JAMES E. MARK AND BURAK ERMAN

Rubberlike Elasticity

A Molecular Primer

SECOND EDITION

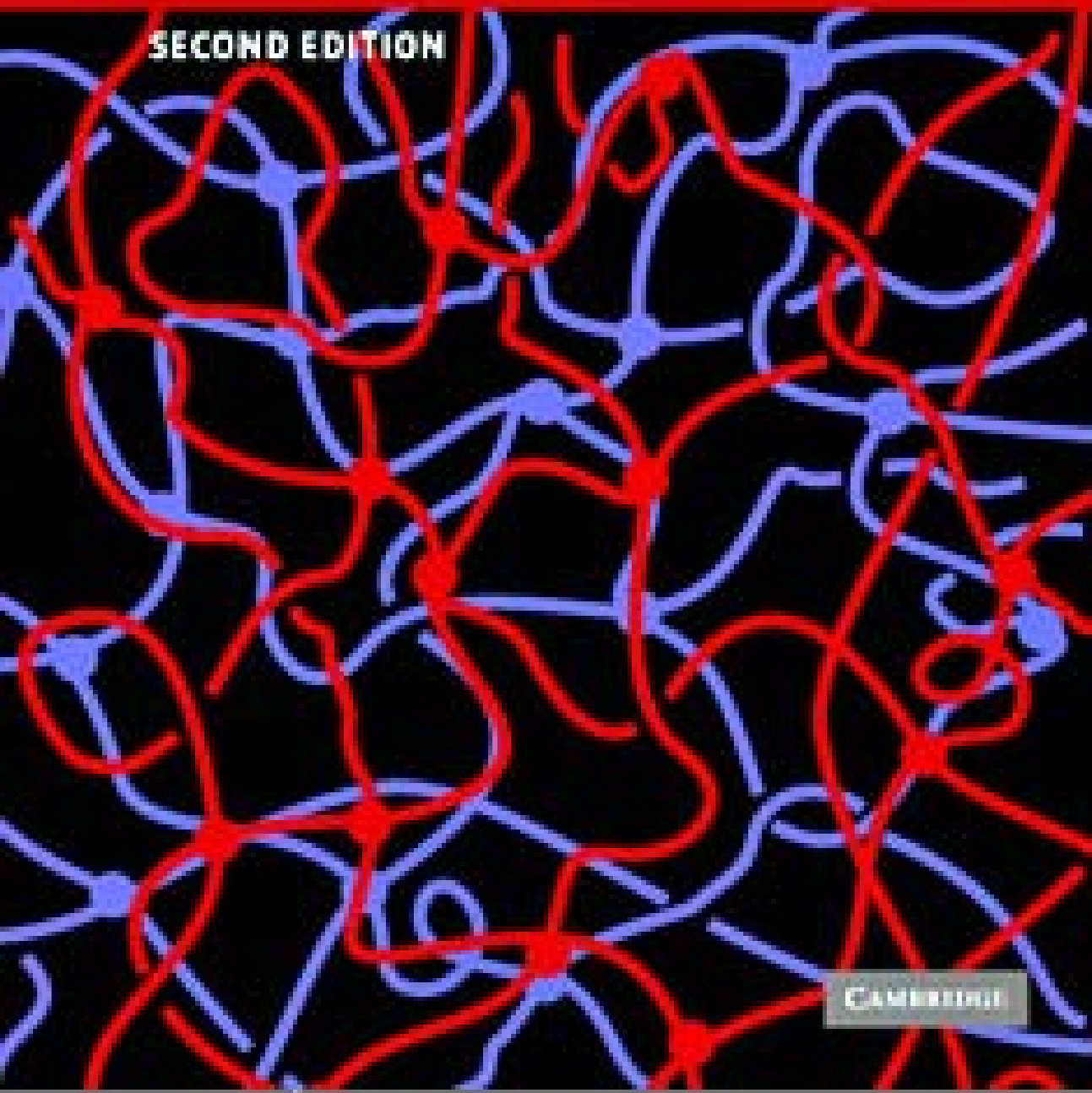

CAMBRIDGE www.cambridge.org/9780521814256

This page intentionally left blank

RUBBERLIKE ELASTICITY

Elastomers and rubberlike materials form critical components in diverse applications that range from tires to biomimetic devices and are used in chemical, biomedical, mechanical and electrical engineering. This updated and expanded edition provides an elementary introduction to the physical and molecular concepts governing the behavior of elastomeric materials. The coverage of fundamental principles has been greatly extended and fully revised, with analogies to more familiar systems such as gases, producing an engaging approach to this phenomenon. Dedicated chapters on novel uses of elastomers, covering bioelastomers, filled elastomers and liquid-crystalline elastomers are included, illustrating established and emerging applications at the forefront of physical science. With problem sets and corresponding solutions, and a list of experiments and demonstrations, this is a self-contained introduction to the topic for graduate students, researchers and industrialists working in the applied fields of physics and chemistry, and polymer science and engineering.

JAMES E. MARK is a Distinguished Research Professor for the Department of Chemistry at the University of Cincinnati, Ohio. He has been a Visiting Professor at several institutions as well as having extensive research and consulting experience in industry. His current research interests pertain to the physical chemistry of polymers, including the elasticity of polymer networks, hybrid organic–inorganic composites, liquid-crystalline polymers, and a variety of computer simulations. A Fellow of the American Physical Society, he is also an editor of the journal *Polymer*. Amongst numerous achievements, he has been awarded the ACS Applied Polymer Science award and was also elected to the Inaugural Group of Fellows (ACS Division of Polymeric Materials Science and Engineering). He is a consultative editor for the Cambridge polymer science list.

BURAK ERMAN is a Professor in the Department of Chemical and Biological Engineering at Koc University in Istanbul, Turkey, where he has been since 2002. His research interests are focused on rubber elasticity, polymer and protein physics and engineering, both experiment and theory, including computer simulations. In 1984 he founded and became Director of the Polymer Research Center at Bogazici University, before moving in 1988 to the Sabanci University in Istanbul where he founded the Chemistry and Materials Science Program. In 1991 he received both the Simavi Science Award and the TUBITAK Science Award. He is founder and member of the Turkish Academy of Sciences.

RUBBERLIKE ELASTICITY

A Molecular Primer

Second Edition

JAMES E. MARK
University of Cincinnati, USA

BURAK ERMAN
Koc University, Turkey

CAMBRIDGE
UNIVERSITY PRESS

CAMBRIDGE UNIVERSITY PRESS
Cambridge, New York, Melbourne, Madrid, Cape Town, Singapore, São Paulo

Cambridge University Press
The Edinburgh Building, Cambridge CB2 8RU, UK

Published in the United States of America by Cambridge University Press, New York

www.cambridge.org
Information on this title: www.cambridge.org/9780521814256

First published in print format 2007

ISBN-13 978-0-511-26925-7 eBook (EBL)
ISBN-10 0-511-26925-0 eBook (EBL)

ISBN-13 978-0-521-81425-6 hardback
ISBN-10 0-521-81425-1 hardback

Contents

Preface to the first edition

This book was prepared to provide a concise, elementary presentation of the most important aspects of rubberlike elasticity. Along with many of our colleagues, we have long felt a need for such an introductory treatment. The present time seems propitious because of new insights into the subject provided by theory and numerous recent developments on the experimental side. We have treated the subject from the point of view of the physical chemist or chemical physicist. Accordingly, there is a very pronounced emphasis on molecular concepts and physical ideas, particularly those underlying some of the more abstract theory. The coverage is restricted to equilibrium properties, with no significant consideration of the huge body of literature on polymer viscoelasticity. The approach is quite tutorial, and the only background required of the reader is familiarity with the basic concepts of physical chemistry. Consequcntly, readers already knowledgeable about some aspects of rubberlike elasticity will be inclined to move through a few of the sections relatively rapidly. Nonetheless, we hope that all readers will benefit from the general overview and will also find some specific topics to be of particular interest and useful in their own research programs. The material presented should be sufficient for a one-term introductory course on the subject.

To a large extent, the book can be divided into two major parts. Part A deals primarily with fundamentals; Part B considers additional topics, many of which are still under intensive investigation and thus necessarily discussed in only a preliminary manner. From a positive point of view, the tentative nature of these capsule summaries should stimulate further work in these areas. For both Parts A and B, some of the more detailed material has been placed in appendixes.

Both of us had the great privilege of collaborating extensively with the late Paul J. Flory, who contributed so remarkably to an understanding of rubberlike elasticity, among other topics in the area of polymer science. Our approach to this subject is largely his, and it would be impossible (and undesirable) to remove these partialities

completely. Although they are there, every effort has been made to provide some balance by commenting on other approaches and schools of thought.

It is a great pleasure to acknowledge the invaluable assistance provided by Mrs. Jane Hershner, who typed all the drafts of the manuscript. She either has the patience of a saint or is a superb actress (probably the latter).

Finally, we wish to dedicate this book to the memory of Paul Flory, because of his seminal contributions to the area of rubberlike elasticity, but more generally on behalf of the countless people he inspired, both as a scientist and an extraordinary, profound human being.

James E. Mark
Cincinnati, Ohio

Burak Erman
Istanbul, Turkey
June 1998

Preface to the second edition

In this edition, we made several changes in both content and organization. In order to reduce cross-referencing, we combined the chapters on elastic equations of state and force as a function of deformation into a single chapter, Chapter 7, under the heading "Elastic equations of state and force–deformation relations". We updated Chapter 10, "Force as a function of structure", under the new heading, "Model elastomers". Since volume phase transitions are now gaining fundamental importance, we moved Chapter 17, "Osmotic compressibility, critical phenomena, and gel collapse" to Part I, under the new name: Chapter 8, "Swelling of networks and volume phase transitions". We joined Chapters 14 and 15 on "Birefringence" and "Segmental orientation" into a single new chapter, Chapter 14, "Birefringence and segmental orientation", because both of these chapters are closely related and this merge reduces redundancy in the treatment of the subject. We significantly condensed and moved Chapter 16, "Rotational isomerization", to the end of the new Chapter 12, "Strain-induced crystallization and ultimate properties". This change was made due to lack of computational work and interest in the field of rotational isomerization in stretched elastomers since the first edition. We feel, however, that the importance of computational work on highly stretched chains should not be underestimated. The new chapter, Chapter 3, "The single molecule: theory and experiment", shows new possibilities in this area. We added a new chapter, Chapter 16, "Liquid-crystalline elastomers", due to the importance gained by this subject in recent years. The book is now reduced to 19 chapters from the original 21 chapters.

Part I

Fundamentals

1

Introduction

General comments

The materials to be discussed in this book are known by a variety of names. The oldest, *rubbers*, is not very illuminating since it refers to their relatively unimportant ability to remove pencil or ink marks from paper by an abrasive rubbing action (Treloar, 1975; Eichinger, 1983; Mark, 2005a). Of much greater importance are their elastic properties, and the term *elastomers* is now much in use. So also is *rubberlike materials*, which emphasizes the similarities between such substances and natural rubber, which is obtained from the Hevea tree.

Rubberlike materials have long been of extraordinary interest and importance. They find usage in items ranging from automobile tires and conveyor belts to heart valves and gaskets in supersonic jet planes (Gent, 1992). The striking nature of their elastic properties and their relationships to molecular structure has attracted the attention of numerous physical chemists and chemical physicists interested in structure–property relationships, particularly those involving polymeric materials (Flory, 1953; Treloar, 1975; Mark and Erman, 1992; Erman and Mark, 1997; Graessley, 2003; Witten, 2004).

Rubberlike elasticity and its molecular requirements

A useful way to begin a discussion of rubberlike elasticity is to define it and then to list the molecular characteristics required to achieve the very unusual behavior described. This is done in Table 1.1. The definition has two parts: very high deformability and essentially complete recoverability. In order for a material to exhibit this type of elasticity, three molecular requirements must be met: (1) the material must consist of polymeric chains; (2) the chains must have a high degree of flexibility and mobility; and (3) the chains must be joined into a network structure (Mark *et al.*, 1993; Mark, 2002a, 2003).

Table 1.1 *Definitions and molecular requirements for rubberlike elasticity*

Two-part definition	Molecular requirements
1. Very high deformability	1. Materials that are constituted of molecules that are: (a) long chains (polymers) (b) highly flexible and mobile
2. Essentially complete recoverability	2. Network structure from cross linking of molecules

The first requirement is associated with the very high deformability. It arises from the fact that the molecules in an elastomeric material must be able to alter their arrangements and extensions in space dramatically in response to an imposed stress, and only a long-chain molecule has the required very large number of spatial arrangements of very different extensions. This versatility is illustrated in Figure 1.1, which depicts a two-dimensional projection of a random spatial arrangement of a relatively short polyethylene chain in the undeformed amorphous state. The spatial configuration shown was computer generated using a Monte Carlo technique in as realistic a manner as possible. The correct bond lengths and bond angles were employed, as was the known preference for *trans* rotational states about the skeletal bonds in any *n*-alkane molecule. A final feature taken into account was the fact that rotational states are interdependent; what one rotatable skeletal bond does depends on what the adjoining skeletal bonds are doing (Flory, 1969; Mattice and Suter, 1994; Rehahn *et al.*, 1997). One important feature of this typical configuration is the relatively high spatial extension of some parts of the chain. This is due to the already mentioned preference for *trans* conformations, which are essentially planar zigzag and therefore of high extension. A feature that is more important in the present context is the fact that, in spite of these preferences, many sections of the chain are quite random and compact. As a result, the chain extension (as measured by the end-to-end separation) is quite small. For even such a short chain, the extension could be increased approximately fourfold by simple rotations about skeletal bonds, without any need for the more energy-demanding distortions of bond angles or increases in bond lengths.

The second characteristic required for rubberlike elasticity also relates to the high deformability. It specifies that the chains be flexible and mobile enough that the different spatial arrangements of the chains are accessible. That is, changes in these arrangements should not be hindered by such constraints as might result from inherent rigidity of the chains, or by decreased mobility as would result from extensive chain crystallization, or from the very high viscosity characteristic of

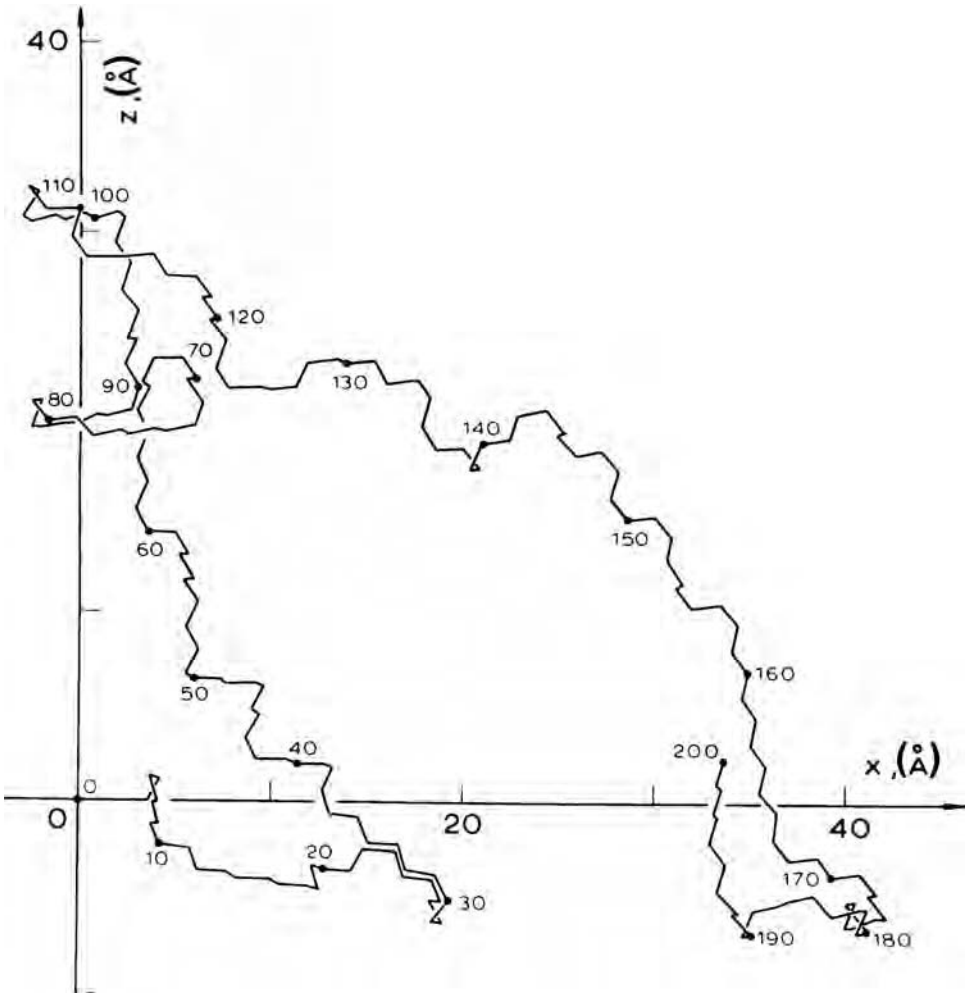

Figure 1.1 A two-dimensional projection of the backbone of an undeformed *n*-alkane chain (or sequence from a longer polyethylene chain) which consists of 200 skeletal bonds (Mark, 1981; Mark *et al*., 1993). This representative arrangement or spatial configuration was computer generated using known values of the bond lengths, bond angles, rotational angles about skeletal bonds, and preferences among the corresponding rotational states. (Reprinted with permission from J. E. Mark *et al*., Eds., *Physical Properties of Polymers*. Copyright 1984, American Chemical Society.)

the glassy state. These two requirements are further discussed in Chapter 2, using specific examples of elastomeric and non-elastomeric materials.

The last characteristic cited is required in order to obtain the recoverability part of the definition. The network structure is obtained by joining together, or cross linking, pairs of segments, approximately one out of every 100, thereby preventing

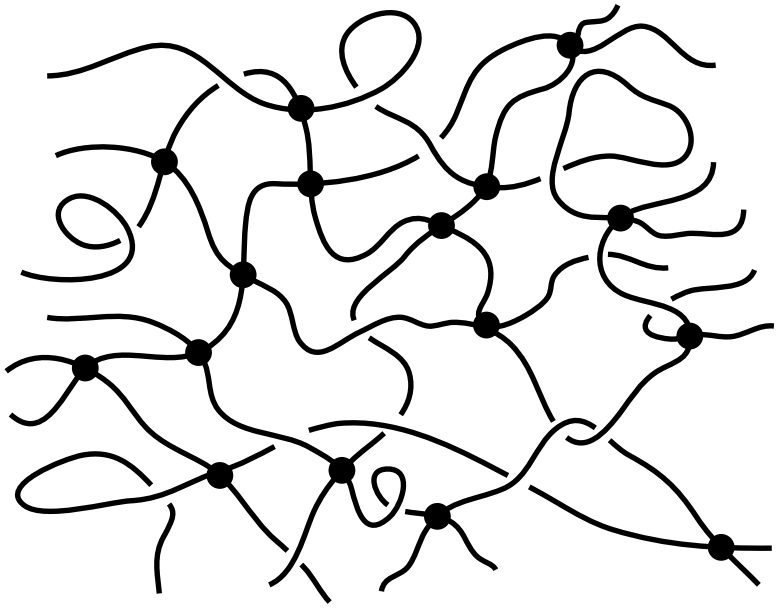

Figure 1.2 Sketch of part of a typical elastomeric network.

stretched polymer chains from irreversibly sliding by one another. The structure obtained in this way is illustrated in Figure 1.2, in which the cross links may be either chemical bonds (as is illustrated by sulfur-vulcanized natural rubber) or physical aggregates, like the small crystallites in a partially crystalline polymer or the glassy domains in a multiphase triblock copolymer (Mark, 2000). Different types of cross linking are discussed in more detail in Chapter 4.

Origin of the elastic force

The molecular origin of the elastic force f exhibited by a deformed elastomeric network can be elucidated through thermoelastic experiments, which involve the temperature dependence of either the force f at constant length L or the length at constant force. Consider first a thin metal strip stretched with a weight W to a point short of that giving permanent deformation, as is shown in Figure 1.3. Increase in temperature (at constant force) would increase the length of the stretched metal strip in what would be considered the usual behavior. Exactly the opposite result, a shrinkage, is observed in the case of a stretched elastomer! For purposes of comparison, the result observed for a gas at constant pressure is included in the figure. Raising its temperature would of course cause an increase in its volume V, as is illustrated by the well-known ideal gas law $pV = nRT$ (Atkins, 1990).

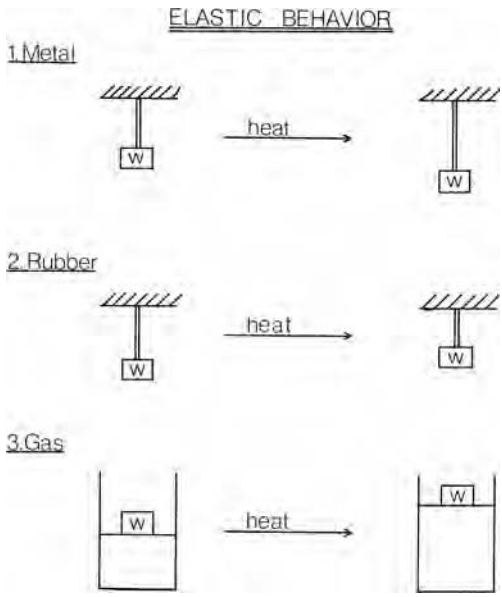

Figure 1.3 Results of thermoelastic experiments carried out on a typical metal, rubber, and gas (Mark, 1981).

The explanation for these observations is given in Figure 1.4 (Mark, 1981). The primary effect of stretching the metal is the increase ΔE in energy caused by changing the values of the distance d of separation between the metal atoms. The stretched strip retracts to its original dimensions upon removal of the force since this is associated with a decrease in energy. Similarly, heating the strip at constant force causes the usual expansion arising from increased oscillations about the minimum in the asymmetric potential energy curve. In the case of the elastomer, however, the major effect of the deformation is the stretching out of the network chains, which substantially reduces their entropy. Therefore the retractive force arises primarily from the tendency of the system to increase its entropy toward the (maximum) value that it had in the undeformed state. Increase in temperature increases the chaotic molecular motions of the chains, which increases the tendency toward the more random state. As a result there is a decrease in length at constant force, or an increase in force at constant length. This is strikingly similar to the behavior of a compressed gas, in which the extent of deformation is given by the reciprocal volume $1/V$. The pressure of the gas is largely entropically derived, with increase in deformation (i.e., increase in $1/V$) also corresponding to a decrease in entropy. Heating the gas increases the driving force toward the state of maximum entropy (infinite volume or zero deformation). Therefore, increasing the temperature increases the volume at constant pressure, or increases the pressure at constant volume.

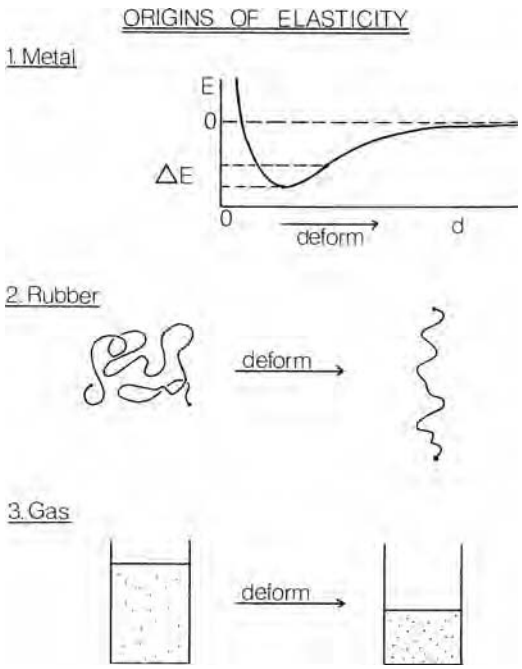

Figure 1.4 Sketches explaining the observations described in Figure 1.3 in terms of the molecular origin of the elastic force or pressure (Mark, 1981).

Some other analogies

The surprising analogy between a gas and an elastomer (which after all is a condensed phase) carries over into the expressions for the work dw of deformation. In the case of a gas, dw is of course $-p\,\mathrm{d}V$. For an elastomer, however, this term is essentially negligible since network deformation (except for swelling) takes place at very nearly constant volume. The corresponding work term now becomes $f\,\mathrm{d}L$, where the difference in sign is due to the fact that positive w corresponds to a decrease in volume of a gas but to an increase in length of an elastomer.

Similarly, adiabatically stretching an elastomer increases its temperature in the same way that adiabatically compressing a gas (for example, in a diesel engine) will increase its temperature. The situation in the case of the elastomer is somewhat more complicated in that if some crystallization is induced by the stretching, then part of the temperature increase would be due to the latent heat of crystallization. In any case, for both the elastomer and the gas, the total entropy change for the reversible process

$$\Delta S = \Delta S(\text{deformation}) + \Delta S(\text{temperature change}) \geq 0 \qquad (1.1)$$

must be positive or zero since the systems are acting as though they are (temporarily) isolated. Therefore, since ΔS(deformation) must be negative, ΔS(temperature change) must be positive, and this has to correspond to a temperature increase. The basic point here is the fact that the retractive force of an elastomer and the pressure of a gas are both primarily entropically derived, and as a result the thermodynamic and molecular descriptions of these otherwise dissimilar systems are very closely related.

As would be expected, letting a stretched elastomer contract adiabatically causes its temperature to decrease. These increases and decreases in temperature can, in fact, be used to construct heat-transfer devices such as refrigerators and air conditioners (DeGregoria, 1994; DeGregoria and Kaminski, 1997). An analogy of this effect in elastomers is provided by adiabatic demagnetization, a technique used to reach very low temperatures (Atkins, 1990). A suitable salt is magnetized isothermally by the application of a strong field, thereby aligning its magnetic moments with an associated decrease in entropy. The field is then removed adiabatically (which is analogous to letting the elastomer snap back), and the moments again spontaneously become disordered. In both cases ΔS(disordering) is positive and is offset by a negative ΔS(temperature change), which of course corresponds to a decrease in temperature.

The fact that heat is given off in the stretching of an elastomer can be used to provide a thermodynamic explanation of the observed shrinkage of a stretched elastomer when its temperature is increased. According to Le Chatelier's principle, "A system at equilibrium, when subjected to a perturbation, responds in a way that tends to eliminate the effect" (Atkins, 1990). Since heat is given off during stretching, adding heat has to cause a contraction. The temperature increase observed upon stretching an elastomer is augmented by heat generated by the wasteful conversion of part of the deformation energy through frictional effects. As a result, the temperature increase during the stretching process is not completely offset by the temperature decrease during the retraction phase. There is therefore a hysteretic buildup in temperature that is highly disadvantageous. Not only does it represent wastage of mechanical energy, but the heat buildup can have a degradative effect on the elastomer. Probably the most important example here is the flexing of an automobile tire as it rotates through its bending–recovery cycles.

Some historical high points

Table 1.2 summarizes some important contributions from early experiments on rubberlike elasticity. The earliest experiments, by Gough in 1805 (Flory, 1953; Treloar, 1975; Mason, 1979), demonstrated the heat effects described in the preceding few paragraphs and also the phenomenon of strain-induced crystallization, which is

Table 1.2 *Some early contributions in the experimental area*

Contribution	Scientists	Date
Heat effects, strain-induced crystallization	Gough	1805
Vulcanization (cross linking)	Goodyear and Hayward	1839
Thermoelasticity	Joule	1859
Volume changes accompanying deformation	Several	*c.* 1930
Physically cross-linked networks such as the thermoplastic elastomers	Numerous	—
Insights from studies of bioelastomers	Numerous	—

discussed in Chapter 12. The discovery of vulcanization (sulfur-based cross linking) by Goodyear and Hayward in 1839 greatly facilitated experimental investigations since cross-linked elastomers could now be brought close to elastic equilibrium (Morawetz, 1985). The more quantitative thermoelasticity experiments described above were first carried out by Joule back in 1859. This was in fact only a few years after the entropy S was introduced as a thermodynamic function. Another important experimental contribution was the observation by several workers that deformations (other than swelling) of rubberlike materials occurred essentially at constant volume, so long as crystallization was not induced (Gee *et al.*, 1950). (In this sense, the deformations of an elastomer and a gas are very different.) Some more recent milestones are physically cross-linked networks such as the thermoplastic elastomers (discussed primarily in Chapter 4), and biomimetic insights from studies of bioelastomers (covered in Chapter 17).

Some early contributions on the theoretical side are described in Table 1.3. A molecular interpretation of the fact that rubberlike elasticity is primarily entropic in origin had to await Hermann Staudinger's later demonstration that polymers were covalently bonded molecules and not some type of association complex best studied by colloid chemists (Morawetz, 1985). Meyer, von Susich, and Valko in 1932 correctly interpreted the observed near constancy in volume to indicate that the changes in entropy must therefore involve changes in the spatial configurations of the network chains. These workers also concluded that the elastic force should be proportional to the absolute temperature (Treloar, 1975). These basic qualitative ideas are shown in the sketch in Figure 1.5, where the arrows represent some typical end-to-end vectors of the network chains. The first step toward making these ideas more quantitative, in the form of an elastic equation of state, was the idea, proposed

Table 1.3 *Some early contributions in the theoretical area*

Contribution	Scientists	Date
Chainlike nature of polymers	Staudinger	*c.* 1920
Chain orientation upon network deformation; elastic force proportional to absolute temperature	Meyer, von Susich, and Valko	1932
Elastic force proportional to number of "molecules"	Kuhn	1936
Elastic force proportional to absolute temperature and to sample length	Guth and Mark	1934
Phantom network theory	James and Guth	1941
Affine network theory	Wall	1942
	Flory and Rehner	1943
Theories with constraints on junctions	Allegra and Ronca	1975
	Flory and Erman	1977
Slip-link theories	Ball, Doi, and Edwards	1981

by Werner Kuhn in 1936, that the elastic force f should be proportional to the number of "molecules" in the elastomer. In the 1930s, Kuhn, Eugene Guth, and Herman Mark first began to develop quantitative theories based on this idea that the network chains undergo configurational changes, by skeletal bond rotations, in response to an imposed stress. Guth and Mark (Guth and Mark, 1934) also concluded from this picture that f should be proportional to the absolute temperature, which turns out to be approximately correct. They also concluded, however, that f should be proportional to the length of the stretched elastomer. This is incorrect since the constant-volume nature of the elongation process requires that the sample dimensions perpendicular to the stretching direction decrease proportionally. Some chains are therefore compressed in an elongation experiment, as is illustrated by the horizontal end-to-end vector shown in the middle of the sample strip in Figure 1.5. As a result, f is not proportional to L or to the elongation $\alpha = L/L_\mathrm{i}$; (L_i being the initial length), but to $(\alpha - \alpha^{-2})$, where the subtractive term α^{-2} results from these compressive effects.

Guth, in collaboration with Hubert James, began development of the phantom network theory of rubberlike elasticity around 1941. Fred Wall, Paul Flory, and John Rehner in 1942 and 1943 then began development of the alternative affine network theory. Later refinements include theories with constraints on junctions, and the slip-link theories. All these developments are described in Chapters 5 and 6.

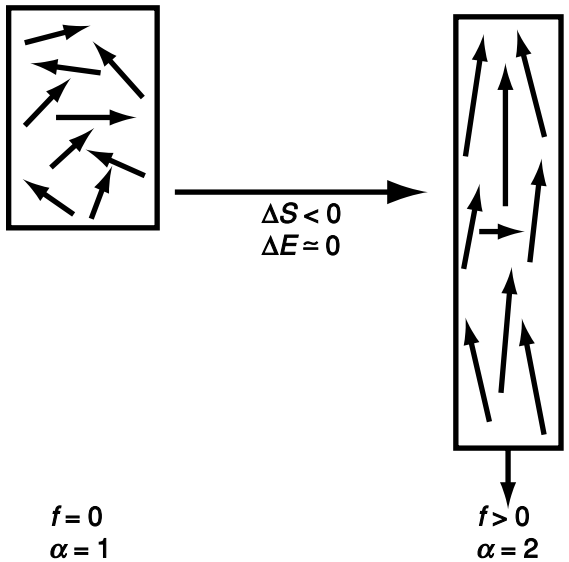

Figure 1.5 Sketch showing changes in length and orientation of network chain end-to-end vectors upon elongation of a network.

Basic postulates

There are two postulates that have been of critical importance in the development of molecular theories of rubberlike elasticity. The most important is:

1. Although intermolecular interactions unquestionably occur in rubberlike materials (they are, after all, condensed phases), these interactions are independent of configuration. They are therefore independent of extent of deformation and therefore play no role in deformations carried out at constant volume and composition (except of course in the case of strain-induced crystallization).

The postulate states that rubberlike elasticity is an *intra*molecular effect, specifically the entropy-reducing orientation of network chains described above. As a repercussion, these chains should be random in the bulk (undiluted) amorphous state, in the absence of any deformation (Flory, 1953). Since intermolecular effects are independent of intramolecular effects, there is no inducement for the spatial configurations of the chains to be altered.

This assumption, probably originally made more out of desperation than anything else, is now supported by a variety of results. First, thermoelastic results are found to be independent of network swelling, as is described in Chapter 9. Second, neutron scattering studies have confirmed that chains in the bulk, amorphous, undeformed state are indeed random (Flory, 1984). They in fact have mean-square dimensions

the same as the unperturbed values $\langle r^2 \rangle_0$ they have in a Θ system, where excluded-volume effects are nullified (Flory, 1953). Finally, the partition function for the system has been found to be separable (to factor) into an intramolecular part and a compositional part (Flory, 1984).

The second postulate is very closely related to the first. It states:

2. The Helmholtz free energy of the network should also be separable into liquid and elastic contributions:

$$A = A_{\text{liq}}(T, V, N) + A_{\text{el}}(\lambda) \tag{1.2}$$

where λ is the strain tensor.

It is thus assumed that the non-elastic (liquid-like) part of the network free energy is independent of deformation. How much of an approximation this involves is not yet entirely clear. Differential sorption measurements on networks may eventually resolve this issue (Yen and Eichinger, 1978; Brotzman and Eichinger, 1983; Erman and Mark, 1997).

In some of the theories, it is further assumed that the deformation is affine, that is, that the network chains move in proportion to the macroscopic dimensions of the elastomeric sample (Flory, 1953; Treloar, 1975; Eichinger, 1983). This assumption was relaxed in the phantom network theories, and in the more modern theories described in Chapter 6.

It is also frequently assumed that the chains have end-to-end distances that follow a Gaussian distribution. This is quite satisfactory except of course for chains that are unusually stiff, very short, or brought close to the limits of their extensibility by the deformation process. Non-Gaussian behavior is described in Chapter 13.

Typical apparatuses for stress–strain measurements

In the case of elongation, the apparatus typically used to measure the force required to give a specified deformation in a rubberlike material is very simple, as can be seen from its schematic description in Figure 1.6 (Mark *et al.*, 1993; Mark and Erman, 1998, 2001). The elastomeric strip is mounted between two clamps, the lower one fixed and the upper one attached to a movable force gauge. A recorder is used to monitor the output of the gauge as a function of time in order to determine when the force is exhibiting the constant, near-equilibrium values suitable for comparisons with theory. The sample is generally protected with an inert atmosphere such as nitrogen to prevent degradation, particularly in the case of measurements carried out at elevated temperatures. Both the sample cell and container with the surrounding constant-temperature bath are made of glass, which permits use of a cathetometer

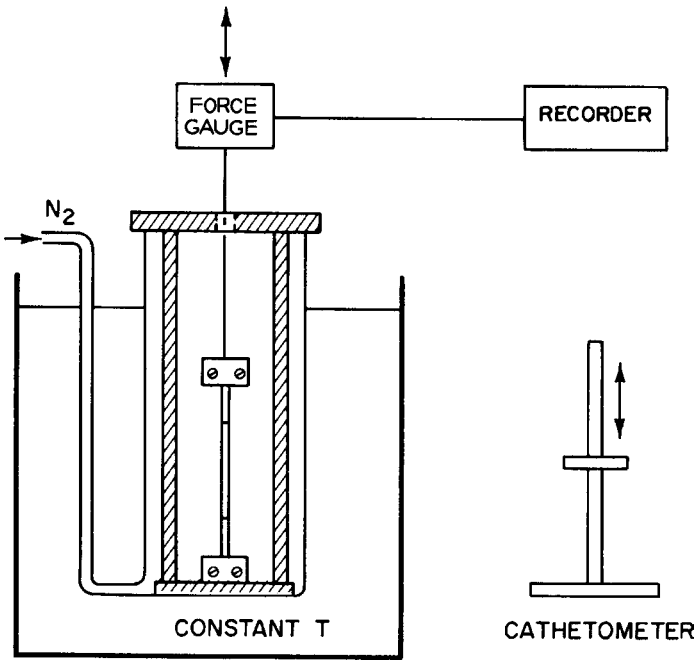

Figure 1.6 Apparatus for carrying out stress–strain measurements on an elastomer in elongation (Mark, 1981). (Reprinted with permission from J. E. Mark *et al.*, Eds., *Physical Properties of Polymers*. Copyright 1984 American Chemical Society.)

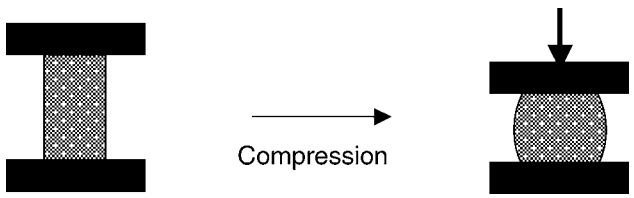

Figure 1.7 Apparatus for carrying out stress–strain measurements on an elastomer in compression.

or traveling microscope to obtain values of the strain by measuring the distance between two lines marked on the central portion of the test sample.

The apparatus is quite different for doing compression measurements, as can be seen from the sketch in Figure 1.7. The compression can be imposed by decreasing the distance between the two parallel confining plates, but this is difficult to do without causing the non-uniform strains commonly called "barreling" (the bulging shown in the sketch). A closely related alternative is simply to stretch a sheet of the material in two perpendicular directions, as illustrated in Figure 1.8. The deformations in the two directions need not be the same, which is the major advantage

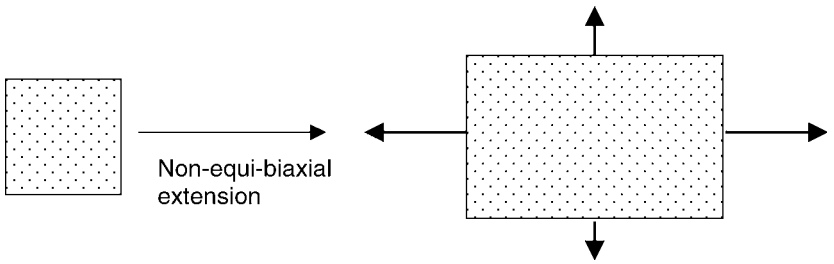

Figure 1.8 Apparatus for carrying out stress–strain measurements on an elastomer in biaxial extension.

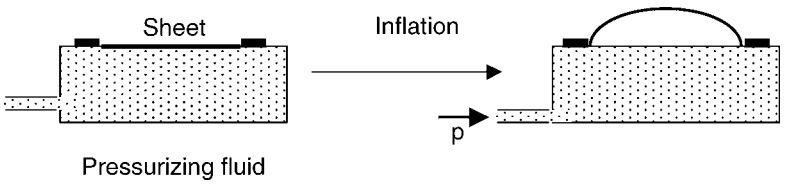

Figure 1.9 Apparatus for carrying out stress–strain measurements on an elastomer by inflation of a sheet.

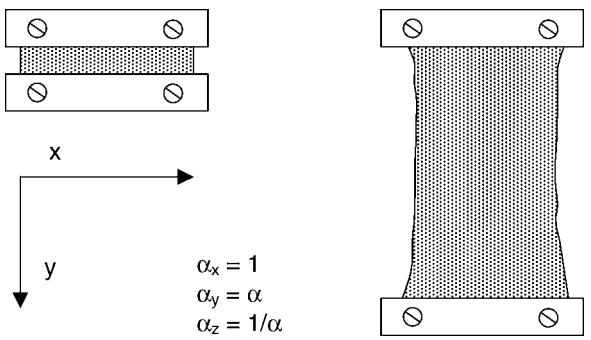

Figure 1.10 Apparatus for carrying out stress–strain measurements on an elastomer in shear.

of this approach. A simpler method involves inflation of the elastomeric sheet, as shown in Figure 1.9. In this case, the deformations in the two directions have to be the same, or "equi-biaxial".

Measurements in shear can be carried out by stretching a very wide but short strip of the elastomer, as shown in Figure 1.10. When stretching is imposed in the direction perpendicular to this larger initial dimension, then this dimension is essentially held constant, as is required in the case of shear.

Finally, torsion can be imposed as the strain, and involves twisting of a cylindrical sample about its axis, as is illustrated in Figure 1.11. The interesting thing about

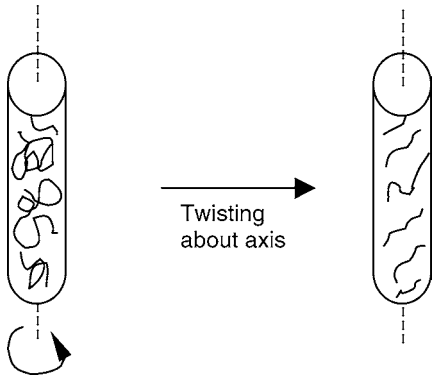

Figure 1.11 Carrying out stress–strain measurements on an elastomer in torsion.

this deformation is the inherent non-uniformity of the strain, being a maximum at the surface of the sample and zero at the axis. The orientations of the stretched-out chains would also be unusual, and this should lead to novel crystallization effects.

Thermoelastic measurements are of course carried out by changing the temperature of the constant-temperature bath in which the experiment is being carried out.

A typical stress–strain isotherm in elongation

A typical stress–strain isotherm obtained on a strip of cross-linked natural rubber in elongation is shown in Figure 1.12 (Mark, 1981; Mark *et al.*, 1993). The units for the force are generally newtons (N), and N mm^{-2} for the nominal or engineering stress f^* (the force divided by the original cross-sectional area). The curves obtained are usually checked for reversibility. In this type of representation, the area under the curve is frequently of considerable interest since it is proportional to the work of deformation $w = \int f \mathrm{d}L$. Its value up to the failure point is the energy required for rupture and is therefore a measure of the toughness of the material. The initial part of the stress–strain isotherm shown is of the expected form in that f^* approaches linearity with elongation α as α becomes sufficiently large to make negligibly small the α^{-2} term in the $(\alpha - \alpha^{-2})$ strain function mentioned above.

The large increase in f^* at high deformation in the case of natural rubber is due largely if not entirely to strain-induced crystallization. The melting point $T_\mathrm{m} = \Delta H_\mathrm{m}/\Delta S_\mathrm{m}$ of the polymer is directly proportional to the heat of fusion ΔH_m and inversely proportional to the entropy of fusion ΔS_m. The latter is significantly diminished (from ΔS_m to $\Delta S'_\mathrm{m}$) when the chains in the amorphous (melted) network remain stretched out because of the applied deformation. The melting point is thereby increased, and it is in this sense that the stretching induces the crystallization of some of the network chains. Figure 1.13 (Mark and Odian, 1984) illustrates

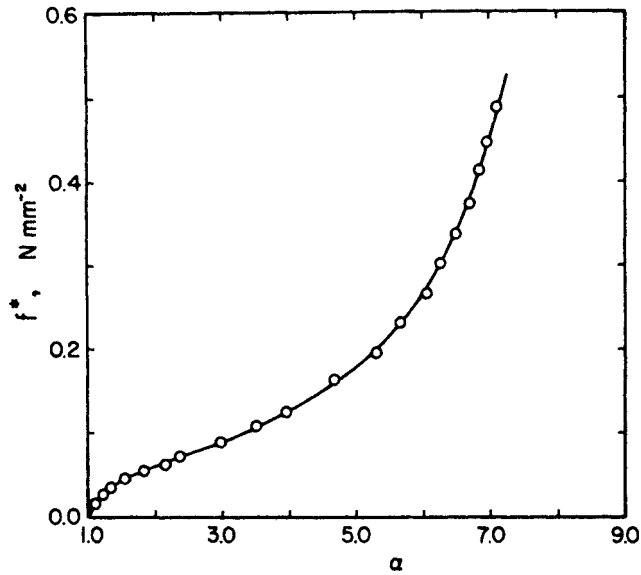

Figure 1.12 Stress–elongation isotherm for natural rubber in the vicinity of room temperature (Mark, 1981, 1993). (Reprinted with permission from J. E. Mark *et al.*, Eds., *Physical Properties of Polymers*. Copyright 1984 American Chemical Society.)

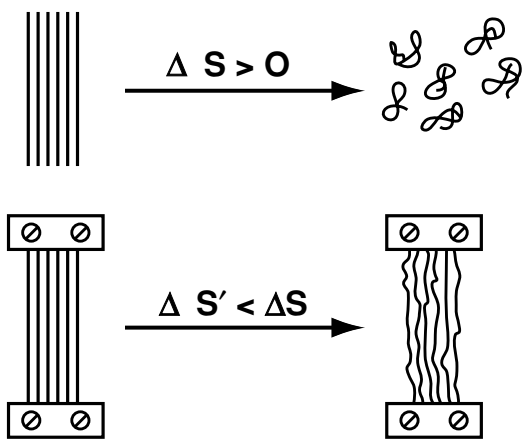

Figure 1.13 Sketch explaining the increase in melting point with elongation in the case of a crystallizable elastomer. (Reprinted with permission from J. E. Mark and G. Odian, Eds., *Polymer Chemistry*. Copyright 1984 American Chemical Society.)

these ideas. The effect is a mechanical analog to suppressing the extent to which chains can randomize themselves by putting a rigid group such as *p*-phenylene in the polymeric repeat unit, as is described in Chapter 12 (Mark and Odian, 1984). It is also qualitatively similar to the increase in melting point generally observed upon increase in pressure on a low-molecular-weight substance in the crystalline state (Atkins, 1990). In any case, the crystallites formed in this way act as physical cross links and reinforcing filler, and they decrease the amount of deformable material in the sample (Mark, 1979b, c). These changes increase the modulus of the network. The properties of both crystallizable and non-crystallizable networks at high elongations are discussed in detail in Chapter 12. Additional deviations from theory are found in the region of moderate deformation, upon careful examination of the data, particularly in terms of the usual plots of modulus against reciprocal elongation. Although early theories predicted the modulus to be independent of elongation, it generally decreases significantly upon increase in α. The interpretation of these deviations is given in Chapter 7.

Scope of the coverage of the subject

As already mentioned in the two Prefaces, the focus will be almost entirely on rubberlike materials at elastic equilibrium. Non-equilibrium, viscoelastic properties have been extensively discussed in a number of other places (Ferry, 1980; Aklonis and McKnight, 1983; Graessley, 2003, 2004; Mark *et al.*, 2004). Interpretations will almost always be in molecular terms, and detailed non-molecular (phenomenological) information will have to be sought elsewhere (Treloar, 1975; Gee, 1980; Ogden, 1986, 1987). Homogeneous (one-phase) systems will be of primary interest, the major exceptions being elastomers undergoing strain-induced crystallization and filled elastomers (when there is some molecular understanding of their properties).

2

Some rubberlike materials

Polymers that are normally rubberlike (unswollen at ambient temperatures)

As mentioned in Chapter 1, the preparation of an elastomeric material requires that the polymer chains being cross linked be relatively long and have significant flexibility and mobility. Examples of polymers meeting these requirements (Morton, 1987; Treloar, 1975; Mark, 2003a, 2004b; Mark *et al.*, 2005b, c) are given in Table 2.1, along with their structures and transition temperatures (Brandrup *et al.*, 1999; Mark, 2005b; Mark *et al.*, 2005b, c). As can be seen from the structures given, these typical chains have no rings as part of the backbone repeat unit, and very few bulky side groups. This is to be expected, since such structural features would give an undesirable decrease in the flexibility of the polymer (Mark *et al.*, 2004). The high flexibility of these chains is demonstrated in part by the relatively low values they exhibit for the *glass transition temperature* T_g, which is the temperature below which flexibility is so reduced that the material becomes glassy (Ngai, 2004).

Natural rubber, which is essentially 100% of the *cis*-1,4 form of polyisoprene, has a relatively low value of T_g. Specifically, non-crystalline regions of this polymer will not lose their rubberlike elasticity until the temperature falls below -73 °C. Significant amounts of crystallinity in the undeformed state interfere with elastomeric behavior since the chain segments packed into crystallites obviously have their flexibility suppressed. The maximum equilibrium melting point of natural rubber is frequently cited to be 28 °C, but T_m is typically depressed significantly when the polymer is compounded with various additives in a commercial elastomer. Therefore, as a practical matter, natural rubber is a good elastomer and is much used in a variety of applications (Nor and Ebdon, 1998; Mark, 2005b), despite the fact that room temperature is below the maximum melting point of the polymer.

Another important elastomer is butyl rubber, which coincidentally has the same low value of T_g as natural rubber. Its melting point of 5 °C is, however, well below room temperature. It has one of the lowest permeabilities of any elastomer and

Table 2.1 *Some polymers that are normally rubberlike*

Polymer	Structure	T_g (°C)	T_m (°C)
Natural rubber[a]	$[C(CH_3)=CH-CH_2-CH_2-]$	–73	28
Butyl rubber[b]	$[C(CH_3)_2-CH_2-]$	–73	5
Poly(dimethylsiloxane)	$[Si(CH_3)_2-O-]$	–127	–40
Poly(ethyl acrylate)[c]	$[CH(COOC_2H_5)-CH_2-]$	–24	None
Styrene–butadiene copolymer	$[CH(C_6H_5)-CH_2-]$, $[CH=CH-CH_2-CH_2-]$	Low	None
Ethylene-propylene copolymer	$[CH_2-CH_2-]$,$[CH(CH_3)-CH_2-]$	Low	None

[a] *Cis*-1,4-polyisoprene.
[b] Polyisobutylene containing a few mole percent unsaturated comonomer for cross linking.
[c] Stereochemically irregular (atactic) polymer.

is therefore used extensively in pneumatic applications, such the inner linings of tires.

Poly(dimethylsiloxane) (PDMS), a semi-inorganic polymer, is used in many specialty applications, particularly those requiring a high-performance elastomer. It remains non-crystalline and elastomeric to very low temperatures ($T_m = -40$ °C), and its excellent thermal stability permits usage at unusually high temperatures (Mark *et al.*, 2005b, c; Mark, 2004a). Its glass transition temperature, -127 °C, is the lowest reported for any polymer. The very high chain flexibility this indicates is due to (1) the relatively long sketetal bonds (1.64 Å), (2) the unusually large bond angles (143° at the O atoms), (3) the small size of the totally unencumbered O atoms, (4) the unusually low torsional barrier about the Si–O bonds, and (5) the ability of the Si–O–Si bonds to invert through the linear (180° state). It is only the methyl groups that distinguish this material from the totally inorganic silicates such as window glass. Therefore, not surprisingly, the polymer is highly inert and can be used in such demanding applications as high-temperature seals and body implants.

Since a large amount of crystallinity in the undeformed state is disadvantageous, some polymers are prepared so as to make them inherently non-crystallizable. In the case of poly(ethyl acrylate), this is done by using a polymerization initiator or catalyst that does not control the stereochemical structure at the substituted (pseudo-asymmetric) carbon atoms in the chain backbone. The resulting "atactic" vinyl polymer is incapable of crystallizing, because of its stereochemical irregularities (Allcock *et al.*, 2003). A polymer chain can also be made structurally irregular by preparing it in a random copolymerization. Copolymers of styrene–butadiene or ethylene–propylene are in this category, and neither typically has a significant amount of crystallinity. Their specific values of T_g depend of course on chemical

Table 2.2 *Some polymers that are not normally rubberlike*

Polymer	Structure	Complication
Polyethylene	[CH_2—CH_2—]	Highly crystalline
Polystyrene	[$CH(C_6H_5)$—CH_2—]	Glassy
Poly(vinyl chloride)	[CHCl—CH_2—]	Glassy
Elastin	[C═ONH—CHR—]	Glassy

composition, but they are known to be low. Thus the two chemical copolymers and the stereochemical copolymer are rubbery under normal conditions and are in fact commercially important elastomers.

Although large amounts of crystallinity in the undeformed state are undesirable, it should be mentioned that the generation of some crystallites during the stretching process can greatly increase the toughness of an elastomer. This type of *strain-induced crystallization* is discussed in Chapter 12.

Polymers that can be made rubberlike by increase in temperature or by swelling

Some typical polymers that are not usually rubberlike are described in Table 2.2. In the case of polyethylene, the chains are inherently flexible, but a high degree of crystallinity in the undiluted (unswollen) state at room temperature reduces their mobility and thus prevents the occurrence of rubberlike elasticity. This interfering crystallinity can be removed by either copolymerization (as mentioned in Table 2.1), increasing the temperature to above the melting point of the polymer ($\sim$130 °C), or by incorporating a swelling diluent (plasticizer) (Fried, 2003). Elastomeric measurements have in fact been carried out on rubbery cross-linked polyethylene, both at high temperatures in the unswollen state and at somewhat lower temperatures when swollen with a non-volatile diluent (Erman and Mark, 1997). These experiments primarily involve network thermoelasticity and are described in Chapter 9. These studies are not as peculiar as it might seem since it was assumed, correctly, that the unusually simple structure of this polymer would facilitate theoretical interpretation of the experimental results. Highly crystallizable *trans*-diene polymers such as *trans*-1,4-polybutadiene [CH═CH—CH_2—CH_2—] (Zhou and Mark, 2004) would also be in this category.

Similarly, cross-linked polystyrene (which is normally glassy) can be made elastomeric either by increasing the temperature to above its value of T_g (-100 °C) or by incorporating a plasticizer. Again, such experiments have actually been done, but in this case primarily because a convenient polymerization reaction of styrene

Table 2.3 *Some polymers that are never rubberlike*

Polymer	Structure	Complication
Polymeric sulfur	[S—]	Chains too unstable
Poly(*p*-phenylene)	[C_6H_4—]	Chains too rigid
Bakelite®	[C_6H_4(OH)—CH_2—], etc.	Chains too short

® Phenol-formaldehyde resin.

was known to give model networks of known structure (Hild, 1998). Poly(vinyl chloride) provides a more practical example. Its rather high value of T_g (∼85 °C) is frequently suppressed to a value below room temperature by means of a non-volatile plasticizer, making it sufficiently elastomeric for a number of applications.

An example from the realm of biopolymers is provided by the protein elastin, whose repeat units have different R side groups, as shown in Table 2.2. This bioelastomer is used by mammals, including man, for a variety of elastomeric applications (Gosline, 1980, 1987, 1992). The dry polymer has a glass transition temperature in the vicinity of 200 °C (according to extrapolations of data), which is much too high for direct use as an elastomer in living systems. Nature, however, also apparently knows about plasticizers; it never uses elastin except as sufficiently highly swollen by aqueous body fluids to bring its T_g well below the operating temperature of mammals, 37 °C (98.6 °F) (Erman and Mark, 1997). Elastin and some related fascinating bioelastomers are discussed further in Chapter 17.

Polymers that are inherently non-rubberlike

There are several classes of polymers that are inherently incapable of exhibiting rubberlike elasticity, and these are described in Table 2.3.

If elemental sulfur is melted, polymerization can occur at these elevated temperatures, and the resulting chains do exhibit some rubbery behavior in the quenched state (Erman and Mark, 2005). The material has never been made truly rubber-elastic, however. The chains could not be cross linked and, because of their instability, could not be kept from reorganizing. Therefore, the required recoverability could not be achieved.

Rigid-rod polymers such as poly(*p*-phenylene) lack the required flexibility because of their chemical structure. In effect, they have none of the compact conformations required for high deformability.

Finally, very highly cross-linked thermosets, such as the phenol-formaldehyde resins (Bakelite®) or the epoxy adhesives, generally consist of chains that are much too short to have the required extensibility and flexibility under any conditions.

Some other, unusual elastomers

As would be expected, there is always the continuing search for new high-performance elastomers (Ameduri *et al.*, 2001; Wrana *et al.*, 2001). As will be described in Chapter 4, there is also strong interest in preparing better (or at least less expensive) thermoplastic elastomers (triblock copolymers that phase separate to give temporary physical cross links) (Holden *et al.*, 1996; Grady and Cooper, 2005). In this regard, there is an interesting analog in a type of "*baro*plastic" elastomer which parallels *thermo*plastic elastomers in that a pressure increase gives the desired softening required for processing (instead of the usual temperature increase) (Pollard *et al.*, 1998; Ruzette *et al.*, 2001; Gonzalez-Leon *et al.*, 2003).

Liquid-crystalline elastomers are of sufficient interest and importance to be discussed separately (in Chapter 16) and, finally, mention should be made of some elastomers modified so as to have permanently hydrophilic surfaces (Noda, 1991).

3

The single molecule: theory and experiment

Introduction

The single chain constitutes the basic building block of elastomers and understanding its structure and properties is necessary before going into the study of rubberlike elasticity. The original picture of a polymer chain as an isolated entity was by Guth and Mark (Guth and Mark, 1934) and Kuhn (Kuhn, 1934). According to this picture, the polymer chain consisted of freely jointed beads. Further developments elucidating the real nature of the single chain and its departure from the simple freely jointed model were made by several authors, notably by Volkenstein (Volkenstein, 1963) and Flory (Flory, 1953, 1969). The elastic properties such as the force–deformation relations of the single chain, to be used in constructing the elasticity theory, then followed through the use of thermodynamic relations. However, after the advance of experiments such as the atomic force microscope (AFM) and optical tweezers, direct experimental observation of the single chain behavior became possible (Chu, 1991; Granzier and Pollack, 2000; Janshoff *et al.*, 2000; Hugel and Seitz, 2001; Strick *et al.*, 2001; Zhang and Zhang, 2003; Hummer and Szabo, 2005; Barbara *et al.*, 2005; Schuler, 2005). In this chapter, we will first outline the theoretical model of the single chain for a few simplified cases, and then relate this to experimental work on single chains.

Different models of the single chain, the end-to-end vector distribution and force–deformation relations

A simplified picture of the single chain is sketched in Figure 1.1, where the projection of the chain to the x-z coordinates is shown. The figure was generated by the Monte Carlo technique (Mark, 1981) for an undeformed n-alkane chain of 200 bonds.

A few bonds of the chain model are shown in Figure 3.1. Four backbone atoms or units, $i-1$ to $i+2$, along the chain are shown. The backbone bond between the

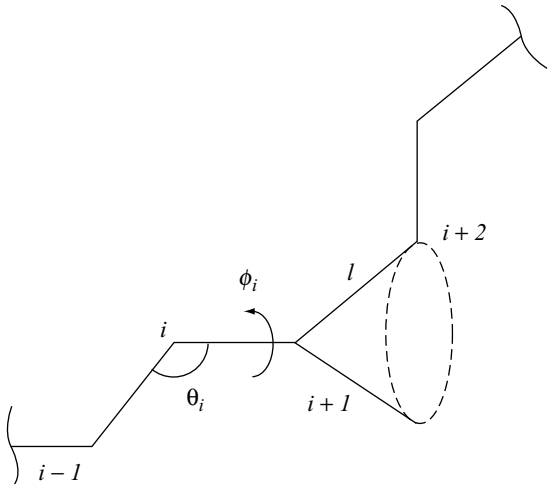

Figure 3.1 A few backbone bonds of a polymer chain, each having a length l. The bond angle between two neighboring bonds at the ith backbone atom is θ_i. Rotation about bond i, $i + 1$ is shown by ϕ_i. If the atoms $i - 1$, i and $i + 1$ are fixed, and rotation is allowed about the bond i, $i + 1$ then the backbone atom $i + 2$ travels along a circular trajectory, shown by the dashed circle.

backbone atoms i and $i + 1$ is the ith bond. Each bond has length l, and the bond angle at the ith backbone atom is shown by θ_i. Rotation about the ith bond is shown as ϕ_i. In the simplest model of the chain, the bonds are freely jointed, i.e., the bond angles θ_i and torsion angles ϕ_i can change freely. An improvement to the freely jointed model is made by assuming freely rotating bonds where bond lengths and θ_i are fixed and only ϕ_i may vary freely. In a more realistic model (Flory, 1969), the rotations about bonds are subject to hindrances that result from the intrinsic torsions of the bonds and the local hindrances of the adjoining atoms. Effects of such hindrances become significant in the presence of bulky groups as is the case in some biological molecules. This will be discussed further in the experimental section below. Both bond lengths and bond angles require relatively large energies of deformation and are assumed fixed. Rotations about bonds, shown by the angle ϕ_i, are possible and subject to a rotational potential determined by the model chosen. If the atoms $i - 1$, i and $i + 1$ are fixed, and rotation is allowed about the bond i, $i + 1$ then the backbone atom $i + 2$ travels along a circular trajectory, shown by the dashed circle in the figure. The chain may change its configurations through such torsional rotations about its bonds and a multitude of chain configurations exists. The unperturbed chain exhibits these rotations due to thermal energy. Stretching the two ends of the chain biases the rotations about bonds. As a result, the configurations allowable to the chain change.

The density distribution $W(r)$ of the end-to-end distance r is central to the analysis of the elasticity of the single chain as well as the network. The density distribution is a measure of the number of configurations allowable to the chain and is related to the entropy $S(r)$ by the relation $S(r) = S_0 + k \ln W(r)$ where k is the Boltzmann constant and S_0 is a function of the absolute temperature, T. Through the use of the thermodynamic relation $A_{el} = U - TS$, and the entropy relation, the elastic free energy (or the Helmholtz free energy) A_{el} of the chain is obtained as (Flory, 1976)

$$A_{el} = c(T) - kT \ln W(r) \tag{3.1}$$

Here, $c(T)$ is a constant that is a function of temperature only. The average force f required to keep the two ends of the chain at the separation r is obtained from Eq. (3.1) through the thermodynamic relation

$$f = -\left(\frac{\partial A_{el}}{\partial r}\right)_T \tag{3.2}$$

Thus, knowing the expression for $W(r)$ yields the force–deformation relations through Eqs. (3.1) and (3.2).

The average dimensions of a chain are suitably represented by the mean-square end-to-end distance $\langle r^2 \rangle$. The unperturbed dimensions are represented by a subscript 0. The unperturbed mean-square end-to-end distance $\langle r^2 \rangle_0$ is defined through the relation

$$\langle r^2 \rangle_0 = \int r^2 W(r) \mathrm{d}r \tag{3.3}$$

Different models of polymer chains yield different expressions for $W(r)$ and $\langle r^2 \rangle_0$. For a freely jointed chain of n bonds with bond length l, $\langle r^2 \rangle_0 = nl^2$. For the freely rotating chain model, $\langle r^2 \rangle_0 = \left(\frac{1 - \cos\theta}{1 + \cos\theta}\right) nl^2$. In general, for a chain subject to bond torsion potentials of any type, $\langle r^2 \rangle_0 = C_n nl^2$, where, C_n is the called the characteristic ratio for a chain with n bonds of length l. The limiting value for C_n for $n \to \infty$ is known for different polymer types and varies typically between 4 and 15 (Flory, 1969; Mattice and Suter, 1994).

The distribution of the end-to-end distance is central to the study of chain elasticity, as can be seen from the foregoing discussion. Here, we consider two such functions, (1) the Gaussian and (2) the inverse Langevin function. The Gaussian distribution is representative of sufficiently long chains that behave as a linear spring. The inverse Langevin function is used to represent the elastic behavior of shorter chains or chains subject to high degrees of extension where in either case stretching results in an upturn in the force–extension curves.

The expression for the Gaussian approximation is

$$W(r) = \Big(\frac{3}{2\pi\langle r^2\rangle_0}\Big)^{3/2} \exp\Big(-\frac{3r^2}{2\langle r^2\rangle_0}\Big) \tag{3.4}$$

Combining Eqs. (3.1), (3.2) and (3.4) leads to the force–extension ratio for the Gaussian chains as

$$f = \Big(\frac{3kT}{\langle r^2\rangle_0}\Big) r \tag{3.5}$$

This is the relation for a linear spring. Thus, a Gaussian chain behaves like a linear spring with spring constant $3kT/\langle r^2\rangle_0$. Specifically, for a freely jointed chain model, the spring constant is $3kT/nl^2$, which shows that shorter chains are stiffer than the long ones. In addition, since the foregoing derivations are all based on the entropy of the chain, the spring constant is proportional to the absolute temperature. For a polyethylene chain consisting of 100 bonds, $\langle r^2\rangle_0 = 15.9\ \text{nm}^2$, and the corresponding spring constant equates to 0.78 pN/nm. The equilibrium elasticity of the Gaussian chain is entropic in nature, in contrast to the elasticity observed in the single-chain experiments to be discussed below, where significant enthalpic and non-equilibrium contributions may be observed.

At high levels of stretching, the force–extension relation becomes non-linear, with an upturn due to finite chain extensibility at the higher levels of stretch and the Gaussian distribution is no longer valid. The inverse Langevin approximation is an example of one that is widely used and shows the upturn. This approximation is based on the freely jointed chain model. The probability density function $W(r)$ given in logarithmic form here (Treloar, 1975) was first derived by Kuhn and Grün (Kuhn and Grün, 1942):

$$\ln W(r) = C - n\Big(\frac{r}{nl}\beta + \ln\frac{\beta}{\sinh\beta}\Big) \tag{3.6}$$

where β is the inverse Langevin function L^{-1}

$$\beta = L^{-1}\Big(\frac{r}{nl}\Big) \tag{3.7}$$

obtained by solving the relation

$$\coth\beta - \frac{1}{\beta} = \frac{r}{nl} \equiv L(\beta)$$

for β. The form of the elastic free energy expression for a freely jointed chain of n bonds is obtained from Eqs. (3.6) and (3.1) as (Treloar, 1975)

$$A_{\mathrm{el}} = kTn\left(\frac{r}{nl}\beta + \frac{\beta}{\sinh\beta}\right) \tag{3.8}$$

Expanding β into series, (Treloar, 1975) and using Eqs. (3.5) and (3.2) leads to the non-linear force–extension relation

$$f = \left(\frac{3kT}{nl^2}r\right)\left\{1 + \frac{3}{5}\left(\frac{r}{nl}\right)^2 + \frac{99}{175}\left(\frac{r}{nl}\right)^4 + \frac{513}{875}\left(\frac{r}{nl}\right)^6 + \cdots\right\} \tag{3.9}$$

The first term of Eq. (3.9) corresponds to the Gaussian approximation for the freely jointed chain. The remaining terms give the experimentally observed upturn at higher extensions.

Experiments on single polymer chains

These types of experimental investigations typically focus on stress–strain measurements in elongation on single molecules or, in the case of some polynucleotides, on double-stranded chains. Much of the work has involved biopolymers, specifically proteins, polynucletides, or polysaccharides, but some synthetic polymers have been studied as well. This is a very active area of research, but the continuing appearance of review articles has been very helpful in providing good overviews of the subject (Chu, 1991; Granzier and Pollack, 2000; Janshoff *et al.*, 2000; Hugel and Seitz, 2001; Strick *et al.*, 2001; Zhang and Zhang, 2003; Barbara *et al.*, 2005; Hummer and Szabo, 2005; Schuler, 2005).

The main challenges in this area are developing techniques for grasping the single chains to be elongated, and developing sufficiently sensitive methods for measuring the stresses and strains involved. With regard to the required attachments, it is obviously advantageous to have this occur at the *ends* of the chains, and this is accomplished by having the chains terminate either with carefully chosen functional groups or with micrometer-sized beads. In the first case, the functional groups can be bonded onto complementary groups on a probe. In the second approach, the bead can be grasped using a micropipette or a laser beam (acting as an "optical tweezer"). Some less controlled experiments have been carried out by simply having one part of the chain physically or chemically adsorbed onto a surface with another part similarly adsorbed onto a probe. The probe in all these cases is typically the cantilever of what is essentially an atomic force microscope. The degree to which it is moved is a measure of the strain (in the range of nanometers), and its deflection a measure of the force of deformation (generally in the range of piconewtons, pN).

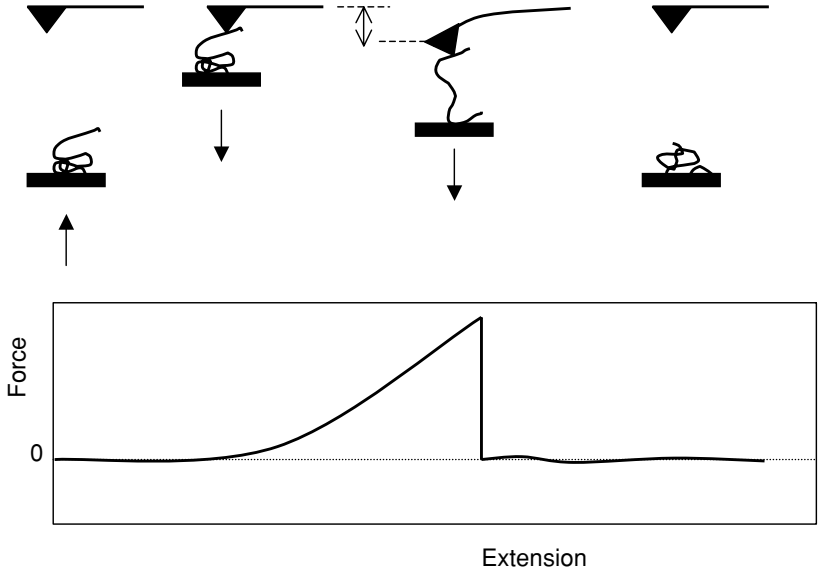

Figure 3.2 Apparatus for doing force–deformation measurements on single molecular chains, and some results obtained on the denatured form of the polysaccharide xanthan. Sketches based on results presented in detail elsewhere (Li *et al.*, 1998).

Simple rubberlike elasticity

A number of studies of this type have been used to characterize relatively simple elastomeric behavior. Typical molecules have included poly(methacrylic acid) (Ortiz and Hadziioannou, 1999), a poly(methyl methacrylate –*b*–poly(4-vinyl pyridine) block copolymer (Yamamoto *et al.*, 2000), poly(acrylamide) and poly(*N*-isopropylacrylamide) (Zhang *et al.*, 2000), denatured xanthan (Li *et al.*, 1998), glycosaminoglycan (Seog *et al.*, 2002), λ-phage DNA (Bustamante *et al.*, 1994), and spider-capture silk (Becker *et al.*, 2003). There has also been detailed theoretical work interpreting some of the more complicated results, for example on polyelectrolytes and DNA (Netz, 2001).

The denatured xanthan experiments (Li *et al.*, 1998) provide illustrative results. The denaturation converts the xanthan, which normally has helical sequences, into a random-coil polymer with conformations similar to those of commercial elastomeric materials. In this case, the simple random-coil spatial configurations make the force–deformation isotherms correspondingly simple. The upper portion of Figure 3.2 illustrates the device and procedure, typically carried out at room temperature. The xanthan sample was absorbed onto a glass substrate and the cantilever tip of an atomic force microscope (AFM) pressed into the sample to adsorb one or more chains onto it. The distance between the substrate and the tip was then gradually increased to the desired values of the strain, up to the point where the chain either ruptured or detached. The resulting force–deformation isotherm is shown

schematically in the lower portion of the figure. The slope of the curve provides an estimate of the modulus, the chain spring constant, and the maximum value of the stress–either the ultimate strength of the chain or the strength of its attachment to the substrate or AFM tip.

The more complicated force–deformation behavior shown by native (undenatured) xanthan (Li *et al.*, 1998) is discussed below, under "Conformational changes".

Orientation, relaxation, and hysteresis

Such elongation experiments can also provide additional information, for example on the retraction of the stretched chains (Chu, 1991; Perkins *et al.*, 1994b, 1995; Schroeder *et al.*, 2003). These studies are frequently carried out on chains labeled so as to be directly observable in fluorescence microscopy. Also, the experiments are carried out in a solvent such as water, as was done in the case of the experiments on single λ-DNA molecules illustrated in the Gaussian region portion of Figure 3.3 (Chu, 1991). The circles represent experimental results and the curve shows the expected behavior when the retractive force f is proportional to the end-to-end distance r remaining at that stage of the retraction. The results indicate that for moderate extensions the stretched DNA chains are still in the Gaussian region, for which the relationship $f = (3kT/\langle r^2\rangle_0)r$ given by Eq. (3.5) predicts the observed proportionality.

In other experiments on this same system, the DNA chains were in fact stretched close to the limits of their extensibility (Perkins *et al.*, 1994a). The results for this more complicated case involving the non-Gaussian as well as the Gaussian region are shown schematically in Figure 3.3. At the higher elongations, the chains are clearly in the non-Gaussian region, as evidenced by a much more pronounced initial drop off in the retractive force. This is then followed by a Gaussian decrease in f once the elongation is sufficiently small to be Gaussian (approximately two-thirds of full extension, as discussed in Chapter 13).

A related experiment on such DNA chains is described in Figure 3.4 (Perkins *et al.*, 1994b), which covers a period of approximately 3 s. The chain now has a loop in it, and it is stretched in an entangled solution. The force decreases the size of the loop, but once the stretching stops, the loop increases back to its original diameter. The force applied to the loop decreased as chain segments from the relaxing end relieved the excess force, permitting the initial loop shape to be restored.

Conformational changes

The xanthan molecule already described also provides an example of a force–deformation isotherm affected by a conformational change (Li *et al.*, 1998). When

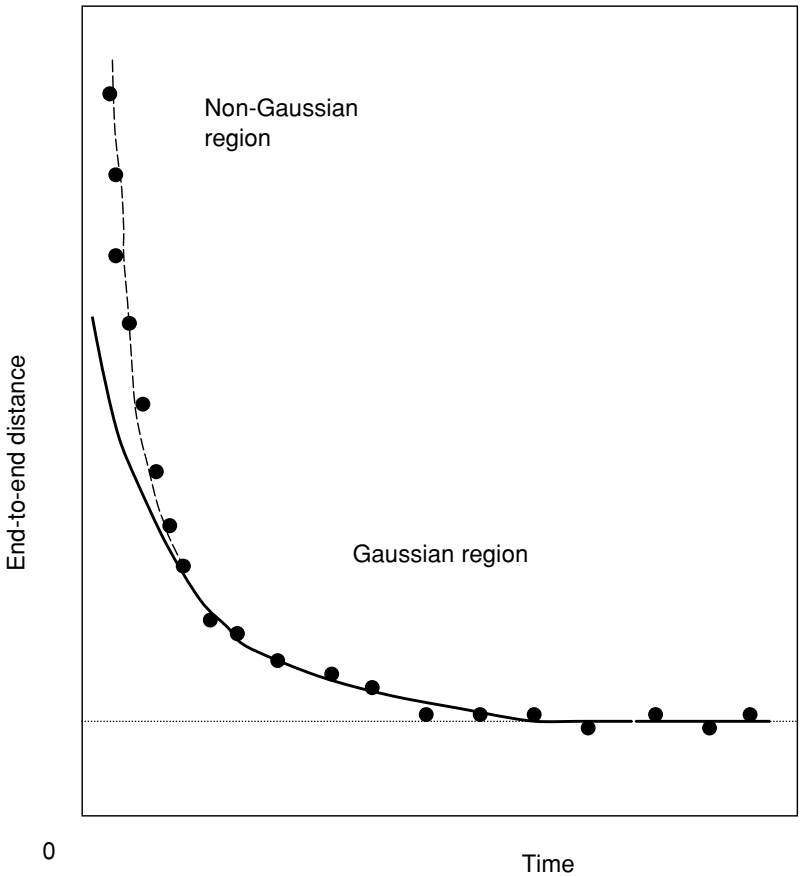

Figure 3.3 Relaxation of λ-DNA molecules when the maximum extent of stretching was either in the Gaussian region, or beyond the Gaussian region. Qualitative sketch based on results presented elsewhere (Chu, 1991; Perkins *et al.*, 1994b).

in the native state it contains helical secondary structures stabilized by non-covalent interactions. As illustrated in Figure 3.5, this apparently gives rise to a plateau when the force reaches the threshold value (400 pN) required to pull the helical sequences into extended random coils. The plateau is then followed by another monotonic increase in force up to the point where either the chain ruptures or one of its ends detaches.

The polysaccharides amylose, dextran, and pullulan provide examples that involve chair–boat transitions of the glucopyranose rings they contain (Marszalek *et al.*, 1998; Zhang *et al.*, 2005). The boat form is approximately 20% longer than the lower energy chair form, and the imposed force increases its population. The effects are illustrated in Figure 3.6. The plateau shown corresponds to these transitions occurring at approximately constant force. This interpretation is supported by

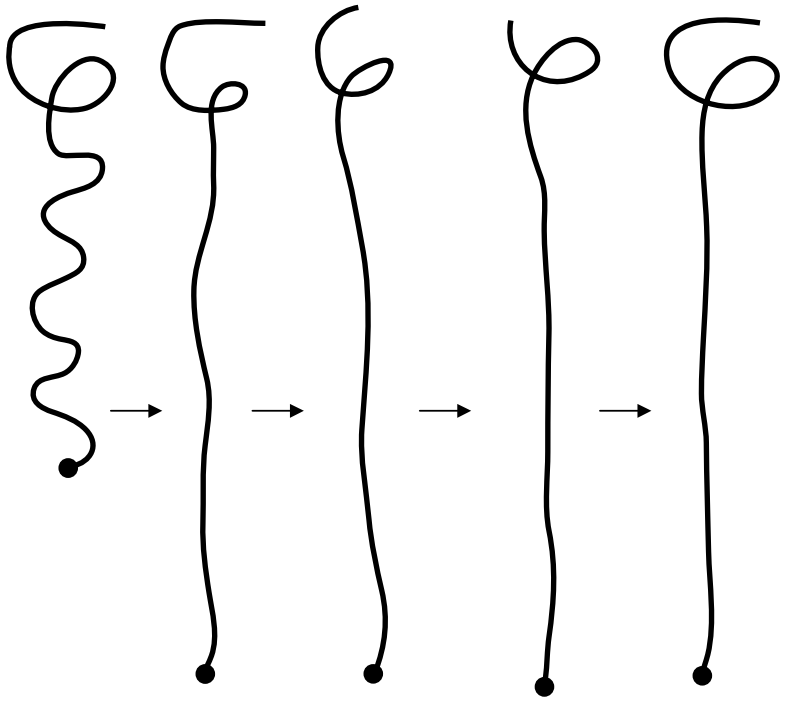

Figure 3.4 A loop in DNA, its decrease in size when the chain is stretched, and the recovery of its original size as the free chain end moved to offset the imposed force. Qualitative sketch based on results presented elsewhere (Perkins *et al.*, 1994b).

the observation that cleaving the rings by mild periodate oxidation removes such plateaus, as is also illustrated in the figure.

Other examples of conformational changes upon stretching can be found elsewhere (Rief *et al.*, 1997; Williams *et al.*, 2002; Xu *et al.*, 2002; Kumaki and Hashimoto, 2003; Kiriy *et al.*, 2003).

Unwinding double helices

An example of this type of experiment involved stretching single molecules of the B-form of double-stranded DNA in which one of the chains is "nicked" (Smith *et al.*, 1996). Some results are shown in Figure 3.7. The initial part of the force–deformation curve characterizes the elastic modulus of this form of DNA. Overstretching into the abnormal region can then cause a transition into a planar structure in which the double chains are now parallel and some of the bases in sequences around the nick become unpaired. Letting the chains retract can give rise to the irreversibility (hysteresis) shown, from the additional time required for some of the base re-pairing to occur.

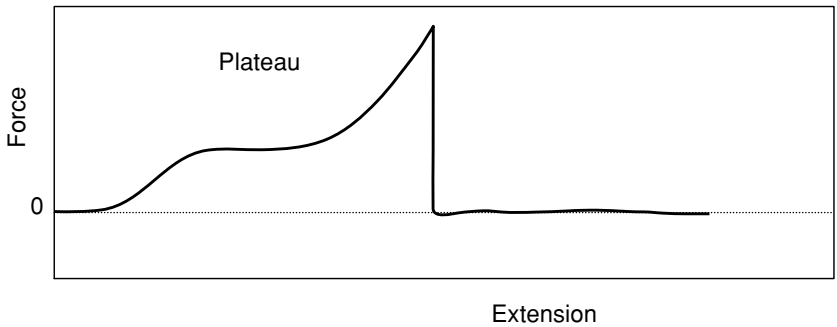

Figure 3.5 Stress–strain (force–deformation) behavior of native (un-denatured) xanthan, showing a plateau arising from a force-induced conformational change from helix to random coil. Qualitative sketch based on results presented elsewhere (Li *et al.*, 1998).

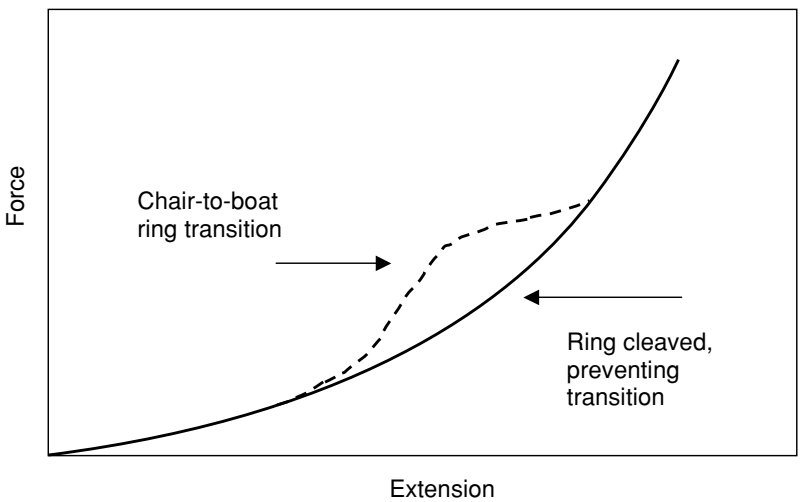

Figure 3.6 Deformation results for a polysaccharide containing glucopyranose rings which can undergo conformational transitions from the chair form to the more extended boat form. The plateau resulting from this transition disappeared when the ring structures were cleaved. Qualitative sketch based on results presented elsewhere (Marszalek *et al.*, 1998).

Unfolding domains

The unfolding of globular domains in response to an imposed force has been the focus of a number of studies (Kellermayer *et al.*, 1997; Oberhauser *et al.*, 1998; Liphardt *et al.*, 2001; Schwaiger *et al.*, 2002; Onoa *et al.*, 2003; Slaughter *et al.*, 2005). An example involving the muscle protein titin is shown in Figure 3.8

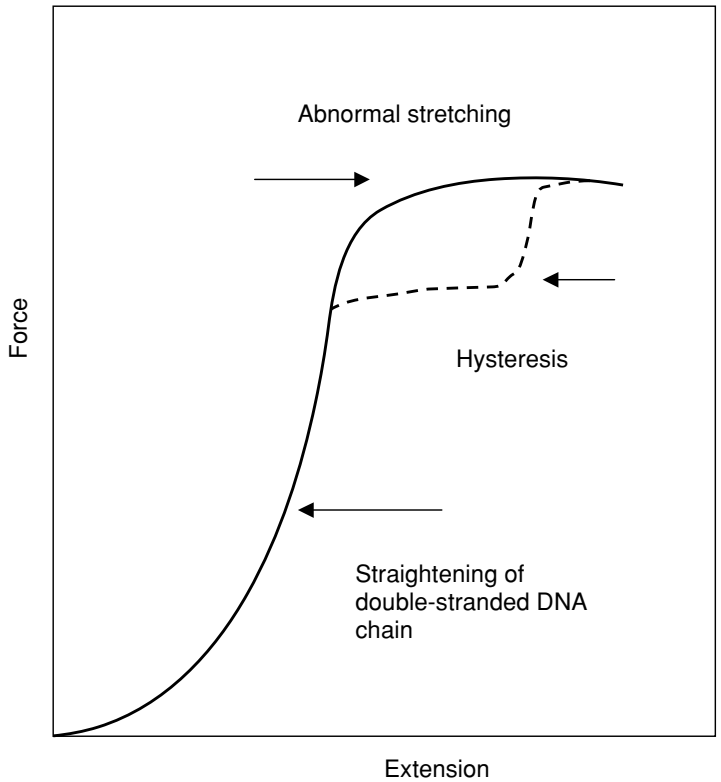

Figure 3.7 Stretching double-stranded DNA into the region where some of the base pairing may be disrupted, giving rise to hysteretic effects. Qualitative sketch based on results presented elsewhere (Smith *et al.*, 1996).

(Kellermayer *et al.*, 1997). This protein contains a linear array of compact domains of the immunoglobulin and fibronectin types. For small deformations, marked by the region a to b, the stress–strain is reversible. Beyond this point, the domains are unfolded, and this gives rise to the hysteresis shown, which corresponds to the time required for these compact domains to reform. Repeating the stretch–retraction cycle causes changes in the titin that prevent it from refolding. This is shown by curves A, B, and C of Figure 3.9 (Kellermayer *et al.*, 1997). The two parts of the cycle eventually superpose into the single curve shown by the heavy line in the figure.

A more complicated case is illustrated by the extracellular protein tenascin, which is used in vertebrates for controlling interactions between cells (Oberhauser *et al.*, 1998). The chains consist of linear arrays of compactly folded immunoglobulin domains. Applying a force to these chains causes a sequential unfolding of the domains, as is illustrated in the upper portion of Figure 3.10. This unfolding, which

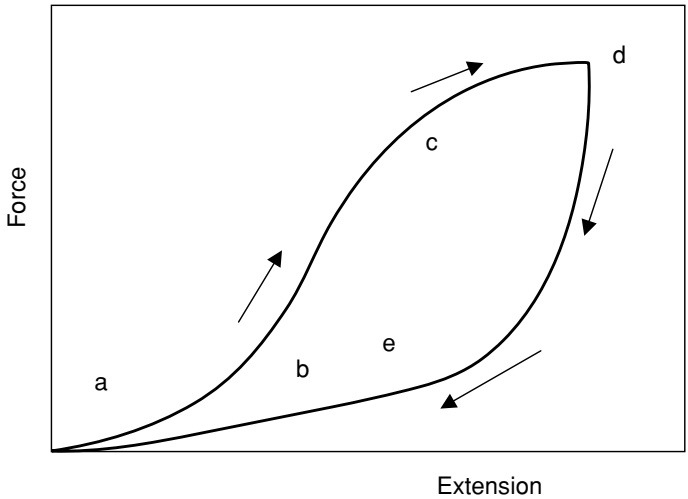

Figure 3.8 Unfolding (a to d) and refolding (d back to a) of the protein titin over one cycle. Qualitative sketch based on results presented elsewhere (Kellermayer *et al.*, 1997).

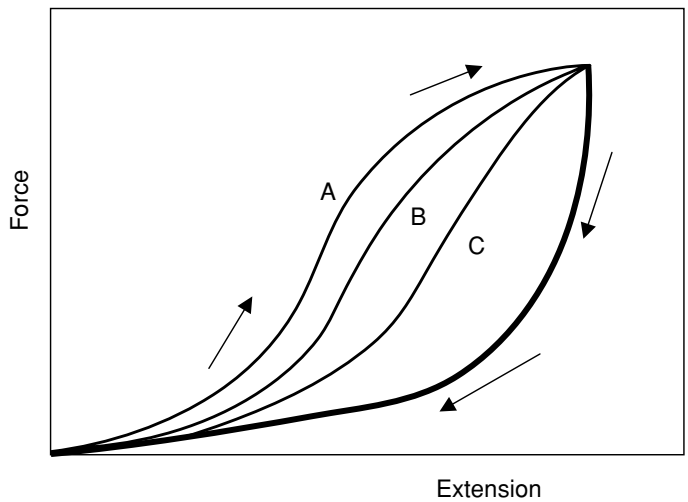

Figure 3.9 Unfolding and refolding of the protein titan over three consecutive cycles, A followed by B, followed by C. Repeated cycling brings the two parts of the cycle into coincidence. Qualitative sketch based on results presented elsewhere (Kellermayer *et al.*, 1997).

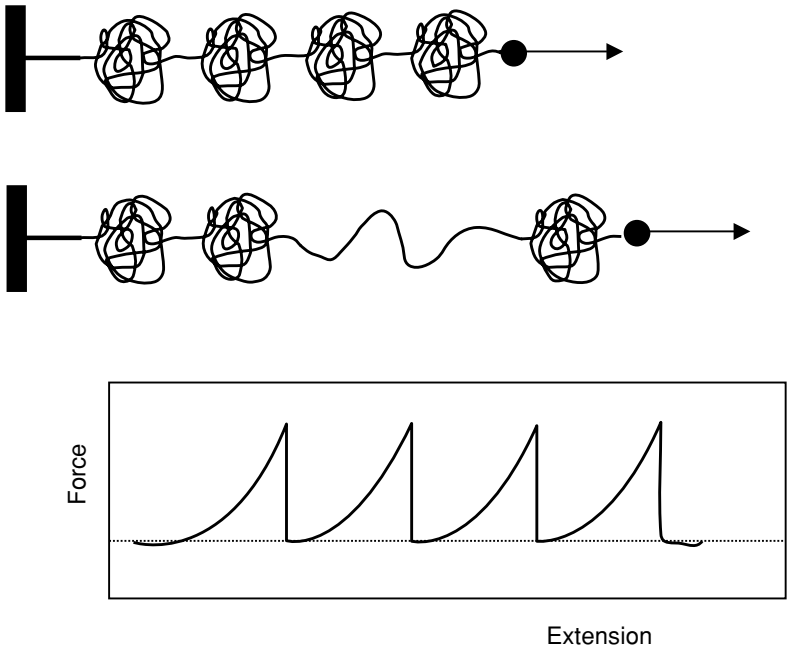

Figure 3.10 Sketch of the protein tenascin and its partial unwinding under an imposed force. The lower portion of the figure shows the saw-tooth pattern observed as each of the compact domains was unwound. Qualitative sketch based on results presented elsewhere (Oberhauser *et al.*, 1998).

occurs at stresses (forces) of approximately 140 pN, gives rise to a saw-tooth pattern with as many as 12 peaks! This is illustrated in the lower portion of the figure. The domains do refold, but in an intriguing manner, with some domains refolding rapidly and some much more slowly.

Transcription of RNA and shortening of DNA

Single-molecule studies of polynucleotides have not been limited to force–deformation measurements such as those described above (Davenport *et al.*, 2000; Bokinsky and Zhuang, 2005). One novel experiment (Davenport *et al.*, 2000) focused on the transcription of single molecules of the enzyme *E. coli* RNA polymerase (RNAP). The RNAP–DNA transcription complex was tethered between two beads, one of which was held by a micropipette and the other located in a liquid flowing away from the first bead. The distance between the two beads at different stages in the transcription was recorded as a function of time. One interesting result was the observation of a number of "pauses" in the transcription process. This suggested that transcribing RNAP molecules have more competent and less competent states, and that the switching between them is relatively slow. Such

detailed information is obviously very helpful in clarifying the mechanisms in gene regulation.

A related application involves another enzyme, lambda exonuclease, which progressively degrades strands of double-stranded DNA (Perkins *et al.*, 2003). In this case, the DNA chain was held between two beads, and contour length of the chain measured as a function of time as the degradation proceeded. There were found to be intervals of constant degradation speed (12 nucleotides/second) interspersed with pauses of variable duration. These pauses may be due to changes in interactions, for example between the enzyme and specific nucleotides in the DNA, particularly in the "frayed" regions thought to exist between the axis of the DNA and the enzyme active site.

Adhesion to surfaces

A final example concerns adsorbing a single polymer chain onto a surface, then pulling it from this surface, while measuring the forces occurring in the adsorption–desorption cycles (Seitz *et al.*, 2003). The measurements are typically done in solution, under both equilibrium and non-equilibrium conditions. Such experiments have been particularly useful in characterizing the interactions between polyelectrolytes and various substrates.

Broader relevance

Although these single-molecule experiments are of tremendous interest in their own right, they are of course incapable of shedding light on most of the major unsolved problems in the area of rubberlike elasticity, which primarily involve the interactions among the *numerous chains* making up a network structure.

4

Preparation and structure of networks

Preparation of networks

A network is obtained by linking polymeric chains together into the form of a three-dimensional structure such as that shown in Figure 1.2. The process is generally known as cross linking, curing, or vulcanization (Coran, 1987, 2005; Akiba and Hashim, 1997; Ignatz-Hoover and To, 2004). The points of linking, called cross links or junctions, may be (1) randomly located along the chains, or (2) restricted to specific locations such as the chain ends or selected repeat units, particularly in the case of bioelastomers (Gosline, 1987; Lillie and Gosline, 1990; Erman and Mark, 1997). The required linking (cross linking or end linking) can be brought about by chemical reactions that form covalent bonds between chains, either randomly or controllably at chosen locations. The linking may also be accomplished, randomly, by the physical aggregation of units from two or more chains. The simplicity of the first technique and the permanence of the structures it provides are advantages for many applications. The main advantage of the second technique is the fact that the elastomer is frequently reprocessable, since the aggregation process is often reversible.

Random chemical reactions

The most important examples of cross linking using chemical reactions that attack the chains at random locations are given in the top part of Table 4.1.

Sulfur is used primarily with elastomers having numerous unsaturated groups, for example, those in the repeat units of the polyisoprenes and polybutadienes. Sulfur adds to some of these double bonds (approximately 1%), resulting in joining two chains of the elastomer. Depending on the other curing ingredients used, this will insert either a single S atom (monosulfidic cross link) or a short chain S_x of

Table 4.1 *Methods of cross linking to form elastomeric network structures*

Type	Example	Comments
Random, chemical	Sulfur cures	Either monosulfidic or polysulfidic
	Peroxide cures	Either vinyl specific or non-specific
	High-energy radiation	Forms ions as well as free radicals
	Copolymerizations	Requires comonomer of functionality greater than two
Controlled, chemical	Terminal group reactions	Important for polysiloxanes and polyurethanes
	Side chain reactions	Important for polymers that are difficult to cross link, and for proteins
Physical aggregation	Adsorption onto filler	"Bound rubber" can cause irreversibility
	Limited crystallization	Reversible, reprocessable
	Ionomer association	Reversible, reprocessable
	Chelation	Reversible, reprocessable
	Triblock phase separation	Reversible, reprocessable. Exemplified by the Kratons

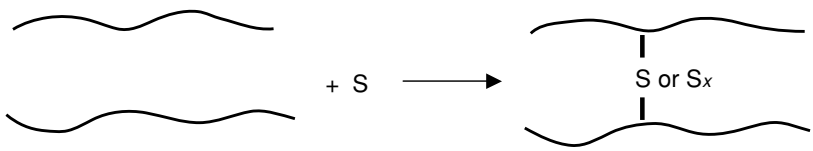

Figure 4.1 Cross linking of two chains in a sulfur cure.

$x = 6-8$ sulfur atoms (polysulfidic cross link) (Flory, 1953). This is illustrated in Figure 4.1 (Coran, 2005).

The cross linking with sulfur is called "vulcanization" and the reactions are surprisingly complex, particularly in the industrial formulations in which it is practiced. A number of additional compounds are typically added to facilitate the reactions, and to improve the properties of the final product. Examples are thiurams and dithiocarbamates added as "accelerators", and zinc oxide and fatty acids added as "activators". Different formulations can lead to very different cross-link structures, as already mentioned. The polysulfidically cross-linked elastomer has the better properties, and this may be due to the chains of sulfur atoms being elastically effective in a "bimodal" network (as described in Chapter 13). Considerable information on the reactions has been obtained in studies using model compounds (Nieuwenhuizen *et al.*, 1997; Hergenrother *et al.*, 2004). Typical small molecules reacted with sulfur in analogous reactions are 2,3-dimethyl-2-butene

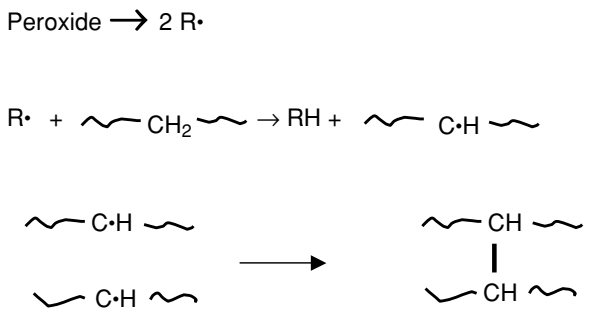

Figure 4.2 Basis steps in a peroxide cure.

$[(CH_3)_2C{=}C(CH_3)_2]$ and 2-methyl-2-pentene $[(CH_3)_2C{=}CCH_2CH_3]$. Since the products of the reactants are not locked into networks, they can be separated and analyzed using standard methods of small-molecule organic chemistry. Another approach, the "chemical probe method", uses reactions that decrease the number of sulfur atoms in a polysulfidic cross link, sometimes to the monosulfidic case (Nieuwenhuizen *et al.*, 1997). This is one way of determining the effect of cross-link length, specifically by doing mechanical property measurements before and after shortening the chains of sulfur atoms.

Peroxide cures can be used for a greater variety of elastomers. A suitably unstable peroxide is homogeneously cleaved into two free radicals R•, each of which then abstracts a hydrogen radical from the polymer chain to become the RH stable molecule. The free radical now present on the polymer migrates along the chain until it is in proximity to a similar radical on another chain. Combination of the two radicals results in a covalent bond that cross links the two chains (Flory, 1953), as shown in Figure 4.2.

The radicals formed from some peroxides are of relatively low reactivity and in order to function must find groups such as vinyl side chains that are more reactive than methylene or methyl groups. Using such "vinyl specific" peroxides with a chain having vinyl side groups, for example, provides some degree of control, since the number of side chains will limit the maximum number of cross links that can be introduced.

The third random technique involves high-energy radiation, such as electrons (e), gamma photons (γ), and ultraviolet (UV) light (Dole, 1973; Mark, 1996a). Free radicals are formed and function as described above, but also of importance is the generation of ions (hence the synonym *ionizing radiation*). The type of cross link formed is shown in Figure 4.3. High-energy irradiation is the most abusive of the cross-linking techniques and generally also causes a great deal of chain scission, resulting in dangling-chain irregularities in the network structure.

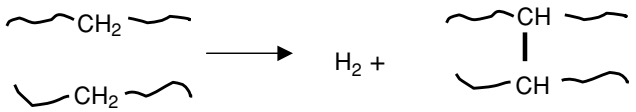

Figure 4.3 Cures using high-energy radiation.

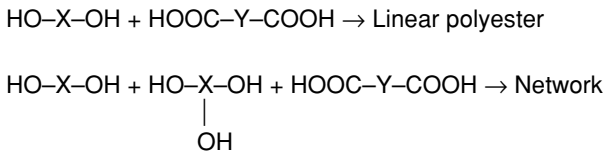

Figure 4.4 Simple condensation polymerization, and the addition of a trifunctional comonomer to give a network structure.

Networks may also be formed by the random copolymerization of monomers, at least one type of which has a functionality ϕ of 3 or greater, where ϕ is the number of sites from which chains can grow. This is illustrated in Figure 4.4. An example is the condensation of a dialcohol ($\phi = 2$) with a dibasic acid ($\phi = 2$) to give a polyester; including the trialcohol glycerol ($\phi = 3$) then yields a cross-linked polymer (Flory, 1953). An example from the area of thermoplastics is the well-known cross linking of polystyrene by including some divinyl benzene to form vinyl side groups as potential cross-linking sites.

Such reactions typically take place in solution, with the system going from a liquid to a solid, specifically to a network structure swollen with any unreacted monomers and whatever solvent was present. The process is called *gelation*, and the resulting swollen network is a *gel*. The molecular aspects of gelation in general have been extensively investigated from the theoretical point of view (Flory, 1953; Leung and Eichinger, 1984a, b; Dusek, 1986; Stepto, 1986; Miller and Macosko, 1987; Braun *et al.*, 2002). This terminology has been extended in that the term gel is now frequently applied also to polymer networks that are swollen by absorption of a diluent after they have been cross linked in the dry state. Swollen polymer networks are discussed further in Chapters 8, 11, and 17.

There are some polymers that cannot be cured by these relatively simple techniques, polyisobutylene being a good example. In order to obtain a curable polymer, isobutylene monomer is copolymerized with a diene comonomer which introduces sites of unsaturation along the chain (Zapp and Hous, 1973; Waddell and Tsou, 2004). These sites are then susceptible to the cross-linking techniques mentioned above. The same approach is used for other polymers that are difficult to cure, an example being the terpolymerization of ethylene, propylene, and diene monomers to yield a curable ethylene–propylene elastomer (Borg, 1973), or the insertion of repeat units with vinyl side chains into a poly(dimethylsiloxane) (Brook, 2000).

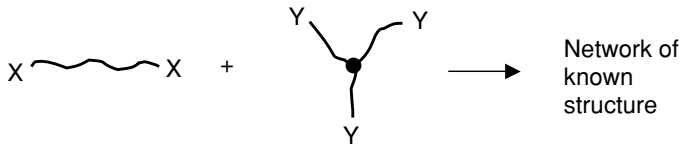

Figure 4.5 End linking of functionally terminated chains.

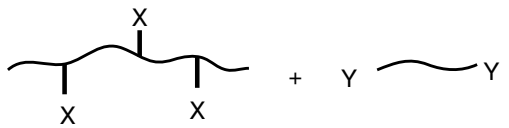

Figure 4.6 Linking chains through specific side chains.

Highly specific chemical reactions

Cross linking by highly specific chemical reactions is illustrated in the center portion of Table 4.1 (Herz *et al.*, 1978; Gottlieb *et al.*, 1981; Mark, 1982b; Leung and Eichinger, 1984a, b; Dusek, 1986; Miller and Macosko, 1987; Hild, 1998). The example of end linking functionally terminated chains is illustrated in Figure 4.5. For example, a chain having hydroxyl groups at both ends can be end linked into a network through either an addition reaction with a triisocyanate [$M(N{=}C{=}O)_3$] (Wirpsza, 1993), or through a condensation reaction with a trifunctional or tetrafunctional alkoxysilane (e.g., $Si(OC_2H_5)_4$). Some of these reactions are discussed further in Chapters 10 and 13. Since the reactive groups are only at the chain ends in this example, the end-linking reactant has to have a functionality ϕ of 3 or greater. The case where $\phi = 2$ merely gives chain extension (Mark and Sung, 1982) rather than cross linking. It is also possible to use dendrimers (with functional groups over their entire surfaces) as very high functionality cross-linking agents (Grayson and Frechet, 2001; Tomalia and Frechet, 2002).

The copolymerization approach mentioned above is an example of reacting side chains to give the desired cross links, as illustrated in Figure 4.6. Since the chains themselves have a very high functionality, the other reactant can have a functionality as low as 2 and still cure the polymer into a network structure. Another example of this approach is given in Chapter 17.

Physical aggregation of chain segments

Some examples of cross linking by the physical aggregation of chains are given in the lower portion of Table 4.1. In the case of fillers, shown in Figure 4.7, the chain segments are adsorbed onto the surface of a finely divided particulate filler of the type used to reinforce elastomers (Boonstra, 1979; Donnet and Custodero,

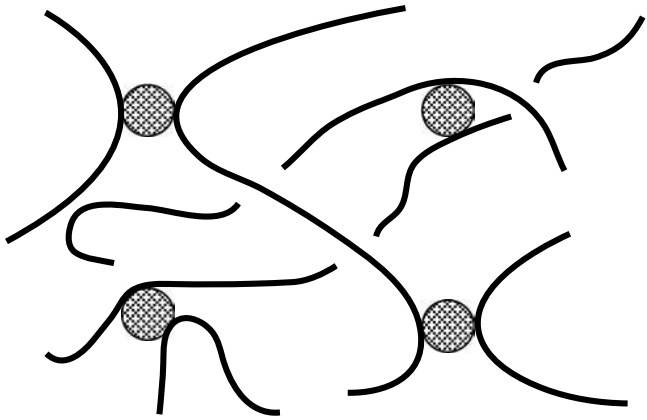

Figure 4.7 Adsorption of chain segments onto filler surfaces.

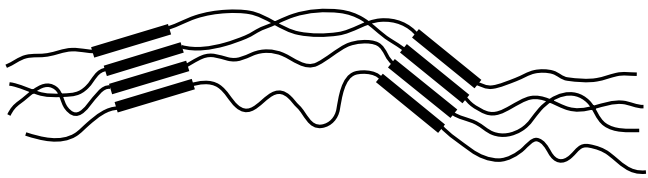

Figure 4.8 Small numbers of small crystallites acting as physical cross links.

2005). Examples would be carbon black (Wampler *et al.*, 2004) added to natural and various synthetic rubbers, and silica (Meon *et al.*, 2004) added to polysiloxane (silicone) elastomers. These and other fillers are discussed in Chapter 18. Of interest here is the fact that reactive groups on the particle surfaces can easily make the adsorption strong enough to effectively cross link the chains, frequently in an essentially irreversible manner (Warrick *et al.*, 1979). It can occur so fast that the material sets (gels) prematurely, thus interfering with its processing. In such cases, some of the reactive groups on the particle surfaces are deactivated by treatment with a low-molecular-weight additive prior to the blending of the filler into the polymer.

The second example involves polymers having a relatively small number of very small crystallites, for example, plasticized poly(vinyl chloride) (Davis, 1973). As shown in Figure 4.8, these microcrystallites can act as cross links of very high functionality. Since this type of aggregation is obviously reversible by heating above the melting point of the polymer, these elastomeric materials are reprocessable.

Ionomers are polymers containing a small number of ionic side chains (typically a few mole percent) (Eisenberg and King, 1977). These ions can be made to aggregate around a metal ion carrying one or more positive charges (M^+), as shown

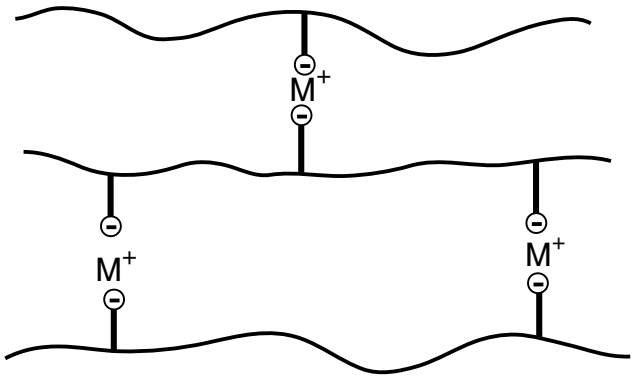

Figure 4.9 Aggregates of charges around a metal ion in an ionomer.

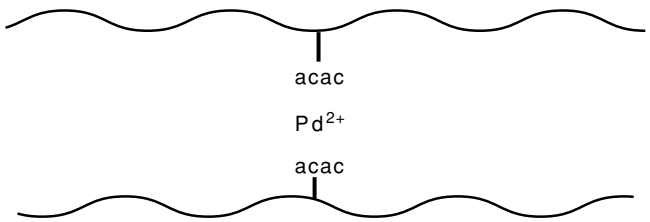

Figure 4.10 Aggregates of acetylacetonate ligands around a metal ion in a chelation polymer.

in Figure 4.9. This type of cross linking (Bagrodia *et al.*, 1987) is also reversible, by increasing the temperature or by adding a solvent. In a very similar technique, as illustrated in Figure 4.10, acetylacetonate (acac) side groups on a polymer are chelated to a metal atom such as palladium (Yeh *et al.*, 1982). Reversal of this curing step is brought about by adding other chelating substances to compete with the groups attached to the polymer chains.

The final example pertains specifically to triblock copolymers (Noshay and McGrath, 1977; Holden *et al.*, 1996; Abraham and McMahan, 2004; Grady and Cooper, 2005; Koo *et al.*, 2005), where the first and third blocks can form hard domains that are glassy or crystalline. In the upper sketch shown in Figure 4.11 (Mark and Odian, 1984), these two blocks consist of the glassy polymer polystyrene and are separated by a block of the elastomeric polymer polybutadiene. The two types of blocks do not mix because of the very low entropy of mixing chainlike molecules. Phase separation thus occurs and is held at the microscopic level by the covalent bonding going through the polystyrene–polybutadiene interfaces. As a result the styrene sequences segregate into domains (having diameters the order of 200 Å), as described in the Table 4.1 and in Figure 4.12 (Mark and Odian,

S·····S–BD·····BD–**S**·····**S**
S·····**S**–BD·····BD–S·····S
S·····S–BD·····BD–**S**·····**S**

DPS·····DPS–DMS·····DMS–**DPS**·····**DPS**
DPS·····**DPS**–DMS·····DMS–DPS·····DPS
DPS·····DPS–DMS·····DMS–**DPS**·····**DPS**

Figure 4.11 Two triblock copolymers, one of styrene–butadiene–styrene, and the other of diphenylsiloxane–dimethylsiloxane–diphenylsiloxane. Some segments coalescing into hard domains acting as physical cross links are shown in bold face.

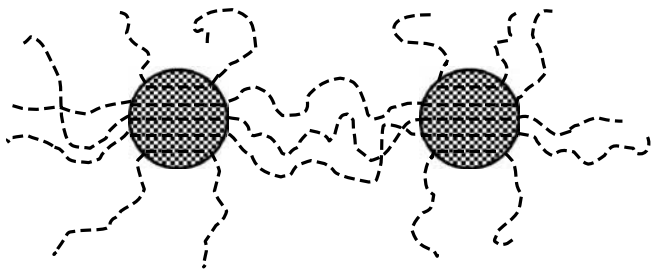

Figure 4.12 Phase separation giving hard domains (for example polystyrene) that effectively cross link a rubbery matrix (for example polybutadiene) into a thermoplastic elastomer.

1984). The domains act as cross links, but the process is obviously reversible. Reprocessable materials of this type are called thermoplastic elastomers, meaning they become "plastic" (moldable) upon increase in temperature. The most important examples are described in Table 4.2. The particular example shown in the upper portion of Figure 4.11 is the one of greatest commercial importance. This material would become reprocessble at a temperature above the glass transition temperature of polystyrene ($-100\ ^\circ$C). In some cases, the glassy blocks are chosen so as to have much higher glass transition temperatures, for example blocks of diphenylsiloxane (DPS), shown in the lower portion of Figure 4.11.

In the case where the hard domains are crystalline, this temperature would have to be above their melting point. In the case of polyethylene, the usually long sequences of crystallizable units are broken into shorter stretches by addition of a comonomer such as *n*-hexene-1 (Kaminsky, 1996). In the case of polypropylene, special catalysts that alternate between adding crystallizable isotactic and non-crystallizable atactic units are used to control the sequence lengths (Coates and Waymouth, 1995; Nele *et al.*, 2001; Myers, 1999; Rajan *et al.*, 2004). The goal is to have sequences long

Table 4.2 *Some types of thermoplastic elastomers*

Polymers	Domains	Variables
Kratons	Glassy polystyrene	Block lengths
Polysiloxanes	Crystalline PDPS	Block lengths
Polyethylene chemical copolymer	Crystalline linear PE sequences	Chemical sequence lengths
Polypropylene stereochemical copolymer	Crystalline isotactic sequences	Stereochemical sequence lengths

enough to crystallize but not have so many of them that the material crystallizes to the usual extent observed in thermoplastics.

In this regard it should also be mentioned that the increased importance of recycling elastomers has led to considerable work on *de-vulcanizing* elastomers so that they may be reused in other materials (Yun and Isayev, 2003; De *et al.*, 2005; Isayev, 2005).

Structure of networks

A network chain (a chain between two junction points) forms the basis of the elementary molecular theory of amorphous polymeric networks (Flory, 1953; Treloar, 1975). In general, network chains exhibit a distribution of molecular weights about an average, which serves as a representative reference quantity in describing network structure. As already mentioned, the number of chains meeting at each junction is called the *functionality* ϕ of that junction. A network may have two or more sets of junctions with different functionalities; it may then be characterized by an average functionality. A chain connected to a junction of the network at only one end is called a *dangling chain*, and one having both of its ends attached to the same junction is called a *loop*. A network with no dangling chains or loops and in which all junctions have a functionality greater than 2 is called a perfect network. Although a perfect network can never be obtained in reality, it forms a simple reference structure around which molecular theories are constructed. For this reason, most of the discussion in this text is based on perfect networks.

The topological structure of a perfect network may be described by various parameters: the average molecular weight between junctions, M_c; the average functionality ϕ; the number of network chains ν; the number of junctions μ; and the cycle rank ξ (which denotes the number of chains that have to be cut in order to reduce the network to a tree with no closed cycles). These five parameters are

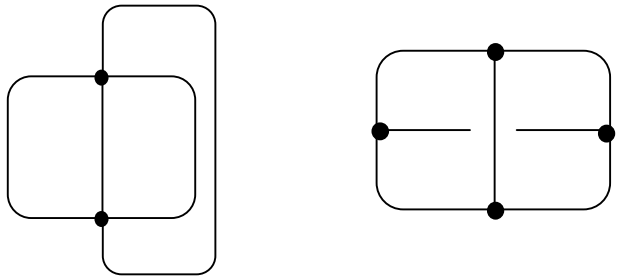

Figure 4.13 Sketches of some simple, perfect networks having (a) tetrafunctional and (b) trifunctional cross links (both of which are indicated by the heavy dots).

not independent, however, and are related by three equations. The first relation, between ν and μ, is very simple to derive (Flory, 1953; Mark, 1982a). Since in the case of a perfect network the method used to form it is irrelevant, it is easiest to consider the process as an end linking of chains. For the network to be perfect, the number of chain ends, 2ν, has to be equal to the number of functional groups, $\phi\mu$, on the end-linking molecules. Thus,

$$\mu = 2\nu/\phi \tag{4.1}$$

which states, for example, that to get ν chains in a perfect tetrafunctional network, only $\mu = \nu/2$ junctions are required. This can easily be seen pictorially from the sketches in Figure 4.13, where the networks are not only perfect but also simple in the sense of having a small enough number of chains and cross links to be easily counted. In the tetrafunctional network shown in the left portion of Figure 4.13, the four network chains require two cross links, as expected. On the other hand, the six chains in the trifunctional network shown in the right portion require four junctions, as expected since the conversion factor $2/\phi$ is now two-thirds instead of one-half. The other two equations are

$$\xi = (1 - 2/\phi)\nu \tag{4.2}$$

$$\xi / V_0 = [1 - 2/\phi)\rho]/[M_c/N_A] \tag{4.3}$$

where V_0 is the volume of network in the state of formation, ρ is the corresponding density, and N_A is Avogadro's number. Equations (4.2) and (4.3) are derived in Appendix A, along with a discussion of the modifications they require for the case of imperfect networks.

5

Elementary statistical theory for idealized networks

As was mentioned in Chapter 1, the elementary molecular theory of polymer networks rests on the postulate that the elastic free energy of a network is equal to the sum of the elastic free energies of the individual chains. The elastic free energy for the single chain was discussed in Chapter 3. Intermolecular contributions to the total elastic free energy are assumed to be insignificant and are entirely neglected in the elementary theory (Flory, 1953; Treloar, 1975). Understanding of the theory thus requires a precise description of the statistical behavior of the individual chains, given in Chapter 3, and of the relationship between their dimensions and the macroscopic strain that will be discussed in this chapter.

The chains in a network formed in the amorphous bulk state exhibit unperturbed dimensions identical to that of a single chain in Θ-solvents (Flory, 1953; Flory, 1976). This results from the fact that the distribution of the end-to-end vectors **r** for the chains in the bulk state is unchanged upon formation of network junctions, i.e., extended chains in the bulk state are equally susceptible to the interlinking or cross-linking reaction as others. The distribution of the end-to-end vector **r** of the chains in the network may therefore be identified with that of the single free chain. In rubber networks, chains that join two cross links typically have 100 to 700 bonds (Flory, 1976). For chains with 100 or more skeletal bonds, the distribution may satisfactorily be approximated by a Gaussian function given by Eq. (3.4) and reproduced here for convenience:

$$W(r) = \left(\frac{3}{2\pi \langle r^2 \rangle_0}\right)^{3/2} \exp\left(-\frac{3r^2}{2\langle r^2 \rangle_0}\right) \tag{5.1}$$

Here, $\langle r^2 \rangle_0$ denotes the mean-squared value of **r** for an unperturbed free chain. Substituting Eq. (5.1) into the thermodynamic expression $A_{el} = c(T) - kT \ln W(r)$ (see Eq. (3.1)) leads to the elastic free energy of a chain at a fixed r

$$A_{el} = A^*(T) + \left(\frac{3kT}{2\langle r^2 \rangle_0}\right) r^2 \tag{5.2}$$

where $A^*(T)$ is a function only of T. As the result of the additivity postulate, Eq. (5.2) is the free energy of both the isolated chain and the chain in the network.

The total elastic free energy ΔA_{el} of the network relative to the undeformed state is obtained by summing Eq. (5.2) over all chains of the network, ν in number:

$$\begin{aligned}\Delta A_{\mathrm{el}} &= \frac{3kT}{2\langle r^2\rangle_0}\sum_{\nu}(r^2 - \langle r^2\rangle_0) \\ &= \frac{3}{2}\nu kT\left(\frac{\langle r^2\rangle}{\langle r^2\rangle_0} - 1\right)\end{aligned} \tag{5.3}$$

The quantity $\langle r^2\rangle = \sum_{\nu}\dfrac{r^2}{\nu}$ represents the average of the mean-squared end-to-end chain vectors in the deformed network. The relationship between the mean-squared chain dimensions $\langle r^2\rangle$ in the deformed network and $\langle r^2\rangle_0$ is required for further development of the theory. A molecular model has to be adopted for such a relationship. The affine and the phantom network models are the two simplest molecular models employed in relating the deformation of the chains to macroscopic deformation.

The three principal extension ratios λ_x, λ_y, λ_z are defined in the laboratory-fixed coordinate system $0xyz$ by

$$\lambda_x = \frac{L_x}{L_{x0}} \qquad \lambda_y = \frac{L_y}{L_{y0}} \qquad \lambda_z = \frac{L_z}{L_{z0}} \tag{5.4}$$

Here L_x, L_y, L_z, and L_{x0}, L_{y0}, L_{z0} denote the deformed and undeformed macroscopic dimensions of a prismatic test sample. For simplicity we consider a homogeneous state of deformation where λ_x, λ_y, λ_z are the same at all points of the deformed sample.

In both the affine and the phantom network models, the chains are assumed to be of equal length. Thus polydispersity is not taken into account. Average chain dimensions are represented in the undeformed state by

$$\langle r^2\rangle_0 = \langle x^2\rangle_0 + \langle y^2\rangle_0 + \langle z^2\rangle_0 \tag{5.5}$$

and in the deformed state by

$$\langle r^2\rangle = \langle x^2\rangle + \langle y^2\rangle + \langle z^2\rangle \tag{5.6}$$

where the angular brackets indicate averaging over all chains of the network at a given instant. Assuming an isotropic network in the state of rest further leads to

$$\langle x^2\rangle_0 = \langle y^2\rangle_0 = \langle z^2\rangle_0 = \frac{\langle r^2\rangle_0}{3} \tag{5.7}$$

The affine network model

The original theory of the affine network model was given by several authors, notably by Kuhn, Wall, Treloar and Flory (Kuhn, 1936; Wall, 1942; Treloar, 1943a, b; Flory, 1953). The junction points in the affine network model are assumed to be embedded in the network. As a result of this assumption, components of each chain vector transform linearly with macroscopic deformation:

$$x = \lambda_x x_0 \qquad y = \lambda_y y_0 \qquad z = \lambda_z z_0 \tag{5.8}$$

$$\langle x^2 \rangle = \lambda_x^2 \langle x^2 \rangle_0 \qquad \langle y^2 \rangle = \lambda_y^2 \langle y^2 \rangle_0 \qquad \langle z^2 \rangle = \lambda_z^2 \langle z^2 \rangle_0 \tag{5.9}$$

Substituting Eq. (5.9) into Eq. (5.6) and using Eq. (5.3) leads to the elastic free energy of the affine network:

$$\Delta A_{\text{el}} = \frac{1}{2} \nu k T \left(\lambda_x^2 + \lambda_y^2 + \lambda_z^2 - 3 \right) \tag{5.10}$$

The phantom network model

According to the phantom network model (James and Guth, 1947; Flory, 1976), the junction points fluctuate over time without being hindered by the presence of the neighboring chains. The extent of the fluctuations is not affected by the macroscopic state of deformation. The term *phantom* derives from the assumed ability of the junctions to fluctuate in spite of their entanglements with network chains.

According to the theory, a small number of junctions are assumed to be fixed at the surface of the network, and the remaining ones are free to fluctuate over time. The instantaneous end-to-end vector of the ith chain may be represented as a sum of a mean $\overline{\boldsymbol{r}}_i$ and a fluctuation $\Delta \boldsymbol{r}_i$ from the mean:

$$\boldsymbol{r}_i = \overline{\boldsymbol{r}}_i + \Delta \boldsymbol{r}_i \tag{5.11}$$

The dot product of both sides of Eq. (5.11) is

$$r_i^2 = \overline{r}_i^2 + 2 \overline{\boldsymbol{r}}_i \cdot \Delta \boldsymbol{r}_i + (\Delta r_i)^2 \tag{5.12}$$

Averaging both sides of Eq. (5.12) over all chains of the network in the state of rest and in the deformed state gives

$$\begin{aligned} \langle r^2 \rangle_0 &= \langle \overline{r}^2 \rangle_0 + \langle (\Delta r)^2 \rangle_0 \\ &= \langle \overline{x}^2 \rangle_0 + \langle \overline{y}^2 \rangle_0 + \langle \overline{z}^2 \rangle_0 + \langle (\Delta x)^2 \rangle_0 + \langle (\Delta y)^2 \rangle_0 + \langle (\Delta z)^2 \rangle_0 \end{aligned} \tag{5.13}$$

$$\begin{aligned} \langle r^2 \rangle &= \langle \overline{r}^2 \rangle + \langle (\Delta r)^2 \rangle \\ &= \langle \overline{x}^2 \rangle + \langle \overline{y}^2 \rangle + \langle \overline{z}^2 \rangle + \langle (\Delta x)^2 \rangle + \langle (\Delta y)^2 \rangle + \langle (\Delta z)^2 \rangle \end{aligned} \tag{5.14}$$

The average of the term $\langle \overline{\boldsymbol{r}}_i \cdot \Delta \boldsymbol{r}_i \rangle$ in Eq. (5.12) is zero because fluctuations of chain dimensions are uncorrelated with the mean chain vectors. At a given instant, the mean positions $\overline{r}$ and fluctuations Δr of all chains exhibit distributions that may be assumed as Gaussian (Flory, 1976). The mean-squared values $\langle r^2 \rangle_0$ and $\langle (\Delta r)^2 \rangle_0$ are related to $\langle r^2 \rangle$ according to theory by

$$\langle \overline{r}^2 \rangle_0 = \left(1 - \frac{2}{\phi}\right) \langle r^2 \rangle_0 \tag{5.15}$$

$$\langle (\Delta r)^2 \rangle_0 = \frac{2}{\phi} \langle r^2 \rangle_0 \tag{5.16}$$

where ϕ is the junction functionality. Derivation of Eq. (5.16) is outlined in Appendix B. The components of mean position $\overline{r}$ of each chain transform affinely with macroscopic deformation while fluctuations Δr are not affected, which results in the following relations:

$$\langle \overline{x}^2 \rangle = \lambda_x^2 \langle \overline{x}^2 \rangle_0 \quad \langle \overline{y}^2 \rangle = \lambda_y^2 \langle \overline{y}^2 \rangle_0 \quad \langle \overline{z}^2 \rangle = \lambda_z^2 \langle \overline{z}^2 \rangle_0 \tag{5.17}$$

$$\langle (\Delta x)^2 \rangle = \langle (\Delta x)^2 \rangle_0 \qquad \langle (\Delta y)^2 \rangle = \langle (\Delta y)^2 \rangle_0 \qquad \langle (\Delta z)^2 \rangle = \langle (\Delta z)^2 \rangle_0 \tag{5.18}$$

Substituting Eqs. (5.17) and (5.18) into Eq. (5.14) and using Eqs. (5.15) and (5.16) with the condition of isotropy in the state of rest, Eq. (5.3), leads to

$$\frac{\langle r^2 \rangle}{\langle r^2 \rangle_0} = \left[\left(1 - \frac{2}{\phi}\right) \frac{\lambda_x^2 + \lambda_y^2 + \lambda_z^2}{3} + \frac{2}{\phi} \right] \tag{5.19}$$

Substituting Eq. (5.19) in Eq. (5.3) leads to the following elastic free energy expression for the phantom network:

$$\Delta A_{\text{el}} = \frac{1}{2} \nu kT \left(1 - \frac{2}{\phi}\right) (\lambda_x^2 + \lambda_y^2 + \lambda_z^2 - 3) \tag{5.20}$$

Equation (5.20) may be written in terms of the cycle rank ξ of the network (using Eqs. (A.1) and (A.2), given in Appendix A) as

$$\Delta A_{\text{el}} = \frac{1}{2} \xi kT \left(\lambda_x^2 + \lambda_y^2 + \lambda_z^2 - 3\right) \tag{5.21}$$

Comparing the two models

The differences between the elastic free energy for an affine model (Eq. 5.10) and the phantom model (Eq. 5.21) arise specifically from the nature of transformations of chain dimensions built into the two models of the elementary theory.

The expression for the elastic free energy for both models may be represented as

$$\Delta A_{\text{el}} = FkT\left(\lambda_x^2 + \lambda_y^2 + \lambda_z^2 - 3\right) \tag{5.22}$$

where the *front factor F* equates to $\nu/2$ for the affine network model and to $\xi/2$ for the phantom network model. For a perfect tetrafunctional network, the front factor for the latter model is half the value for the former. Failure to recognize the differences in the assumptions of the two models led to a long series of heated arguments in the literature (Wall and Flory, 1951; James and Guth, 1953), which was finally resolved in the classic paper by Flory (Flory, 1976). The simplified derivation of the elastic free energy for the affine network model presented in this chapter deviates from that obtained by Flory (1953) using more rigorous statistical mechanical analysis. According to Flory, the elastic free energy expression contains an additional logarithmic term that is a gaslike contribution resulting from the distribution of the cross links over the sample volume. Thus the correct expression for the elastic free energy of the affine network model is

$$\Delta A_{\text{el}} = \frac{1}{2}\nu kT(\lambda_x^2 + \lambda_y^2 + \lambda_z^2 - 3) - \nu kT \ln\left(\frac{V}{V_0}\right) \tag{5.23}$$

where V_0 and V are the initial and final volumes of the network. The presence of the logarithmic term is inconsequential for the force–deformation relations presented in Chapter 7. However, its presence is required in considering the equilibrium degree of swelling, as outlined in Chapter 8.

A more realistic theory, which subsumes the two limiting theories discussed here, is the subject of the following chapter.

6

Statistical theory for real networks

As already mentioned, the basic challenge in the molecular theory of rubber elasticity is to relate the state of deformation at the molecular level to the externally applied macroscopic deformation. The two models described in the previous chapter, the affine network and phantom network models, are the two simplest models adopted for this purpose. In the affine network model, the junctions are assumed to be embedded securely in the network structure, showing no fluctuations over time. As a consequence of being embedded in the network, the junctions translate affinely with macroscopic strain. No assumption is made with regard to the parts of a chain between its junctions. The junctions in the phantom network model, on the other hand, reflect the full mobility of the chains subject only to the effects of the connectivity of the network. The position of each junction may be defined in terms of a time-averaged mean location and an instantaneous fluctuation from it. According to this other extreme case (James and Guth, 1947), the mean locations of junctions transform affinely with macroscopic deformation, whereas the instantaneous fluctuations are not affected. The independence of the instantaneous fluctuations from the macroscopically applied state of deformation is a consequence of the phantomlike nature of the chains. During the course of their fluctuations the chains may pass freely through each other, being unaffected by the volume exclusion effects of neighboring chains and therefore by the macroscopically applied deformation.

Constrained junction model

A real network is expected to exhibit properties that fall between those of the affine and phantom network models, in that junction fluctuations do occur but not to the extent present at the phantom limit. Also, the magnitudes of the fluctuations are expected to depend on macroscopic deformation, being less in the undeformed network and significantly more when the network is stretched and more space is accessible for them to take place. This was first suggested by Ronca and Allegra

(1975). A quantitative model of a network with fluctuations of junctions dependent non-affinely on the macroscopic state of strain is given by the so-called *constrained junction* model of real networks (Flory, 1977). Detailed descriptions of its physical basis are given elsewhere (Flory, 1985a, b; Erman and Flory, 1978, 1982, 1983a, b; Flory and Erman, 1982). According to this model, the fluctuations of junctions are affected by the copious interpenetration of their pendent chains with the spatially neighboring junctions and chains. The degree of interpenetration of a chain with its environment is of critical importance. This is described schematically for a tetrafunctional network in Figure 6.1a where the four filled circles represent the junctions that are topological neighbors of a given junction (empty circle). The spatially neighboring junctions are shown by $\times$s. The average number Γ of junctions within this domain is given by (Erman and Flory, 1982)

$$\Gamma = \frac{4\pi}{3}\langle r^2\rangle_0^{3/2}\frac{\mu}{V_0} \tag{6.1}$$

where μ/V_0 represents the number of junctions per unit volume in the reference state of the network. For typical networks, Γ is in the range $25-100$. Unlike the limiting case of the phantom networks, a significant degree of rearrangement of junctions in the domain shown by the dashed circle is expected to occur upon macroscopic deformation of the network. This has the very important effect of rendering the junction fluctuations dependent on strain.

In the constrained junction network model, a given junction is assumed to be under the joint action of the phantom network and the constraint domains, as shown in Figure 6.1b. Point A locates the mean position of the junction in the phantom network. The large dashed circle of radius $\langle(\Delta R)^2\rangle_{\text{ph}}^{1/2}$ represents the root-mean-square of the fluctuation domain for the junction in the phantom network. Point B locates the mean location of constraints, which is at a distance $\overline{s}$ from the phantom center. The small dashed circle of radius $\langle(\Delta s)^2\rangle_0^{1/2}$ represents the root-mean-square size of the constraint domain in which the junction would fluctuate under the effect of constraints only. Point C locates the mean position of the junction under the combined action of the phantom network and constraints. Point D denotes the instantaneous location of the junction at a distance of ΔR, Δs, and δR from points A, B, and C, respectively. A quantitative measure of the strength of the constraints is given by the ratio

$$\kappa = \langle(\Delta R)^2\rangle_{\text{ph}} \,/\, \langle(\Delta s)^2\rangle_0 \tag{6.2}$$

If constraints are inoperative, $\langle(\Delta s)^2\rangle_0 \to \infty$ and $\kappa = 0$ from Eq. (6.2). This corresponds to the phantom limit. On the other hand, if constraints are infinitely strong so as to suppress all junction fluctuations, then $\langle(\Delta s)^2\rangle_0 = 0$ and $\kappa \to \infty$. This corresponds to the affine limit.

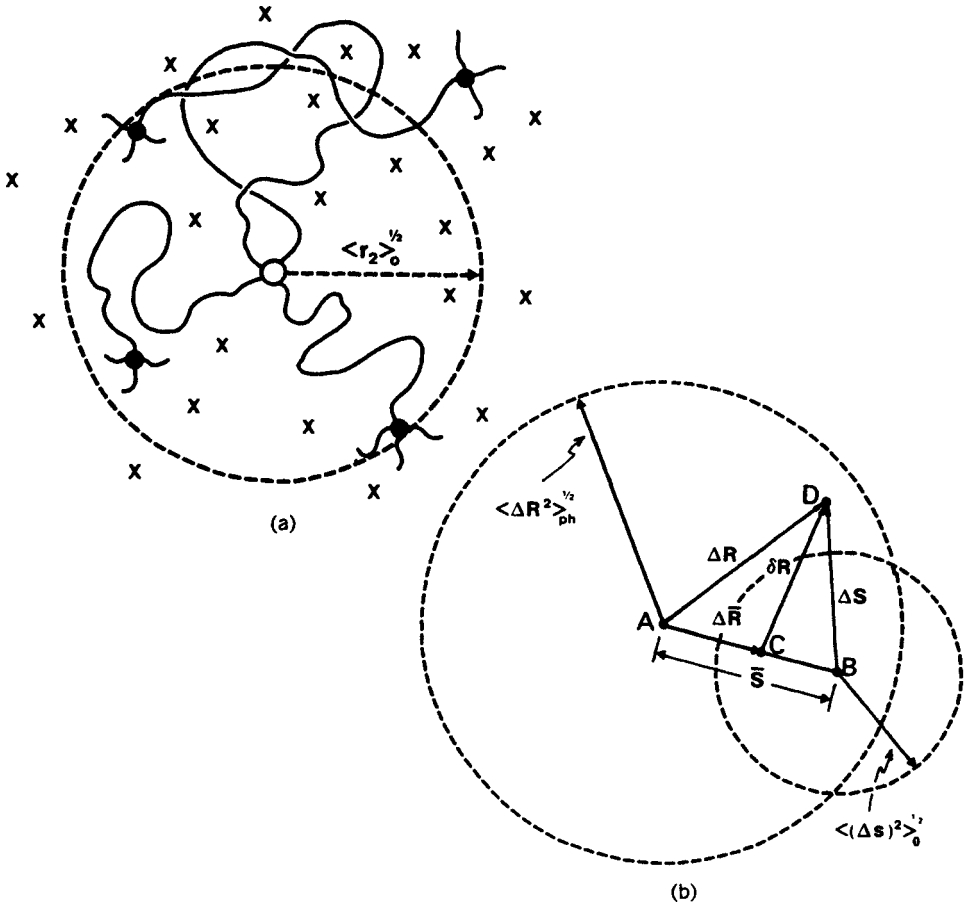

Figure 6.1 (a) Tetrafunctional junction (empty circle) surrounded by spatially neighboring junctions ($\times$s) and four topological junctions (filled circles). The dashed line indicates the radius of the average volume pervaded by a network chain. (b) Various variables defining the mean and instantaneous positions of a given junction. Point A is the mean position of the junction in the phantom network. Point B is the center of entanglements, located at a distance $\overline{S}$ from point A. Point D is the instantaneous location of the junction in the real network, located at a distance ΔR from the phantom center and ΔS from the constraint center. The large dashed circle of radius $\langle(\Delta R)^2\rangle_{\rm ph}^{1/2}$ denotes the average region in which the junction would fluctuate in the absence of constraints. The small dashed circle of radius $\langle(\Delta s)^2\rangle_0^{1/2}$ denotes the region in which the junction would fluctuate under the action of constraints only. Point C is the center about which the junction fluctuates under the combined effects of the phantom network and the constraints.

The elastic free energy of the network is obtained as the sum of the phantom network and constraint free energies, ΔA_{ph} and ΔA_c:

$$\Delta A_{el} = \Delta A_{ph} + \Delta A_c \tag{6.3}$$

where the phantom network elastic energy is given by Eq. (5.21). The elastic free energy change due to constraints is given in terms of the components of the principal extension ratios:

$$\Delta A_c = \frac{1}{2}\mu kT \sum_t [B_t + D_t - \ln(B_t + 1) - \ln(D_t + 1)] \qquad t = x, y, z \tag{6.4}$$

where

$$B_t = \kappa^2(\lambda_t^2 - 1)(\lambda_t^2 + \kappa)^{-2} \qquad D_t = \lambda_t^2 \kappa^{-1} B_t \tag{6.5}$$

The derivation of Eq. (6.4) is based on a statistical treatment whose mathematical formulation would be out of place in the present brief review. The formulation rests essentially on determination of the distribution of fluctuations δR from the mean position of the junction under the combined action of the phantom network and constraint effects in the deformed network. The reader is referred to the original paper (Flory, 1977) for the mathematical derivation of the additional elastic free energy ΔA_c due to the action of constraints on δR. For $\kappa = 0$, $\Delta A_c = 0$ and the elastic free energy of the network is equal to that of the phantom network. As κ increases indefinitely, the elastic free energy converges to that of the affine network given by Eq. (5.23). Thus the constrained junction model represents a network with elastic free energy intermediate in value between the phantom and the affine network limits. As will be described in more detail in Chapter 7, the behavior of the real network is closer to that of the affine network model at low deformations and approaches the phantom network model as the deformation increases.

The κ parameter of the constrained junction model, defined by Eq. (6.2), can be interpreted in terms of the molecular constitution of the network (Erman and Flory, 1982) by assuming it to be proportional to the average number of junctions in the domain occupied by a network chain (see Eq. 6.1). Thus

$$\begin{aligned} \kappa &= I(N_A d/2)^{3/2}(\langle r^2\rangle_0/M)^{3/2}(\xi/V_0)^{-1/2} \\ &= I(2/\phi)(N_A d)(\langle r^2\rangle_0/M)^{3/2} M_c^{1/2} \end{aligned} \tag{6.6}$$

where I is the constant of proportionality, N_A is Avogadro's number, d is the network density, and M is the molecular weight of a chain with end-to-end mean-square length $\langle r^2\rangle_0$. Equation (6.6) indicates that κ is inversely proportional to the square

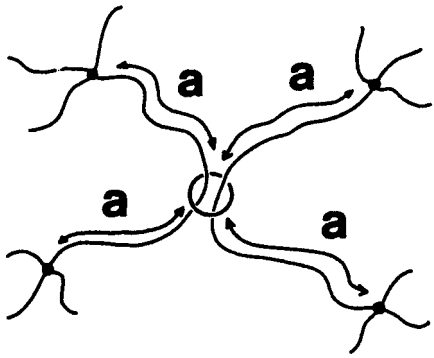

Figure 6.2 Slip link joining two chains. The slip link is assumed to slide a distance a along the chains.

root of cycle rank density ξ / V_0, inversely proportional to the functionality ϕ, and directly proportional to the square root of network chain molecular weight M_c.

Slip-link model

The theory of rubber elasticity based on the phantom, affine, and constrained junction models focuses attention on the junctions. Factors that may be affecting points along the chain contours do not appear explicitly in the formulation. An alternative model by Edwards and colleagues (Ball *et al.*, 1981), referred to as the *slip-link model*, incorporates the effects of entanglements along the chain contour into the elastic free energy. According to this model, a link joins two different chains as shown in Figure 6.2. The link may slide a distance along the contour length of the chains. The actions of the slip links are held to be equivalent to additional cross links in the network, but not of course with a one-to-one correspondence. The statistical derivation of the free energy is based on a highly sophisticated mathematical model, referred to as the replica model. The resulting equation is

$$\Delta A_{el} = \frac{1}{2} N_c kT \left\{ \sum_{i=1}^{3} \lambda_i^2 + \frac{N_s}{N_c} \sum_{i=1}^{3} \left[\frac{(1+\eta)\lambda_i^2}{1+\eta\lambda_i^2} + \log\left(1+\eta\lambda_i^2\right) \right] \right\} \tag{6.7}$$

where N_c and N_s are the number of chemical cross links and slip links, respectively, and $\eta = 0.2343\ldots$ The first term on the right-hand side of Eq. (6.7) is the elastic energy of the phantom network. The second term denotes contributions to ΔA_{el} from slip links and corresponds to ΔA_c of Eq. (6.3). There is no restriction on the number of slip links N_s. Thus, the ratio N_s/N_c may be quite large, and the elastic free energy of the network with slip links may exceed that of the affine network.

This differs significantly from the predictions of the constrained junction model, according to which the upper limit of ΔA_{el} is that for an affine network.

Other models

There are still other molecular approaches to a general theory of real networks, some of which we list below.

1. Diffused-constraint model. In this model, the confining harmonic potential affects not only the fluctuations of junctions but fluctuations of points along the network chain (Kloczkowski *et al.*, 1995a, b; Erman and Monnerie, 1989, 1992)
2. Edwards' tube model. In this model, the topological constraints act along the whole chain and restrict the fluctuations of all monomers of the chain, restricting their fluctuations to a *confining tube* which is independent of deformation (Edwards, 1967; Gaylord, 1982, 1983; Edwards and Vilgis, 1988)
3. Non-affine tube model. According to this model, the confining tube is rendered deformation dependent (Heinrich, 1983, 1984, 1987a, b; Rubinstein and Panyukov, 2002)
4. Van der Waals model (Kilian *et al.*, 1986; Vilgis and Boue, 1986)

Various aspects of the other molecular approaches are discussed in some detail in more recent work (Everaers, 1998, 1999; Vilgis *et al.*, 1989).

7

Elastic equations of state and force–deformation relations

Introduction

An equation of state is an equation interrelating the various properties required to characterize a system. The elastic equation of state for a rubber network thus specifies the relationship between the applied forces, the resulting deformations, and the molecular structure of the network. It is obtained according to the thermodynamic expression

$$\tau_t = V^{-1}\lambda_t(\partial \Delta A_{\mathrm{el}}/\partial\lambda_t)_{T,V} \qquad t = 1, 2, 3 \tag{7.1}$$

where τ_t is the "true" stress along the tth coordinate direction, and is defined as the force per unit deformed area (Flory, 1961). ΔA_{el} is the elastic free energy. The quantity λ_t is the ratio of the final length to the reference length along that direction. The subscripts *T, V* indicate that the differentiation is performed at fixed temperature and volume. The index t may take values 1, 2, 3, as indicated in Eq. (7.1), or x, y, z, as given in Chapter 5.

Equation (7.1) may conveniently be interpreted by considering a prismatic block of a network with sides L_{01}, L_{02}, and L_{03}, and volume V_0 in the reference state (Figure 7.1a*)* that represents the state of formation of the network. In the case of network formation in solution, V_0 represents the total volume of polymer and solvent. Figure 7.1b shows the dimensions L_{11}, L_{12}, and L_{13} of the network at the start of the experiment, where the volume V may be different from V_0 depending on the amount of solvent present relative to that during formation. Figure 7.1c depicts the deformed state under forces f_1, f_2, and f_3 applied along the three coordinate directions. The equality of the volumes before and after the application of the stresses, as indicated in Figures 7.1b and 7.1c, is the result of assuming incompressibility. As mentioned in Chapter 1, experimental data in simple tension show that the volume change in ordinary networks is negligibly small in comparison to changes in linear dimensions.

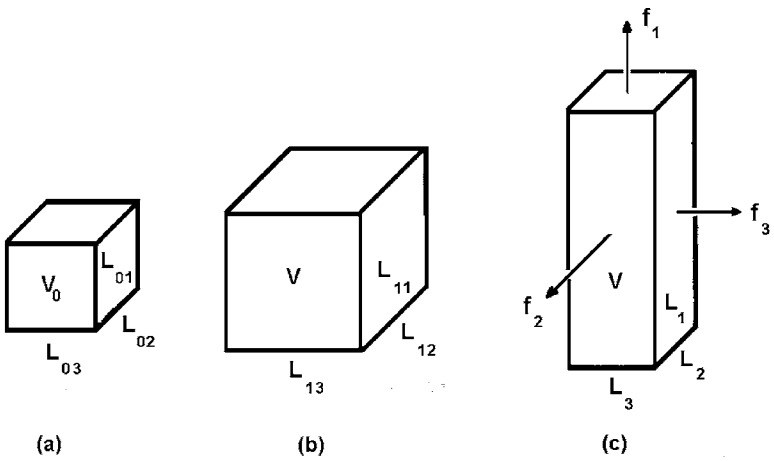

Figure 7.1 (a) A prismatic block at the reference volume V_0. The reference state is the state at which the network was formed. (b) The same block at the initial state before the application of the deformation. The volume V may be different from V_0 due to a difference in amount of solvent present or in temperature. (c) The final dimensions of the block after the stresses are applied. Equivalence of volumes at the initial and final states indicates that the volume of the network remains constant and that no solvent enters or leaves during deformation.

The deformation ratio λ_t along the direction t is defined as

$$\lambda_t = L_t/L_{0t} \qquad t = 1, 2, 3 \tag{7.2}$$

Thus, three deformation ratios are related to the final volume and reference volume by

$$\lambda_1\lambda_2\lambda_3 = V/V_0 \tag{7.3}$$

Inasmuch as V_0 and V are fixed quantities in a given experiment, Eq. (7.3) states that only two of the three λ_t terms are independent. The deformation ratio α_t relative to the initial undistorted but swollen dimensions is defined by

$$\alpha_t = \frac{L_t}{L_{it}} = \frac{L_t}{L_0}\frac{L_0}{L_{it}} = (V/V_0)^{-1/3}\lambda_t \qquad t = 1, 2, 3 \tag{7.4}$$

The fourth term of Eq. (7.4) follows from the assumption that the network is isotropic in the undistorted state.

Knowledge of the volume fraction of polymer present during network formation and during the stress–strain experiment is essential for any interpretation by the molecular theory in terms of equations of state. The two volume fractions defined

for this purpose are

$$v_{2c} = V_d / V_0 \tag{7.5}$$

$$v_2 = V_d / V_i \tag{7.6}$$

where, V_d is the volume of the dry network, and V_i is the volume of the network plus solvent at the start of the stress–strain experiment. Thus the conversion factor $(V/V_0)^{-1/3}$ in Eq. (7.4) can be alternatively written as $(v_{2c}/v_2)^{1/3}$.

The deformation ratios λ_1, λ_2, and λ_3 are not independent of one another due to the requirement indicated by Eq. (7.3). It is therefore necessary to write Eq. (7.1) in the form

$$\tau_t = V^{-1}\lambda_t \sum_{i=1}^{3} \left(\partial \Delta A_{el}/\partial \lambda_i^2\right) \partial \lambda_i^2/\partial \lambda_t \tag{7.7}$$

For the phantom or the affine network model, using the relation $\Delta A_{el} = (FkT)(\lambda_1^2 + \lambda_2^2 + \lambda_3^2 - 3)$ from Eq. (5.22), Eq. (7.7) becomes

$$\tau_t = \left(\frac{FkT}{V}\right)\lambda_t \sum_{i=1}^{3} \partial \lambda_i^2/\partial \lambda_t \tag{7.8}$$

An alternative derivation of the stresses is possible by the use of the so-called Treloar relations involving differences in stresses (Treloar, 1975).

Specification of the λ_t in Eq. (7.8) for any type of deformation then gives the desired corresponding equation of state. Setting $F = \nu/2$ yields the affine limit and $F = \xi/2$ the phantom limit. For a perfect network, $\xi = \nu(1 - 2/\phi)$. Derivations of the equations of state for the constrained junction model are presented in Appendix C.

Uniaxial extension (or compression)

The state of deformation for simple extension or compression along the 1-direction is

$$\lambda_1 = \alpha(V/V_0)^{1/3} \tag{7.9a}$$

$$\lambda_2 = \lambda_3 = \alpha^{-1/2}(V/V_0)^{1/3} \tag{7.9b}$$

where α is the ratio of the final length along the direction of stretch to the initial undistorted length at volume V. For compression, $\alpha < 1$. Writing Eq. (7.8) as

$$\tau_1 = \left(\frac{FkT}{V}\right)\lambda_1 \sum_{i=1}^{3} \frac{\partial \lambda_i^2}{\partial \alpha}\frac{\partial \alpha}{\partial \lambda_1} \tag{7.10}$$

and using Eqs. (7.9) leads to the expression for the true stress along the x-direction

$$\tau_1 = 2\left(\frac{FkT}{V}\right)\left(\frac{V}{V_0}\right)^{2/3}(\alpha^2 - \alpha^{-1}) \tag{7.11}$$

The force f acting along the x-axis is obtained by multiplying both sides of Eq. (7.11) by the deformed area, $A = V/\alpha L_{i1}$ (L_{i1} denoting the length of the undistorted swollen sample):

$$f = 2\left(\frac{FkT}{L_{i1}}\right)\left(\frac{V}{V_0}\right)^{2/3}(\alpha - \alpha^{-2}) \tag{7.12}$$

Experimental data are generally represented in terms of the *reduced stress* $[f^*]$ defined as

$$[f^*] \equiv \frac{f v_2^{1/3}}{A_d(\alpha - \alpha^{-2})} \tag{7.13}$$

where A_d is the cross-sectional area of the undeformed, dry sample. Using Eq. (7.12) in Eq. (7.13) leads to

$$[f^*] = 2\left(\frac{FkT}{V_d}\right)v_{2c}^{2/3} \tag{7.14}$$

The applied force f in uniaxial extension has two effects on the network at the molecular level. Part of the force is used in changing the configurations of the network chains to a less disordered state. This component changes the entropy of the network only, and is referred to as the entropic component. The remaining part of the force is used in changing the energy but not the entropy of each chain, simply by forcing the chains to assume configurations of different energy. This component, denoted by f_e is referred to as the energetic contribution to the total force (Flory *et al.*, 1960). From thermodynamics (see Appendix D) we have

$$\frac{f_e}{f} = -T\left[\frac{\partial \ln(f/T)}{\partial T}\right]_{L,V} \tag{7.15}$$

where the subscripts L, V denote that differentiation is performed at constant length and volume. Equation (7.15) gives rise to a very simple general relationship between f_e/f and the chain dimensions that is most easily derived in the case of a phantom network. Dividing the right-hand side of Eq. (7.12) by T, taking the logarithm, and differentiating with respect to T at constant L and V (and therefore at constant α) leads to the simple result

$$\frac{f_e}{f} = \frac{T\,\mathrm{d}\ln\langle r^2\rangle_0}{\mathrm{d}T} \tag{7.16}$$

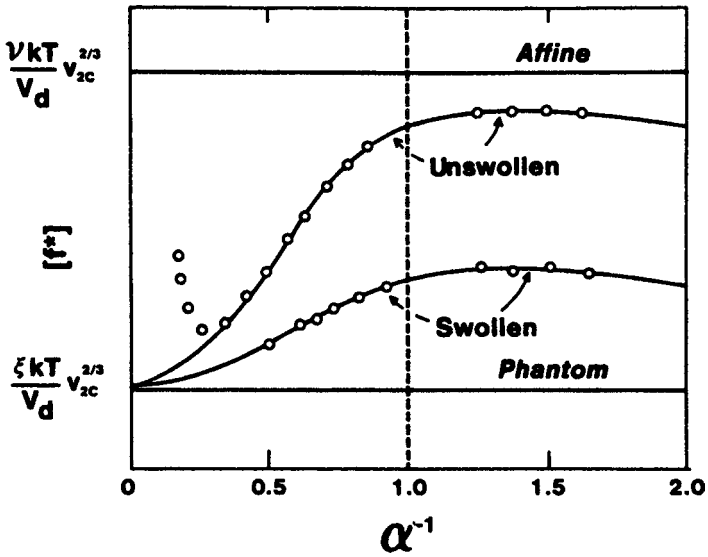

Figure 7.2 Reduced stress as a function of reciprocal extension ratio. The upper and lower horizontal lines represent results from affine and phantom network models, respectively. Circles show representative data from experiments, and the curves are from the constrained junction theory.

where the relation $\dfrac{\mathrm{d}\ln\langle r^2\rangle_0}{\mathrm{d}T} = \dfrac{2}{3}\dfrac{\mathrm{d}\ln V_0}{\mathrm{d}T}$ is used. The term $\dfrac{\mathrm{d}\ln\langle r^2\rangle_0}{\mathrm{d}T}$ is a molecular parameter referred to as the temperature coefficient of the unperturbed mean-squared end-to-end distance (Flory, 1969). Experiments are commonly carried out at constant pressure rather than at constant volume. In this case, further correction terms are added to Eq. (7.16). Detailed discussion of such terms and experimental analysis are given in Chapter 9.

The reduced stress $[f^*]$ given by Eq. (7.14) is independent of deformation in both the phantom and the affine network models. The reduced stress may be interpreted as the shear modulus of a phantom or an affine network. Experiments show, however, that it depends rather strongly on deformation (Treloar, 1975; Mark, 1975). This dependence of $[f^*]$ on α is well predicted by the constrained junction model. The expression for the reduced stress at small deformations has been given recently and compared with those of the phantom and affine models (Erman and Mark, 2005). In Figure 7.2 the reduced force is shown as a function of reciprocal α by the two horizontal lines for the affine and the phantom network models. The advantage of this type of representation is that the data in elongation can be well represented by a straight line over a wide range in α^{-1}. Thus, elongation data have very frequently

been fitted to the relationship (Mooney, 1948, Rivlin, 1948a, b, c, d)

$$[f^*] = 2C_1 + 2C_2\alpha^{-1} \tag{7.17}$$

where $2C_1$ and $2C_2$ are constants independent of α (Treloar, 1975; Mark, 1975). Thus $2C_1$ has been taken as an estimate of the high-deformation modulus (the phantom network model limit). Similarly, $2C_1 + 2C_2$ has been used as an estimate of the low-deformation modulus (the affine network model limit). Correspondingly, $2C_2$ and its normalized value $2C_2/2C_1$ can represent a measure of the extent to which the deformation becomes non-affine as α increases. In Figure 7.2, the circles represent typical results of experiments (Erman and Flory, 1978; Pak and Flory, 1979; Mark, 1979b, c). The upper set of points denotes results on networks deformed in the unswollen state. Data points are approximately independent of deformation in the compression region ($\alpha^{-1} > 1$), whereas a steady decrease is observed in tension ($\alpha^{-1} < 1$), accompanied by a sharp increase at low values of α^{-1}. Thus, real networks exhibit reduced forces ranging in values from those close to the affine network model limit in compression and at low extensions, to those closer to the phantom network model limit at higher extensions. The upturn at high extensions results from either strain-induced crystallization or finite chain extensibility, as discussed in further detail in Chapter 12.

The lower set of circles shows typical results of experiments on networks deformed in the swollen state. Experiments indicate that the variation of $[f^*]$ with α^{-1} becomes weaker, in general, with increasing degree of swelling. Also, if the upturn in $[f^*]$ were due to strain-induced crystallization, it would be diminished or entirely suppressed by the melting-point depression caused by the solvent (Flory, 1953; Mark, 1979b, c). At high degrees of swelling ($v_2 < 0.2$) the data points coincide practically with the phantom network model limit over the entire range of α^{-1}. Similarly, dependence of $[f^*]$ on α weakens in networks prepared in solution and studied dried, as is described in Chapters 8 and 11. The curves through the representative data points in Figure 7.2 indicate predictions of the constrained junction theory (Erman and Flory, 1982), for which the expression for $[f^*]$ is given in Appendix C. The theory has been successful in predicting data in tension and compression at different degrees of swelling. According to the molecular model on which the constrained junction theory is based, the constraints are more pronounced at low deformations. This renders the transformations of junction positions strongly dependent on macroscopic deformation. The behavior is therefore closer to that of the affine network at low deformations. At high extensions or swelling, the effects of constraints diminish and the network approaches the phantom network model.

Biaxial extension

The state of deformation for biaxial extension, where the dimensions of the network are changed independently along axes l and 2, is given by

$$\begin{aligned}\lambda_1 &= \alpha_1 (V/V_0)^{1/3} \\ \lambda_2 &= \alpha_2 (V/V_0)^{1/3} \\ \lambda_3 &= (\alpha_1 \alpha_2)^{-1} (V/V_0)^{1/3}\end{aligned} \tag{7.18}$$

where α_1 and α_2 denote the ratios of final to undistorted initial lengths along directions l and 2, respectively. Substitution of Eqs. (7.18) into Eq. (7.8) leads to

$$\begin{aligned}\tau_1 &= 2\left(\frac{FkT}{V}\right)\left(\frac{V}{V_0}\right)^{2/3}\left(\alpha_1^2 - \frac{1}{\alpha_1^2\alpha_2^2}\right) \\ \tau_2 &= 2\left(\frac{FkT}{V}\right)\left(\frac{V}{V_0}\right)^{2/3}\left(\alpha_2^2 - \frac{1}{\alpha_1^2\alpha_2^2}\right)\end{aligned} \tag{7.19}$$

For equi-biaxial extension, such as obtained in the inflation of a spherical balloon, $\alpha_1 = \alpha_2 = \alpha$. Therefore, from Eq. (7.19),

$$\tau = 2\left(\frac{FkT}{V}\right)\left(\frac{V}{V_0}\right)^{2/3}(\alpha^2 - \alpha^{-4}) \tag{7.20}$$

A state of biaxial extension is obtained by stretching a thin sheet of elastomer in two directions in its own plane. The state of deformation is represented by Eqs. (7.19), where directions 1 and 2 are in the plane of the sheet and direction 3 is perpendicular to it: The extension ratios α_1 and α_2 may be varied independently. Although experimental analysis of the network in biaxial extension is more complicated than in simple uniaxial extension, results verify the validity of the statistical theory, as is shown in Figure 7.3. The circles in the figure show results of measurements by Kawai *et al.* (Obata *et al.*, 1970), on unswollen rubber sheets by keeping the α_1 values constant and modifying the α_2 values. The ordinate values represent the stress difference $\tau_1 - \tau_2$. The dashed curves are calculated from the elementary molecular theory using Eqs. (7.19), and the solid curves are obtained from the constrained junction theory (Erman, 1981). The improvement provided by the latter theory at lower extensions is readily seen.

Pure shear

The state of pure shear is essentially a biaxial loading under the stresses τ_1 and τ_2 such that there is no change in length along the 2-direction. Thus, the state of

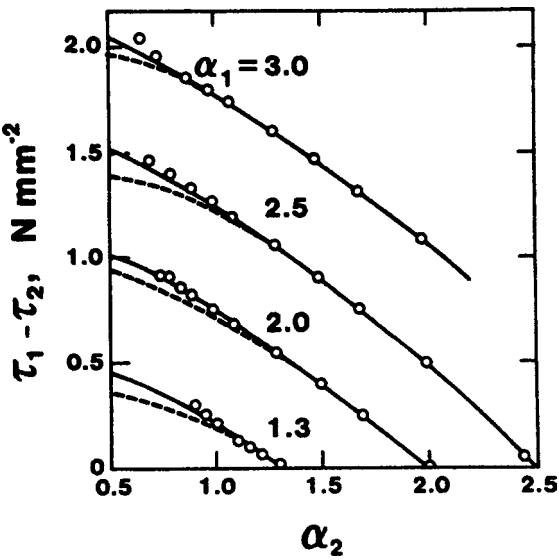

Figure 7.3 Difference of true stresses, $\tau_1 - \tau_2$, in biaxial extension shown as a function of extension ratio α_2. Circles represent data from Obata *et al.* (1970). Dashed and solid curves were calculated according to the elementary molecular and constrained junction theories, respectively.

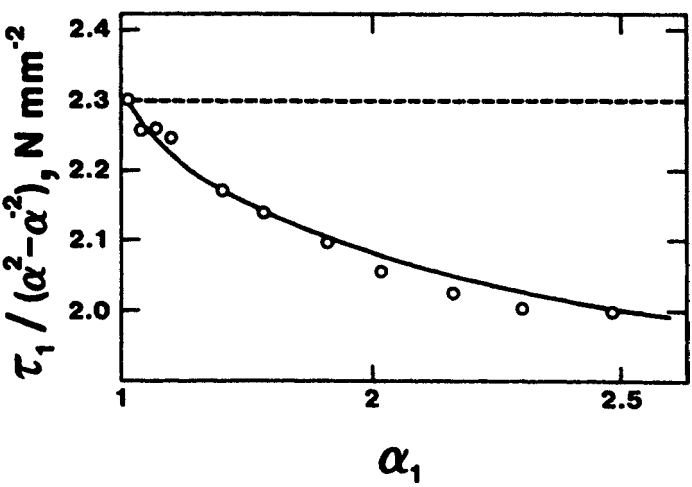

Figure 7.4 Comparison of experiment and theory for pure shear. The sample is fixed in the x_2 direction, and τ_1 and α_1 represent the stress and extension ratio along the x_1 direction, respectively. The circles represent data from Rivlin and Saunders (1951). The horizontal dashed line is obtained from the elementary molecular theory, and the solid curve, which falls very close to the experimental points, is from the constrained junction model.

deformation is described by Eq. (7.19) with $\alpha_2 = 1$. Letting $\alpha_1 = \alpha$, $\alpha_2 = 1$ in Eq. (7.19), the stresses obtained are

$$\begin{aligned} \tau_1 &= 2\left(\frac{FkT}{V}\right)\left(\frac{V}{V_0}\right)^{2/3}\left(\alpha^2 - \frac{1}{\alpha^2}\right) \\ \tau_2 &= 2\left(\frac{FkT}{V}\right)\left(\frac{V}{V_0}\right)^{2/3}\left(1 - \frac{1}{\alpha^2}\right) \end{aligned} \tag{7.21}$$

Results of pure shear experiments are presented in Figure 7.4. The sample is fixed in the x_2-direction, and τ_1 and α_1 represent the stress and extension ratio along the x_1-direction, respectively. The circles represent data from Rivlin and Saunders (1951). The horizontal dashed line is obtained from the elementary molecular theory, and the solid curve, which falls very close to the experimental points, is from the constrained junction model (Erman, 1981). Experimental data show significant deviations from the predictions of Eq. (7.21) obtained according to either the phantom network or the affine network models. The data, however, are in satisfactory agreement with predictions of the constrained junction theory, as derived in Appendix C.

8

Swelling of networks and volume phase transitions

All synthetic and biological networks swell when exposed to low molecular weight solvents. The degree of swelling at equilibrium depends on factors such as temperature, length of the network chains, size of the solvent molecules, and the strength of thermodynamic interaction between the polymer chains and solvent molecules.

As in the previous applications, the thermodynamics of the system may be described by the change in the Gibbs free energy ΔG of the system, which is related to the change in the Helmholtz free energy ΔA by $\Delta G = \Delta A + \Delta(pV)$. At constant pressure, the pressure–volume product does not change significantly in swelling, and ΔG can be replaced by ΔA. The total change results from the change in the elastic free energy ΔA_{el} of the network upon isotropic dilation with the introduction of the solvent and from the change in the free energy of mixing ΔA_{mix} of the solvent molecules with the chains constituting the network. It is assumed (Flory, 1953; Treloar, 1975; Erman and Flory, 1985; Erman and Mark, 2005) that the change in the total free energy is the direct sum of the two terms, i.e.,

$$\Delta A = \Delta A_{\text{el}} + \Delta A_{\text{mix}} \tag{8.1}$$

Expressions for ΔA_{el} for an affine network and a phantom network are given by Eqs. (5.10) and (5.21), respectively. The deformation ratios λ_1, λ_2, and λ_3 in these equations must now correspond to the state of isotropic dilation, that is,

$$\lambda_1 = \lambda_2 = \lambda_3 = \left(\frac{V_{\text{m}}}{V_0}\right)^{1/3} \equiv \left(\frac{v_{2\text{c}}}{v_{2\text{m}}}\right)^{1/3} \tag{8.2}$$

where V_{m} is the volume of solvent plus polymer, and $v_{2\text{m}}$ is the volume fraction of polymer at equilibrium (maximum) degree of swelling when exposed to excess solvent. Substituting Eq. (8.2) into Eqs. (5.10) and (5.21), respectively, leads to

$$\Delta A_{\text{el}} = \frac{3\nu kT}{2}\left[\left(\frac{v_{2\text{c}}}{v_{2\text{m}}}\right)^{2/3} - 1\right] - \mu kT \ln\frac{v_{2\text{c}}}{v_{2\text{m}}} \qquad \text{(affine)} \tag{8.3}$$

$$\Delta A_{\text{el}} = \frac{3\xi kT}{2}\left[\left(\frac{v_{2\text{c}}}{v_{2\text{m}}}\right)^{2/3} - 1\right] \qquad \text{(phantom)} \tag{8.4}$$

The logarithmic term in Eq. (8.3) does not appear in Eq. (5.10) which was derived simply for an affine network in the dry state. However, this term is required for swollen networks (Flory, 1953). The second term of Eq. (8.1), ΔA_{mix}, for mixing polymer chains with solvent is given by the Flory–Huggins relationship (Flory, 1953):

$$\Delta A_{\text{mix}} = kT(n_1 \ln v_1 + n_2 \ln v_2 + \chi n_1 v_2) \tag{8.5}$$

where n_1 and n_2 are the numbers of solvent and polymer molecules, respectively. For a cross-linked network, $n_2 = 1$. The quantity χ is the interaction parameter for the polymer–solvent system (Flory, 1953).

Introduction of solvent molecules into the system results in (1) an increase in ΔA_{el} due to the decrease of entropy of the network chains upon dilation, and (2) a decrease in ΔA_{mix} primarily due to the increase in the entropy of mixing the solvent molecules with the network chains. A state of equilibrium swelling is obtained when the two changes balance each other. At this state, the chemical potential, μ_1, of solvent inside the swollen network is equal to that, μ_1^0, of the solvent. Mathematically this state is expressed as

$$\Delta\mu_1 \equiv \mu_1 - \mu_1^0 = \Delta\mu_{1,\text{el}} + \Delta\mu_{1,\text{mix}} \tag{8.6}$$

where $\Delta\mu_{1,\text{el}}$ and $\Delta\mu_{1,\text{mix}}$ are the elastic and mixing chemical potentials. Using the thermodynamic definitions for the chemical potentials and equating $\Delta\mu_1$ to zero,

$$\left(\frac{\partial \Delta A}{\partial n_1}\right)_{T,p} = \left(\frac{\partial \Delta A_{\text{el}}}{\partial n_1}\right)_{T,p} + \left(\frac{\partial \Delta A_{\text{mix}}}{\partial n_1}\right)_{T,p} = 0 \tag{8.7}$$

where n_1 is the number of solvent molecules in the swollen network and the subscripts T, p indicate that the differentiations are made at constant temperature and pressure. Performing the differentiations indicated in Eq. (8.7) (Queslel and Mark, 1985a, 1989; Erman and Flory, 1985), one obtains for an affine network

$$\ln(1 - v_{2\text{m}}) + \chi v_{2\text{m}}^2 + v_{2\text{m}} + B\left(\frac{\phi}{\phi - 2}\right)\left[\left(\frac{v_{2\text{m}}}{v_{2\text{c}}}\right)^{1/3} - \frac{\mu}{\nu}\frac{v_{2\text{m}}}{v_{2\text{c}}}\right] = 0 \tag{8.8}$$

and for a phantom network

$$\ln(1 - v_{2\text{m}}) + \chi v_{2\text{m}}^2 + v_{2\text{m}} + B\left(\frac{v_{2\text{m}}}{v_{2\text{c}}}\right)^{1/3} = 0 \tag{8.9}$$

where

$$B = \left(\frac{V_1}{RT}\right)\left(\frac{\xi kT}{V_0}\right) \tag{8.10}$$

In Eq. (8.10), V_1 is the molar volume of solvent. The details of the calculations that lead to Eqs. (8.8) and (8.9) are given in Erman and Mark (1997).

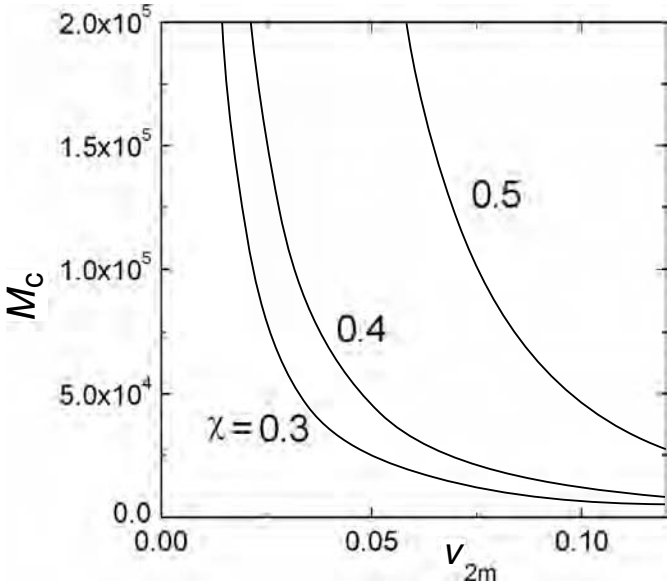

Figure 8.1 Relationship between network chain molecular weight, M_c, and the equilibrium degree of swelling, v_{2m}, calculated from Eq. (8.11) for three different values of the interaction parameter, χ.

In the highly swollen state, the constrained junction theory (Flory, 1977) indicates that a real network exhibits properties closer to those of the phantom network model. Consequently, Eq. (8.9) is a more realistic representation for equilibrium swelling.

Equation (8.9) may thus be used to estimate the average chain length M_c between cross links. Using the relation $\xi kT/V_0 = (1 - 2/\phi)\rho RT/M_c$ obtained from Eq. (4.3) and solving Eq. (8.9) for M_c leads to

$$M_c = -\frac{\rho(1 - 2/\phi)V_1 v_{2c}^{2/3} v_{2m}^{1/3}}{\ln(1 - v_{2m}) + \chi v_{2m}^2 + v_{2m}} \tag{8.11}$$

Characterization of the network chain length in this manner requires precise measurement of v_{2m}. The value of v at this value of v_{2m} is also required. The relationship between v_{2m} and M_c calculated from Eq. (8.11) is shown in Figure 8.1 for different values of χ. The strong dependence of the degree of swelling on the interaction parameter is worth noting. For various polymer–solvent systems, the χ parameter exhibits strong dependence on the amount of solvent. For the polyisobutylene–benzene system, for example, the dependence of ξ on v_{2m} is given by the following relation (Erman and Flory, 1985; Eichinger and Flory, 1968)

$$\chi = 0.500 + 0.30v_{2m} + 0.3v_{2m}^2 \tag{8.12}$$

This dependence plays a major role in driving the system to the critical state and volume phase transitions as discussed below (Okay, 2000). Application of Eq. (8.11) is further illustrated by an example in the Problems.

Alternatively, Eq. (8.9) may serve as a convenient means of evaluating the χ parameter. Solving Eq. (8.9) for χ, one obtains

$$\chi = -\frac{\ln(1 - v_{2m}) + v_{2m} + B v_{2c}^{2/3} v_{2m}^{1/3}}{v_{2m}^2} \tag{8.13}$$

The value of the cross-link density as embodied in the factor B and the corresponding value of v_{2m} are required for evaluating χ from Eq. (8.13). Use of several network samples with different cross-link densities leads of course to an estimate of χ as a function of v_{2m} (Bahar *et al.*, 1987).

Swelling is also frequently used as a preliminary to elongation measurements. In this application, a large-enough quantity of a solvent, generally non-volatile, is introduced into the network to facilitate the approach to elastic equilibrium or to suppress crystallization. This also has the advantageous effect of decreasing the extent to which the reduced stress changes with elongation (Mark, 1975; Treloar, 1975), as is described in Chapter 7. However, a complication can occur in the case of networks of polar polymers at relatively high degrees of swelling. The observation is that different solvents at the same degree of swelling can have significantly different effects on the elastic force (Yu and Mark, 1974). This is apparently due to a specific solvent effect on the unperturbed dimensions or on $V_0 \propto \langle r^2 \rangle_0^{3/2}$. It is described further in Chapter 10.

Volume phase transitions

In recent years, much emphasis has been placed on swelling of networks and their phase transitions under different activities of the network–solvent system. The pioneering work of Tanaka and collaborators stimulated the work in this area (Tanaka, 1978, 1981, 1992; Tanaka *et al.*, 1987, 1995; Kokufuta *et al.*, 1995; Tsuchiya *et al.*, 1994; Suzuki and Tanaka, 1990; Annaka and Tanaka, 1992; Li and Tanaka, 1992; Matsuo and Tanaka, 1992; Zhang *et al.*, 1992; Grinberg *et al.*, 2000). In the studies of volume phase transitions, usually low degrees of cross linking are used in the interest of observing large differences between the swollen and the collapsed states. As a convention, swollen networks with low degrees of cross linking are referred to as "gels". Large-scale volume transitions triggered by small changes in environmental variables directed attention to possible uses of swollen gels in the field of responsive materials technologies. The transition involves the gel exuding solvent, for example upon decrease in temperature. The resulting shrinkage ("syneresis") is widely known as "gel collapse", which is mostly studied on

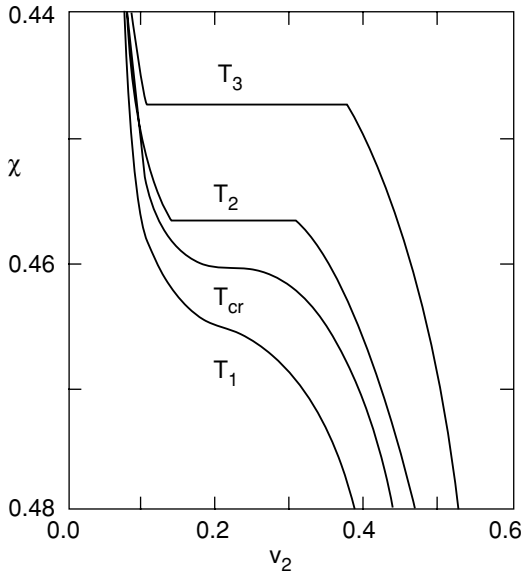

Figure 8.2 Dependence of the degree of swelling on the χ parameter, sketched for a network at different temperatures. The curve labeled with T_{cr} exhibits critical behavior. At T_1, the network shrinks as the χ parameter decreases but does not show an abrupt collapse. At T_2 and T_3, the network exhibits collapse as the χ parameter is decreased.

networks having a small number of charges on chains. The presence of charges facilitates the volume phase transitions in swollen gels. The shrinkage, critical state, and collapse of a gel is shown schematically in Figure 8.2 where the abscissa indicates the volume fraction of polymer in the swollen gel, and the ordinate shows the values of the χ parameter. The four curves are obtained at different temperatures, where for each curve the χ parameter is varied. Thus, the χ parameter plays the role of the environmental variable, which for example may depend on the pH of the system or the composition of the solvent if it consists of two or more components.

The change in environmental variables such as temperature, the quality of solvent, and the amount of charge on network chains may cause the system to go through critical conditions and, with the fulfillment of the necessary conditions, may result in triphasic equilibrium. In Figure 8.2, the curve marked with T_{cr} passes through the critical point as the interaction parameter is varied. The curve below the T_{cr} curve exhibits changes in volume as χ is varied; however, the system does not go through a phase transition. The two curves above the T_{cr} curve exhibit phase transitions. The quantity relevant to the study of phase transitions is the chemical

potential. In the presence of charged groups on network chains, the chemical potential of the network satisfies the equation

$$\Delta\mu_1/RT = \Delta\mu_{1,\mathrm{el}}/RT + \Delta\mu_{1,\mathrm{mix}}/RT + \Delta\mu_{1,i}/RT = -\ln a_1 \tag{8.14}$$

where $\Delta\mu_{1,\mathrm{el}}/RT$ and $\Delta\mu_{1,\mathrm{mix}}/RT$ are defined by Eqs. (8.6) and (8.7) above, a_1 is the activity of solvent surrounding the swollen network that equates to unity for pure solvent, and $\Delta\mu_{1,\mathrm{i}}/RT$ for the ionic groups is given by (Flory, 1953; Erman and Flory, 1985)

$$\frac{\Delta\mu_{\mathrm{i}}}{RT} = -i\nu\left(\frac{V_1}{V_0 N_{\mathrm{A}}}\right)\left(\frac{v_{2\mathrm{m}}}{v_{2\mathrm{c}}}\right) \tag{8.15}$$

where i is the number of ionic groups per chain.

At the critical point, the following three conditions hold

$$\frac{\Delta\mu_1}{RT} = -\ln\, a_1 \qquad \frac{\partial\mu_1}{\partial n_1} = 0 \qquad \frac{\partial^2\mu_1}{\partial n_1^2} = 0 \tag{8.16}$$

The solution of Eqs. (8.16) uniquely determines the critical state of the swollen network.

When the system exhibits a phase transition, three phases are in equilibrium: (1) the pure solvent, (2) a highly swollen gel, with polymer volume fraction v_2, and (3) a less swollen, more concentrated gel with polymer volume fraction v_2'. Conditions of phase transition are obtained when the following equations are satisfied:

$$\Delta\mu_1(v_2) = \Delta\mu_1(v_2') = -RT\,\ln\, a_1 \tag{8.17}$$

$$\Delta\mu_2(v_2) = \Delta\mu_2(v_2') \tag{8.18}$$

where $\Delta\mu_2$ is the chemical potential of the polymer phase.

Several applications of volume phase transitions are presented in the two volume series by Dusek (1993a, b).

When the network chains contain ionic groups, there will be additional forces that affect their swelling properties. Translational entropy of counterions, Coulomb interactions, and ion pair multiplets are forces that lead to interesting phenomena in ion-containing gels. These phenomena were studied in detail by Khokhlov and collaborators (Khokhlov and Philippova, 1996, 2002; Philippova, 2000; Khokhlov, 1992).

A network chain of a polyampholyte gel contains both positive and negative charges. The liquid phase in the swollen polyampholyte gel may contain additional counterions. The theoretical and experimental literature on polyampholyte gels was reviewed by Nisato and Candau (2002). In an ion-containing gel, when ion-containing groups are fully dissociated, the gel swells excessively because of the

tendency of the free counterions to occupy as much space as possible. In the other extreme case, called the ionomer regime, counterions are condensed on oppositely charged monomer units, forming ion pairs followed by formation of multiplets. This decreases the osmotic pressure of the gel and results in its collapse. The conditions for ion pair formation and physical and chemical factors leading to gel swelling and collapse have been discussed by Khokhlov and Philippova (2002).

9

Force as a function of temperature

Introduction

As was illustrated in Chapter 5, one of the most important thermodynamic quantities is the free energy. It is a state function and has been given this particular name because it represents that portion of the energy available ("free") to do work under specified conditions (Atkins, 1990). The type of free energy used in Chapter 5 is called the Helmholtz free energy $A \equiv E - TS$, and is most useful under conditions of constant temperature and constant volume. (The fact that the theory proceeds through the Helmholtz free energy complicates things for experimentalists. They must either do the experiment at constant volume, which is very difficult, or correct their constant-pressure data to constant volume, which requires model-based approximations.)

The second type of free energy of interest to physical chemists is the Gibbs free energy, $G \equiv H - TS$. It is more convenient for analysis of systems at constant temperature and constant pressure. For such a process G must decrease, consistent with nature's attempt to decrease the energy of a system while simultaneously increasing its entropy, or disorder.

Its relevance to rubberlike elasticity can be illustrated by analysis of force–temperature (thermoelastic) measurements (Flory *et al.*, 1960). Such experiments, first described qualitatively in Chapter 1, have now been carried out quantitatively for a wide variety of elastomers. The basic question in this analysis was raised in a preliminary manner in Chapter 7. It concerns the nature of the free energy increase attending the deformation of an elastomer, or the free energy decrease accompanying its spontaneous retraction when the deforming stress is removed. Specifically, how much of the free energy change is due to changes in energy and how much to changes in entropy? If the experiments are carried out at constant V, ΔA_{el} is of greatest interest; experiments at constant p, however, shift the focus to ΔG_{el},

that is, to the change in the Gibbs elastic free energy. The usual thermodynamic analysis, summarized in Appendix D, pertains directly to experiments at constant V, and this part is based entirely on purely thermodynamic arguments. Subsequent adoption of a molecular model then permits modification of these equations to make them applicable to the much simpler experiments carried out at constant pressure.

As was mentioned in Chapter 1, the pressure exhibited by an ideal gas is entirely due to entropy effects, specifically the tendency for the gas to increase its entropy by increasing its volume (Atkins, 1990). This absence of energy effects results from the fact that the gas molecules are assumed not to repel one another through an excluded-volume effect, nor to attract one another through the usual non-bonded intermolecular interactions. One repercussion is the prediction, from $pV = nRT$, that, at constant volume, the pressure should be directly proportional to the absolute temperature.

An ideal elastomer can be analogously defined as one in which the elastic force is entirely due to entropy effects, specifically, the tendency of the network chains to increase their entropy by retracting to more random conformations. This ideality would occur when (1) intermolecular interactions do not depend on degree of deformation (one of the major assumptions of the molecular theories), (2) the dependence of intermolecular interactions on the spacing between chains is nullified by constraining measurements to constant volume, and (3) the conformational energies of the network chains do not change with deformation. The assumption of ideality results in the equation of state for the stress or the stress–deformation relations given by Eq. (7.11), according to which, the force or stress at constant elongation is proportional to absolute temperature.

Theory

The described proportionality between f^* and T is generally not observed, since different conformations of a polymer chain generally do not correspond to the same energy. The extent of this thermodynamic non-ideality can be represented by the energetic contribution to the total elastic force (Flory *et al.*, 1960; Mark, 1973, 1976; Treloar, 1975; Godovsky, 1986). In the case of uniaxial deformation (elongation or compression) it is given by

$$f_e = \left(\frac{\partial E}{\partial L}\right)_{T,V} \tag{9.1}$$

The most useful form for representing such information is the fraction f_e/f of the total force that is of energetic origin. Purely thermodynamic analysis, described

in Appendix D, shows this ratio to be given by the expression

$$\frac{f_e}{f} = -T\left[\frac{\partial \ln(f/T)}{\partial T}\right]_{L,V} \tag{9.2}$$

and it is thus seen to be immediately accessible from force–temperature measurements at constant length and volume. Some thermoelastic studies have indeed been carried out at constant volume (Allen *et al.*, 1971), as required by this thermodynamically exact equation but, because of severe experimental difficulties encountered in meeting this requirement, most experiments are conducted at constant pressure. Transformation of Eq. (9.2) to a form suitable for analysis of such isobaric data requires recourse to an appropriate elastic equation of state. Here, we adopt the equation of state resulting from the simplest molecular or statistical theories of polymer networks.

As demonstrated in Chapter 7, the equation of state characterizing the uniaxial deformation of a Gaussian network, either unswollen or swollen with a constant amount of diluent, may be written (Erman and Mark, 1997)

$$f = 2\left(\frac{FkT}{L_i}\right)\left(\frac{V}{V_0}\right)^{2/3}(\alpha - \alpha^{-2}) \tag{9.3}$$

where F equates to $\nu/2$ for the affine network model and to $\xi/2$ for the phantom network model, ν and ξ being the number of chains in the network, and the cycle rank, respectively. k is the Boltzmann constant, V is the volume of the sample at the prevailing T, p, and f, and V_0 is a reference volume so chosen that the mean-square end-to-end lengths of the network chains would be unchanged by removal of the cross links. Comparison of results obtained by differentiating this equation with respect to temperature under conditions of constant L and V, L and p, and finally α and p, give the relationships (Flory *et al.*, 1960; Erman and Mark, 1997)

$$\left[\frac{\partial \ln(f/T)}{\partial T}\right]_{L,V} = \left[\frac{\partial \ln(f/T)}{\partial T}\right]_{L,p} + \frac{\beta_L}{\alpha^3 - 1} \tag{9.4}$$

$$\left[\frac{\partial \ln(f/T)}{\partial T}\right]_{L,V} = \left[\frac{\partial \ln(f/T)}{\partial T}\right]_{\alpha,p} - \frac{\beta_\alpha}{3} \tag{9.5}$$

The quantities β_L and β_α are the thermal volume expansion coefficients of the sample at constant length and constant α, and may to very good approximation be replaced by β, the thermal volume expansion coefficient of the sample in the undeformed state (Flory *et al.*, 1960). Equations (9.4) and (9.5) are derived in Appendix D. Results on swollen networks require of course the value of β characterizing the network at the same degree of swelling employed in the thermoelasticity

measurements (Flory *et al.*, 1960). Equations (9.4) and (9.5) transform Eq. (9.2) into the experimentally more practical forms

$$\frac{f_e}{f} = -T\left[\frac{\partial \ln(f/T)}{\partial T}\right]_{L,p} - \frac{\beta T}{\alpha^3 - 1} \tag{9.6}$$

$$\frac{f_e}{f} = -T\left[\frac{\partial \ln(f/T)}{\partial \mathrm{T}}\right]_{\alpha,p} + \frac{\beta T}{3} \tag{9.7}$$

These equations thus give the desired thermodynamic quantity f_e/f in terms of experimentally accessible force–temperature data obtained at constant pressure.

In addition to this thermodynamic information, it is possible to obtain a molecular interpretation of thermoelastic data and the ratio f_e/f derived therefrom. The energy changes accompanying the deformation of the network are assumed to be entirely intramolecular in origin, an assumption that will be discussed in detail below. Analysis then proceeds through the alternative form (Barrie and Standen, 1967; Chen *et al.*, 1973)

$$f = 2\left(\frac{FkT}{L_i}\right)\left[\frac{\langle r^2\rangle_{\mathrm{i}}}{\langle r^2\rangle_0}\right](\alpha - \alpha^{-2}) \tag{9.8}$$

of the theoretically derived elastic equation of state, where $\langle r^2\rangle_{\mathrm{i}}$ is the mean-square end-to-end distance of a network chain in the undistorted state of volume V, and $\langle r^2\rangle_0$ (the "unperturbed dimension") is the corresponding quantity for the same chain free of the constraints imposed by the network cross links. As will be demonstrated below, excluded volume interactions have no effect on the dimensions of the network chains. Differentiation of this equation with respect to temperature at constant L and V gives the result (Erman and Mark, 1997)

$$\left[\frac{\partial \ln(f/T)}{\partial T}\right]_{L,V} = -\frac{\mathrm{d}\ln\langle r^2\rangle_0}{\mathrm{d}T} \tag{9.9}$$

Comparison of Eqs. (9.2) and (9.9) then demonstrates that

$$\frac{f_e}{f} = T\frac{\mathrm{d}\ln\langle r^2\rangle_0}{\mathrm{d}T} \tag{9.10}$$

an equation also derivable, of course, from differentiation of Eq. (9.3) at constant L and p, or at constant α and p. This equation is of considerable importance in thermoelastic analysis, because it establishes the connection between the purely thermodynamic quantity f_e/f, and its molecular counterpart, the temperature coefficient of the unperturbed dimensions of the network chains. The latter quantity may be calculated from the rotational isomeric state theory of chain configurations (Flory, 1969; Mattice and Suter, 1994) as is described in Appendix D, thereby providing detailed insight into the molecular changes associated with either the

deformation of a polymer network at constant temperature, or a change in the temperature of a network subsequent to its deformation.

The equations characterizing a network in torsion are very similar to those for uniaxial deformation, with f and L being replaced by the torsion couple M and angle of torsion ϕ, respectively. These relationships may be summarized by (Treloar, 1975)

$$M_e = \left(\frac{\partial E}{\partial \phi}\right)_{V,T,L} \tag{9.11}$$

$$\frac{M_e}{M} = -T\left[\frac{\partial \ln(M/T)}{\partial T}\right]_{V,\phi,L} = -T\left[\frac{\partial \ln(M/T)}{\partial T}\right]_{p,\phi,L} + \beta T$$

$$= T\frac{\mathrm{d}\ln\langle r^2\rangle_0}{\mathrm{d}T} \tag{9.12}$$

that parallels Eq. (9.10) obtained for uniaxial deformation. The thermoelastic equations characterizing networks in simple shear also parallel very closely those already presented here.

As described above, the energy changes may be assumed to be intramolecular, resulting from changes in conformational energies of the network chains. (Thus, since the non-ideality is intramolecular, it cannot be removed by diluting the chains (swelling the network) or by increasing the lengths of the chains (decreasing the degree of cross linking). In this respect, elastomers are different from gases, which can be made to behave ideally by decreasing the pressure to a sufficiently low value (Atkins, 1990).) Because f_e is intramolecular, the same theoretical equation of state mentioned above may also be used to obtain a molecular interpretation of thermoelastic data and the quantity f_e/f derived therefrom. The result given by Eq. (9.10) is of considerable importance for two reasons (Mark, 1976). It permits the comparison of results of thermoelastic measurements on polymer chains in the bulk, in network structures, with results of viscosity measurements on chains of the same, essentially isolated, polymer in dilute solution. It also establishes the relationship between the purely thermodynamic quantity f_e/f and its molecular counterpart $\mathrm{d}\ln\langle r^2\rangle_0/\mathrm{d}T$, which can be interpreted in terms of the rotational isomeric state theory of chain configurations (Flory, 1969).

Some experimental details

It is, of course, important to note that use of the thermodynamic relationships derived in Appendix D and the previous section requires that the polymer network be brought as closely as possible to elastic equilibrium at each temperature of investigation. Thus, only those thermoelastic data found to be reproducible upon

subsequent changes in temperature are suitable for the purposes at hand. Swelling a network with non-volatile solvent is frequently used to facilitate the approach to equilibrium.

Direct use of the equations pertaining to the condition of constant volume has the considerable advantage of not requiring recourse to an elastic equation of state of non-thermodynamic origin. Such experiments, however, generally require the imposition of a sizable hydrostatic pressure on the sample to keep its volume constant with changing temperature, and this requirement introduces considerable experimental difficulty (Allen *et al.*, 1971). Because of this complication, such experiments have been restricted to very small temperature ranges, typically intervals of only a few degrees, thereby introducing additional uncertainties.

Measurements at constant pressure are much easier to carry out but require for their interpretation adoption of an elastic equation of state based on a particular model of the network, as already described. In the case of uniaxial elongation or compression at constant pressure, measurements at constant deformation α have an advantage in that calculation of values of f_e/f involves a correction term $\beta/3$, which is independent of deformation (Treloar, 1975). The advantage of involving a deformation-independent correction term is shared by measurements in torsion or shear in general. (Measurements at constant α are of course somewhat inconvenient in that the temperature dependence of L_i requires readjustment of the length L of the sample at each new temperature, or the application of the appropriate correction for thermal expansion of the network in the unstrained state.) Correction of measurements at constant length, however, requires the term $\beta/(\alpha^3 - 1)$, which tends to have very large values in the region of small deformation (Shen, 1975; Mark, 1976). This term can be made negligibly small in elongation by choosing sufficiently large values of α (but no such simplification is possible in the case of compression (Mark, 1976). Finally, thermoelastic data equivalent to those described above may, of course, be obtained from a series of stress–strain isotherms, or from measurements of sample length as a function of temperature at constant force (Mark, 1976).

Some typical data

Figure 9.1 shows some typical thermoelastic data, in elongation at constant length, directly represented as the dependence of force on temperature. From the slopes of curves such as these, the derivatives required in Eqs. (9.6) and (9.7) may be obtained.

At low elongations, the increased tendency for the chains to retract (increase in f) with increase in temperature is overcome by the usual thermal expansion of the network (Treloar, 1975). At a somewhat higher elongation, called the inversion value, the two effects just offset one another, and the force becomes independent of

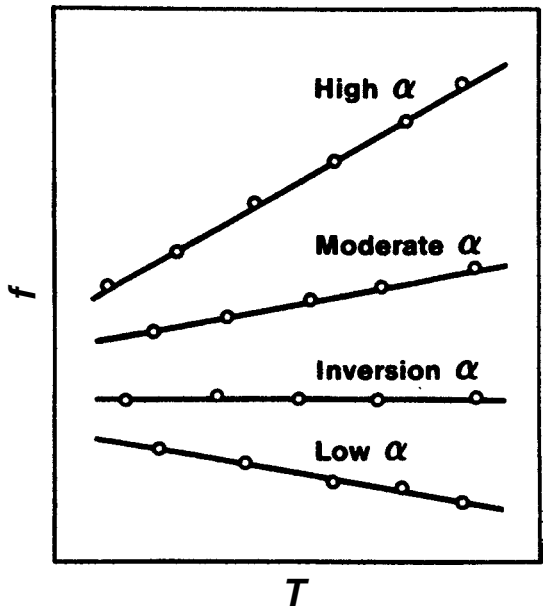

Figure 9.1 Typical thermoelastic results at various elongations.

temperature. At still higher but moderate values of α, the usual easily measurable increase in f with T occurs, and this is the region where the most reliable thermoelasticity data are obtained. Very high elongations have the advantage of making the correction term $\beta/(\alpha^3 - 1)$ negligibly small, but they also have the possible disadvantage of introducing complications from strain-induced crystallization or from non-Gaussian effects due to limited chain extensibility (Mark, 1979b, c).

Some typical results

Table 9.1 summarizes some typical values of f_e/f and $\mathrm{d}\ln\langle r^2\rangle_0/\mathrm{d}T$ (Mark, 1976). As can be seen, most values of these quantities are positive, which means that extended chain conformations are generally of higher energy. Since an increase in temperature would then increase the frequency of these more extended conformations, this would also explain the positive values of $\mathrm{d}\ln\langle r^2\rangle_0/\mathrm{d}T$. More detailed interpretations in terms of rotational isomeric state theory (Flory, 1969) are discussed later in this chapter.

Evaluation and importance of thermoelastic results

Despite the experimental difficulties attending the study of unswollen polymer networks under the constraint of constant volume, a number of studies meeting

Table 9.1 *Some typical thermoelastic results*

Elastomer	$\frac{f_e}{f}$[a]	$10^3 \frac{d \ln \langle r^2 \rangle_0}{dT} (K^{-1})$[b]
Natural rubber	0.18	0.60
cis-1,4-Polybutadiene	0.13	0.44
Poly(dimethylsiloxane)	0.20	0.67
Polyisobutylene	−0.06	−0.20
Polyethylene	−0.42	−1.41
Elastin[c]	0.26	0.87

[a] Fraction of the force that is of energetic origin
[b] Temperature coefficient of the unperturbed dimensions, in the vicinity of 298 K
[c] An elastomeric protein present in mammals
Data from Mark (1976)

Table 9.2 *Values of f_e/f obtained at constant volume and constant pressure*

Elastomer	Constant V	Constant p
Natural rubber	0.12	0.17
Poly(dimethysiloxane)	0.25	0.20
Polyisobutylene	−0.09	−0.06

Data from Mark (1976); Treloar (1975)

this thermodynamic requirement have been successfully carried out by Allen and coworkers (Allen *et al.*, 1971). Such studies are of great importance in evaluating the statistical theory of rubberlike elasticity, of course, since they permit the calculation of f_e/f directly from Eq. (9.2), a thermodynamically exact equation. Thermoelastic results thus obtained therefore serve as an important check of results obtained at constant pressure and interpreted by using the equation of state derived from the statistical theory.

Values of f_e/f obtained to date by the use of these methods are summarized in Table 9.2; included for purposes of comparison are the most reliable values of f_e/f obtained for the same polymer networks from measurements at constant pressure (Treloar, 1975; Mark, 1976). For the three polymers thus studied, values of f_e/f obtained from constant-pressure experiments and treated according to Eqs. (9.4) or (9.5) are generally in good agreement with those obtained at constant volume.

Although the great majority of thermoelasticity studies have been carried out on networks in simple uniaxial elongation, several studies have now been reported

Table 9.3 *Values of f_e/f obtained using different types of deformation*

Polymer	Elongation	Compression	Torsion	Shear[a]	Swelling equilibrium
Natural rubber	0.17	0.18	0.17	0.18	—
cis-1,4-Polybutadiene	0.12	0.14	0.10	—	—
Poly(dimethylsiloxane)	0.20	0.13	—	—	∼0.1
Polyisobutylene	−0.06	—	−0.03	—	—

[a]Elongation data converted into shear moduli
Data from Mark (1976); Treloar (1975)

Table 9.4 *Comparison of calorimetric and thermoelastic values of f_e/f*

Elastomer	Type of deformation	Calorimetric values	Thermoelastic values
Natural rubber	Elongation	0.18	0.17
	Torsion	0.20	0.15
cis-1,4-Polybutadiene	Elongation	0.11	0.12
	Torsion	0.14	0.11

Data from Mark (1976); Treloar (1975)

in which the deformation was uniaxial compression, torsion, shear, or isotropic swelling. Results obtained for the same polymers that have been studied in more than one type of deformation are presented in Table 9.3 (Treloar, 1975; Mark, 1976). The fact that results obtained from measurements in elongation are in good agreement with those from other types of deformation is of considerable importance since interchain ordering, if present, could be expected to respond differently to different types of network deformation and thus manifest itself through a dependence of f_e/f on the type of deformation employed. No such effect is evident from the results. Similarly, f_e/f has been found to be independent of cross-linking conditions, degree of cross linking, and extent of deformation (Mark, 1976).

Direct calorimetric measurements carried out on a polymer network during the deformation process can also be used to determine values of f_e/f. Some of the most reliable calorimetric values thus obtained are given in Table 9.4 (Treloar, 1975; Mark, 1976), and are seen to be in good agreement with thermoelastic results reported for the same two polymers.

One of the most direct confrontations of theory with experiment may be achieved by the thermoelastic study of networks swollen with diluent, either at constant composition or in swelling equilibrium. The effects of such diluents on f_e/f for

Table 9.5 *Constancy of f_e/f upon swelling*

Elastomer	Unswollen networks	Swollen networks
Natural rubber	0.17	0.16
cis-1,4-Polybutadiene	0.12	0.11
trans-1,4-Polyisoprene	−0.1	−0.17
Polyethylene	−0.42	−0.52

Data from Mark (1976); Treloar (1975)

Table 9.6 *Comparison of thermoelastic and viscometric values of temperature coefficient of unperturbed dimensions*

	$10^3 \frac{d \ln \langle r^2 \rangle_0}{dT^b} (K^{-1})$	
Polymer	Thermoelastic	Viscometric
Poly(dimethylsiloxane)	0.59	0.52
Polyisobutylene	−0.19	−0.26
Polyethylene	−1.05	−1.06
Isotactic poly(*n*-pentene-1)	0.34	0.52

Data from Mark (1976)

several elastomers are summarized in Table 9.5 (Mark, 1976). A wide variety of polymers and diluents has been employed in such studies, and a wide range of degrees of swelling has been investigated, down to a volume fraction of polymer of 0.18. Nonetheless, there is no apparent effect of dilution on f_e/f. This is an important result, since any ordering of polymer chains in the amorphous state would certainly be dispersed by the relatively large amounts of diluent incorporated into the networks in these studies (Flory, 1973; Mark *et al.*, 1984). It also supports the assumption that intermolecular interactions have little effect on rubberlike elasticity.

Conversion of the thermodynamic quantity f_e/f to $d \ln \langle r^2 \rangle_0 / dT = f_e / f T$ permits comparison of values of the temperature coefficient of the unperturbed dimensions of the network chains as obtained from thermoelasticity measurements with values obtained from intrinsic viscosity–temperature ($[\eta]-T$) measurements on chains of the same polymer dispersed in a solvent at infinite dilution. Table 9.6 (Mark, 1976) lists some polymers that have been studied both in thermoelastic investigations and in viscometric studies in which proper account has been taken of polymer–solvent interactions and their variation with temperature. The excellent

Table 9.7 *Summary and conclusions, thermoelasticity studies*

A. Evidence
1. Values of $f_e/f = T\,\mathrm{d}\ln\langle r^2\rangle_0/\mathrm{d}T$ are independent of cross-linking conditions, degree of cross linking, type and extent of deformation, and presence of diluent in a network.
2. Values of $\mathrm{d}\ln\langle r^2\rangle_0/\mathrm{d}T$ from thermoelastic studies are in good agreement with values from $[\eta]$–T experiments.
B. Conclusions
1. Intermolecular interactions must be independent of the extent of deformation (i.e., f_e/f must be intramolecular).
2. Chains in the bulk amorphous state must be in random, unordered configurations.
3. The molecular representation of the results is well interpreted by rotational isomeric state theory.

agreement obtained between values of $\mathrm{d}\ln\langle r^2\rangle_0/\mathrm{d}T$ for the same polymer chains under such vastly different conditions is extremely important since it is inconceivable that such agreement would be obtained if intermolecular interactions varied with configuration or if significant molecular ordering occurred in the amorphous state (Flory, 1973; Mark *et al.*, 1984). Since intermolecular interactions do not affect the force, they must be independent of the extent of the deformation and thus the spatial configurations of the chains. This in turn indicates that the spatial configurations must be independent of intermolecular interactions; that is, the amorphous chains must be in random, unordered configurations, the dimensions of which should be the unperturbed values. This conclusion has now been amply verified, in particular by neutron scattering studies on undiluted amorphous polymers (Flory, 1973).

The major conclusions reached in thermoelastic studies are summarized in Table 9.7.

Rotational isomeric state interpretation

In the case of polyethylene, the thermoelastic data indicate that the energetic contribution to the elastic force is large and negative (Flory, 1969). These results may be understood using the information given in Figure 9.2 (Mark, 1981). The preferred (lowest-energy) conformation of the chains is the all-*trans* form, since *gauche* states (at rotational angles of $\pm 120^\circ$) cause steric repulsions between CH_2 groups. Since this conformation has the highest possible spatial extension, stretching a polyethylene chain requires switching some of the *gauche* states (which are of course present in the randomly coiled form) to the alternative *trans* states. These changes decrease the conformational energy and are thus the origin of the negative type of ideality

Results

$$\frac{f_e}{f} = T\frac{\mathrm{d}\ln\langle r^2\rangle_0}{\mathrm{d}T} = -0.42$$

Interpretation

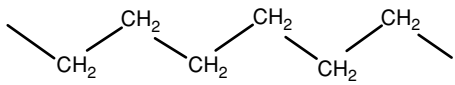

Figure 9.2 Thermoelastic results on (amorphous) polyethylene networks and their interpretation in terms of the preferred all-*trans* conformation of the chain (Mark, 1981).

Results

$$\frac{f_e}{f} = T\frac{\mathrm{d}\ln\langle r^2\rangle_0}{\mathrm{d}T} = 0.20$$

Interpretation

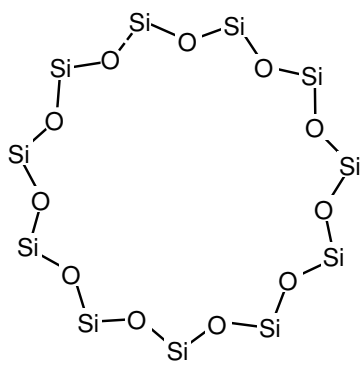

Figure 9.3 Thermoelastic results on poly(dimethylsiloxane) networks and their interpretation in terms of the preferred all-*trans* conformation of the chain (Mark, 1981). For purposes of clarity, the two methyl groups on each silicon atom have been deleted.

represented in the experimental value of f_e/f. (This physical picture also explains the decrease in unperturbed dimensions upon increase in temperature. The additional thermal energy causes an increase in the number of the higher-energy gauche states, which are more compact than the *trans* ones (Flory, 1969).)

The opposite behavior is observed in the case of poly(dimethylsiloxane) (PDMS), as is described in Figure 9.3 (Mark, 1981). The all-*trans* form is again the preferred

conformation; the relatively long Si–O bonds and the unusually large Si–O–Si bond angles reduce steric repulsions in general, and the *trans* conformation places CH_3 side groups at distances of separation where they are strongly attractive. Because of the inequality of the Si–O–Si and O–Si–O bond angles, however, this conformation is of very low spatial extension. Stretching a poly(dimethylsiloxane) chain therefore requires an increase in the number of *gauche* states. Since these are of higher energy, this explains the fact that deviations from ideality for these networks are found to be positive (Flory, 1969).

As here illustrated, rotational isomeric state theory can be used to give an insightful molecular interpretation of the thermoelastic properties of polymer networks.

10

Model elastomers

Effects of network structure on elastomeric properties

General approach

Until recently, there was relatively little reliable quantitative information on the relationship of stress to structure, primarily because of the uncontrolled manner in which elastomeric networks were generally prepared (Flory, 1953; Treloar, 1975; Erman and Mark, 1997). Segments close together in space were linked irrespective of their locations along the chain trajectories, thus resulting in a highly random network structure in which the number and locations of the cross links were essentially unknown. Such a structure was shown in Figure 1.2. New synthetic techniques are now available, however, for the preparation of "model" polymer networks of known structure. More specifically, if networks are formed by end linking functionally terminated chains instead of haphazardly joining chain segments at random, then the nature of this very specific chemical reaction provides the desired structural information (Erman and Mark, 1997; Mark, 2004a; Mark *et al.*, 2004). Thus, the functionality of the cross links is the same as that of the end-linking agent, and the molecular weight M_c between cross links and its distribution are the same as those of the starting chains prior to their being end linked.

An example is the reaction shown in Figure 10.1, in which hydroxyl-terminated chains of a polymer such as poly(dimethylsiloxane) (PDMS) are end linked using tetraethyl orthosilicate (alternatively called tetraethoxysilane). Characterizing the uncross-linked chains with respect to molecular weight M_n and molecular weight distribution, and then carrying out the specified reaction to completion gives elastomers in which the network chains have these characteristics: in particular a molecular weight M_c between cross links equal to M_n; a network chain-length distribution the same as that of the starting chains; and cross links having the functionality of the end-linking agent. It is also possible to use chains having a known number of

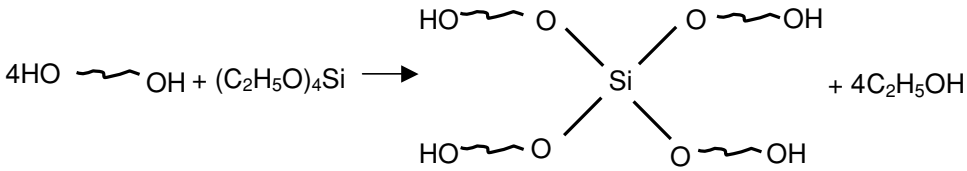

Figure 10.1 End linking by a condensation reaction between hydroxyl groups at the ends of a polymer chain and the alkoxy groups on a tetrafunctional end-linking agent. The number-average molecular weight M_n of the precursor chains becomes the critically important molecular weight M_c between cross links, and the distribution of M_n also characterizes the distribution of M_c (i.e., network chain lengths).

potential cross-linking sites placed as side chains along the polymer backbone, so long as their distribution is known as well (Falender *et al.*, 1979).

Because of their known structures, such model elastomers are now the preferred materials for the quantitative characterization of rubberlike elasticity. Such very specific cross-linking reactions have also been shown to be useful in the preparation of some of the liquid-crystalline elastomers (Disch *et al.*, 1995; Zentel and Brehmer, 1995) discussed in Chapter 16.

Effects of junction functionality

Trifunctional and tetrafunctional PDMS networks can be prepared in this way, and have been used to test the molecular theories of rubber elasticity with regard to the increase in non-affineness of the network deformation with increasing elongation. Typical results are shown in Figure 10.2 (Mark *et al.*, 1979). The ratio $2C_2/2C_1$ decreases with increase in cross-link functionality from three to four because cross links connecting four chains are more constrained than those connecting only three (Mark, 1993). There is therefore less of a decrease in modulus brought about by the fluctuations which are enhanced at high deformation and give the deformation its non-affine character, as described in Chapter 6. The decrease in $2C_2/2C_1$ with decrease in network chain molecular weight is due to the fact that there is less configurational interpenetration in the case of short network chains. This decreases the firmness with which the cross links are embedded and thus the deformation is already highly non-affine even at relatively small deformations.

A more thorough investigation of the effects of cross-link functionality requires use of the more versatile chemical reaction illustrated in Figure 10.3 (Mark, 1993). Specifically, vinyl-terminated PDMS chains are end linked using a multi-functional silane (Mark, 1993). In the study summarized in Figure 10.4 (Llorente and Mark, 1980) this reaction was used to prepare PDMS model networks having functionalities ranging from 3 to 11, with a relatively unsuccessful attempt to achieve a

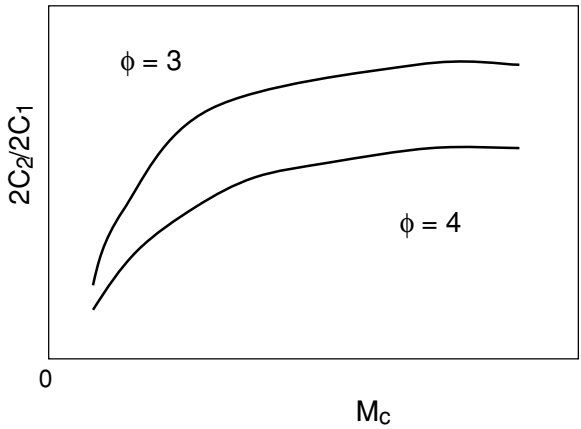

Figure 10.2 Values of the ratio $2C_2/2C_1$ (where $2C_2$ is a measure of the increase in non-affineness of the deformation as the elongation increases, and $2C_1$ approximates the high-deformation modulus). The ratio decreases with decrease in network chain molecular weight, and with increase in junction functionality, as predicted by theory (Flory and Erman, 1982).

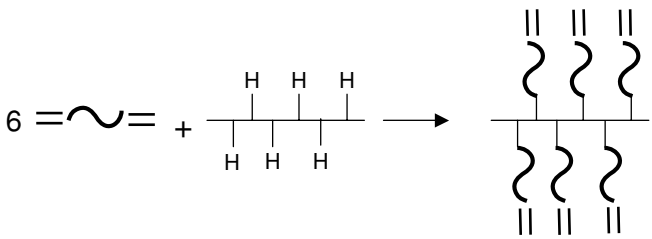

Figure 10.3 End linking by an addition reaction between vinyl groups at the ends of a polymer chain and the active hydrogen atoms on silicon atoms in an oligomeric poly(methyl hydrogen siloxane), in this illustrative case giving a junction functionality of six.

functionality of 37. As shown in the figure, values of $2C_2$ relative to $2C_1$ both decrease, for the reasons described in the discussion of Figure 10.2.

Effects of entanglements

Such model networks may also be used to provide a direct test of molecular predictions of the modulus of a network of known degree of cross linking. Some experiments on model networks (Sharaf, 1992; Eichinger and Akgiray, 1994; Sharaf and Mark, 1995; Erman and Mark, 1997) have given values of the elastic modulus in good agreement with theory. Others (Gottlieb *et al.*, 1981; Miller and Macosko,

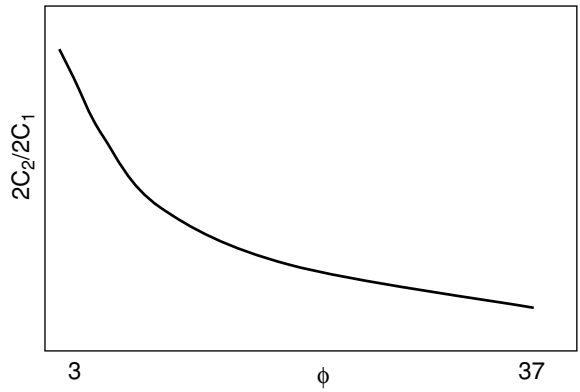

Figure 10.4 The effect of cross-link functionality on $2C_2/2C_1$.

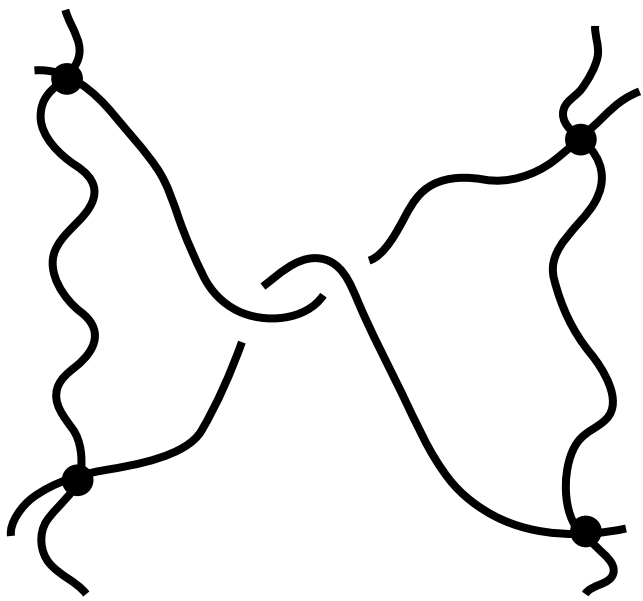

Figure 10.5 Sketch of an interchain entanglement.

1987; Patel *et al.*, 1992; Venkatraman, 1993; Gent *et al.*, 1994; Graessley, 2003) have given values significantly larger than predicted (Erman and Mark, 1997), and the increases in modulus have been attributed to contributions from "permanent" chain entanglements of the type shown in Figure 10.5. There are disagreements, and the issue has not yet been resolved. Since the relationship of modulus to structure is of such fundamental importance, there has been a great deal of research activity in this area.

Aspects of greatest importance appear to be (1) studying the effects of cross linking in solution, (2) studying the effects of swelling on networks cross linked in the bulk (dry) state, (3) building on the demonstration by Vilgis and Erman (1993) that the constraint models and slip-link models have much in common, (4) studying the effects of cross-link functionality and degree of cross linking, (5) studying a variety of elastomeric polymers, particularly those having very different values of the plateau modulus (Ferry, 1980) and (6) generalizing rubber elasticity models to include viscoelastic effects as well.

For purposes of illustration, it is useful to consider some studies of Oppermann (Oppermann and Rennar, 1987; Rennar and Oppermann, 1992) on end-linked PDMS networks of different functionalities, since some of these issues arose in the detailed and careful analysis of their experimental data (Erman and Mark, 1997). Here, studies of the small-strain shear modulus of end-linked PDMS networks with pentafunctional junctions were carried out as a function of network chain density. The data agree with predictions of the molecular theories at larger values of the chain or junction densities. At lower junction densities, however, the measured moduli are significantly larger than the predicted ones. Part of the difference, but probably not all of it, is due to problems in bringing such lightly cross-linked networks to elastic equilibrium in the unswollen state. Finally, the moduli tended to zero as the junction density went to zero.

The departure of the experimental results from the simple molecular theory when the network chains are long indicates the presence of additional contributions to the modulus. The reasons behind this departure are not yet clear and the problem clearly remains open. The understanding of entanglement phenomena is perhaps based on answering the question of whether the stated departures result from trapped entanglements or simply from the presence of other chains, sharing the volume of a given network chain. One important difference between the two types of constraints involves their dependence on network swelling. The localized, permanent entanglements should be independent of swelling, while the more diffuse interchain interactions should decrease with increase in swelling. The contributions from trapped entanglements should therefore persist even in highly swollen networks, and therefore contribute to the phantom modulus. For these reasons, it is quite important to carry out measurements of the modulus at a series of degrees of swelling, with the results at the highest degrees of swelling presumably being least complicated by non-equilibrium effects.

It should be noted that if one makes a network in the extremely dilute state so that there is no chain interpenetration during its formation, the phantom-structure state will be obtained, by definition. Experimentally, one indeed sees that network formation in the dilute state decreases both the modulus and its dependence on elongation (the "C_2 effect") (Erman and Mark, 1997). It was observed that the

entanglements resulting from the disperse interpenetration of chains in the cross-linked state were far more numerous than the specific localized points along the chain defined by explicit reference to the plateau modulus. Definitive experiments of this type would do much to resolve this issue of the nature and importance of chain entanglements in network structures at elastic equilibrium.

Interpretation of ultimate properties

This section focuses on the discussion of unfilled elastomers at high elongations, with an emphasis on ultimate properties and how model networks can clarify issues in this area. Of particular interest are the upturns in modulus frequently exhibited by elastomers at very high elongations (Flory, 1953; Treloar, 1975; Mark, 1981; Mark *et al.*, 1993) and the commercially important increases in ultimate strength associated with them. Such an upturn in modulus was illustrated in the stress–strain isotherm shown in Figure 1.12. This increase is very important since it corresponds to a significant toughening of the elastomer. Its molecular origin, however, had been the source of some controversy (Andrady *et al.*, 1980). It had been widely attributed to the "limited extensibility" of the network chains, i.e., to an inadequacy in the Gaussian distribution function, specifically that it does not assign a zero probability to a configuration unless its end-to-end separation r is infinite. However, the increase in modulus had generally been observed only in networks that could undergo strain-induced crystallization, which could account for the increase in modulus, primarily because the crystallites thus formed would act as additional cross links in the network. These effects of strain-induced crystallization are mentioned briefly below, and discussed further in Chapter 12.

This type of reinforcement resulting from strain-induced crystallization was identified by the fact that the higher the temperature, the lower the extent of crystallization and the worse the ultimate properties. The effects of increase in swelling were found to parallel those for increase in temperature, as was expected, since diluent also suppresses network crystallization (Mandelkern, 1989, 2003). On the other hand, in those cases where the upturns are due to limited chain extensibility, increase in temperature has relatively little effect on the upturns (Erman and Mark, 1997). Also, in these cases swelling can even make the upturns more pronounced because of the already-imposed stretching of the chains from the dilational effects of the swelling. Thus, studying the effects of increase in temperature or introduction of a swelling solvent represents a way to determine whether the upturns in modulus are due to strain-induced crystallization or to a non-Gaussian contribution arising from limited-chain extensibility.

Attempts to observe upturns from non-Gaussian effects in non-crystallizable networks were observed by the use of some of end-linked, non-crystallizable model PDMS networks described above. These networks have high extensibilities,

presumably because of their very low incidence of dangling-chain network irregularities. They have particularly high extensibilities when they are prepared from a mixture of very short chains (around a few hundred g mol^{-1}) with relatively long chains (around 18 000 g mol^{-1}), giving a bimodal distribution of network chain lengths (Mark, 1994). Apparently, the very short chains in such networks are important because of their limited extensibilities, and the relatively long chains because of their ability to retard the rupture process. Such "bimodal" model networks are discussed further in Chapter 13.

Stress–strain measurements on such bimodal PDMS networks exhibited upturns in modulus, which were much less pronounced than those in crystallizable polymer networks. Furthermore, they are independent of temperature and are not diminished by incorporation of solvent. These characteristics are what is to be expected in the case of limited chain extensibility (Andrady *et al.*, 1980; Mark *et al.*, 1984). Thus these results permit interpretation of properties such as the elongation at the upturn in the modulus and the elongation at rupture ("maximum extensibility").

Dangling-chain networks

Since dangling chains represent imperfections in a network structure, their presence should have a detrimental effect on ultimate properties such as the tensile strength, as gauged by the stress f_r^* at rupture. This expectation is confirmed by an extensive series of results obtained on PDMS networks which had been tetrafunctionally cross linked using a variety of techniques. Some pertinent results are shown schematically, as a function of the molecular weight between cross links, in Figure 10.6 (Andrady *et al.*, 1981). The largest values of f_r^* were obtained for the networks prepared by selectively joining functional groups occurring as chain ends (or as side groups) on the chains. This is to be expected, because of the relatively low incidence of dangling ends in such networks. As expected, the lowest values of the ultimate properties generally occur for the networks cured by radiation (UV light, high-energy electrons, and γ radiation). The peroxide-cured networks are generally intermediate to these two extremes, with the ultimate properties presumably depending on whether or not the free radicals generated by the peroxide are sufficiently reactive to cause some chain scission. Similar results were obtained for the maximum extensibility (Andrady *et al.*, 1981). These observations are at least semi-quantitative and certainly interesting, but are somewhat deficient in that information on the number of dangling ends in these networks is generally not available.

Such quantitative information has been obtained using the very specific chemical reactions used to form ideal elastomers, but now modified to prepare intentionally non-ideal networks containing known numbers and lengths of dangling-chain irregularities. This is illustrated in Figure 10.7 (Mark, 1990). If more chain ends are present than reactive groups on the end-linking molecules, then dangling ends will

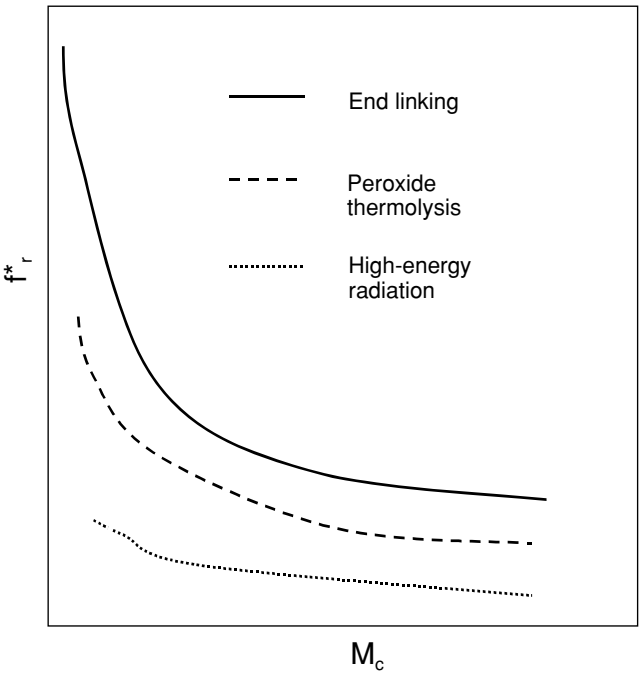

Figure 10.6 Values of the ultimate strength shown as a function of the molecular weight between cross links, for three cross-linking methods.

be produced and their number is directly determined by the extent of the stoichiometric imbalance. Their lengths, however, are of necessity the same as those of the elastically effective chains, as shown in Figure 10.7a. This constraint can be removed by separately preparing monofunctionally terminated chains of any desired lengths and attaching them as shown in Figure 10.7b.

Such more definitive results have in fact been obtained by investigation of a series of model networks prepared by end linking vinyl-terminated PDMS chains (Andrady *et al.*, 1981). The tetrafunctional end-linking agent was used in varying amounts smaller than that corresponding to a stoichiometric balance between its active hydrogen atoms and the chains' terminal vinyl groups. The ultimate properties of these networks, with known numbers of dangling ends, were then compared with those obtained on networks previously prepared so as to have negligible numbers of these irregularities (Andrady *et al.*, 1981). Values of the ultimate strength f_r^* of the networks containing the dangling ends were found to be lower than those of the more nearly perfect networks, with the largest differences occurring at high proportions of dangling ends (low $2C_1$), as expected (Andrady *et al.*, 1981). These results, shown schematically in Figure 10.8, thus confirmed the less definitive results shown in Figure 10.6. The values of the maximum extensibility showed a similar dependence, as expected.

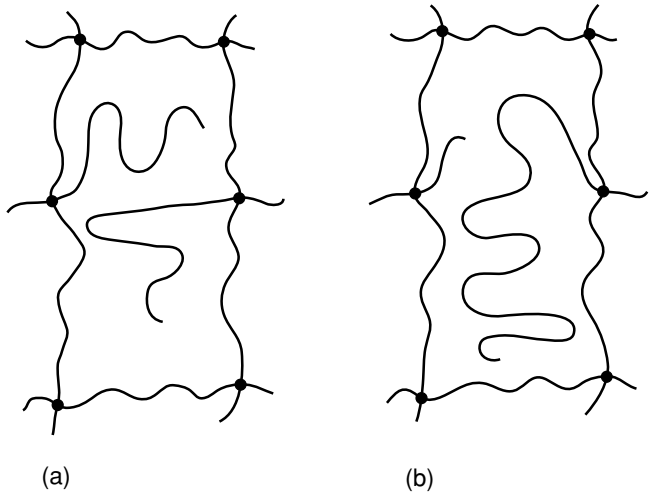

Figure 10.7 Two end-linking techniques for preparing networks with known numbers and lengths of dangling chains. In (a), the dangling chains are produced by having more chain ends than complementary groups on the end-linking agent, and in (b) by preparing some chains so as to have reactive groups on only one of the two chain ends.

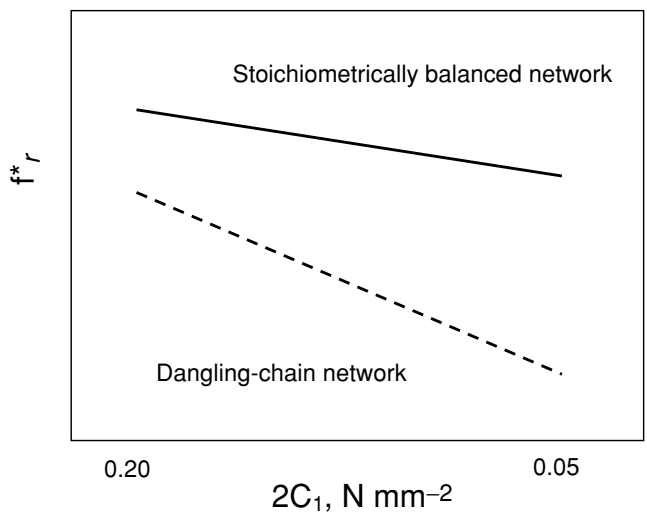

Figure 10.8 The ultimate strength shown as a function of the high deformation modulus for networks that either contain a negligible number of dangling ends (stoichiometrically balanced) or contain dangling ends introduced by using less than the stoichiometrically required amount of end-linking agent. In the latter case, decrease in $2C_1$ corresponds to increase in the number of dangling ends.

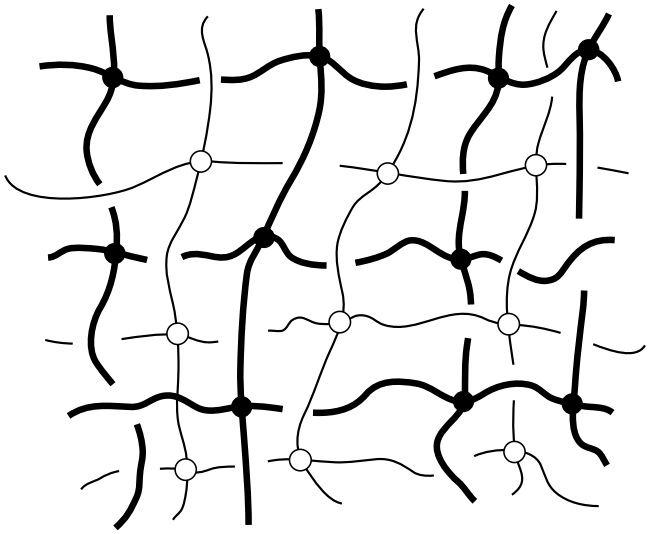

Figure 10.9 An interpenetrating network structure, in which one network is generated by a condensation end-linking reaction, and the other by an addition end-linking reaction (heavier lines). The two types of cross links are shown by the open and filled circles, respectively.

Interpenetrating networks

If two types of chains have different end groups, then it is possible to end link them simultaneously into two networks that *interpenetrate* one another (Sperling, 1981). Such a network could, for example, be made by reacting hydroxyl-terminated PDMS chains with tetraethoxysilane (in a condensation reaction), while reacting vinyl-terminated PDMS chains mixed into them, with a multifunctional silane (in an addition reaction) (Mark and Ning, 1985). This is illustrated in Figure 10.9. Interpenetrating networks can be very unusual with regard to both equilibrium and dynamic mechanical properties. For example, such materials can have considerable toughness and unusual damping characteristics.

Sorption and extraction of diluents

General approach

As illustrated by the above examples, the study of networks of controlled structures has provided considerable useful information leading to a better molecular understanding of the properties of elastomeric materials. The present application is different in that it involves swelling as the elastomeric deformation, and specifically addresses questions related to the rate at which diluent absorbs into a network of

known and controlled "pore size", and how rapidly it can subsequently be extracted (Mark and Zhang, 1983; Garrido and Mark; 1985, Mark, 1989). The rate of absorption or extraction can be used to estimate diffusion coefficients. Extraction efficiencies can be used to obtain information on the extents of reaction in the end-linking procedure used to form the network, and the degree to which the extractable chains are entangled with the network chains that impede their removal from within the network structure. Of obvious interest is the dependence of these quantities on the molecular weight M_c of the network chains (as a measure of pore size), the molecular weight M_d of the diluent, the structure of the diluent (linear, branched, or cyclic), and whether or not the diluent is present during the end-linking process.

Linear diluents

One way of obtaining a network swollen with diluent is to form the network in a first step, and then absorb an unreactive diluent into it. Alternatively, the same diluent can be mixed into the reactive chains prior to their being end linked into a network structure. In either case, oligomeric and polymeric diluents are of greatest interest, and they must be functionally inactive for them to "reptate" through the network rather than being bonded to it. Both types of networks can then be extracted to determine the ease with which the various diluents can be removed, as a function of M_d and M_c.

The ease with which a diluent could be removed from a network was found to decrease with increase in M_d and with decrease in M_c, as expected. High molecular weight diluents are extremely hard to remove at values of M_c of interest in the preparation of model networks, a circumstance complicating the analysis of soluble polymer fractions in terms of degrees of perfection of the network structure. The diluents added after the end linking were the more easily removed, possibly because they were less entangled with the network structure, and this could correspond to differences in chain conformations of the diluent.

Branched diluents

The extraction of diluents that are branched has considerable potential importance. For example, in the preparation of networks by radiation cross linking there are presumably large numbers of soluble molecules formed that are highly branched (because of the essentially uncontrolled formation and coupling of free-radical species) (Dole, 1973). Another example occurs in the area of controlled release of drugs from cross-linked reservoirs (Peppas and Langer, 1994). Some of the drugs diffusing out of such delivery systems are assuredly "non-linear", and the problems of understanding such diffusion are likely to become more important as interest

shifts to larger and larger molecules (such as polypeptides). Finally, it should be mentioned that molecules with long branches can greatly affect the flow characteristics of a polymer (Graessley, 1993), to the extent that they can be used as processing aids in polymeric systems that will subsequently be cross linked. The ultimate in branched systems, the "dendrimers" (Frechet, 1994; Tomalia, 1995; Grayson and Frechet, 2001; Tomalia and Frechet, 2002) should also find applications in network structures.

Polar diluents

There is a complication, however, which can occur in the case of networks of polar polymers at relatively high degrees of swelling (Yu and Mark, 1974, Mark *et al.*, 1984). The observation is that different solvents, at the same degree of swelling, can have significantly different effects on the elastic force. This is apparently due to a "specific solvent effect" on the unperturbed dimensions, which appear in the various molecular forms of the elastic equations of state. Although frequently observed in studies of the solution properties of uncross-linked polymers (Hoeve and O'Brien, 1963; Dondos and Benoit, 1971), the effect is not yet well understood. It is apparently partly due to the effect of the solvent's dielectric constant on the Coulombic interactions between parts of a chain, but probably also to solvent–polymer segment interactions that change the conformational preferences of the chain backbone (Yu and Mark, 1974).

Trapping of cyclics within network structures

Experimental results

If cyclic molecules are present during the end linking of chains, some of them will be trapped because of having been threaded by the linear chains prior to the latter being chemically bonded into the network structure (Garrido *et al.*, 1985a, b; Clarson *et al.*, 1986, 1987; Erman and Mark, 1997). This is illustrated in Figure 10.10. The fraction trapped is readily estimated from solvent extraction studies. Some typical results, in terms of the fraction trapped as a function of degree of polymerization of the cyclic are shown schematically in Figure 10.11 (DeBolt and Mark, 1987a, b). The results were found to be independent of the amount of time given for the cyclics and linear chains to intermingle (Clarson *et al.*, 1987), thus demonstrating the very high mobility of the PDMS chains. As expected, very small cyclics do not get trapped at all, but almost all of the largest cyclics do. The following section describes the interpretation of these results in terms of the configurational characteristics of PDMS chains.

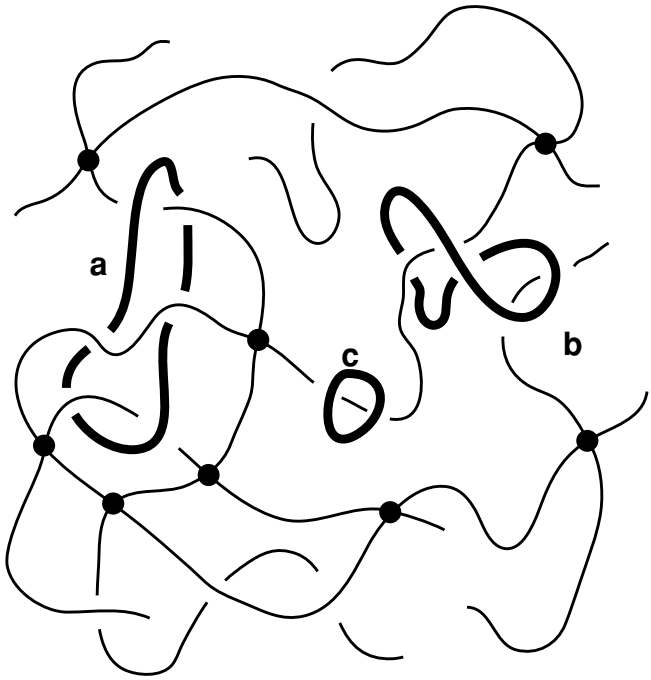

Figure 10.10 A tetrafunctional network containing cyclics (heavy lines). Cyclics a and b were trapped by linear chains that passed through them prior to their being end linked into a network structure.

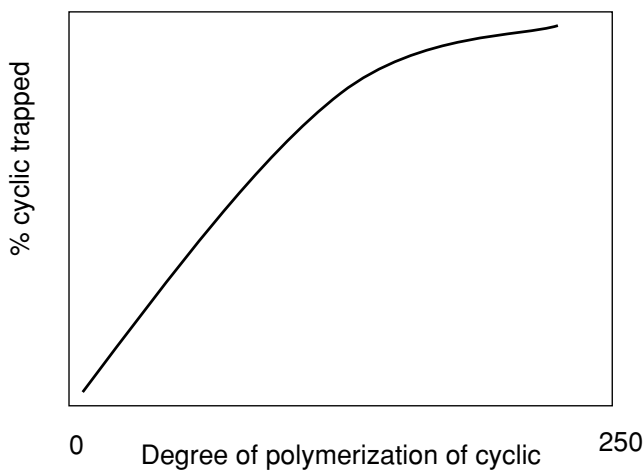

Figure 10.11 Trapping efficiencies for cyclics as a function of cyclic size.

These cyclics can change the properties of the network in which they are "incarcerated". Since they restrict to some extent the motions of the network chains, they should increase the modulus of an elastomer. Some small but possibly significant increases in low-deformation modulus have in fact been observed (Garrido *et al.*, 1985b). Also, when PDMS cyclics are trapped in a thermoplastic material, they can act as a plasticizer that is in a sense intermediate to the usual external (dissolved) and internal (copolymerized) varieties. Interesting changes in mechanical properties have been observed in materials of this type (Fyvie *et al.*, 1987; Huang *et al.*, 1990).

Theoretical interpretations

The trapping process has been simulated using Monte Carlo methods based on a rotational isomeric state model (Flory, 1969; Mattice and Suter, 1994; Rehahn *et al.*, 1997) for the cyclic chains (DeBolt and Mark, 1987a, b). The first step was generation of a sufficient number of cyclic chains having the known geometric features and conformational preferences, and the desired degree of polymerization. This was done for a large number of linear chains, using the methods of matrix multiplication standard to rotational isomeric state theory. Up to this point, the method is identical to that used to generate distribution functions for a non-Gaussian approach to rubberlike elasticity (Mark and Curro, 1983). In the present application, however, a chain having an end-to-end distance less than a threshold value was considered to be a cyclic. The coordinates of each "cyclic" chain thus generated were stored for detailed examination of the chain's configurational characteristics, in particular the size of the "hole" it would present to a threading linear chain. Of particular interest was the size of this hole in comparison with the known diameter, 7–8 Å, of the PDMS chain.

The trapping process was simulated using a torus centered around each repeat unit in the cyclic (DeBolt and Mark, 1987a, b). Any torus found to be "empty" was considered to provide a pathway for a chain of specified diameter to pass through, threading it and then "incarcerating" it once the end-linking process has been completed. The simulation results thus obtained gave a good representation of the experimental trapping efficiencies. It is also possible to interpret these experimental results in terms of a power law for the trapping probabilities and fractal cross sections for the PDMS chains (Galiatsatos and Eichinger, 1987).

Olympic networks

It may also be possible to use this technique to prepare networks having no cross links whatsoever (Rigbi and Mark, 1986). Mixing linear chains with large amounts

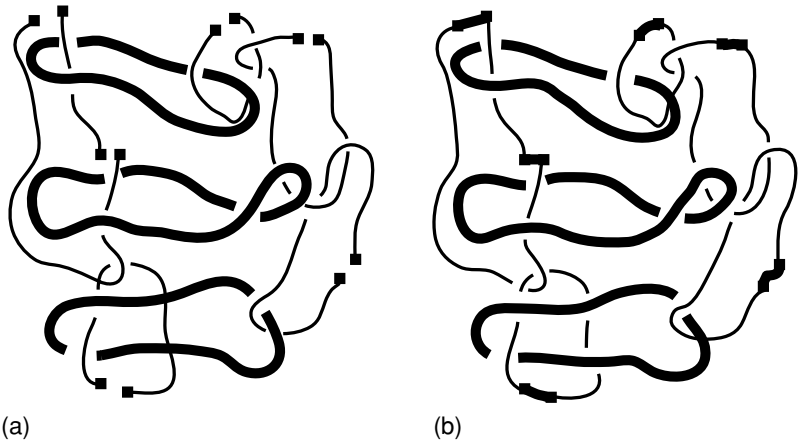

Figure 10.12 Preparation of a chain-mail or Olympic network that has no cross links at all. Linear chains (light lines) passing through the cyclics (heavy lines) in (a) are difunctionally end linked to form a series of interpenetrating cyclics in (b).

of cyclic and then *di*functionally end linking them could give sufficient cyclic interlinking to yield an "Olympic" or "chain-mail" network (de Gennes, 1979; Garrido *et al.*, 1985a). This is illustrated in Figure 10.12. Such materials would be very interesting topologically, and would be similar in some respects to the catenanes and rotaxanes that have long been of interest to a variety of scientists and mathematicians (Frisch and Wasserman, 1961; Gibson *et al.*, 1994; Gong and Gibson, 1997). Computer simulations (Iwata and Ohtsuki, 1993) could be particularly useful with regard to establishing the conditions most likely to produce these novel structures.

Part II

Additional topics

11

Networks prepared under unusual conditions

Introduction

As can be gathered from Chapter 10, it is very difficult to obtain information on the topology of a network. Some studies have therefore taken an indirect approach. Networks were prepared in a way that could be expected to simplify their topologies, and their properties were measured and interpreted in terms of reduced degrees of network chain entangling.

The two techniques employed involved separating the chains prior to their cross linking by either dissolution (Johnson and Mark, 1972) or stretching (Greene *et al.*, 1965). After the cross linking, the solvent is removed or the stretching force is relaxed, and the network is studied (unswollen) with regard to its stress–strain properties, typically in elongation.

Cross linking in solution

The preparation of networks by cross linking in solution followed by removal of the solvent (Erman and Mark, 1997) is shown schematically in Figure 11.1. Success in obtaining elastomers that had fewer entanglements was supported by the observation that such networks came to elastic equilibrium much more rapidly than elastomers cross linked in the dry state. Results of this type obtained on PDMS networks cross linked in solution by means of γ radiation are shown in Table 11.1 (Johnson and Mark, 1972, Mark *et al.*, 1984). Note the continual decrease in the time required to reach elastic equilibrium, t_{eq}, and in the extent of stress relaxation as measured by the ratio of equilibrium to initial values of $[f^*]$, upon decrease in the volume fraction of polymer present during the cross linking. These observations are qualitatively explained in Figure 11.2. When a network is cross linked in solution and the solvent then removed, the chains collapse in such a way that there is reduced overlap in their configurational domains. This reduces the type of chain-junction entangling embodied in the various constraint theories.

Table 11.1 *PDMS networks compared at approximately constant modulus*

v_{2S}[a]	t_{eq} (hr)	[f^*](equil)/[f^*](init)	$2C_2$ (N mm^{-2})
1.00	0.70	0.95	0.062
0.75	0.48	0.98	0.057
0.62	0.10	0.99	0.059
0.55	0.30	0.99	0.062
0.48	0.02	1.00	0.067
0.40	0.03	1.00	0.039
0.30	0.00	1.00	0.031

[a]Volume fraction of polymer in the solution being irradiated in the cross-linking reaction, which is generally somewhat larger than the volume fraction v_{2c} actually successfully incorporated in the gel.
Source: Johnson and Mark (1972); Mark *et al.* (1984). Reprinted with permission from J. E. Mark *et al.*, Eds., *Physical Properties of Polymers*. Copyright 1984 American Chemical Society.

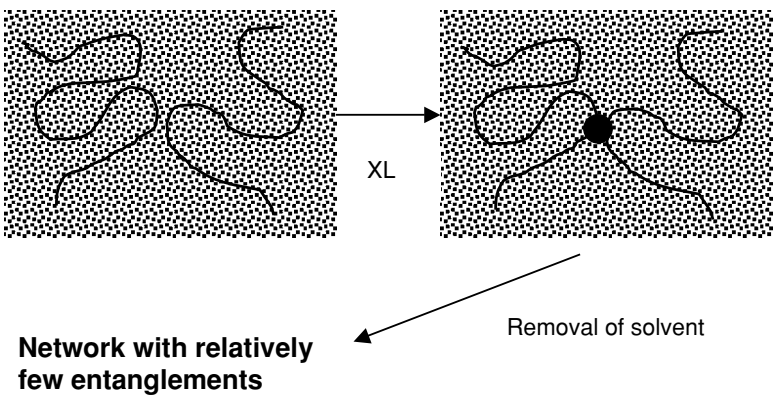

Figure 11.1 Cross linking in solution to prepare networks of simpler topology.

In terms of the constrained junction theory, described in Chapters 6 and 7, the constraint parameter κ is decreased. It is primarily in this regard – namely, decreased chain-cross-link entangling – that solution-cross-linked samples have simpler topologies. Specifically, the theory was found to give a good account of these results when the constraint parameter κ was decreased with decrease in volume fraction v_{2c} of polymer present during the cross linking (Erman, 1987). The values of κ obtained are within the range of values obtained in other comparisons of theory and experiment, as are the values of an additional, relatively unimportant heterogeneity parameter ζ (Flory and Erman, 1982). The values of κ generally

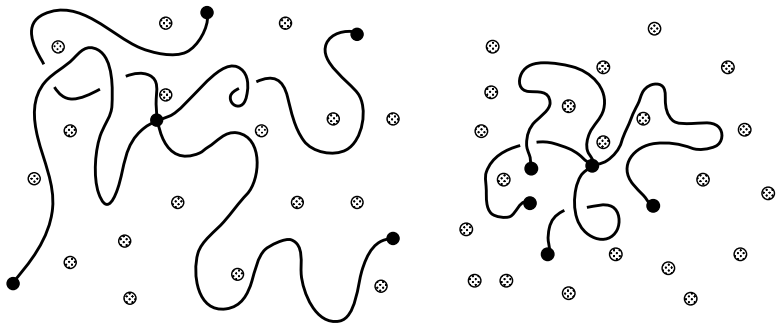

Figure 11.2 Typical configurations of four chains emanating from a tetrafunctional cross link in a polymer network. In the left sketch, the network had been prepared in the undiluted state, and in the right sketch, it had been prepared in solution and then dried.

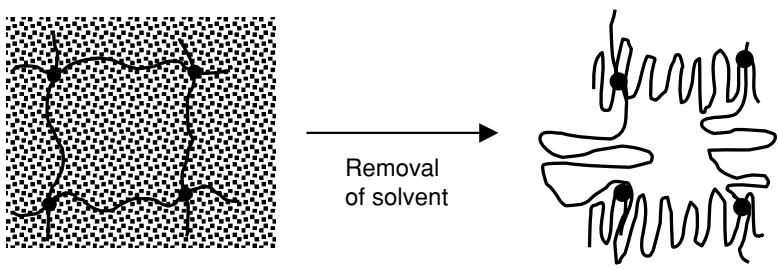

Figure 11.3 "Super-compression" of the network chains when a network formed in solution is dried.

decrease with decrease in the volume fraction v_{2c} of polymer present during the cross linking, and with increase in degree of cross linking as represented by the constant $2C_1$ (described in Chapter 7). The dependence of κ on v_{2c} is significantly stronger than that suggested by theory, however, indicating a particularly strong effect of dilution on the degree of network chain interpenetration.

These elastomers also exhibited stress–strain isotherms in elongation that were closer in form to those expected from the simplest molecular theories of rubber-like elasticity. Specifically, there were large decreases in the Mooney–Rivlin $2C_2$ correction constant described in Chapter 7.

In these procedures, removal of the solvent has the additional effect of putting the chains into a "supercontracted" state (Figure 11.3) (Erman and Mark, 1997). Experiments on strain-induced crystallization carried out on such solution-cross-linked elastomers indicated that the decreased entangling was less important than the supercontraction of the chains, in that crystallization required larger values of

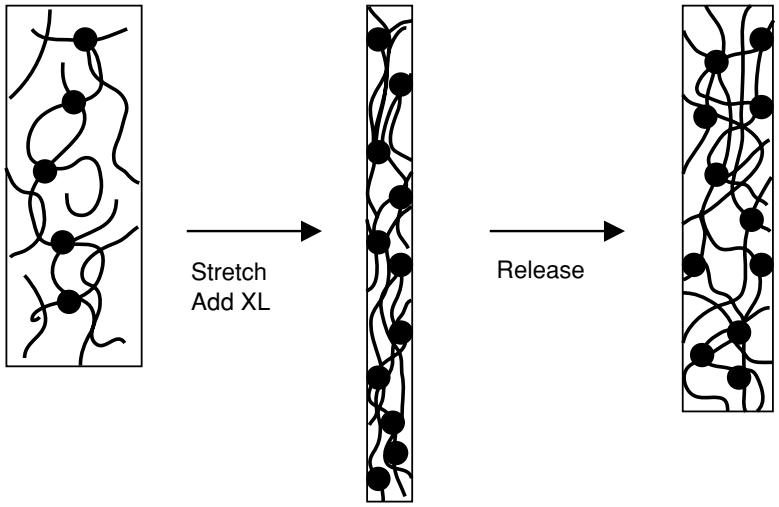

Figure 11.4 Cross linking in the elongated state to prepare networks of simpler topology.

the elongation than was the case for the usual elastomers cross linked in the dry state (Premachandra and Mark, 2002; Premachandra *et al.*, 2002). The most recent work in this area has focused on the unusually high extensibilities of such elastomers (Urayama and Kohjiya, 1997, 1998; Kohjiya *et al.*, 1997).

Cross linking in the deformed state

In this approach a first network is generally introduced in the undeformed state, the resulting elastomer is elongated, and a second network is introduced in the stretched state. Release of the stress permits the network to retract, but the second network of this "double-network" structure prevents retraction down to the original dimensions. This is illustrated in Figure 11.4. The most interesting feature of the retracted network is the fact that it is anisotropic in structure and properties.

In some cases, double networks have shown increases in orientability and strain-induced crystallization (Roland and Warzel, 1990), and improved fatigue resistance (Santangelo and Roland, 2003). In fact, some results show that there may be less of a compromise between failure properties in general and the modulus (Santangelo and Roland, 1994, 1995), which may be due in part to the decreased hysteresis observed for some of these elastomers (Wang *et al.*, 2005). There have even been reports of improved thermal stability (Aprem *et al.*, 2004), although it is hard to visualize how this would occur! Finally, electrical resistivities are found to be more sensitive to strain in carbon-black reinforced double networks (Roland and Peng, 1991). Better

molecular understandings of these observations are being sought with, for example, extensive studies of residual strains and birefringence (Mott and Roland, 2000).

Results such as those cited above have generally been obtained on double networks in the unswollen state. Very recent results, however, now indicate that swelling double networks gives gels that have extremely high mechanical strengths (Gong *et al.*, 2003; Na *et al.*, 2004) and fracture energies (Tanaka *et al.*, 2005).

12

Strain-induced crystallization and ultimate properties

Some general comments on crystallization

As already mentioned in Chapter 2, large amounts of crystallization in an undeformed network interfere with rubberlike behavior because they suppress the mobility of the network chains. They can also enhance the degree of intermolecular correlations. A relatively small number of very small crystallites present in an undeformed network are no problem, however, and can in fact function as temporary cross links, as described in Chapter 4.

Even better are polymers with melting points a little below room temperature, since these materials can undergo strain-induced crystallization at typical temperatures of utilization (Mark, 2004a, b). As mentioned in Chapter 2, this type of crystallization occurs because the melting point $T_m = \Delta H_m / \Delta S_m$ is elevated by the decrease in entropy of the stretched network chains. Specifically,

$$\Delta S_m = S_{amorp} - S_{cryst} \tag{12.1}$$

It is S_{amorp} that is decreased by the stretching, and, since $S_{cryst} = 0$ (at least for perfect order), ΔS_m is decreased as well, and T_m increases.

The elevation of the melting point of natural rubber with stretching is shown schematically in Figure 12.1 (Mark and Odian, 1984). The melting point of very carefully annealed natural rubber is as high as 28 °C, but under most conditions, the melting point T_m in the unstretched state is below room temperature. Thus unstretched natural rubber generally is totally amorphous at room temperature. Stretching a network of the polymer, however, increases T_m considerably. The extent to which it exceeds the test temperature (for example, room temperature) is called supercooling, as is illustrated in the figure. Crystallization now occurs (is "induced"), as is readily shown by X-ray diffraction and scattering measurements (Toki *et al.*, 2004, 2005; Trabelsi *et al.*, 2004), and by NMR spectroscopy (Lin *et al.*, 2004). Permitting the natural rubber to retract decreases T_m back to

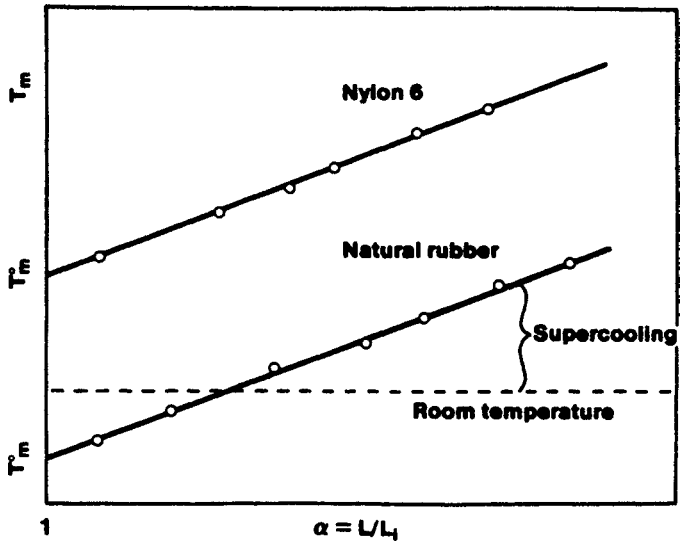

Figure 12.1 Comparison of strain-induced elevation of the melting point T_m^0 of an elastomer (natural rubber) and of a fiber (Nylon 6). A typical extent of supercooling relative to room temperature is indicated for the elastomer. (Reprinted with permission from J. E. Mark and G. Odian, Eds., *Polymer Chemistry*. Copyright 1984 American Chemical Society.)

T_m^0 and the crystallites melt since the melting point is again back below room temperature.

Rather different behavior is observed for a polymer (such as Nylon 6) having a melting point T_m^0 above room temperature. Stretching can now induce additional crystallization, but this crystallinity will persist even upon retraction of the polymer, as is also shown in the figure.

It should be mentioned that a type of "law of corresponding states" applies to this phenomenon. For example, if room temperature were somewhat lower (as, for example, on another planet), natural rubber would be very similar to Nylon 6 in that they would both be fibrous at this new ambient temperature. Similarly, if room temperature were much higher, then Nylon 6 would be very similar to natural rubber, in that under these conditions they would both be elastomers.

Strain-induced crystallization can reinforce an elastomer, as is described below. It is an advantage that natural rubber enjoys over silicone elastomers, which generally cannot exhibit strain-induced crystallization because of their very low melting points (~ -40 °C) in the undeformed state (Mark, 1996a, 1999b). There are now attempts to increase T_m of silicone-type elastomers by stiffening the chains. This is illustrated by the two silphenylene polymers shown in Figure 12.2. The *para* phenylene group shown in the upper portion of the figure is seen to have the larger stiffening effect, as expected: it causes the larger increase in glass transition

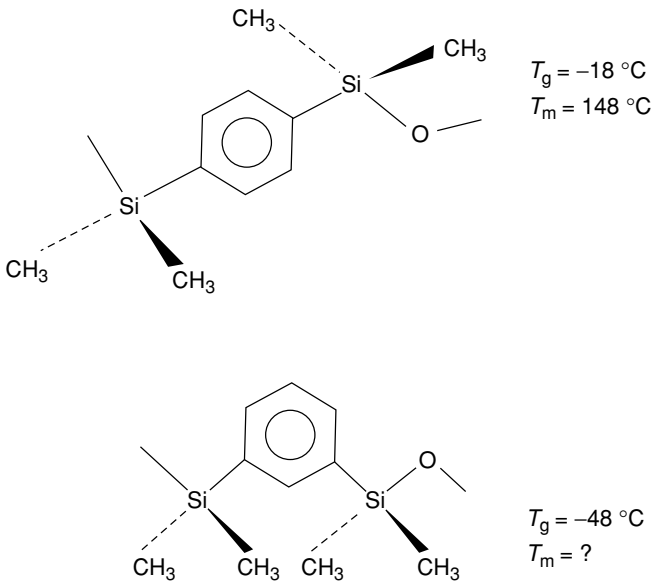

Figure 12.2 Structures, glass transition temperatures, and melting points of two silphenylene polymers. The upper portion shows the *para* structure, and the lower portion the *meta*.

temperature and increases the melting point to well above room temperature. No melting point has yet been reported for the *meta* polymer shown in the lower part of the figure, but it could well undergo strain-induced crystallization. In the area of elastomeric materials, this would make it much more important than the *para* polymer, which is obviously a thermoplastic at room temperature.

Upturns in the reduced stress at high elongations

As was already described in Figure 1.12, some (unfilled) networks show a large and rather abrupt increase in modulus at high elongations. This increase is further illustrated for natural rubber in the Mooney–Rivlin representation in Figure 12.3. This behavior is very important in a practical sense since it corresponds to a significant toughening of the elastomer. Its molecular origin, however, has been the source of considerable controversy. It has been widely attributed to the limited extensibility of the network chains, that is, to an inadequacy in the Gaussian distribution function (Treloar, 1975). This potential inadequacy is readily evident in the exponential in Eq. (5.1), specifically that this function does not assign a zero probability to a configuration unless its end-to-end separation r is infinite. This limited-extensibility explanation was viewed with skepticism by some workers since the increase in modulus was generally observed only in networks that could undergo strain-induced

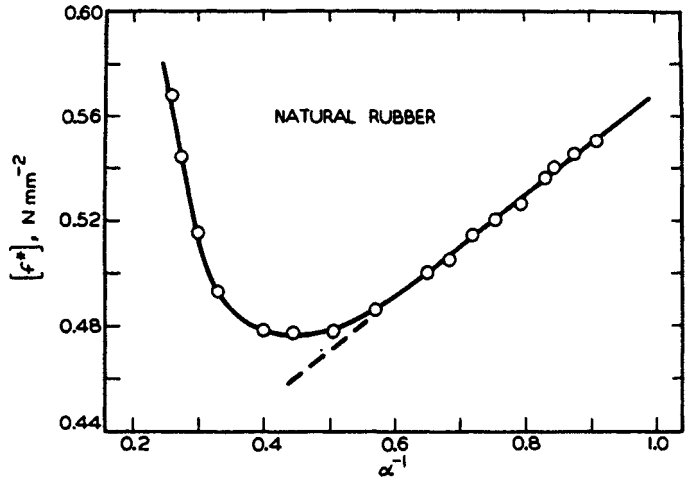

Figure 12.3 Stress–strain isotherm for an unfilled rubber network in the vicinity of room temperature showing the anomalous increase in modulus at high elongation (Mark, 1979d).

crystallization (Mark, 1979b, d). Such crystallization in itself could account for the increase in modulus, primarily because the crystallites thus formed would act as additional cross links in the network.

Attempts to clarify the problem by using non-crystallizable networks were not convincing since such networks were incapable of the large deformations required to distinguish between the two possible interpretations. The issue has now been resolved, however, by the use of end-linked, non-crystallizable model PDMS networks, as described in Chapter 10. These networks have high extensibilities, presumably because of their very low incidence of dangling-chain network irregularities (Mark, 2004a, b). They have particularly high extensibilities when they are prepared from a mixture of very short chains (around a few hundred g mol^{-1}) with relatively long chains (around 20 000 g mol^{-1}) (Mark, 2003c). Apparently the very short chains are important because of their limited extensibilities, and the relatively long chains are important because of their ability to retard the rupture process. As described in Chapter 13, these bimodal networks show upturns that are diminished by neither increase in temperature nor swelling. This non-Gaussian effect is therefore due to the limited extensibility of the network chains. Such results will be extremely useful for the reliable evaluation of the various non-Gaussian theories of rubberlike elasticity.

Crystallizable networks such as natural rubber show upturns that do diminish with increase in temperature or swelling. These upturns are obviously caused by strain-induced crystallization (Mark, 1979c, d). The crystallization is due to the elevation of the melting point by the decrease in the entropy of fusion, as described

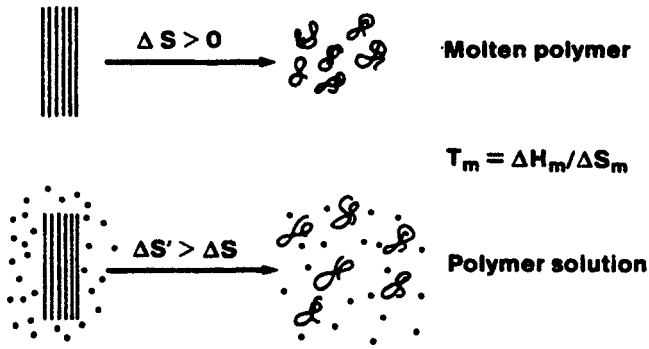

Figure 12.4 Sketch showing how the presence of a solvent (small circles) can reduce the melting point of a polymer. (Reprinted with permission from J. E. Mark and G. Odian, Eds., *Polymer Chemistry*. Copyright 1984 American Chemical Society.)

in this chapter and in Chapter 2. The increase in the melting point can be very substantial, with the elevated T_m frequently lying above the decomposition temperature of the polymer. The suppression of the upturn by the increase in temperature or presence of solvent is due to suppression of the crystallization. In the case of the increase in temperature, the effect is simply the melting of the crystallites. The solvent, on the other hand, has the indirect effect of lowering the melting point, as illustrated in Figure 12.4 for the simpler case of an uncross-linked polymer (Flory, 1953; Mark and Odian, 1984). When the polymer chains leave the crystalline lattice, they can further disorder themselves by mixing with the solvent. This increases ΔS of the process and thus decreases T_m.

Downturns in the reduced stress at high elongations

In the case of crystallizable networks, there is frequently a downturn in the reduced stress just prior to its upturn, as illustrated in Figure 12.5 (Mark, 1979c, d). Such decreases in the upturns with swelling are due to suppression of some of the strain-induced crystallization by the solvent, as already described. Also, the initiation of the strain-induced crystallization (as evidenced by departure of the isotherm from linearity) is facilitated by the presence of the low-molecular-weight diluent, presumably by increasing the mobility of the network chains. Thus, in a sense this kinetic effect acts in opposition to the thermodynamic effect, which is primarily the suppression of the polymer melting point by the diluent. The most interesting point has to do with the decrease in the modulus prior to its increase. As shown schematically in Figure 12.6 (Mark, 1979b), this is probably due to the fact that the crystallites are oriented along the direction of stretching (Figure 12.6a), and the chain sequences within a crystallite are in regular, highly extended conformations

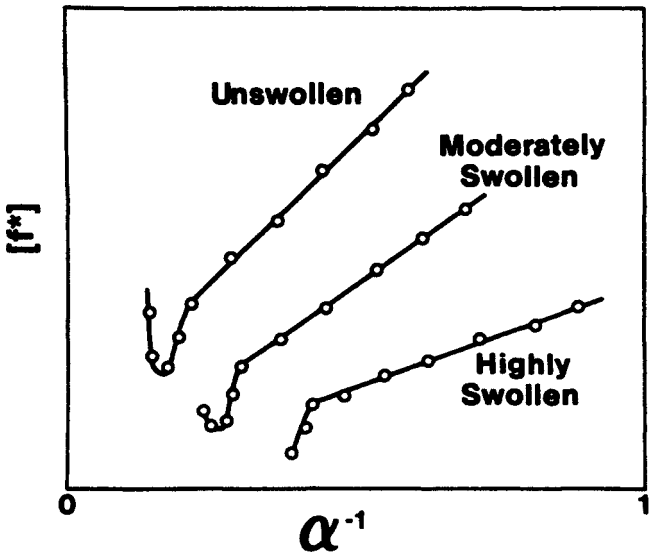

Figure 12.5 Stress–strain isotherms for a crystallizable network showing downturns in the reduced stress.

(Figure 12.6b). The straightening and aligning of portions of the network chains thus decrease the deformation in the remaining amorphous regions, with an accompanying decrease in the stress.

Ultimate properties

In this section we continue the discussion of unfilled elastomers at high elongations but emphasize ultimate properties, namely, the ultimate strength and maximum extensibility. Some illustrative results on the effects of strain-induced crystallization on ultimate properties are given for *cis*-1,4-polybutadiene in Table 12.1 (Su and Mark, 1977, Mark, 2004a, b). The higher the temperature, the lower the extent of crystallization and, correspondingly, the lower the ultimate properties. The effects of increase in swelling parallel those for increase in temperature, since diluent also suppresses network crystallization. For non-crystallizing networks, however, neither change is very important, as illustrated by the results shown for PDMS networks in Table 12.2 (Chiu and Mark, 1977, Mark, 2004a, b).

Crystallization in other deformations

Little has been done to investigate strain-induced crystallization in deformations other than simple elongation. Measurements in shear do show upturns in modulus similar to those in elongation, but the upturns are less pronounced, suggesting lower degrees of crystallinity (H. Sun, R. Patil and J. E. Mark, 2005, unpublished). In the

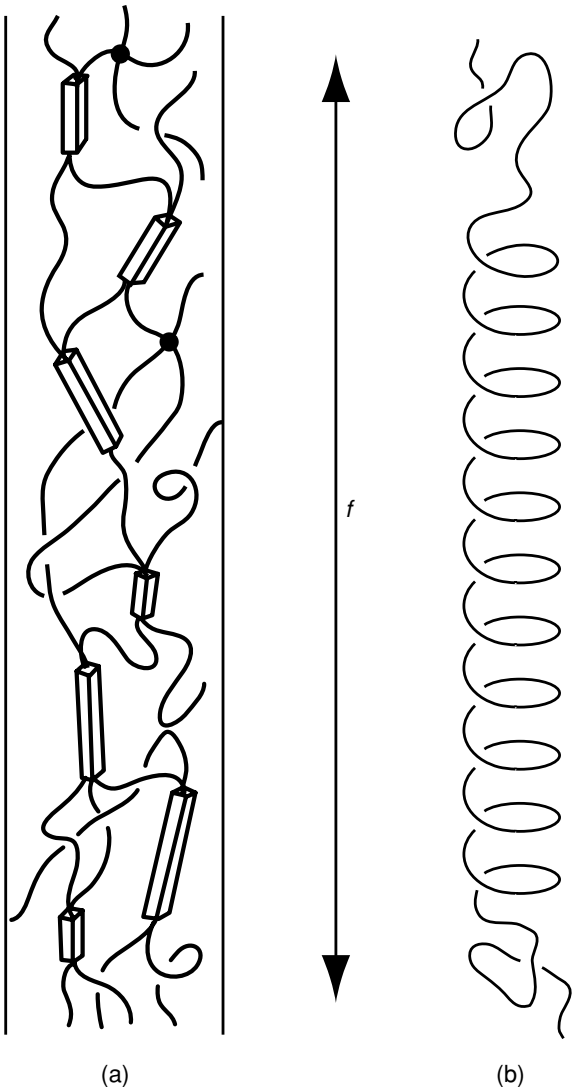

Figure 12.6 Strain-induced crystallization in a polymer network that has been elongated by a force along the vertical direction. (a) Strain-induced crystallites, oriented preferentially along the fiber direction; (b) the straightening out of a portion of one of the network chains because of the crystallization. (Reprinted with permission from Mark (1979d). Copyright 1979, American Chemical Society.)

case of torsion, upturns have not been observed, but it is not known whether this is due to failure to reach sufficiently high deformations or to some fundamental differences in this type of deformation. As was mentioned in Chapter 1, unusual crystallization effects might occur in torsion, because of the non-uniform strain field and orientations of the chains in the cylinder being twisted around its axis.

Table 12.1 *Ultimate properties for crystallizable* cis-*1,4-polybutadiene networks*

		Ultimate properties	
T (°C)	α at upturn	Max upturn in [f^*] (%)	α at rupture
5	3.27	54.2	6.64
10	3.48	30.1	6.22
25	4.03	4.3	5.85
40	—	0.0	5.68

Source: Chiu and Mark (1977); Mark (2004a, b)

Table 12.2 *Ultimate properties for non-crystallizing PDMS networks*

v_2	λ_r	$[f^*]_r$ (N mm^{-2})
1.00	4.90	0.0362
0.80	4.42	0.0342
0.60	4.12	0.0338
0.40	4.16	0.0336

Source: Chiu and Mark (1977); Mark (2004a, b)

One might expect, for example, that the crystallites would have unusual tangential orientations, with the degree of crystallinity a maximum at the surface of the cylinder and a minimum close to the deformation axis.

Crystallization in biaxial extension would also have some novel aspects. In the case of the equi-biaxial case, the deformation can be imposed by the inflation of a sheet of the elastomer. If this is viewed as a two-step process, then the first step would be stretching the chains by simple elongation, and this would clearly decrease their entropies in the usual manner. The second step would then involve stretching the sheet in the perpendicular direction. It is not obvious whether the more important effect is generally the possible additional stretching out of the chains (an entropy decrease) or the randomizing of the directions of the end-to-end vectors (an entropy increase).

It is easier to make the above ideas more quantitative and relevant to experiments by considering the deformations in the two directions to occur simultaneously. In the unusual aspect of this deformation, the network chain vectors would undergo a large decrease in magnitude along the direction of the film thickness, as illustrated

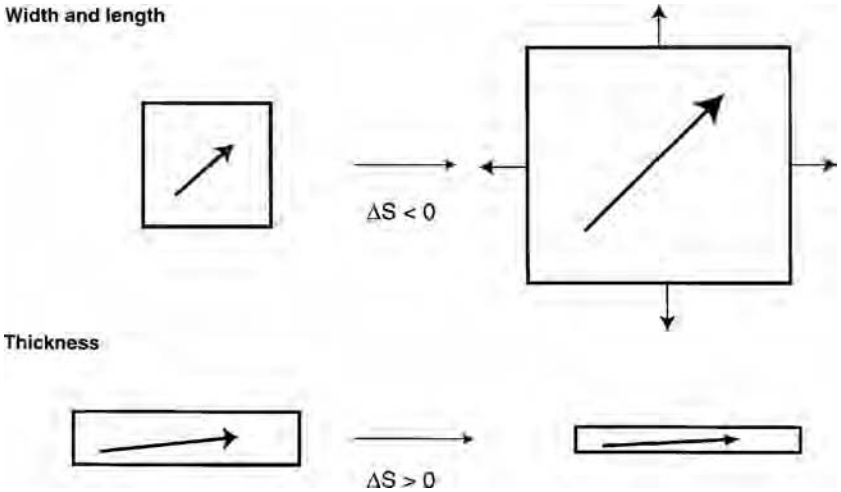

Figure 12.7 End-to-end network chain vectors in equi-biaxial deformations.

in the lower part of Figure 12.7. The corresponding increase in entropy could be easily overcome by the decrease in the other two directions, illustrated in the upper portion of the figure, but the mechanism of the resulting crystallization is not understood at all. The segments within the plane of the elastomeric film would undergo a pure dilation, with the angle between the two segments being unchanged by the equi-biaxial deformation. Thus, the chains would not be aligned, and there would be isotropy within the plane of the film. As a result, the usual birefringence measurements used to characterize uniaxially stretched materials would be of little utility. Such random crystallite orientations are illustrated in Figure 12.8.

Some simulations on crystallinity

There is now considerable interest in using simulations for characterizing crystallization in copolymeric materials. Of particular interest is a model capable of simulating chain ordering in copolymers composed of two comonomers, at least one of which is crystallizable (Hanna and Windle, 1988). Typically, the chains are placed in parallel, two-dimensional arrangements. Neighboring chains are then searched for like-sequence matches in order to estimate extents of crystallinity. Chains stacked in arbitrary registrations are taken to model quenched samples. Annealed samples, on the other hand, are modeled by sliding the chains past one another longitudinally to search for the largest possible matching densities (Mark, 2003a). The longitudinal movement of the chains relative to one another, out of register, approximately models the lateral searching of sequences in copolymeric chains during annealing (Mark, 2001a; Madkour and Mark, 2002).

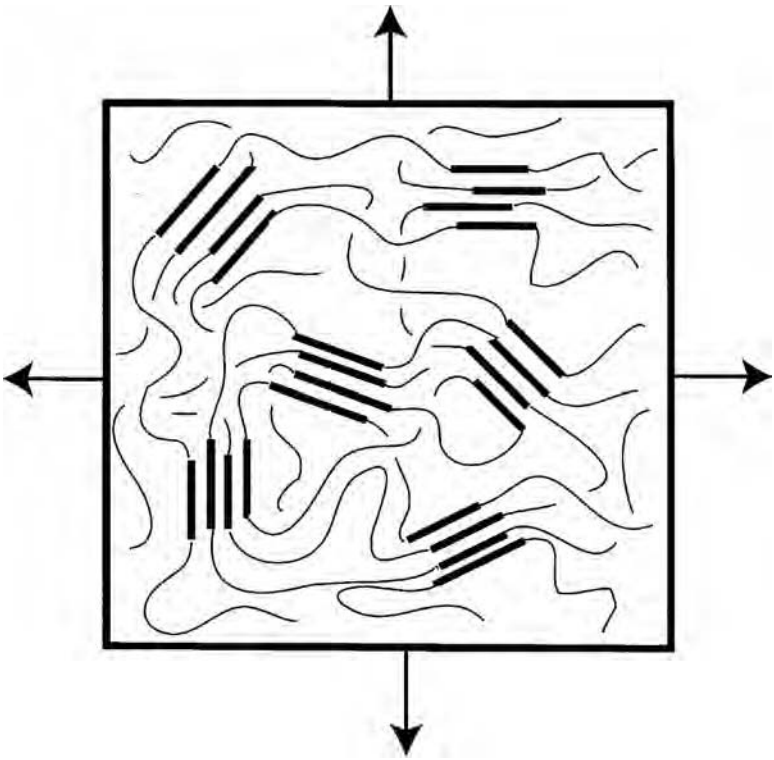

Figure 12.8 Random crystallite orientations in equi-biaxial deformations.

Two examples of elastomers studied by such simulations are poly (diphenylsiloxane-co-dimethylsiloxane) (Madkour and Mark, 1994a, b, Madkour *et al.*, 1994), and thermoplastic polypropylene (Madkour and Mark, 2002).

Statistical theory of strain-induced crystallization

The basic features of the statistical theory of strain-induced crystallization have been given by Flory (1947). The treatment is based on several simplifying assumptions and is therefore of a qualitative nature, in contrast to refined theories of the amorphous state. The assumptions and approximations of Flory's formulation are:

1. Crystallization is assumed to occur in a state of equilibrium. Such a state is reached experimentally, for example, by stretching the network at high temperature to a fixed length and subsequently decreasing the temperature to obtain crystallization. Most experiments on strain-induced crystallization are carried out at non-equilibrium conditions, where crystallization occurs while stretching.

2. Entropy changes associated with the formation of crystal nuclei are assumed to be negligible.
3. Crystallites are assumed to be oriented parallel to the axis of elongation. This assumption has subsequently been relaxed in a more refined treatment (Allegra, 1980) in which crystallites are taken to form parallel to the end-to-end vector of each chain.
4. Chain folding is disregarded and each chain is assumed to traverse the crystallite only once, in the sense of direction of increasing chain vectors. This assumption was removed later (Smith, 1976) by permitting a chain to enter a crystallite in either direction. Chain folding has also been considered explicitly by Gaylord (1976).
5. Chains are assumed to be Gaussian.

The theory developed under these assumptions (Flory, 1947) is applicable only under conditions of incipient crystallization. It gives explicit expressions for the degree of crystallinity and the incipient crystallization temperature as functions of the extension ratio, and for the applied force as a function of the extension ratio and the degree of crystallization. These relations are:

1. The fractional degree of crystallization ψ:

$$\Psi = \left[\frac{\frac{3}{2} - \phi(\alpha)}{\frac{3}{2} - \theta} \right]^{1/2} \tag{12.2}$$

where α is the extension ratio in simple tension, and

$$\phi(\alpha) = \frac{2\alpha\beta l}{\pi^{1/2}} - \frac{\alpha^2/2 + 1/\alpha}{n} \tag{12.3}$$

$$\theta = (h_\mathrm{f}/R)\left(1/T_\mathrm{m}^0 - 1/T\right) \tag{12.4}$$

Here, n is the number of segments in a freely jointed chain, l is the segment length, and $\beta = (3/2n)^{1/2}l$. The quantity h_f is the heat of fusion per segment, R is the gas constant, and T_m^0 is the incipient crystallization temperature for the undeformed polymer.

2. The incipient crystallization temperature T_m of the stretched network:

$$1/T_\mathrm{m} = 1/T_\mathrm{m}^0 - (R/h_\mathrm{f})\phi(\alpha) \tag{12.5}$$

3. The applied force, f^*:

$$f^* = \frac{nkT}{V_0} \frac{(\alpha - \alpha^{-2}) - (6n/\pi)^{3/2}\psi}{1 - \psi} \tag{12.6}$$

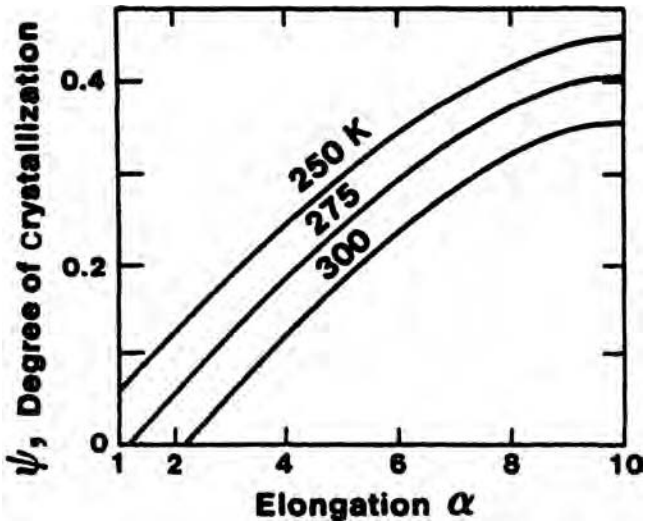

Figure 12.9 Degree of crystallization ψ at equilibrium as a function of elongation at the three temperatures indicated (Flory, 1947).

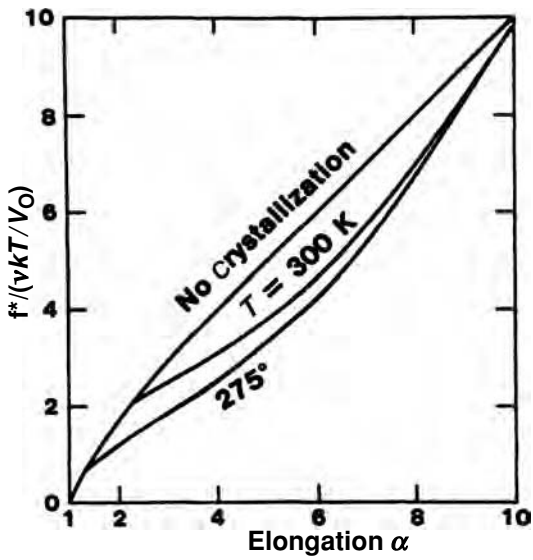

Figure 12.10 Stress–strain curves without crystallization and with equilibrium crystallization at the two temperatures indicated (Flory, 1947).

The relationship of the degree of crystallinity to the extension ratio given by Eq. (12.2) is shown in Figure 12.9 for three temperatures, and for $n = 50$, $h_f = 600R$, and $T_m^0 = 250$ K. The failure of the $T = T_m^0 = 250$ K curve to reach zero crystallinity at $\alpha = 1$ results from the simplifying assumptions on which the theory is based.

The relationship of the dimensionless ratio $f^*/(\nu kT/V_0)$ to α obtained from Eq. (12.6) is depicted in Figure 12.10. The parameters used are the same as those for Figure 12.9. The decrease in force under equilibrium crystallization predicted by Eq. (12.6) and shown in Figure 12.9 may be identified with the downturns exhibited by the experimental data of Figure 12.5.

13

Multimodal networks

Introduction

The main purpose of this chapter is to illustrate how manipulating the distribution of network chain lengths in an elastomer can give large improvements in its mechanical properties. This approach is very novel in that the effect of network chain-length distribution (Flory, 1953; Treloar, 1975) is one aspect of rubberlike elasticity that has not been studied very much until recently. There are two primary reasons for this lack of attention. On the experimental side, the cross-linking techniques traditionally used to prepare the required network structures have been random, uncontrolled processes (Flory, 1953; Treloar, 1975; Erman and Mark, 1997). The resulting network chain-length distributions are unimodal and probably very broad. On the theoretical side, it has turned out to be convenient, and even necessary, to assume a distribution of chain lengths that is not only unimodal, but *monodisperse* (Flory, 1953; Treloar, 1975; Erman and Mark, 1997)!

There are a number of reasons for developing techniques for determining or, even better, controlling network chain-length distributions. One is to check the "weakest-link" theory (Bueche, 1962) for elastomer rupture, which states that a typical elastomeric network consists of chains with a broad distribution of lengths, and that the shortest of these chains are the "culprits" in causing rupture. This is attributed to the very limited extensibility associated with their shortness, which is thought to cause these chains to break at relatively small deformations and then act as rupture nuclei.

The preparation of such networks of controlled structures obviously requires special cross-linking reactions, such as those described in Chapters 4 and 10. One of the most important networks of this type consists of those having unusual *distributions* of the chain lengths. The most novel elastomer of this type has a *multimodal* distribution of network chain lengths. In the *bimodal* case, it consists of a combination of unusually short network chains (molecular weights of a few hundred) and the much

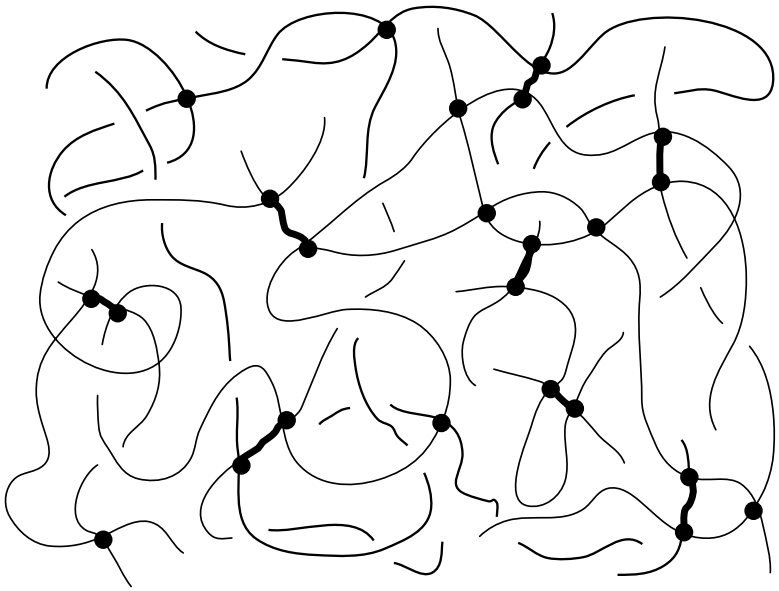

Figure 13.1 A network having a bimodal distribution of network chain lengths. The short chains are arbitrarily shown by heavier lines than the long chains, and the dots represent the cross links, typically resulting from the end linking of functionally terminated chains.

longer chains typically associated with elastomeric behavior (molecular weights of ten or twenty thousand). Such a network is sketched in Figure 13.1. Another use of elastomers having such a bimodal distribution is to clarify the dependence of ultimate properties on non-Gaussian effects arising from limited-chain extensibility. Yet another is to seek synergistic effects that might maximize the ultimate properties of an elastomer. The following parts of the chapter provide more detail on these applications, and on others as well.

Bimodal networks

"Bimodal" elastomers prepared by these end-linking techniques have very good ultimate properties, and for this reason there is currently much interest in preparing and characterizing such materials (Erman and Mark, 1997; Mark, 1999a, 2003d, 2004a), and there have been several patents in the area (Jeram and Striker, 1976; Lee *et al.*, 1979; Galiatsatos and Subramanian, 1994). In addition to this experimental work, there are now theoretical studies addressing the novel mechanical properties of bimodal elastomers (Erman and Mark, 1988; Termonia, 1990; Kloczkowski *et al.*, 1991; Sakrak *et al.*, 1994; Vasilevskaya and Semenov, 1994; Bahar *et al.*, 1995; Hagn *et al.*, 1997; Sotta, 1998; von Lockette and Arruda, 1999).

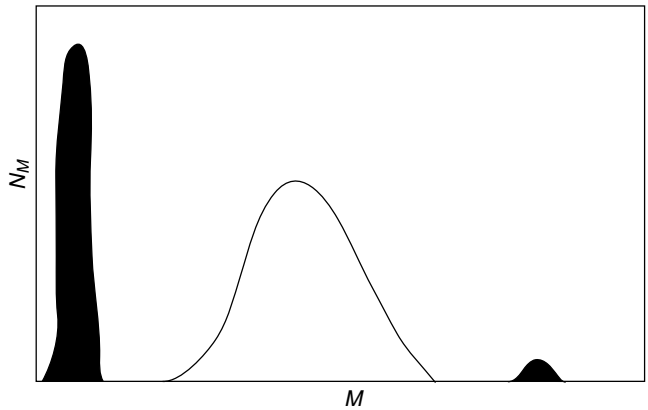

Figure 13.2 Network chain-length distributions, in which N_M is the number of chains in an infinitesimal interval around the specified value of the molecular weight M. For reference purposes, a unimodal distribution is shown between the two parts of the bimodal distribution.

Materials and synthetic techniques

Most bimodal networks synthesized to date have been prepared from poly (dimethylsiloxane) (PDMS) [–$Si(CH_3)_2O$–] (Mark, 1999a, 2003d). One reason for this choice is the fact that the polymer is readily available with either hydroxyl or vinyl end groups, and the reactions these groups participate in are relatively free of complicating side reactions. The end-linking reactions have generally involved hydroxyl-terminated chains, which are readily obtained from the usual ring-opening polymerizations of the corresponding cyclic trimer or tetramer (Clarson and Mark, 1993). The ends of the chains are reacted with the alkoxy groups in a multifunctional organosilicate, as described in Chapters 4 and 10. In the application of interest here, a mixture of two hydroxyl-terminated polymers is being cross linked, one consisting of very short chains and the other of much longer chains. An alternative approach involves the addition reaction between vinyl groups at the ends of a polymer chain and the active hydrogen atoms on silicon atoms in the [$Si(CH_3)HO$-] repeat units in an oligomeric poly(methyl hydrogen siloxane). These ideas can obviously be extended to higher modalities (trimodal, etc.)

The distribution of network chain lengths in a bimodal elastomer can be extremely unusual, and much different from the usual unimodal distribution obtained in less-controlled methods of cross linking. Figure 13.2 shows a schematic distribution for the important example in which there is simultaneously a large number percentage of short chains and a large weight percentage of long chains. The major difference is the significant numbers of both very short chains and very long chains in the bimodal network, which contrasts sharply with the *small* amounts

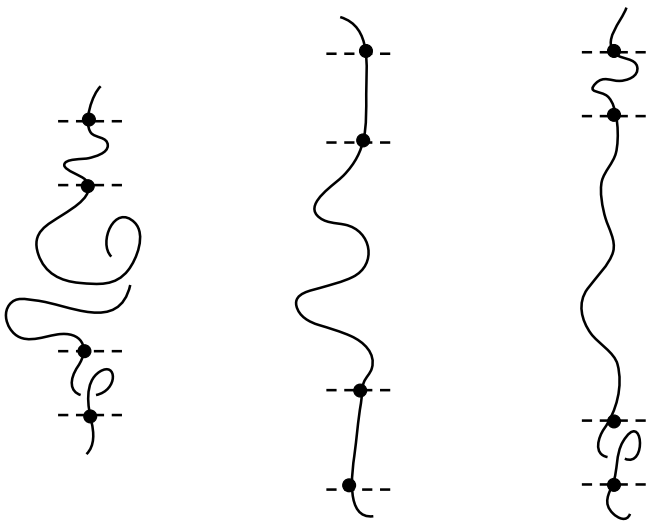

Figure 13.3 The effect of deformation on an idealized network segment consisting of a relatively long chain bracketed by two very short chains. The left sketch shows the undeformed segment, and the middle and right sketches show the segment deformed affinely and non-affinely, respectively.

of such chains in a typical unimodal distribution. The case shown here, where the short chains predominate numerically, is of particular interest with regard to improvements in mechanical properties (Erman and Mark, 1997). Obviously, such peculiar distributions can be obtained only by carefully controlled techniques such as the end-linking reactions being described. One of their uses has been to test the molecular description of elastomer rupture, as described in the following section.

Testing of the weakest-link theory

The weakest-link theory (Bueche, 1962) was tested by preparing end-linked networks containing increasing amounts of short chains, the order of 10–20 mol% (Mark, 1979a; Erman and Mark, 1997). Remarkably, these elastomers showed no significant decreases in ultimate properties with these increases in the numbers of short chains, in striking disagreement with the suggested mode of elastomer failure. Networks are apparently much more resourceful than given credit for in this theory. Apparently, the strain is continually being reapportioned during the deformation, in such a way that the much more easily deformed long chains bear most of the burden of the deformation. This is illustrated in Figure 13.3. Thus, the short chains do not contribute significantly until just prior to rupture. This is consistent with Nature preferring the low-energy route, unless overruled by entropy increases. The flaw in the weakest-link theory is thus the implicit assumption that all parts of the

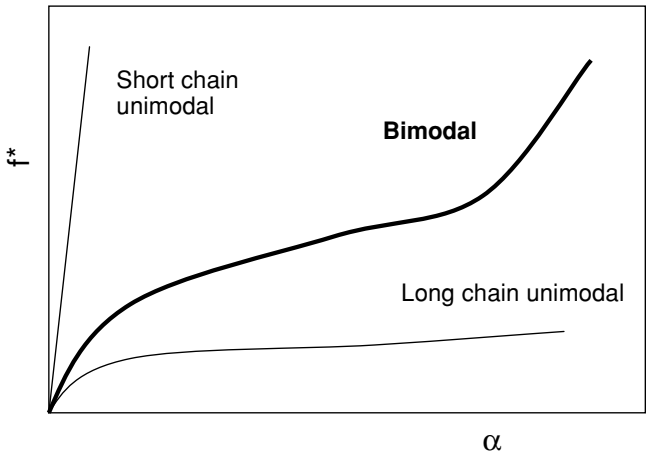

Figure 13.4 Typical dependence of nominal stress against elongation for two unimodal networks having either all short chains or all long chains, and a bimodal network having some of both.

network deform in exactly the same way, i.e., "affinely", whereas the deformation is markedly non-affine (Erman and Mark, 1997).

The weakest-link issue having been resolved, it became of interest to see what would happen in the case of bimodal networks having such overwhelming numbers of short chains that they cannot be ignored in the network's response. As already mentioned, there turns out to be an exciting bonus if one does put a very large number of short chains into the bimodal network. Specifically, there is a synergistic effect leading to mechanical properties that are better than those obtainable from the usual unimodal distribution! These results are the focus of most of the remaining parts of this chapter.

Elongation results

The great majority of studies of mechanical properties of bimodal elastomers of any type have been carried out in elongation, because of the simplicity of this type of deformation. There are a smaller number of studies using types of deformation other than elongation, for example, equi-biaxial extension (compression), shear, and torsion. Some typical studies of this type are also discussed later in this chapter.

In the case of the bimodal elastomers, many of the stress–strain isotherms in elongation were obtained on PDMS elastomers in the vicinity of 25 °C, a temperature sufficiently high to suppress strain-induced crystallization. The results thus determined were of considerable interest since they indicated that the bimodal nature of the distribution greatly *improved* the ultimate properties of the elastomer (Mark, 1999a, 2003d). This is illustrated schematically in Figure 13.4, in which

the area under the stress–strain isotherm up to the point of failure corresponds to the energy required for rupture. If the network consists entirely of the short-chain component, then it is brittle (which means that the maximum extensibility is very small). Similarly, if the network consists of only the long-chain component, its ultimate strength is very low. As a result, neither type of unimodal material has a large area under its stress–strain curve and, thus, neither is a tough elastomer. As can readily be seen from the figure, the bimodal networks are much-improved elastomers in that they can have a high ultimate strength without the usual diminished maximum extensibility. This corresponds to high values of the energy required for rupture, which makes them unusually tough elastomers, even in the unfilled state. Apparently, the short chains act primarily to increase the ultimate strength through their limited deformability, while the long chains somehow thwart the spread of rupture nuclei that would otherwise lead to catastrophic failure. If true, this could be analogous to what executives like to call a "delegation of responsibilities". Related improvements in mechanical properties have also been reported for other bimodal materials, for example, polyurethane elastomers (Kim *et al.*, 1986).

It should be pointed out that there are three requirements for obtaining these improvements. The first is that the ratio M_S/M_L of molecular weights of the short and long chains be very small (i.e., that their molecular weights be very different). The second is that the short chains be as short as possible, for example as low as 200 g/mol. Finally, there should be a large *number* concentration of the short chains, typically around 95 mol%.

Since this internally generated improvement in properties is of considerable practical and fundamental interest, a number of studies on PDMS elastomers were carried out to determine its dependence on the molecular weights of the short chains, the proportions of short and long chains, and cross-link functionality (Mark, 1999a, 2003d). For example, the ultimate strength was found to go through a maximum with increase in the amount of short chains, frequently in the vicinity of 95 mol% short chains. Too low a concentration of short chains does not take full advantage of the approach, and too many may begin to make the elastomer brittle. These results are important in that they can be used to optimize improvements in mechanical properties.

The syntheses and properties of several additional types of bimodal networks were also investigated. The first of these involves pre-reacting the short chains prior to incorporating the long ones in the bimodal structure (Mark and Andrady, 1981). This makes the resulting network spatially as well as compositionally heterogeneous, in that many of the short chains will be segregated into densely cross-linked domains which are only lightly cross linked to other such domains (Mark and Andrady, 1981). These networks could serve as models for inhomogeneously

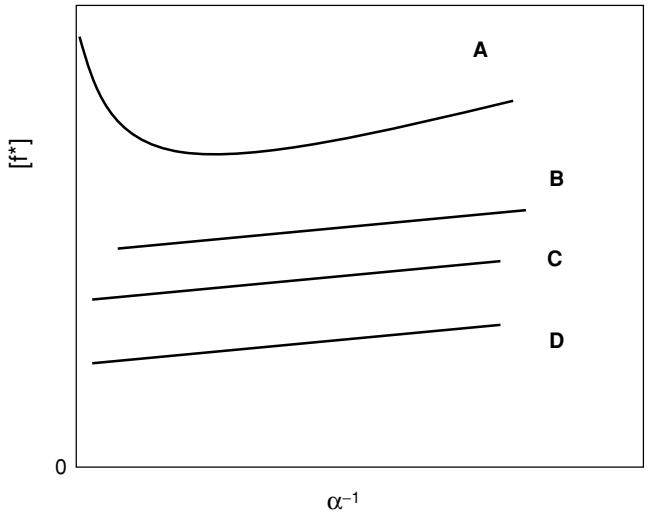

Figure 13.5 Schematic stress–strain isotherms in elongation for a unimodal elastomer, in the Mooney–Rivlin representation. The top three are for a crystallizable network: curve A for a relatively low temperature, B for an increased temperature, and C for the introduction of a swelling diluent. Isotherm D is for an unswollen unimodal network that is inherently non-crystallizable.

cross-linked elastomers, for example those cured by thermolysis of a partially immiscible peroxide. Another type is based on the fact that the condensation and addition types of end-linking reactions can be carried out simultaneously and independently. This can give rise to the interpenetrating network structure (Erman and Mark, 1997). The distribution of network chains can obviously be made bimodal, even though the short chains and long chains communicate only through their entanglements. Finally, it is also possible to reinforce any type of bimodal network with filler particles, thereby further improving its mechanical properties (Erman and Mark, 1997).

Measurements of the mechanical and optical properties of these networks as a function of temperature and degree of swelling were used to test further the conclusion cited above that crystallization or other intermolecular organization was not the origin of the improved properties (Erman and Mark, 1997; Mark, 1999a, 2003d). For example, stress–strain measurements on such bimodal PDMS networks exhibited upturns in modulus which were much less pronounced than those in crystallizable polymer networks such as natural rubber or *cis*-1,4-polybutadiene. The upturns in the case of a crystallizable elastomer are illustrated in the top portion of Figure 13.5. They decrease or disappear upon either an increase in temperature or addition of a diluent, as shown by two of the additional isotherms. Also illustrated

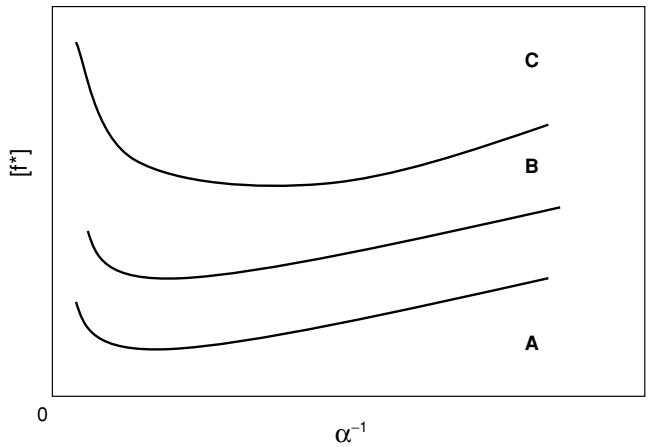

Figure 13.6 Schematic isotherms for a non-crystallizable bimodal network: curve A for a relatively low temperature, B for an increased temperature, and C for the introduction of a swelling diluent.

is the fact that upturns due to crystallization are of course also absent in the case of an elastomer that is inherently non-crystallizable, such as a stereoirregular acrylate. In related experiments, temperature was found to have little effect on the Mooney–Rivlin isotherms for bimodal networks of (non-crystallizing) PDMS, as would be expected in the case of the present explanation in terms of limited chain extensibility. This is shown by the lower two isotherms in Figure 13.6. Also, stress–temperature ("thermoelastic") and birefringence–temperature measurements showed no discontinuities or discernible changes of slope. Rather strikingly, swelling can even make the upturns in modulus *more pronounced* (Andrady *et al.*, 1980; Mark *et al.*, 1993). This is also shown schematically by the upper isotherm in Figure 13.6. Apparently, the enhanced upturns are due to the chains being stretched out in the solvent dilation process, prior to their being stretched further in the elongation experiments. In contrast, as already mentioned, the upturns in crystallizable polymer networks *disappear* upon sufficient swelling. A final experiment of relevance concerns the spatially heterogeneous PDMS networks mentioned in which the short chains are clustered. If the upturns in modulus had been due to some type of intermolecular organization such as crystallization, then it would presumably have been affected by this change in spatial heterogeneity. Instead, there was no discernible effect on the measured elastomeric properties.

The above findings argue against the presence of any crystallization or other type of intermolecular ordering, and the upturns thus seem to be intramolecular in origin. The observed increases in modulus and ultimate strength therefore have to be due to the limited extensibility of the very short network chains. In qualitative terms, the

chains soon exhaust their spatial configurations, their entropies plummet, and the elastic force rises correspondingly. It is possible to characterize this non-Gaussian limited extensibility more quantitatively in a number of ways, some of which are described below.

The first involves the interpretation of limited chain extensibility in terms of the configurational characteristics of the PDMS chains making up the network structure (Mark *et al.*, 1993). The first important characteristic of limited chain extensibility is the elongation at which the increase in modulus first becomes discernible. The values obtained indicate that the upturn in modulus generally begins at approximately 60–70% of maximum chain extensibility (Mark *et al.*, 2004). The present estimate is approximately twice the value which had been estimated previously (Treloar, 1975) from stress–strain isotherms of elastomers which may have been undergoing strain-induced crystallization not accounted for in reaching this conclusion.

More quantitative characterization of this limited chain extensibility requires, of course, a non-Gaussian distribution function (Treloar, 1975) for the end-to-end separation r of the short network chains. Ideal for this case is the Fixman–Alben distribution (Fixman and Alben, 1973), which was used (Erman and Mark, 1988) to calculate stress–strain isotherms in elongation for bimodal PDMS networks. Good agreement was found between theory and experiment. Other non-Gaussian distribution functions have also been successfully used for this purpose (Llorente *et al.*, 1984; Menduina *et al.*, 1986; Erman and Mark, 1997). The experimental isotherms can also be interpreted using the van der Waals theory of rubberlike elasticity (Kilian, 1990; Erman and Mark, 1997).

Another approach, Monte Carlo simulations, utilizes the wealth of information that rotational isomeric state theory provides on the spatial configurations of chain molecules. In brief, Monte Carlo calculations based on the rotational isomeric state approximation are used to simulate spatial configurations and thus distribution functions for the end-to-end separations of the chains (Erman and Mark, 1988; Curro and Mark, 1984). These distribution functions are then used in place of the Gaussian function in the standard three-chain model (Treloar, 1975), in the affine limit to give the desired non-Gaussian theory of rubberlike elasticity. Stress–strain isotherms calculated in this way are strikingly similar to the experimental isotherms obtained for the bimodal networks (Erman and Mark, 1988, 1997). The overall theoretical interpretations are thus quite satisfactory and would encourage other applications of these distributions, for example to segmental orientation in networks containing very short chains. Such segmental orientation is of critical importance, for example with regard to strain-induced crystallization.

A second important characteristic of an elastomeric network is the value of the elongation at which rupture occurs. The present results on PDMS indicate that

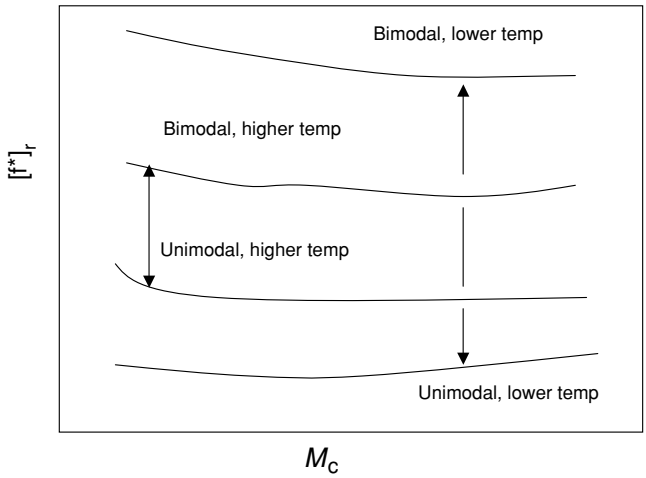

Figure 13.7 Ultimate strength, as represented by the modulus at rupture, shown as a function of the molecular weight between cross links for a unimodal and bimodal elastomer compared at two temperatures. The improvement from using a bimodal elastomer is larger at the lower temperature, presumably due to enhanced strain-induced crystallization.

rupture generally occurred at approximately 80–90% of maximum chain extensibility (Erman and Mark, 1997).

PDMS networks were found to be unsuitable for characterizing the effects of bimodality on strain-induced crystallization, because of their very low crystallization temperatures. The polymer chosen instead for these end-linked bimodal networks was poly(ethylene oxide), which has a relatively high melting point (∼65 °C) (Mark, 1996a, 1999b; Brandrup *et al.*, 1999) and thus readily undergoes strain-induced crystallization. Decrease in temperature was found to increase the extent to which the values of the ultimate strength of the bimodal networks exceed those of the unimodal ones (Sun and Mark, 1987a). A schematic representative of this is shown in Figure 13.7. These results suggest that bimodality facilitates strain-induced crystallization (Erman and Mark, 1997), possibly through increased orientation of the longer, more easily crystallizable chains, into crystallization nuclei. Similar conclusions have been reached in studies of elongated bimodal networks of poly(tetrahydrofuran) (Hanyu and Stein, 1991).

In practical terms, the above results demonstrate that short chains of limited extensibility may be bonded into a long-chain network to improve its toughness. It is also possible to achieve the converse effect. Thus, bonding a small number of relatively long elastomeric chains into a short-chain PDMS thermoset greatly improves both its energy of rupture and impact resistance (Tang *et al.*, 1984). This is shown schematically in Figure 13.8. Approximately 95 mol% short chains gives

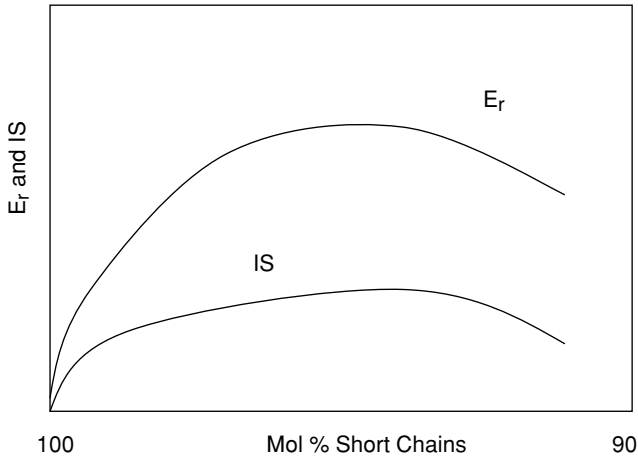

Figure 13.8 The energy required for rupture E_r and the impact strength IS shown as a function of composition for typical bimodal networks that are sufficiently brittle for such testing.

the maximum effect for the molecular weights involved. Lower concentrations give smaller improvements than can otherwise be achieved, and higher concentrations will gradually convert the composite from a relatively hard material to one that is more rubberlike.

Results in other mechanical deformations

There are numerous other deformations of interest, including compression, biaxial extension, shear, and torsion (Treloar, 1975; Mark and Erman, 2001). Equi-biaxial extension results have been obtained by inflating sheets of unimodal and bimodal networks of PDMS (Xu and Mark, 1992). Upturns in the modulus were found to occur at high biaxial extensions, as expected. Also of interest, however, are pronounced maxima preceding the upturns. A schematic representative of this is shown in Figure 13.9. Such dependences represent a challenging feature to be explained by molecular theories addressed to bimodal elastomeric networks in general.

Elastomeric networks can be studied in pure shear by stretching a sheet of the material which has a large ratio of width to length, in the direction perpendicular to the width. In shear measurements on some unimodal and bimodal networks of PDMS (Wang and Mark, 1992), the bimodal PDMS networks showed large upturns in the pure-shear modulus at high strains which were similar to those reported for elongation and biaxial extension.

Very little work has been done on elastomers in torsion (twisting a cylindrical sample around its long axis). More results are presumably forthcoming, particularly

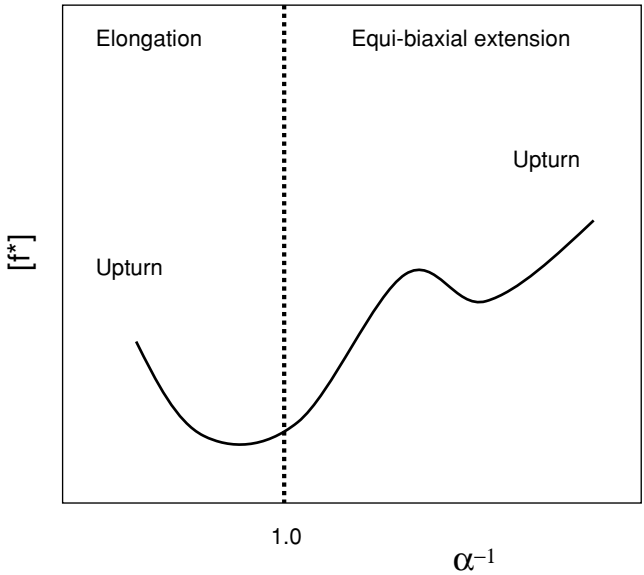

Figure 13.9 Representative stress–strain isotherm for a bimodal elastomer in both uniaxial extension (left side) and biaxial extension (right side).

on bimodal networks and on networks containing some of the unusual fillers introduced *in situ* by hydrolyses of organometallic compounds such as silicates or titanates (Mark, 1999a). In any case, the same types of bimodal PDMS networks showed rather different behavior in torsion (Wen and Mark, 1994a). Specifically, no unambiguous upturns in modulus were observed at large deformations. It has not yet been established whether this is due to the inability, to date, of reaching sufficiently large torsions, or whether this is some inherent difference in this type of deformation.

Tear tests have been carried out on bimodal PDMS elastomers (Yanyo and Kelley, 1987; Smith *et al.*, 1990; Shah, 1996, 2004), using the standard "trouser-leg" method. Tear energies were found to be considerably increased by the use of a bimodal distribution, with documentation of the effects of compositional changes and changes in the ratio of molecular weights of the short and long chains. The increase in tear energy did not seem to depend on tear rate (Yanyo and Kelley, 1987), an important observation that seems to suggest that viscoelastic effects are not of paramount importance in explaining the observed improvements. Some of these results are shown schematically in Figure 13.10.

A subsequent series of shear tests (Smith *et al.*, 1990) established the dependence of the tearing properties on the composition of the bimodal networks and the lengths of the chains used to prepare them. Of particular interest was the dependence of the tearing energy on the amount of the short-chain component, since the maxima

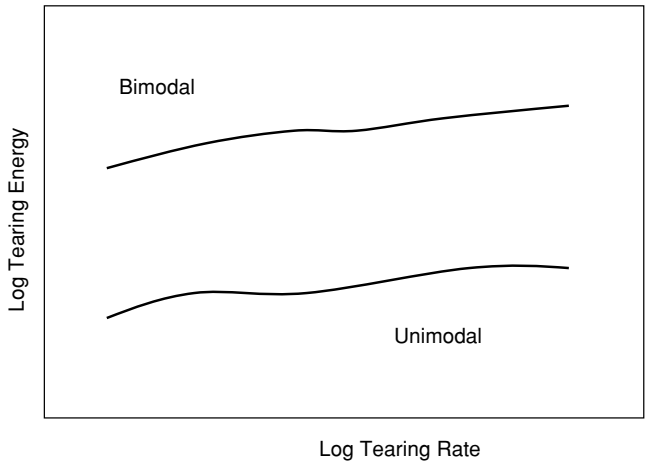

Figure 13.10 Tearing energies for a unimodal and bimodal elastomer as a function of tearing rate.

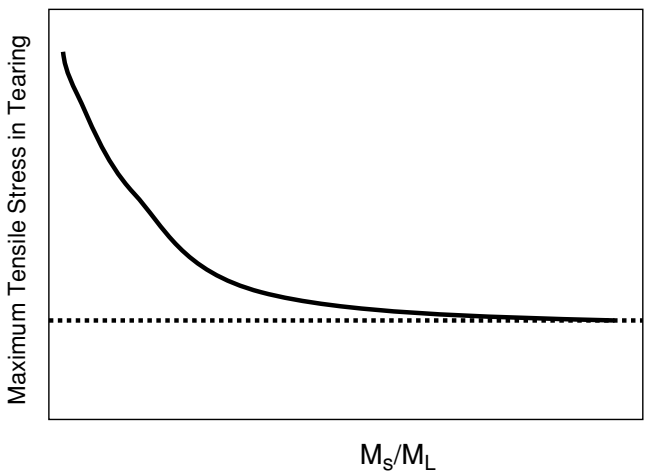

Figure 13.11 Maximum tensile strengths in tearing for bimodal elastomers as a function of the ratio of the molecular weights of the short and long chains.

in such curves locate the compositions giving the greatest increases in tear energy. Also of importance are experiments showing how the tensile strength depends on the ratio M_S/M_L of molecular weights of the two components. Figure 13.11 shows these results schematically. The observed increases in strength with decrease in the molecular weight of the short chains must eventually become decreases when the chains become too short to have any elastic effectiveness at all. It would obviously be important to carry out additional studies to establish the molecular weight at

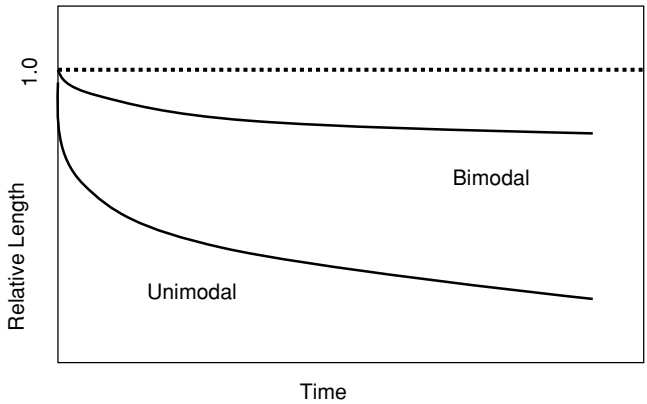

Figure 13.12 Dependence of relative length of a sample on cyclic compressive stress as a function of time for a unimodal and bimodal elastomer.

which this occurs, for a variety of types of deformation and a number of different elastomers.

Some Rheovibron viscoelasticity results have been reported for bimodal PDMS networks (Andrady *et al.*, 1991). To provide guidance for the desired interpretations, measurements were first carried out on unimodal networks consisting of the types of chains used in combination in the bimodal networks. One of the important observations was the dependence of crystallinity on the network chain-length distribution.

Some measurements have been made on permanent set for PDMS networks in compressive cyclic deformations (Wen *et al.*, 1994). They are shown schematically in Figure 13.12. There appeared to be less permanent set or creep in the case of the bimodal elastomers. This is consistent in a general way with some early results for polyurethane elastomers (Kaneko *et al.*, 1980). Specifically, cyclic elongation measurements on unimodal and bimodal networks indicated that the bimodal ones survived many more cycles before the occurrence of failure from fatigue. The number of cycles to failure is approximately an order of magnitude higher for the bimodal network, at the same modulus Mod_{10} at 10% deformation (Erman and Mark, 1997)!

Results on non-mechanical properties

Birefringence measurements have been shown to be very sensitive to bimodality, and have therefore also been used to characterize non-Gaussian effects resulting from it in PDMS bimodal elastomers (Erman and Mark, 1997; Riande and Saiz, 1992; Galiatsatos *et al.*, 1996). Relevant here is the effect of strain on the stress–optical coefficient (defined as the ratio of the birefringence to the stress) (Galiatsatos and Mark, 1987). There was found to be a large decrease in this coefficient over a

relatively small range in elongation, presumably from the limited extensibility of the short chains in the bimodal structure. It is therefore a sensitive way of characterizing non-Gaussian effects in network deformation.

Another method called "thermoporometry" is based on the fact that solvent molecules constrained to small volumes form only relatively small crystallites upon crystallization, and therefore exhibit lower crystallization temperatures (Jackson and McKenna, 1991; Goldstein *et al.*, 1992; Grobler and McGill, 1993; Baba *et al.*, 2003; Hoei *et al.*, 2003; Billamboz *et al.*, 2005). Some differential scanning calorimetry measurements on solvent molecules constrained in the pores of PDMS elastomers gave evidence for several crystallization temperatures, which could be indicative of an unusual distribution of pore sizes (Madkour and Mark, 1993). The types of curves obtained indicate that the effects are most pronounced for trimodal networks, which are discussed later in this review.

Calorimetric measurements on bimodal poly(ethylene oxide) networks indicated that the short chains seemed to decrease the amount of crystallinity in the unstretched state (Clarson *et al.*, 1992). This is an intriguing result since they *increase* the extent of crystallization in the stretched state.

When cyclic molecules are present during the end-linking reaction, the larger ones tend to get trapped by being threaded with chains subsequently bonded into the network structure. Such experiments have also been carried out using a bimodal distribution of end-linkable PDMS chains (Clarson *et al.*, 1987).

Additional insights into the dynamics and structure of bimodal elastomers have been obtained from experiments using dynamic light scattering (Oikawa, 1992) and nuclear magnetic resonance spectroscopy (Saalwachter and Kleinschmidt, 2004; Saalwachter, 2003, 2004), neutron scattering calculations (Kloczkowski *et al.*, 1991), and computer simulations on chain orientations and network mechanical properties (Sakrak *et al.*, 1994).

Trimodal networks

Experimental results

As mentioned above, there have been differential scanning calorimetry measurements on solvent molecules constrained in the pores of a variety of PDMS elastomers. Some results on networks having a trimodal distribution have been reported (Madkour and Mark, 1993). The several crystallization temperatures which were observed for the benzene in such networks could possibly be used to obtain additional information on the pore sizes present.

Although there have been attempts to evaluate the mechanical properties of trimodal elastomers, this has not been done in any organized manner. The basic problem is the large number of variables involved, specifically three molecular weights and two independent composition variables (mol fractions); this makes it practically

impossible to do an exhaustive series of relevant experiments. For this reason, the only mechanical property experiments that have been carried out have involved arbitrarily chosen molecular weights and compositions (Madkour and Mark, 1993; G. T. Burns, 1995, Dow Corning Corporation, unpublished). Not surprisingly, only modest improvements have been obtained over the bimodal materials.

Results from theory and simulations

Some recent computational studies (Sakrak *et al.*, 1994), however, indicate that it is possible to do simulations to identify those molecular weights and compositions which should maximize further improvements in mechanical properties. Such simulations are being extended to search for optimum properties of trimodal networks, specifically (1) the elastic modulus, (2) maximum extensibility, (3) tensile strength, and (4) segmental orientability. Results to date (Erman and Mark, 1998) suggest that a trimodal network prepared by incorporating small numbers of very long chains into a bimodal network of long and short chains could have significantly improved ultimate properties.

Networks of very high modality

The interpretation of the attractive mechanical properties of bimodal networks has been in terms of a "delegation of responsibilities", with the short chains serving in one role and the long chains in another. If this picture is true, then it would be interesting to prepare and study networks having extraordinarily broad molecular weight distributions, in that there would be network chains of all conceivable lengths, available for any possible mechanism that would improve properties (Erman and Mark, 1997). Polymer prepared from a single polymerization would not have a broad enough distribution, but the combination of a series of samples of gradually differing average molecular weights could provide the desired broadness. This is illustrated in Figure 13.13. An elastomer of this type might well have unusually attractive mechanical properties (Viers, 1998).

Elastomers that may have been inadvertently bimodal

Elastomers cured with sulfur frequently have improved mechanical properties when the curing conditions are chosen to give cross links that consist of *chains* of sulfur atoms (Nasir and Teh, 1988). It has been suggested that if such polysulfidic cross links can themselves act as elastomeric network chains, then a bimodal network is produced, albeit inadvertently. Figure 13.14 shows this possibility. Calculations conducted to take into account this possible bimodality gave results in good agreement with experiment (Sharaf and Mark, 1991).

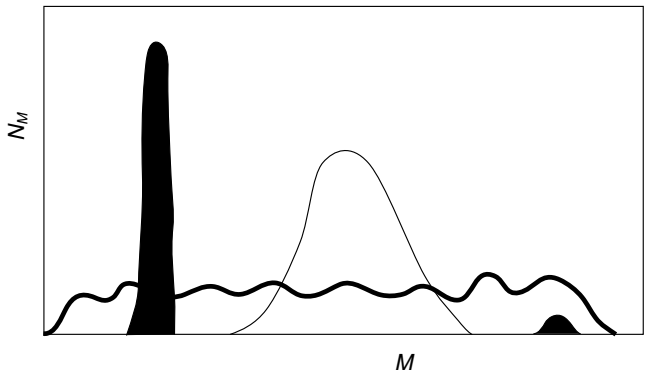

Figure 13.13 The network chain-length distributions shown in Figure 13.2, with the addition of the extremely broad "pseudo-unimodal" distribution obtainable by combining a number of samples of the same polymer made in different polymerizations.

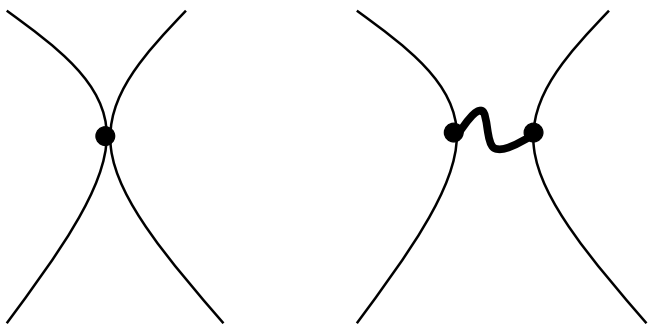

Figure 13.14 Sketch showing the difference between a monosulfidic cross link (left portion), and a polysulfidic one (right portion). In the latter case, the chains of sulfur atoms can possibly act as additional elastically effective chains in what is essentially a bimodal network.

A similar situation may occur in the case of networks end linked using the addition reaction involving vinyl chain ends and hydrogen atoms in an oligomeric poly(methyl hydrogen siloxane) (Sharaf and Mark, 1993, 1995; Erman and Mark, 1997). In the case of incomplete reactions, the segments between the reacted silicon atoms on the oligomer may be long enough to act as elastically effective chains in a bimodal structure. Finally, a bimodal chain-length distribution has also been proposed to explain some unusual properties of polysiloxane networks that have been post cured (Quan, 1989), elastomers prepared from two cross-linking systems (Madkour and Hamdi, 1996), and elastomers after being reclaimed by ultrasonic devulcanization (Isayev *et al.*, 1997; Yun *et al.*, 2001).

Other materials in which bimodality might be advantageous

There appear to be other cases where a bimodal distribution of chain length or some other physical property can be advantageous, possibly again through this idea of a delegation of responsibilities (Erman and Mark, 1997).

For example, in the area of thermosets, there seems to be an improvement in mechanical properties when the polymer being cured has a bimodal distribution of molecular weights (Holmes and Letton, 1994). In this case, the improvements may be due to different morphologies and degrees of inhomogeneity (Wu *et al.*, 1990; Tan *et al.*, 1999) resulting from the fact that the long chains in a bimodal distribution could have considerably lower solubilities than the short chains. Also, it is well known that the flow characteristics of a polymer during processing (Ferry, 1980) can frequently be adjusted by the addition of a small amount of polymer of either very low or very high molecular weight. Another example is in the area of rubber-toughened thermoplastics in which an elastomer is dispersed as domains within the thermoplastic matrix to improve its mechanical properties (Bucknall, 1977; Donald and Kramer, 1982). It has been reported that a bimodal distribution of particle sizes gives the largest improvements (Okamoto *et al.*, 1991; Chen and Jan, 1992; Demirors, 1998). Perhaps the small particles are most efficient at stopping one type of failure mechanism, and the large particles another type. In a related application, there is the possibility that a mixture of two chemically different particles, such as silica (SiO_2) and titania (TiO_2) (Wen and Mark, 1995a) could have significant advantages in elastomer reinforcement, with one perhaps functioning best at moderate temperatures and the other at elevated temperatures.

14

Birefringence and segmental orientation

Introduction

The directions of chain segments are isotropically distributed in an undistorted network. Macroscopic distortion of the network, however, results in anisotropy at the microscopic level in that the distribution of segment orientations is no longer the same in all directions. The anisotropy resulting from macroscopic deformation is accompanied by optical anisotropy associated with these varying orientations of the polarizability tensors of the repeat units. Consequently the refractive indices of the network along different directions become unequal, and the network is said to be birefringent. The theory of birefringence of affine networks has been outlined by Treloar (Treloar, 1975). In this chapter, the derivation of birefringence will be given for both affine and phantom networks, followed by a more general discussion of the problem of segmental orientation and its experimental determination.

Birefringence of affine and phantom networks

First, we consider a single chain in the network whose ends are fixed at the origin and at the point (x, y, z) of a laboratory-fixed coordinate system $0xyz$. The x-axis is chosen to lie along the direction of stretch of the network. The segments of the chain are assumed to experience all possible spatial configurations subject to the constancy of the end-to-end vector $\mathbf{r}$. The polarizability tensor for the chain with a given configuration is obtained as the sum of the polarizability tensors of structural units comprising the chain (Volkenstein, 1963; Flory, 1969). A chain with a fixed end-to-end vector will assume different values of polarizability depending on the spatial configurations of the structural or repeat units. The difference between the x-component and the two lateral components, y and z, of the polarizability tensor averaged over all possible configurations of the chain at fixed r (Volkenstein, 1963; Nagai, 1964) is given approximately by

$$\left[\alpha_{xx} - \frac{(\alpha_{yy} + \alpha_{zz})}{2}\right]_r = \Gamma_2 \frac{x^2 - (y^2 + z^2)/2}{\langle r^2 \rangle_0} \tag{14.1}$$

Here, α_{xx}, α_{yy}, and α_{zz} represent the x, y, and z components of the polarizability tensor for the chain averaged over all configurations. The subscript r denotes that this averaging is performed for the chain with fixed ends. On the right-hand side of Eq. (14.1) x, y, and z represent the respective components of r, and $\langle r^2 \rangle_0$ is the mean-squared end-to-end distance of the corresponding free chain. The quantity Γ_2 (Nagai, 1964; Flory, 1969) is defined by

$$\Gamma_2 = \frac{9}{10} \sum_i \frac{\langle r^{\mathrm{T}} \hat{\alpha}_i r \rangle_0}{\langle r^2 \rangle_0} \tag{14.2}$$

where the summation is over all the structural units comprising the chain and $\hat{\alpha}_i$ is the anisotropic part of the polarizability tensor of the ith structural unit. The quantity r^{T} is the transpose of r and subscript 0 denotes that the average is performed over all configurations of the free chain. Equation (14.1) may be written similarly for the y and z components. For a sufficiently long freely jointed chain, $\Gamma_2 = 3\Delta a/5$, where Δa is the difference in the components of the bond polarizability tensor parallel and perpendicular to the bond axis. Assuming the x, y and z axes to be the principal directions of macroscopic deformation and averaging Eq. (14.1) over all chains of the network leads to

$$\begin{aligned} \langle \alpha_{xx} - (\alpha_{yy} + \alpha_{zz})/2 \rangle &= \nu^{-1} \sum_{i=1}^{\nu} [\alpha_{xx} - (\alpha_{yy} + \alpha_{zz})/2] \\ &= \Gamma_2 \frac{\langle x^2 \rangle - (\langle y^2 \rangle + \langle z^2 \rangle)/2}{\langle r^2 \rangle_0} \\ &= \left(\frac{\Gamma_2}{3}\right) \left[\Lambda_x^2 - \frac{\left(\Lambda_y^2 + \Lambda_z^2\right)}{2}\right] \end{aligned} \tag{14.3}$$

Here, the second line follows by the use of Eq. (14.1). The symbols Λ_x^2, Λ_y^2 and Λ_z^2 in the third line of Eq. (14.3) are the components of the microscopic deformation tensor (Erman and Flory, 1983a, b) defined as

$$\Lambda_x^2 = \frac{\langle x^2 \rangle}{\langle x^2 \rangle_0} \qquad \Lambda_y^2 = \frac{\langle y^2 \rangle}{\langle y^2 \rangle_0} \qquad \Lambda_z^2 = \frac{\langle z^2 \rangle}{\langle z^2 \rangle_0} \tag{14.4}$$

According to the Lorentz–Lorenz relation, the refractive index difference $\Delta n \equiv n_x - (n_y + n_z)/2$ is

$$\Delta n = \left(\frac{2\pi}{9}\right) \left(\frac{\nu}{V}\right) \left[\frac{(n^2 + 2)^2}{n}\right] \left\langle \alpha_{xx} - \frac{\alpha_{yy} + \alpha_{zz}}{2} \right\rangle \tag{14.5}$$

where n is the mean refractive index and V is the volume of the network during the experiment. Using Eq. (14.3) in Eq. (14.5) leads to

$$\Delta n = \left(\frac{2\pi}{27}\right)\left(\frac{\nu}{V}\right)\left[\frac{(n^2+2)^2\Gamma_2}{n}\right]\left[\Lambda_x^2 - \frac{\Lambda_y^2+\Lambda_z^2}{2}\right] \tag{14.6}$$

For an affine network, Λ_x^2, Λ_y^2 and Λ_z^2 are obtained from Eq. (5.9) and (14.4), as

$$\Lambda_x^2 = \lambda_x^2 \qquad \Lambda_y^2 = \lambda_y^2 \qquad \Lambda_z^2 = \lambda_z^2 \tag{14.7}$$

where λ_x^2, λ_y^2, λ_z^2 are the components of the macroscopic deformation tensor along the x, y, and z axes, respectively. Substituting Eq. (14.7) into Eq. (14.6) leads to the expression for the birefringence of an affine network,

$$(\Delta n)_{\text{af}} = \left(\frac{\nu}{V}\right)kTC\left[\lambda_x^2\frac{\lambda_y^2+\lambda_z^2}{2}\right] \tag{14.8}$$

where

$$C = 2\pi(n^2+2)^2\frac{\Gamma_2}{27}nkT \tag{14.9}$$

For a phantom network, the components Λ_x^2, Λ_y^2 and Λ_z^2 are obtained from Eqs. (5.14)–(5.18) as

$$\begin{aligned}\Lambda_x^2 &= (1-2/\phi)\lambda_x^2 + 2/\phi \\ \Lambda_y^2 &= (1-2/\phi)\lambda_y^2 + 2/\phi \\ \Lambda_z^2 &= (1-2/\phi)\lambda_z^2 + 2/\phi\end{aligned} \tag{14.10}$$

Using Eqs. (14.10) in Eq. (14.6) leads to the birefringence of a phantom network:

$$(\Delta n)_{\text{ph}} = \left(\frac{\xi}{V}\right)kTC\left[\lambda_x^2 - \frac{\lambda_y^2+\lambda_z^2}{2}\right] \tag{14.11}$$

The expression for birefringence may be written in general as

$$\Delta n = 2\left(\frac{FkT}{V}\right)C\left[\lambda_x^2 - \frac{\lambda_y^2+\lambda_z^2}{2}\right] \tag{14.12}$$

where $F = \nu/2$ for an affine network and $\xi/2$ for a phantom network.

Most birefringence experiments are performed in uniaxial extension for which the state of deformation is given by Eqs. (7.9a, b). Substituting Eqs. (7.9a, b) into Eq. (14.12) leads to the birefringence for uniaxial extension:

$$\Delta n = 2\left(\frac{FkT}{V}\right)\left(\frac{V}{V_0}\right)^{-1/3}C[\alpha^2 - \alpha^{-1}] \tag{14.13}$$

According to the theory of strain birefringence developed by Erman and Flory (1983b), the birefringence of real networks should lie between that of the affine and phantom network models. The presence of short-range intermolecular orientational correlations in the network, however, leads to a significant increase of birefringence over the theoretically predicted values.

The true stress τ in simple tension is given as

$$\tau = 2\left(\frac{FkT}{V_0}\right)\left(\frac{V}{V_0}\right)^{-1/3}(\alpha^2 - \alpha^{-1}) \tag{14.14}$$

as may be obtained from Eq. (7.11). Dividing Eq. (14.13) by Eq. (14.14) leads to

$$\frac{\Delta n}{\tau} = C \tag{14.15}$$

The constant C is referred to in the literature as the stress–optical coefficient (Treloar, 1975).

Some uses of birefringence measurements

The most fundamental use of birefringence measurements is to evaluate the molecular theory giving rise to the equations in the preceding section. More specifically, the equations may be tested by measurements of Δn as a function of strain and temperature for networks having different degrees of cross linking (with the cross links possibly introduced at different reference volumes V_0) and different degrees of swelling (frequently with solvents of varying geometric asymmetry). The experimental results, some of which have been summarized by Stein and Hong (1976), are generally in good agreement with theory.

This testing of the Gaussian theories can be extended to non-Gaussian theories, particularly by the use of bimodal PDMS elastomers having very high deformability (Galiatsatos and Mark, 1987). Measurements of Δn as a function of α are very useful, for example in locating the onset of non-Gaussian behavior. Thus the birefringence data can supplement the more extensive mechanical property data (Treloar, 1975) in the evaluation of non-Gaussian theories in general.

Since birefringence is very sensitive to ordering of any type, it can also be used to determine small amounts of crystallinity (Stein and Hong, 1976). Specific examples are the detection of small amounts of strain-induced crystallization in networks of highly amorphous ethylene–propylene copolymers (Llorente and Mark, 1981) and stereochemically irregular polybutadiene (Mark and Llorente, 1981). Also relevant in this regard was the (unsuccessful) search for crystallinity in bimodal PDMS networks over a wide range in temperature (Zhang and Mark, 1982). Bimodal and other multimodal networks were discussed in Chapter 13.

A related application is the study of the short-range correlations occurring between polymer segments and diluent, particularly as a function of the geometric asymmetry of the diluent molecule (Gent, 1969; Treloar, 1975; Llorente *et al.*, 1983). An important result (Liberman *et al.*, 1972, 1974) is the finding that use of a swelling diluent that is as nearly spherical as possible gives values of Δn that are most suitable for interpretation in terms of rotational isomeric state theory (Flory, 1969).

In such theoretical analyses, properties related to the birefringence are compared with corresponding results calculated using a rotational isomeric state model of the network chains. These comparisons between experiment and theory then yield chain conformational energies that can be used to predict other configuration-dependent properties. Alternatively, if the conformational energies are already known, then it is possible to obtain polarizabilities and optical anisotropies useful in the prediction of other optical properties.

Segmental orientation

Strain birefringence, presented above, is a measure of the orientation of the polarizability tensors associated with structural units of the chains and may therefore be adopted as an average indication of segmental orientation. It should be noted, however, that birefringence is only a crude qualitative estimate of such orientation because of uncertainties in the polarizability tensor resulting from intra- and intermolecular effects and solvent–chain interactions. Recent developments in spectroscopic techniques (Ward, 1975; Bokobza *et al.*, 1998; Koenig, 2004) allow more accurate measurement of orientations of specific vector directions within chain segments. For example, infrared dichroism, ^{2}H NMR spectroscopy, and fluorescence polarization are three of the more widely used methods.

The degree of orientation of segments in a deformed network is given usually in terms of the orientation function S defined by

$$S = (3\langle\cos^2\theta\rangle - 1)/2 \tag{14.16}$$

Here $\langle\cos^2\theta\rangle$ represents the mean-squared projection of the segment vectors on a laboratory-fixed axis, where θ is the angle between the segment direction and the axis. If all segments are directed along the given axis, $\langle\cos^2\theta\rangle = 1$ and $S = 1$. In the case where all segments are perpendicular to the given axis, $\langle\cos^2\theta\rangle = 0$ and $S = -1/2$. For random orientation of segments, $\langle\cos^2\theta\rangle = 1/3$ and $S = 0$.

Evaluation of S in terms of molecular parameters for a given network is made by first considering a network chain with fixed end-to-end vector $\mathbf{r}$ as shown in Figure 14.1. In this figure, $0xyz$ is a laboratory-fixed coordinate system. The sample is assumed to be stretched (or compressed) along the x axis; y and z axes are lateral

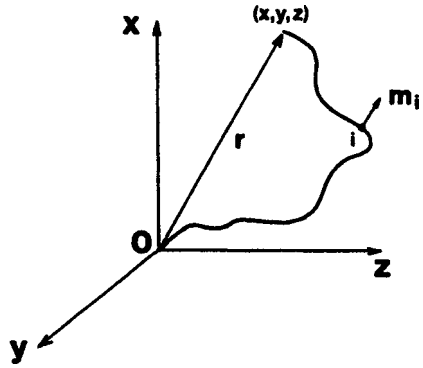

Figure 14.1 Schematic representation of a chain with fixed end-to-end vector **r**, and a vector $\mathbf{m}_i$ affixed to unit i of the chain.

directions. The vector $\mathbf{m}_i$ is affixed to the ith structural unit of the chain. It may be associated with a fictitious direction in the unit or may be identified with an actual bond. The angle between $\mathbf{m}_i$ and the x axis (not shown in the figure) is θ. As the chain undergoes configurational transitions, subject to the constancy of **r**, the angle θ takes different values. The average $\overline{\cos^2\theta}$ over all configurations of the chain is given according to the statistical treatment (Nagai, 1964, Flory, 1969) as

$$\overline{\cos^2\theta} = \frac{1}{3}\left\{1 + 2D_0\left[\frac{x^2}{\langle x^2\rangle_0} - \frac{1}{2}\left(\frac{y^2}{\langle y^2\rangle_0} + \frac{z^2}{\langle z^2\rangle_0}\right)\right]\right\} \tag{14.17}$$

where

$$D_0 = \frac{3\langle r^2\cos^2\Phi\rangle_0/\langle r^2\rangle_0 - 1}{10} \tag{14.18}$$

with Φ indicating the angle between $\mathbf{m}_i$ and the chain vector **r**. The subscript zero in Eqs. (14.17) and (14.18) indicates that the averaging is performed on free chains. The average $\overline{\cos^2\theta}$ given by Eq. (14.17) indicates an average over all configurations of the chain with one end at the origin and the other kept fixed at point (x, y, z). Averaging Eq. (14.17) over all chains of the network leads to

$$\langle\cos^2\theta\rangle = \frac{1}{3}\left\{1 + 2D_0\left[\Lambda_x^2 - \frac{1}{2}\left(\Lambda_y^2 + \Lambda_z^2\right)\right]\right\} \tag{14.19}$$

where $\Lambda_x^2 = \langle x^2\rangle/\langle x^2\rangle_0$, $\Lambda_y^2 = \langle y^2\rangle/\langle y^2\rangle_0$, $\Lambda_z^2 = \langle z^2\rangle/\langle z^2\rangle_0$ denote the components of the molecular deformation tensor given by Eqs. (14.4). Substituting Eq. (14.19) into Eq. (14.16) leads to the orientation function in terms of the components of the molecular deformation tensor and the molecular quantity D_0:

$$S = D_0\left[\Lambda_x^2 - \left(\Lambda_y^2 + \Lambda_z^2\right)/2\right] \tag{14.20}$$

The derivation of Eq. (14.20) is based on the assumption of Gaussian chains that are sufficiently below their finite extensibility limits. At higher deformations, the approximation given by Eq. (14.17) is not sufficient and additional terms are required.

Components of the molecular deformation tensor are given in terms of macroscopic deformation for an affine and a phantom network by Eqs. (14.7) and (14.10), respectively. Thus the orientation function for an affine network follows by substituting Eq. (14.7) into Eq. (14.20) to get

$$S = D_0 \left[\lambda_x^2 - \left(\lambda_y^2 + \lambda_z^2\right)/2\right] \tag{14.21}$$

Similarly, for a phantom network, using Eq. (14.10) in Eq. (14.20) leads to

$$S = D_0 \left(1 - \frac{2}{\phi}\right) \left[\lambda_x^2 - \left(\lambda_y^2 + \lambda_z^2\right)/2\right] \tag{14.22}$$

Simple extension is the most widely used deformation for measurements of segmental orientation. Using $\lambda_x = (v_{2c}/v_2)^{1/3}\alpha$ and $\lambda_y = \lambda_z = (v_{2c}/v_2)^{1/3}\alpha^{-1/2}$ for simple extension in Eqs. (14.21) and (14.22) leads to

$$S = D_0 \left(\frac{v_{2c}}{v_2}\right)^{2/3} [\alpha^2 - \alpha^{-1}] \qquad \text{(affine)} \tag{14.23}$$

and

$$S = D_0 \left(1 - \frac{2}{\phi}\right) \left(\frac{v_{2c}}{v_2}\right)^{2/3} [\alpha^2 - \alpha^{-1}] \qquad \text{(phantom)} \tag{14.24}$$

By analogy with the reduced stress $[f^*]$, a reduced orientation function may be defined, by using Eq. (14.24) for the phantom network, as

$$\begin{aligned} [S] &\equiv \frac{S}{\left(1 - \frac{2}{\phi}\right) \left(\frac{v_{2c}}{v_2}\right)^{2/3} [\alpha^2 - \alpha^{-1}]} \\ &= D_0 \end{aligned} \tag{14.25}$$

The second line of Eq. (14.25) suggests that the reduced orientation function should be independent of deformation, as was the case for the reduced stress of a phantom network. Experiments show, however, that $[S]$ depends rather strongly on α. Typical results of experiments (Queslel and Mark, 1985a) are shown in Figure 14.2. The circles represent experimental data, for dry and swollen samples. The horizontal dashed line, representing the reduced orientation defined in Eq. (14.25) is given an arbitrary location along the ordinate in the figure. The solid curves are obtained according to the constrained junction theory (Erman and Monnerie, 1985; Queslel and Mark, 1985b). The strong dependence of $[S]$ on swelling shown by the data

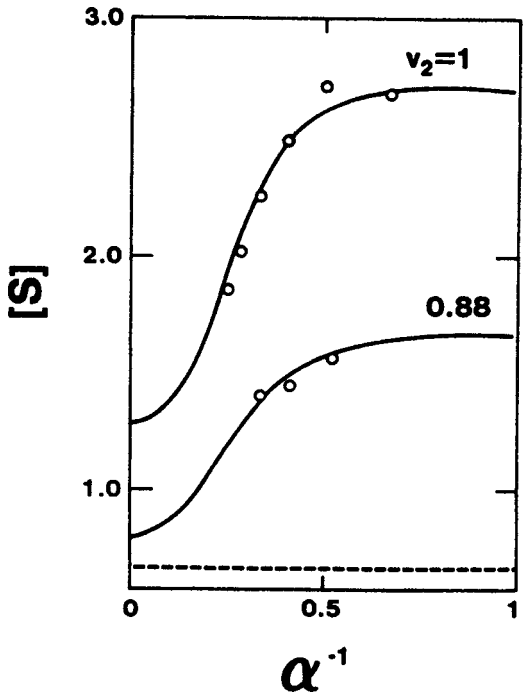

Figure 14.2 Reduced orientation as a function of the reciprocal extension ratio α^{-1}. Circles are from experiments of Queslel and Mark (1985a) on dry ($v_2 = 1$) and swollen ($v_2 = 0.88$) networks, where v_2 is the value of the volume fraction of polymer for each curve. The horizontal dashed line represents the prediction of the elementary molecular theory, and the solid curves are from the constrained junction theory.

points indicates the presence of short-range intermolecular orientational correlations that diminish rapidly upon swelling. The original theory on segmental orientation (Kuhn and Grün, 1942) is based on an affine network with freely jointed chains under simple tension. For this case, and with $v_{2c} = v_2 = 1$, Eq. (14.23) reduces to

$$S = \frac{1}{5N}[\alpha^2 - \alpha^{-1}] \tag{14.26}$$

where N is the number of links in the chain. In comparing predictions of Eq. (14.26) with experimental data on networks whose chains are not freely jointed, the number of bonds N has to be reinterpreted as the number of Kuhn segments in the chain.

The expressions for S given by Eqs. (14.23) and (14.24) for the affine and phantom network models reflect segmental orientation in the absence of intermolecular orientational correlations. Such correlations in real networks result in larger values of S. Dilation of the network with an isotropic solvent leads to rapid removal of such correlations, however, as mentioned above. Identification of the various

contributions to segmental orientation seems to be of major importance for correct interpretation of experimental data in this area.

Experimental determination of segmental orientation

Fluorescence polarization

Fluorescence polarization is based on labeling a small fraction of the network chains by fluorescent molecules, which absorb and emit light along specific directions. The orientations of these fluorescent groups may then be determined by exciting them with polarized light and measuring the emitted intensity along different directions (Monnerie, 1983). The major advantage of this technique is that the orientations of specific points along the chain are measured directly. One disadvantage is that the introduction of fluorescent groups into a chain may perturb its configurational character.

A different use of fluorescence polarization is to introduce structurally anisotropic fluorescent probes into the network in the form of solvent molecules. Experiments indicate that anisotropic solvent molecules are orientationally coupled with the segments of the network molecules. Measurements of the orientations of the probes thus give information on the segmental orientation in the networks.

Deuterium NMR

Deuterium nuclear magnetic resonance (NMR) is based on deuterating a fraction of the network chains and measuring the splitting of the NMR lines. The magnitude of the measured splitting is proportional to the orientation function (Deloche and Samulski, 1981; Deloche *et al.*, 1986; Dubault *et al.*, 1987; Sotta *et al.*, 1987, 1991, 1995; Sotta and Deloche, 1990, 1993; Deloche, 1993; Depner *et al.*, 1994) associated with the orientations of the hydrogen or deuterium bonds or labels in the chains. This technique seems to give the most sensitive measure of orientation, enabling one to determine minute levels of orientation in deformed networks. As in fluorescence polarization, the deuterium NMR technique may be used for measuring the orientations of deuterated solvent molecules, or probes, that are introduced into the network by swelling.

Polarized infrared spectroscopy

This technique is based on the measurement of orientations of specific transition dipole moment directions having known infrared absorption bands. It is based on

the determination of the dichroic ratio for a deformed network. For a network under simple tension, this ratio is defined as

$$D = \frac{A_{\parallel}}{A_{\perp}} \tag{14.27}$$

where $A_{\parallel}$ and $A_{\perp}$ are the absorbances of radiation polarized along and perpendicular to the direction of stretch, respectively. For an isotropic, unoriented network, the dichroic ratio equals unity, and the deviation of D from unity is proportional to the orientation function (Read and Stein, 1968; Flory, 1969; Amram *et al.*, 1986; Besbes *et al.*, 1992; Bokobza *et al.*, 1998; Bokobza and Erman, 2000). Calculations based on the rotational isomeric state theory provide the relationship between the experimentally measured value of the dichroic ratio and the desired orientation function. Two more recent general references relevant to birefringence and segmental orientation in networks are (Riande and Saiz, 1992, Riande and Diaz-Calleja, 2004).

15

Neutron scattering from networks

Introduction

One of the first relevant applications of neutron scattering measurements confirmed that chains in the bulk, undeformed amorphous state exhibit their unperturbed dimensions (Flory, 1984), as we mentioned in Chapter 1. Of much greater current interest, however, are measurements on deformed networks, which we describe here. Establishing the proper relationship between an externally applied state of deformation and the corresponding changes at the molecular level is essentially the most important problem in the molecular theory of rubber elasticity. The phantom and the affine network models make different assumptions for this necessary relationship between the macroscopic and the microscopic states of deformation. An experimental test of these relations is possible by the small-angle neutron scattering (SANS) technique. According to this technique, the shape and size of network chains in the undeformed and deformed states can be measured directly. The basic principle rests on labeling certain sites, such as the junctions or points along the chains, by replacing hydrogen atoms with deuterium and then measuring the intensity of scattering from the labeled molecules. In this way, scattering from individual molecules may be measured, whereas in the more conventional light and X-ray scattering techniques, contributions from a group of neighboring molecules cannot be separated.

SANS studies of networks were initiated by Benoit and collaborators (Munch *et al.*, 1976) and have generated wide interest in subsequent years (Hinckley *et al.*, 1978; Clough *et al.*, 1980; Beltzung *et al.*, 1982; Bastide *et al.*, 1984). Most of the fundamental problems and experimental work are given in the two more recent monographs (Higgins and Benoit, 1994; Roe, 2000).

Theory of scattering

The geometrical variables that describe scattering from two deuterated points i and j of a polymer chain are shown in Figure 15.1. The vector from i to j is identified

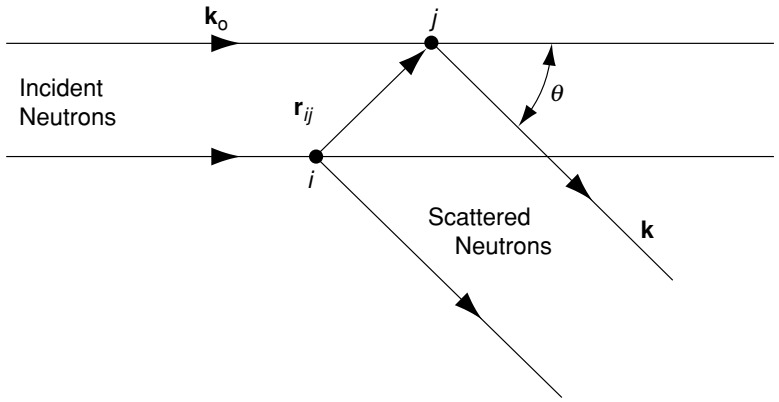

Figure 15.1 Scattering from two points i and j separated by the vector $\mathbf{r}_{ij}$. The quantity θ is the scattering angle, and $\mathbf{k}_0$ and $\mathbf{k}$ are wave propagation vectors for incident and scattered neutrons, respectively.

as $\mathbf{r}_{ij}$ and $\mathbf{k}_0$ and $\mathbf{k}$ are the wave propagation vectors for incident and scattered neutron rays, respectively. The angle between their directions is θ. Magnitudes of $\mathbf{k}_0$ and $\mathbf{k}$ are equal, $|k_0| = |k| = 2\pi/\lambda$ where λ is the wavelength of the radiation. The scattering vector $\mathbf{q}$ is defined as

$$\mathbf{q} = \mathbf{k} - \mathbf{k}_0 \tag{15.1}$$

where

$$|q| = \frac{4\pi}{\lambda} \sin \frac{\theta}{2} \tag{15.2}$$

The two points i and j may be the junctions or points along a chain. The intensity of radiation scattered in direction $\mathbf{q}$ from a collection of labeled points (Flory, 1969) is

$$\begin{aligned} S(q) &\equiv I(\theta)/I_0 \\ &= (n+1)^{-2} \sum_{i,j} \exp(\mathrm{i}q \cdot r_{ij}) W(r_{ij}) \mathrm{d}r_{ij} \end{aligned} \tag{15.3}$$

Here I_0 is the scattering intensity when $\theta = 0$, $\mathrm{i} = \sqrt{-1}$, and n is the number of scattering centers under observation. The ratio $I(\theta)/I_0$ represented by the term $S(q)$ is referred to as the scattering law. The intensity given by Eq. (15.3) is averaged over all possible configurations of each pair as acknowledged by the integration. $W(r_{ij})$ indicates the probability distribution of r_{ij} referred to as the intramolecular pair correlation function. When labeled chains are well separated from each other, the intensity given by Eq. (15.3) corresponds to scattering from a single chain.

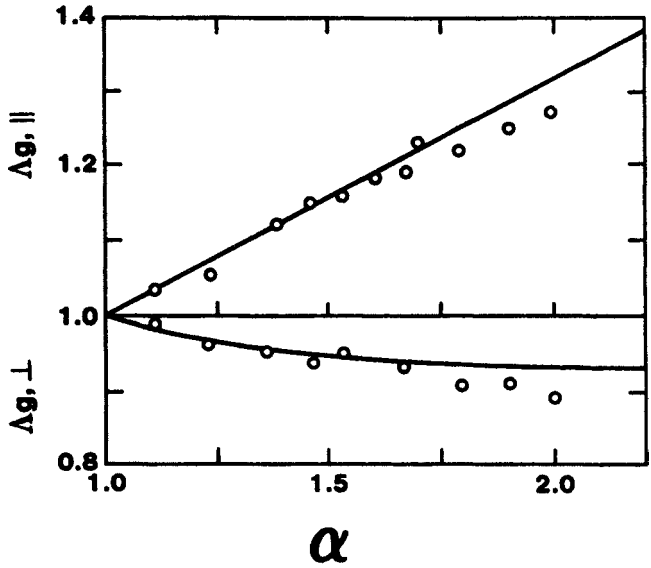

Figure 15.2 Scattering from PDMS networks (Beltzung *et al.*, 1984). The ordinate values show the ratios, $\Lambda_{\parallel} = (\langle s^2\rangle_{\parallel}/\langle s^2\rangle_{\parallel,0})^{1/2}$ and $\Lambda_{\perp} = (\langle s^2\rangle_{\perp}/\langle s^2\rangle_{\perp,0})^{1/2}$. Curves are calculated from Eq. (15.6) for a tetrafunctional network.

This constitutes the advantage of neutron scattering over all other experimental techniques.

For a chain in a network in simple tension, the scattering law given by Eq. (15.3) may be approximated in the long wavelength (small angle) limit (Pearson, 1977) as

$$\begin{aligned} S(q_{\parallel}) &= 1 - q_{\parallel}^2\langle s^2\rangle_{\parallel} \\ S(q_{\perp}) &= 1 - q_{\perp}^2\langle s^2\rangle_{\perp} \end{aligned} \tag{15.4}$$

Here, $q_{\parallel}$ and $q_{\perp}$ indicate the components of the scattering vector parallel and perpendicular to the direction of stretch, respectively. $\langle s^2\rangle_{\parallel}$ and $\langle s^2\rangle_{\perp}$ are the components of the mean-squared radius of gyration of the chain.

Experimental measurements of $S(q_{\parallel})$ and $S(q_{\perp})$ thus allow the determination of chain dimensions in a deformed network. For an affine network at uniaxial extension α, the two components of the radius of gyration are

$$\begin{aligned} \langle s^2\rangle_{\parallel} &= \left(\frac{v_{2c}}{v_2}\right)^{2/3} \alpha^2\langle s^2\rangle_{\parallel,0} \\ \langle s^2\rangle_{\perp} &= \left(\frac{v_{2c}}{v_2}\right)^{2/3} \alpha^{-1}\langle s^2\rangle_{\perp,0} \end{aligned} \tag{15.5}$$

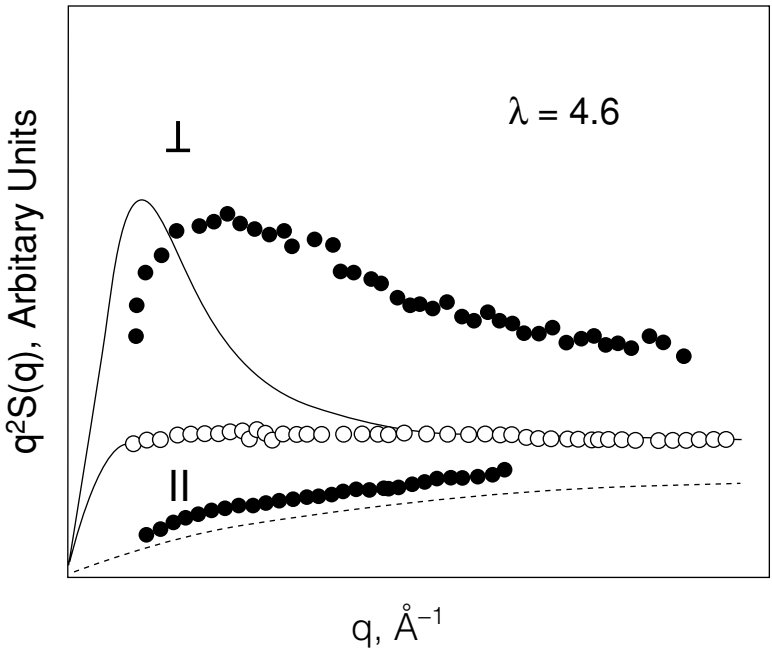

Figure 15.3 Kratky plots for uniaxially deformed (filled circles) and swollen (empty circles) PDMS networks (Bastide and Boue, 1986). Points are from experiments and the dotted lines are from Eqs. (15.4) and (15.6).

For a phantom network, the two components of $\langle s^2 \rangle$ are calculated (Pearson, 1977; Ullman, 1979, 1982; Erman, 1987) to be

$$\langle s^2 \rangle_{\parallel} = \left[\left(\frac{1}{2} - \frac{1}{\phi} \right) \left(\frac{v_{2c}}{v_2} \right)^{2/3} \alpha^2 + \left(\frac{1}{\phi} + \frac{1}{2} \right) \right] \langle s^2 \rangle_{\parallel,0}$$

$$\langle s^2 \rangle_{\perp} = \left[\left(\frac{1}{2} - \frac{1}{\phi} \right) \left(\frac{v_{2c}}{v_2} \right)^{2/3} \alpha^{-1} + \left(\frac{1}{\phi} + \frac{1}{2} \right) \right] \langle s^2 \rangle_{\perp,0} \qquad (15.6)$$

Figure 15.2 shows the results of SANS experiments (Beltzung *et al.*, 1984) on tetrafunctional PDMS networks compared with the predictions of Eq. (15.6). The ordinate quantities are $\Lambda_{\parallel} = (\langle s^2 \rangle_{\parallel} / \langle s^2 \rangle_{\parallel,0})^{1/2}$ and $\Lambda_{\perp} = (\langle s^2 \rangle_{\perp} / \langle s^2 \rangle_{\perp,0})^{1/2}$. Experimental data indicate that the radius of gyration in the network deforms similarly to that expected for the phantom network. The plot of the quantity $q^2 S(q)$ as a function of q is called a Kratky plot. In Figure 15.3 Kratky plots for uniaxially deformed and swollen PDMS networks are presented for directions that are parallel or perpendicular to the direction of the extension. The points represent experimental data (Bastide and Boue, 1986), and the filled points are for samples under tension. The

open circles show results obtained from isotropic samples, and the dotted curves were calculated from Eq. (15.6).

Neutron scattering experiments are also used to investigate the local deformations around a chain in a strained network. Effects of topological constraints, which are now accepted to act like confining tubes around each chain, with diameters in the order of chain diameters, are deduced from such experiments (Straube *et al.*, 1995).

16

Liquid-crystalline elastomers

Introduction

The two parts of the adjective "liquid-crystalline" are not as contradictory as they seem. In qualitative terms, the "crystalline" part refers to the fact that these materials are sufficiently ordered to diffract an X-ray beam in a way analogous to that of normal crystalline materials (with their three-dimensional order). On the other hand, the "liquid" part specifies that there is sufficient disorder for the material to flow like a liquid, at least under some conditions (Collings, 1990). The disorder is typically in one dimension as is the case, for example, with rodlike molecules having their axes all parallel but out of register with regard to their lengths. Because of their intermediate status between crystalline and amorphous materials, they are also called "mesophases" (with "meso" meaning middle).

Both low molecular weight materials (Collings, 1990) and polymers (Ciferri, 1991; Donald and Windle, 1992) can show liquid crystallinity. In the case of polymers, it frequently occurs in very stiff chains such as the Kevlars© and other aromatic polyamides. It can also occur with flexible chains and it is these flexible chains in the elastomeric state that are the focus of the present discussion. One reason such liquid-crystalline elastomers are of particular interest is the fact that (1) they can be extensively deformed (as described for elastomers throughout this book), (2) the deformation produces alignment of the chains, and (3) alignment of the chains is central to the formation of liquid-crystalline phases. Because of fascinating properties related to their novel structures, liquid-crystalline elastomers have been the subject of numerous studies, as described in a number of detailed reviews (Barclay and Ober, 1993; Warner and Terentjev, 1996, 2003a). The purpose here will be to mention some typical elastomers showing liquid crystallinity, to describe some of their properties, and to provide interpretations of some of these properties in molecular terms.

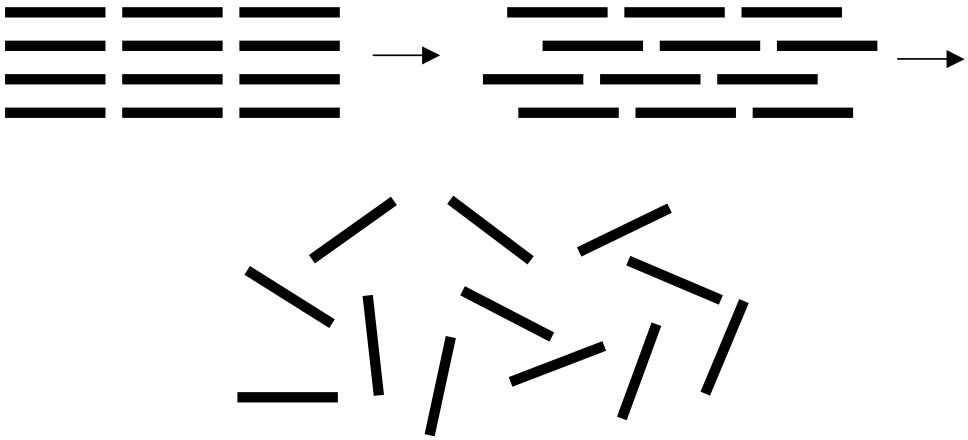

Figure 16.1 Decrease in order on going from the crystalline state to the nematic mesomorphic state, and then to the amorphous or liquid (isotropic) state.

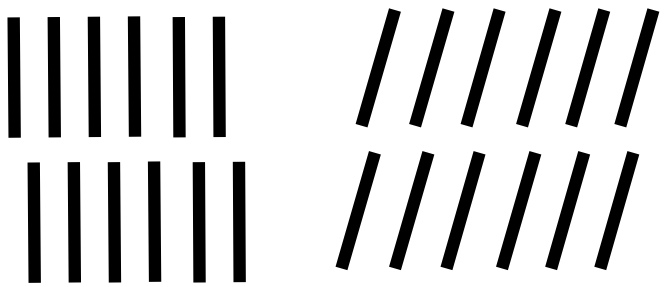

Figure 16.2 Layered arrangements in two types of smectic liquid-crystalline states.

The types of liquid-crystalline phases of interest can be illustrated with some rudimentary sketches, in which the direction of the preferred orientation is given by the "director". Figure 16.1 shows the usual completely ordered (crystalline) and completely disordered (isotropic) phases, with a *nematic* liquid-crystalline phase between them. The bars represent entire molecules in the case of small molecules, but sequences along the chain backbone in the case of polymers. In this case, the disorder is the already-mentioned sliding of segments relative to one another to place them out of register. There are also a variety of *smectic* liquid-crystalline phases, in which layers of molecules or chain sequences occur in layers that are disordered relative to one another. Two such phases are shown in Figure 16.2. In contrast, *cholesteric* phases have layers of nematic arrangements that are stacked in rotated arrangements, as is illustrated in Figure 16.3. A similar stacking occurs in the case of the *discotics* shown in Figure 16.4.

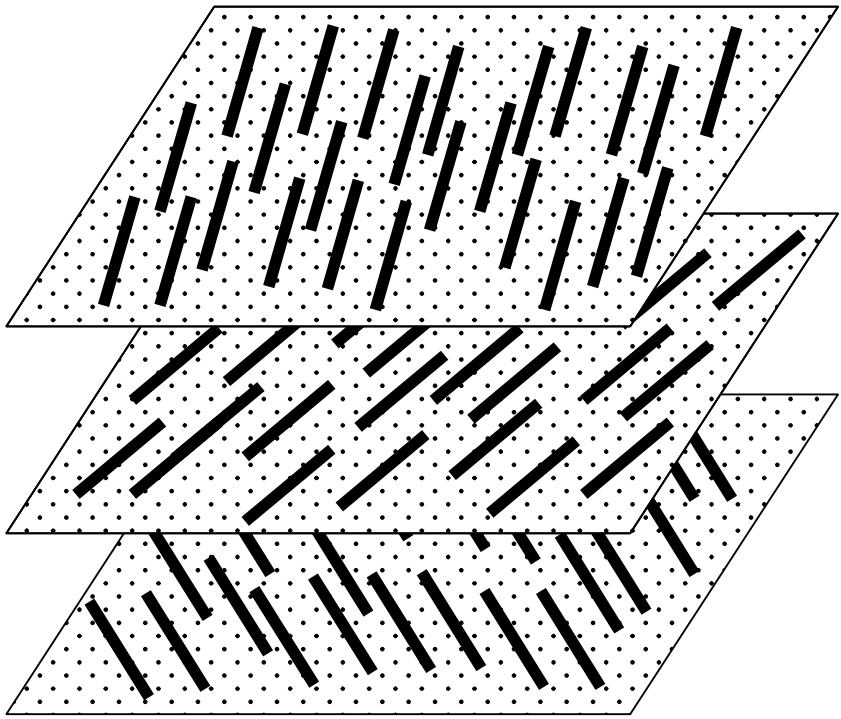

Figure 16.3 The cholesteric liquid-crystalline state.

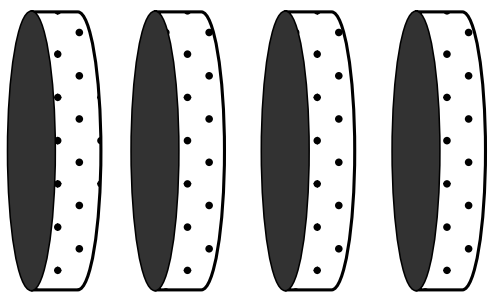

Figure 16.4 The discotic liquid-crystalline state.

In the case of polymers, there can be liquid-crystalline arrangements that involve the side chains attached to the chain backbones. Figure 16.5 illustrates the three possibilities: groups that can form liquid-crystalline phases occurring in the backbone, in the side chains, and in both (in what's called "combined" structures). In the case of the side-chain structures, the length of the "spacer" connecting the group to the backbone is of great importance. Polymer chains that are very stiff can also appear in *rigid-rod networks*, as shown in Figure 16.6. Such networks deform in

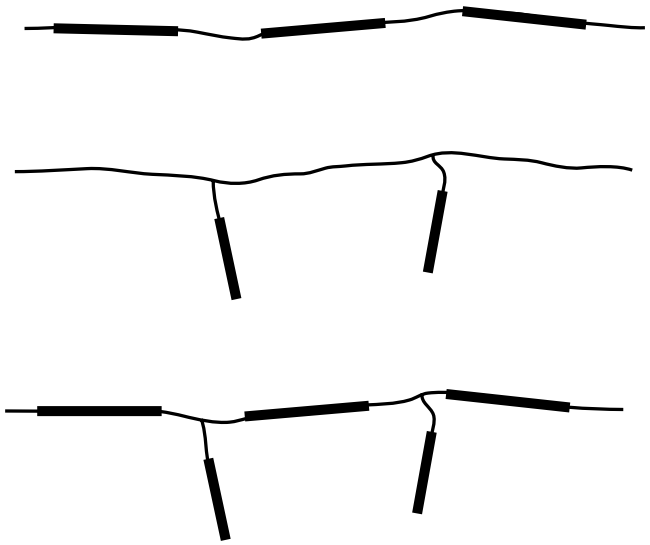

Figure 16.5 Liquid-crystalline polymers in which the mesomorphic sequences occur in the side chain, in the chain backbone, or in both ("combination" structures).

response to a stress by rearranging these rigid chains relative to one another instead of unwinding a flexible chain from a compact state to one that is more extended in the direction of the strain.

Main-chain liquid-crystalline elastomers

Poly(diethylsiloxane)

The polymer in this category that has been the most studied is poly(diethylsiloxane) (PDES) [$-Si(C_2H_5)_2O-$]. Of greatest interest has been its formation of a nematic mesophase, and relevant studies have included (1) heat capacities (Beatty and Karasz, 1975), (2) dielectric relaxations (Pochan *et al.*, 1975), (3) nuclear magnetic resonance (NMR) characterization (Kanesaka *et al.*, 2004), (4) structural changes during transitions (Miller *et al.*, 1990), (5) effects of stretching on the transitions (Papkov *et al.*, 2002), (6) optical properties such as refractive indices and optical rotations (Shibanov, 1989), (7) thermoelastic (force–temperature) properties (Godovsky *et al.*, 1991; Godovsky and Valetskaya, 1991), (8) mechanical properties in general (Godovsky, 1992), (9) end linking of the chains into "model networks" (Out *et al.*, 1994; Hedden *et al.*, 2000), (10) effects of molecular weight (Godovsky and Papkov, 1999), (11) characterization using atomic force microscopy (Godovsky *et al.*, 2001) or X-ray diffraction (Inomata *et al.*, 2000), (12) thermopolarization effects (cooling a heated sample in an electric field) (Voischchev *et al.*, 1999), (13) swelling behavior (Hedden *et al.*, 2000), (14) segmental orientation (Hedden

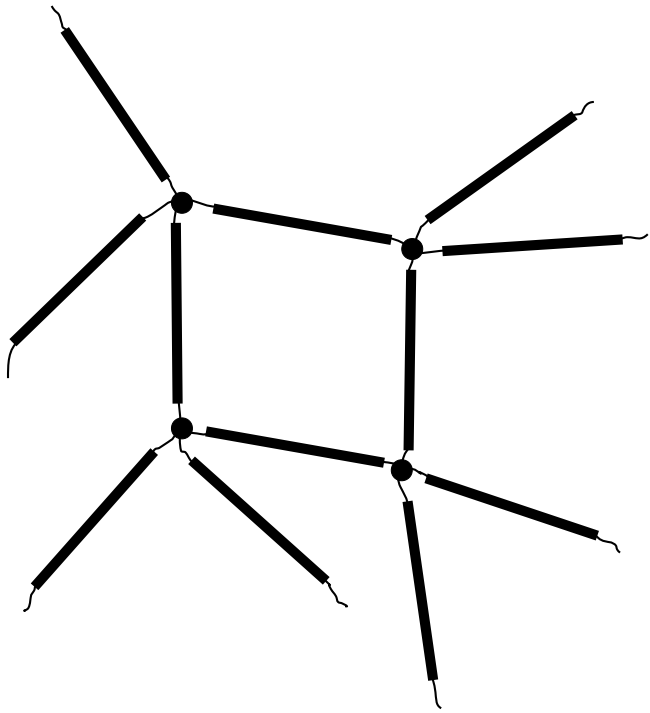

Figure 16.6 A rigid-rod elastomeric network.

et al., 2001), and (15) responses of guest chains in deformed PDES elastomers (Batra *et al.*, 2003).

One item of great interest with regard to these materials is the temperature at which the nematic liquid-crystalline phase becomes isotropic. Table 16.1 lists such *isotropization* ("clearing") temperatures T_i for a variety of symmetric polysiloxane polymers having repeat units $[Si((CH_2)_mCH_3)_2{-}O{-}]$. Although the focus is on PDES, with $m = 1$ methylenes in the side chain, it is preceded in the table by poly(dimethylsiloxane) (PDMS), with $m = 0$, for purposes of comparison. Also included are polymer molecular weights M, where important, and some relevant melting points, T_m. PDMS is very different from PDES in that it does not show a liquid-crystalline phase, and this situation is explained in the following section. PDES show values of T_i that significantly decrease with decrease in molecular weight. In fact, the liquid-crystalline phase *does not form at all* if M is below approximately 25 000 g mol^{-1}. This is in sharp contrast to the behavior of low molecular weight liquid-crystalline molecules; many cholesterol molecules that show mesophases have molecular weights down in the hundreds!

Since stretching a PDES aligns the chains in the direction of the liquid-crystalline structures, the values of T_i should also increase with elongation. Results

Table 16.1 *Transition temperatures for some symmetric polysiloxane elastomers having repeat units [Si((CH$_2$)$_m$CH$_3$)$_2$–O–]*

Polymer	m	$10^{-3}M$ (g/mol)	T_m (°C)	T_i (°C)
Poly(dimethylsiloxane)[a]	0	High	–43	None
Poly(diethylsiloxane)[b]	1	765		53
		425	–	52
		172	–	46
		100	–	34
		58	–	23
		∼25	–	None
Poly(di-*n*-propyl-siloxane)[b]	2	87	–	207
		68	–	177
		51	–	172
		43	–	145
		∼10	–	None
Poly(di-*n*-butyl-siloxane)[b]	3	128	–	299
		28	–	216
Poly(di-*n*-pentyl-siloxane)[b]	4	High	–	330
Poly(di-*n*-hexyl-siloxane)[b]	5	High	–	330
Poly(di-*n*-heptyl-siloxane)[c]	6	High	375[d]	None
Poly(di-*n*-octyl-siloxane)[c]	7	High	28[d]	None
Poly(di-*n*-nonyl-siloxane)[c]	8	High	31[d]	None
Poly(di-*n*-decyl-siloxane)[c]	9	High	47[d]	None

[a] Kuo (1999)
[b] Godovsky and Papkov (1999)
[c] Turetskii *et al.* (1995)
[d] Crystallization of the side chains, rather than the backbones

demonstrating this (Godovsky *et al.*, 1991; Godovsky and Valetskaya, 1991) are shown schematically in Figure 16.7. The dashed portion of the curve is what one would expect for higher elongations, where the effect should eventually saturate, with values of T_i leveling off.

Other acyclic polysiloxanes

Symmetric polysiloxanes having $m = 2-9$ have also been investigated, with some properties listed in several articles in a handbook (Godovsky and Papkov, 1999). These specific polymers and some recent relevant studies on them are cited below:

(1) poly(di-*n*-propyl-siloxane) (Molenberg *et al.*, 1997; Belousov *et al.*, 1999), (2) poly(di-*n*-butyl-siloxane) (Out *et al.*, 1995; Molenberg *et al.*, 1997),

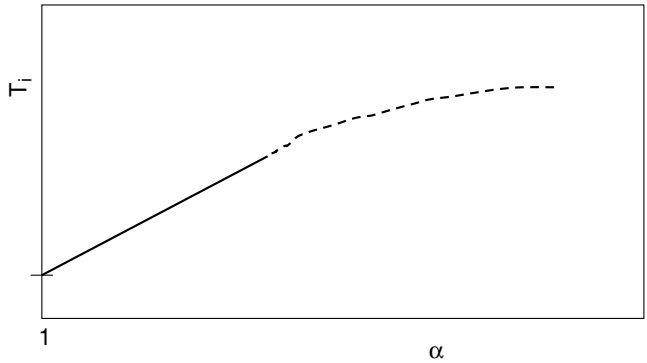

Figure 16.7 Sketch of the typical dependence of the isotropization temperature T_i on elongation.

(3) poly(di-*n*-pentyl-siloxane) (Out *et al.*, 1994; Molenberg *et al.*, 1997), (4) poly (di-*n*-hexyl-siloxane) (Out *et al.*, 1994; Molenberg *et al.*, 1997), (5) poly(di-*n*-heptyl-siloxane) (Turetskii *et al.*, 1995), (6) poly(di-*n*-octyl-siloxane) (Turetskii *et al.*, 1995), (7) poly(di-*n*-nonyl-siloxane) (Turetskii *et al.*, 1995), and (8) poly (di-*n*-decyl-siloxane) (Out *et al.*, 1994; Turetskii *et al.*, 1995).

The isotropization temperatures reported in these studies show a very interesting increase with increase in the number m of methylene groups in the side chains (Godovsky *et al.*, 1985). The trend is illustrated schematically in Figure 16.8, which includes the trend shown by the melting points of the same polymers. The first vertical shows the results of cooling in the case of PDMS ($m = 0$) and the second for cooling for polysiloxanes with m in the range 2–5. The two lines cross in such a way that the predicted value of T_i for PDMS lies *below* its value of T_m. This means that PDMS does not show a liquid-crystalline phase because it crystallizes before it gets to the lower temperature required.

Another interesting feature of the table pertains to the melting points cited for the polymers having $m = 6-9$. The crystallites these temperatures refer to involve the side chains, which are now long enough to crystallize themselves. Such side-chain crystallization has also been involved in polysilane homopolymers (Winokur and West, 2003), and chemical copolymers of polyethylene (Wagner and Phillips, 2001; Zhang *et al.*, 2002), the so-called linear low-density polyethylenes. In any case, such crystallization presumably could also interfere with the mesophases that might otherwise form.

Some polysiloxanes with cyclic groups in the backbone

Polysiloxanes in this category typically contain cyclics of $-Si(CH_3)_2-O-$ siloxane units of various sizes, or such siloxane units mixed with some carbosiloxanes (with

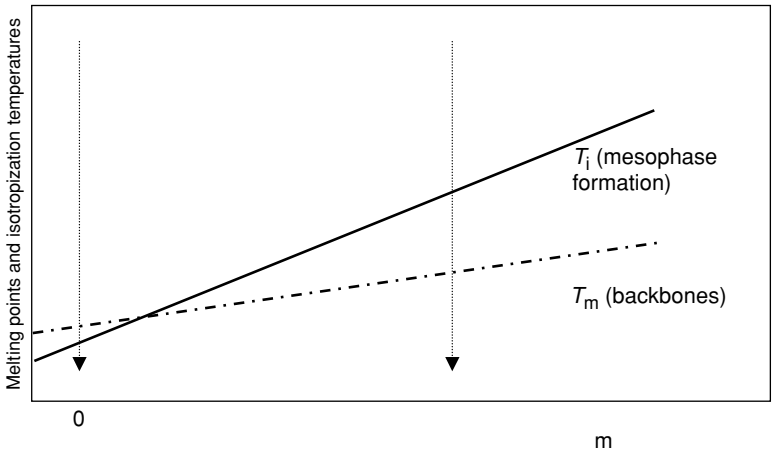

Figure 16.8 Sketch of typical dependences of the isotropization temperature T_i and the melting temperature T_m on the number of side-chain methylene groups in symmetric polysiloxane elastomers having repeat units $[Si((CH_2)_mCH_3)_2–O–]$. The vertical lines show temperature decreases for $m = 0$, corresponding to poly(dimethylsiloxane), and a typical larger value in the range $m = 2$–5 that corresponds to a polysiloxane showing a mesophase.

additional $–CH_2–$ sequences) (Bergmann *et al.*, 1997; Belousov *et al.*, 1999; Ganicz and Stanczyk, 2003). The cyclic portions can add considerable stiffness, resulting in isotropization temperatures above the polymers' decomposition temperatures.

Polyphosphazenes

A number of polyphosphazenes of repeat unit [–PRR′N–] also exhibit liquid-crystalline phases (Cypryk *et al.*, 1992; Miyata *et al.*, 1994; Kojima *et al.*, 1995). It is certainly intriguing that apparently the only classes of flexible chains that extensively exhibit liquid-crystalline phases are the polysiloxane and polyphosphazene semi-inorganic polymers.

Some mechanical properties in elongation

One aspect of this type of behavior involves the already-mentioned increase in the isotropization temperatures with increase in elongation (Disch *et al.*, 1994; Kupfer and Finkelmann, 1994; Kundler and Finkelmann, 1995). Also of importance, of course, are the stress–strain isotherms themselves. Some obtained for PDES as a function of degree of mesomorphic structure are shown schematically in Figure 16.9 (Papkov *et al.*, 2002). The curves show yield points akin to those

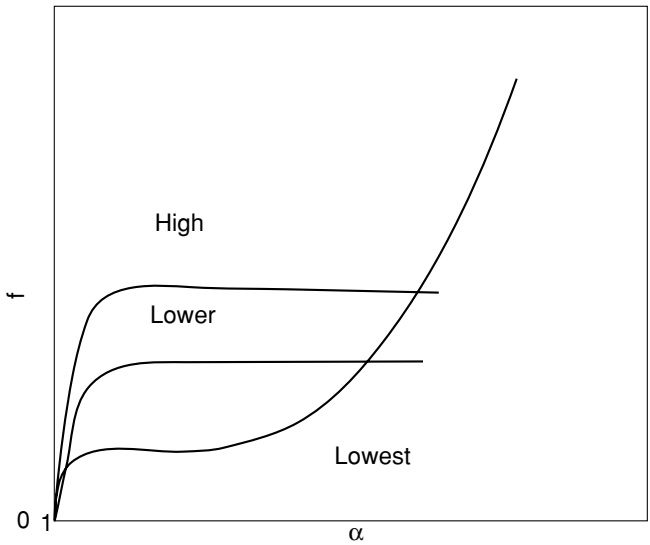

Figure 16.9 Illustrative stress–strain isotherms for poly(diethylsiloxane), as a function of the amount of mesophase present.

shown by partially crystalline polymers, and the overall shapes of the curve differ greatly with decrease in the amounts of mesophase present, either present initially or induced by the deformation. As is generally the case, formation of a second phase leads to irreversibility in the stress–strain isotherms. This is illustrated by the elongation–retraction curves shown in Figure 16.10 (Papkov *et al.*, 2002). The larger the elongation during the deformation, the larger the irreversibility (hysteresis) upon completing the retraction part of the cycle.

Side-chain liquid-crystalline elastomers

Some general aspects

In this category, the units giving rise to the liquid-crystalline behavior can be in the backbone (as already discussed), in the side chains, or in both (Zentel and Reckert, 1986). Of considerable interest is the orientation of the mesogenic groups and the chain backbones to which they are attached (Anglaret *et al.*, 2005; Tammer *et al.*, 2005). Frequently studied backbones include siloxanes and acrylates (Lacey *et al.*, 1998; Shenoy *et al.*, 2003; Gilles *et al.*, 2003), but a variety of other structures have also been studied, including amphiphilics (Loffler and Finkelmann, 1990; Brintzinger *et al.*, 1995).

The side chains in these structures can rearrange into positions either parallel or perpendicular to the deformed chain backbone (Zentel and Benalia, 1987), as

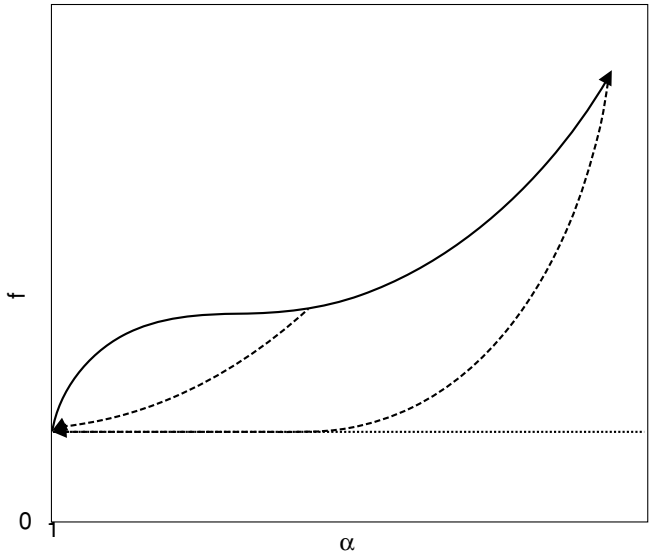

Figure 16.10 Illustrative stress–strain isotherms for poly(diethylsiloxane), showing the effects of irreversibility.

is illustrated in Figure 16.11. The outcome depends particularly on the nature and length of the flexible spacer connecting the mesogenic groups to the chain backbone. As expected the physical properties can become strongly anisotropic (Hammerschmidt and Finkelmann, 1989).

It has been long known that some liquid-crystalline materials of this type could be oriented by imposing an electric or magnetic field (Finkelmann *et al.*, 1984). The chains could also be aligned when these liquid-crystalline elastomers are deformed (generally in elongation but also in some cases in compression), and then cross linked into network structures. The major focus in these experiments was how the mechanical deformation affected the nature of the mesophase (in particular its axial direction relative to the direction of the strain), and its isotropization temperature. The studies generally involved measurements of both stress and birefringence as a function of strain, and the ratio of the former to the latter (the "stress–optical coefficient" mentioned in Chapter 14). The mesogenic behavior of such networks obviously depends strongly on their structures. For example, the effects of degree of cross linking, and composition in the case of copolymers, have been documented (Mitchell *et al.*, 1987).

The phase transitions depend significantly on spacer length, as has been demonstrated, for example, for oligo-oxyethylene spacers (Percec and Hsu, 1990). Closer coupling between the mesogenic groups and the polymer backbone tends to make

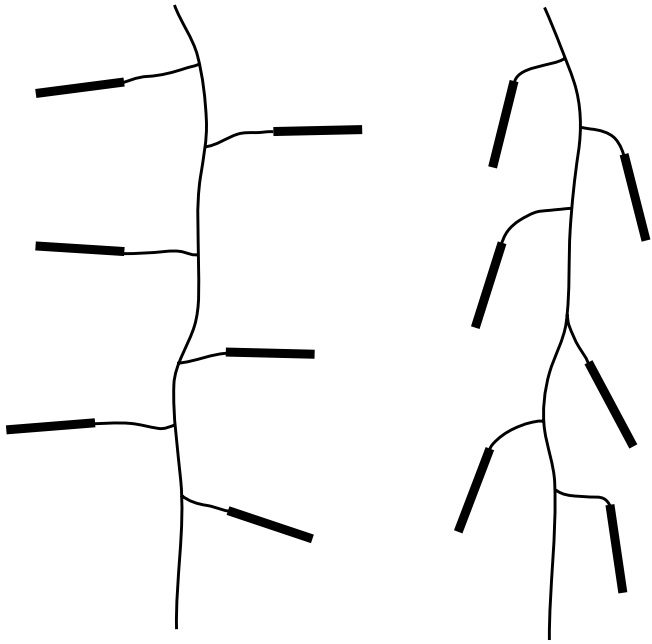

Figure 16.11 Approximately perpendicular and parallel arrangements of mesogenic side groups on a chain backbone stretched in the vertical direction.

the system more sensitive to the mechanical deformation, at least in the case of methylene groups making up the spacer (Kaufhold *et al.*, 1991).

Cross linking can generally be induced by γ radiation or chemical means (Zubarev *et al.*, 1996), and it has been observed that relatively high degrees of cross linking can be introduced without destroying the liquid crystallinity (Davis *et al.*, 1990). IR spectroscopy and stress–strain measurements in extension indicated that relatively low strains can frequently induce significant organization. One relevant experiment involved two cross-linking procedures: the first cross linking produced a network in which the mesogenic units could be oriented (Kupfer and Finkelmann, 1991), while the second subsequently locked in the network anisotropy. Samples were found to be clear and to have X-ray diffraction patterns characteristic of a highly ordered nematic material. Also of interest was the fact that transitions from the isotropic phase to the nematic phase caused significant increases in length. Using one or two cross-linking agents in the presence of a magnetic field could also be used to prepare "monodomain" nematics (in which the director alignment is claimed to be macroscopically uniform) (Lacey *et al.*, 1998).

The thermoelastic behavior of these materials has also been reported (Talroze *et al.*, 1990). Such experiments resolve the nematic to isotropic transition into entropic

and enthalpic contributions and provide values of the corresponding energetic and entropic parts of the force, f_e and f_S (Shenoy *et al.*, 2003).

Discotic, cholesteric, and smectic elastomers

Considerably less work has been done on discotic liquid-crystalline elastomers (Bengs *et al.*, 1993; Disch *et al.*, 1995) and cholesteric elastomers (Jia *et al.*, 2004). The same seems to be true for smectic elastomers (Hanus *et al.*, 1990; Beyer and Zentel, 2005; He *et al.*, 2005), even though some of them have the additional interesting property of being chiral (Zentel *et al.*, 1989; Semmler and Finkelmann, 1995)!

Ferroelectric and piezoelectric elastomers

In addition, some liquid-crystalline elastomers are ferroelectric (possess spontaneous electric polarization) (Zentel and Brehmer, 1995; Kremer *et al.*, 2001), or piezoelectric (become electrically polarized when mechanically strained, and become mechanically strained when exposed to an electric field) (Wendorff, 1991; Hirschmann *et al.*, 1992).

Photonic elastomers

Finally, some liquid-crystalline elastomers exhibit interesting photonic effects (Gleim and Finkelmann, 1987; Warner and Terentjev, 2003b). Of particular importance are non-linear optical properties. These involve interactions of light with the elastomer in a way that some of the characteristics of the incident light change, specifically its phase or frequency (including frequency doubling or frequency mixing) (Benne *et al.*, 1994, 1995).

Theory

As would not be surprising, given the unusual properties cited in this overview, liquid-crystalline elastomers have been the focus of numerous theoretical investigations (Brand, 1989; Erman *et al.*, 1990; Barclay and Ober, 1993; Yang *et al.*, 1995; Warner and Terentjev, 1996, 2003a; Wang and Warner, 1997). These theoretical treatments extend over a wide range of sophistication and rigor. The simplest physical picture of nematic elasticity can be visualized by the lattice theory, in which semiflexible chains are assumed to be embedded in an isotropic lattice of solvent molecules. The semiflexible chains consist of rods of m freely jointed segments of length l, which determines their stiffness. Stretching of the chains orients

the segments in a way that increases strongly with increasing stiffness of the chains. Calculations based on a lattice model (Erman *et al.*, 1990) show an abrupt jump in the segmental orientation function at a finite stretch ratio, and this corresponds to the isotropic–nematic transition. Below the transition, the sample behaves close to isotropic Gaussian elasticity. At a fixed uniaxial force, the transition is marked by a sudden elongation, resulting from the abrupt alignment of the segments along the direction of the force during the transition. Above the transition point the segments are highly oriented along the direction of stretch, and the network is nematic.

17

Bioelastomers

Introduction

Bioelastomers, or elastomeric biopolymers, are utilized by living organisms in a variety of tissues for a number of purposes. In vertebrates, including mammals such as humans, examples of tissues are the skin, arteries and veins, and organs such as the lungs and heart. As is obvious, all these tissues involve the already-mentioned characteristics of deformability with recoverability.

There are two general reasons for studying the elasticity of such materials. The more fundamental one is the simple desire to understand rubberlike elasticity in as broad a context as possible. The more practical one is to learn how nature designs and produces these materials, so as possibly to obtain some guidance on the commercial preparation of more useful non-biopolymeric elastomers.

The bioelastomers that have been investigated with regard to their rubberlike elasticity are listed in Table 17.1. All are proteins and thus have the repeat unit shown in Figure 17.1, where the side group R is different for the different α-amino acids that produce this chain structure. Although there are a variety of bioelastomers, elastin has been the most studied by far. It is thus emphasized in following sections.

Structural choices

Elastin is, of course, a chemical copolymer, and its repeat unit sequence is sufficiently irregular that it is always totally amorphous. This use of copolymerization to suppress the large amounts of crystallinity that would interfere with elastomeric behavior is also practiced by synthetic polymer chemists. For example, introduction of some propylene units into what would otherwise be highly crystalline polyethylene results in elastomeric ethylene–propylene copolymers that are of considerable commercial importance (Borg, 1973). Similarly, copolymerization of perfluorocarbon monomers (which would separately yield highly crystalline

Table 17.1 *Bioelastomers investigated with regard to their rubberlike elasticity*

Bioelastomer	Occurrence
Elastin	Vertebrates
Denatured collagen[a]	Vertebrates
Resilin	Insects[b]
Abductin[c]	Mollusks[c]
Octopus arterial elastomers	Octopuses
Viscid silk	Spider webs

[a] Elastomeric only after denaturation (melting of the normally crystalline collagen fibers)
[b] Present in ligaments and tendons, particularly in jumping insects such as fleas
[c] Present in elastic hinges to antagonize (counteract) the muscles that close the mollusk shells

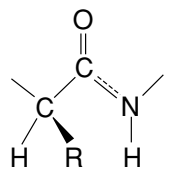

Figure 17.1 The polypeptide or protein repeat unit. (Reprinted with permission from J. E. Mark and G. Odian, Eds., *Polymer Chemistry*, Short Course Manual, Copyright American Chemical Society 1984.)

homopolymers) is used to prepare a number of high-performance fluoroelastomers (Brydson, 1978).

The chain flexibility required for rubberlike elasticity is achieved in elastin through the use of R side groups that are generally very small. The relevant information for mammalian elastin is summarized in the first three rows of Table 17.2 (Gosline, 1980, 1987). Specifically, three unusually small side groups make up a total of 68 mol% of those occurring in this type of elastin. An analogous avoidance of numerous large groups can be seen in the structures of the typical non-biopolymeric elastomers described in Chapter 2. It is also interesting to note, as shown in the final row of Table 17.2, that non-polar units predominate, making elastin one of the most hydrophobic proteins known. This was thought to illustrate Nature's attempt to avoid strong intermolecular interactions, such as Coulombic attractions, since they could interfere with desired chain mobility. This seems not to be the case, however, judging from two additional pieces of information (Gosline, 1987). First, some bioelastomers are significantly more polar than elastin. Second, the elastin

Table 17.2 *Composition of mammalian elastin*

Amino acid	R side group[a]	Mole%
Glycine	H	31
Alanine	CH_3	24
Valine	$CH(CH_3)_2$	13
Various	Non-polar	89

[a] In the [CHR—CO—NH—] repeat unit
Source: Gosline (1980, 1987)

chains would in any case interact only weakly, since they are well separated by the solvent molecules, which swell elastin as it functions in the organism. (The volume fraction v_{2m} of the polymer in elastin at swelling equilibrium is only approximately 0.6.) This swelling or plasticization with aqueous body fluids is crucial to the functioning of elastin since the dry protein would be expected to have a high glass transition temperature T_g. An analogous example is the already-cited use of typical ester plasticizers to increase the pliability of poly(vinyl chloride) (Davis, 1973), which otherwise has a T_g of 82 °C.

Cross linking

Elastin chains are cross linked in a highly specific manner, very unlike the usual techniques used to cure commercial elastomers (Gosline, 1980). The cross linking occurs through lysine repeat units, the number and placement of which along the chains are carefully controlled in the synthesis of the elastin in the ribosomes. The reactions involved are shown schematically in Figure 17.2.

The functionality of the cross link shown would appear to be eight, but this is not the case. The four lysine units involved occur as two pairs, and the two units in each pair are relatively closely spaced along the same chain. The functionality is thus four, as is illustrated in Figure 17.3.

An analogous reaction is very useful with regard to perfluoroelastomers, which are usually very difficult to cross link. Nitrile side groups placed along the chains are trimerized to triazine, thus giving similarly stable, aromatic cross links with a functionality of six. The reaction is shown in Figure 17.4.

In the case of the elastin, the lysine units involved in the cross linking are preceded and succeeded by sequences of alanine units. These sequences are thought to be α-helical, which is very intriguing since it suggests that Nature carefully positions the potential cross-linking sites spatially as well as sequentially (along the chain backbone).

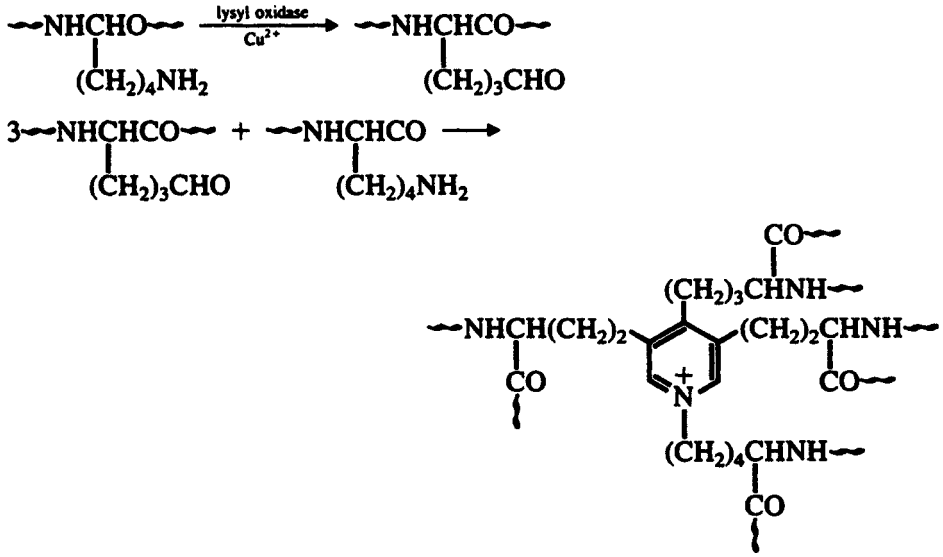

Figure 17.2 The highly specific cross-linking reaction in elastin.

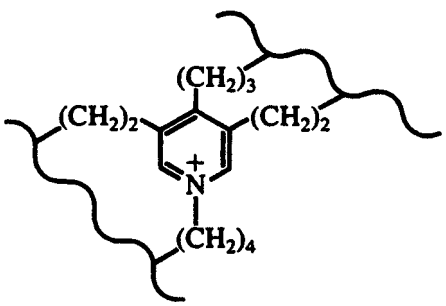

Figure 17.3 Nature of the cross links in elastin.

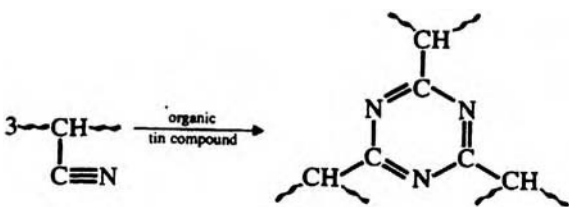

Figure 17.4 The highly specific cross-linking reaction in some perfluoroelastomers.

It should also be mentioned that the uncross-linked precursor protein for elastin is laid down among fibers of partially crystalline collagen, as is discussed further below. This gives the cross-linked elastin an elongated shape, but since the elastin is itself not crystalline, its "fibers" are isotropic (once the collagen is removed). Failure to understand this has led some workers to expect highly regular (anisotropic) structures in what is essentially an irregular (isotropic) system.

Complications in thermodynamically semi-open systems

An *open system* in the thermodynamic sense is one that can exchange its constituent matter with its surroundings (Atkins, 1990). In vivo elastin (and presumably the other bioelastomers as well) is immersed in excess amounts of aqueous body fluids, which bring it to a state of swelling equilibrium. It is thus a *semi-open* system, which, as mentioned in Chapter 8, can exchange diluent (but not polymer) with its surroundings. As also mentioned earlier, changes in temperature or deformation could then significantly change the degree of equilibrium swelling.

Experimental studies have generally been carried out with the elastin swollen with water, to closely approximate in vivo conditions. Because of the volatility of water and the open nature of in vivo elastin, these measurements have generally been carried out in excess solvent. This has caused a great deal of interpretative difficulty. In one of the most important cases, calorimetric measurements were reported for the elongation of elastin swollen and immersed in excess water (Weis-Fogh and Andersen, 1970). Large amounts of heat were given off, and these negative enthalpy changes were held to be inconsistent with the standard random network (described in Chapter 1), in that the magnitude of the fraction of the force of energetic origin (f_e/f) was not relatively small. One model proposed to replace it consisted of interconnected protein globules ("oil drops") with water consigned to the spaces between them. Stretching this assembly would distort the spherical droplets to ellipsoids of larger surface area, and the increased exposure of hydrophobic groups to the water would then account for the observed large enthalpy changes (Weis-Fogh and Andersen, 1970). Reexamination of the problem, however, showed that the enthalpy changes were dilution effects accompanying the increased swelling that invariably occurs upon elongation of an elastomer in swelling equilibrium with excess solvent (Hoeve and Flory, 1974; Treloar, 1975). This conclusion was confirmed by thermoelasticity measurements that were carried out at constant composition ("closed" thermodynamic systems). The experiments utilized either (1) a non-volatile diluent (Andrady and Mark, 1980), or (2) water as diluent with the water-swollen samples totally immersed in oil (Gosline, 1987). Also relevant are some theoretical calculations based on Monte Carlo simulations, rotational isomeric state theory (Flory, 1969), and the standard random network model. They showed that no unusual

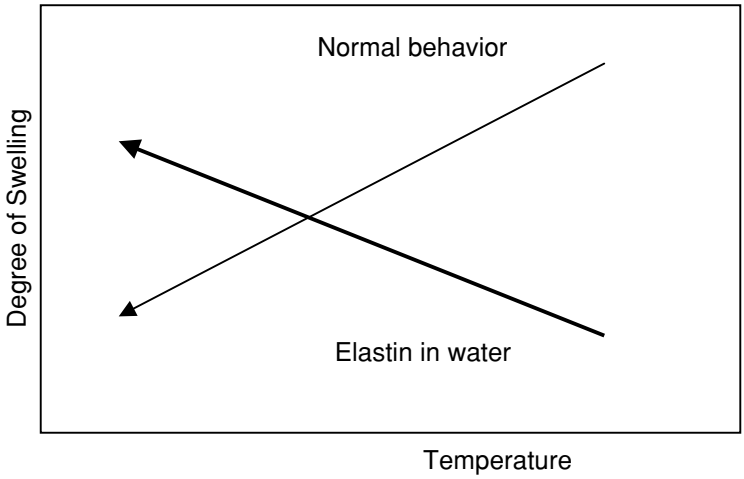

Figure 17.5 Temperature dependence of the degree of swelling of an elastomer in the usual case where a temperature decrease causes a deswelling, and the unusual case of elastin in water, where a temperature decrease causes an *increase* in swelling.

structures such as globular droplets or β-spirals (Urry *et al.*, 1982) are required to reproduce the experimental thermoelastic results (DeBolt and Mark, 1987a, b; Erman and Mark, 1997).

The basic mechanism for the elasticity of elastin is thus the usual entropy reduction accompanying the deformation of random network chains. Nonetheless, hydrophobic interactions and their change with deformation could have an effect on the elastic free energy of a swollen elastin network. They thus would contribute to the elastic force exhibited by elastin in an open system, such as occurs in in vivo deformations (Gosline, 1987).

Thermoelasticity measurements have also been carried out on a number of other bioelastomers (Erman and Mark, 1997). These include resilin from dragonflies (Weis-Fogh, 1961; Gosline, 1987), abductin from scallops (Alexander, 1966; Gosline, 1987), and arterial elastomers from octopuses (Shadwick and Gosline, 1985; Gosline, 1987). As expected, the elastic forces in these materials were also found to be almost entirely entropic, and well represented by the standard, random network model (Erman and Mark, 1997). Less is known about the thermoelasticity of any of the spider web silks (Vollrath, 1992). The fact that these materials can be partially crystalline, with the nature and amount of this crystallinity depending on swelling, deformation, and temperature, could make such data essentially uninterpretable with regard to thermoelastic properties (Erman and Mark, 1997).

It should also be mentioned that elastin in water or in aqueous body fluids exhibits a highly unusual negative temperature coefficient of swelling. This is illustrated in Figure 17.5, which shows elastin swelling more as the temperature is lowered rather

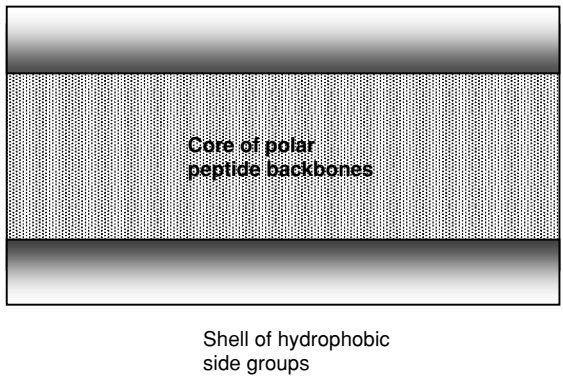

Figure 17.6 The unusual structure of elastin which might be the origin of its unusual swelling–temperature behavior: a polar core surrounded by an oily shell or coating of hydrophobic side chains.

than swelling less (as would be expected from the usual decrease of solvent power at lower temperatures). This permits the survival of fish whose body temperatures decrease when they swim into colder water. The decrease in temperature *increases* the degree of swelling of the elastin, thus further decreasing its T_g and keeping the chains flexible at the lowered temperature (Gosline, 1987). The usual decrease in swelling with decrease in temperature observed for other elastomers would have disastrous consequences for the fish. This very unusual behavior could be due to the preponderance of non-polar side groups, presumably surrounding the polar elastin backbone. This is illustrated in Figure 17.6 in a core-shell structure that is reminiscent of the structure of nerves, with an electrically conductive core insulated by a sheath of myelin.

Stress–strain behavior

Stress–strain isotherms obtained on swollen strips of elastin are generally different in shape from those observed for non-biological elastomers, even when the reinforcing collagen fibers have been removed by extractions. Specifically, they are not of the form shown in Chapter 1, frequently even at relatively low elongations. This is apparently due to the fact that such a strip is made up of a multitude of elastin fibers that are generally not "in register" (Hoeve and Flory, 1974). That is, different fibers have different amounts of slackness in the undeformed strip and thus experience different elongations as the deformation proceeds. The problem has been solved using single elastin fibers (also swollen), carrying out the measurements microscopically (Aaron and Gosline, 1981).

The elongation isotherms thus obtained show some upturns in reduced stress at high elongations. The increases in stress as the rupture point is approached

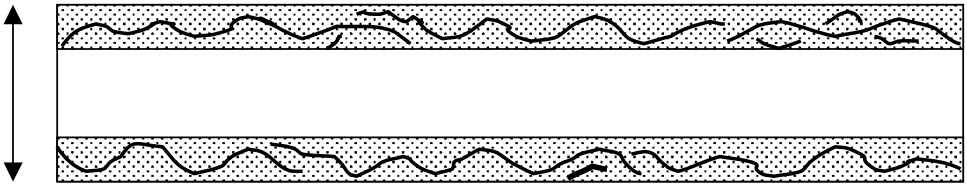

Figure 17.7 Sketch of an artery in which the elastin is laid down around a mesh of partially crystalline collagen fibers. The arrow shows the radial direction in which the artery must expand from the blood during the pressure pulse from the heart.

represent increases in ultimate strength, and could therefore be very advantageous to the organism. This increase in strength is possibly a non-Gaussian effect, due to the limited extensibility of the elastin chains. This interpretation is supported by the pattern of theoretical stress–strain isotherms calculated from distribution functions generated using Monte Carlo simulations applied to a rotational isomeric state model of typical elastin sequences (DeBolt and Mark, 1988).

In the case of an artery reinforced by the collagen fibers, the structure is similar to that of commercial pressure tubing, with its Nylon fibers reinforcing the rubber tubing. The collagen fibers are in a much more sophisticated arrangement, however, specifically with some slack (Gosline, 1980), as is shown in Figure 17.7. This arrangement permits an artery to expand radially during the systolic part of the heart's pumping cycle, and its subsequent recovery helps to keep the blood flowing smoothly. If a weak part of the arterial wall forms a bulge (an aneurism), however, some of the collagen fibers become taut. This greatly increases the modulus of the artery, permitting it to act as a "smart material". The corresponding stress–strain curve occurs so frequently in Nature that it is called the "J curve". It is shown in Figure 17.8, along with a barely acceptable linear dependence, and what would be a disastrous *decrease* in modulus with increase in elongation.

There has been a lot of additional work on other elastomeric gels of a biological nature (Clark and Ross-Murphy, 1987; Gosline, 1987; Erman and Mark, 1997; Kavanagh and Ross-Murphy, 1998). Examples include gelatin (collagen), carrageenans (partially sulfated polysaccharides from seaweed), agar, alginates (salts of alginic acid), xanthan, proteoglycans, cellulose esters and ethers, pectins, starch (amylose and amylopectin), and guar galactomannan. Finally, there are the globular biopolymers that can aggregate into rodlike structures that ultimately aggregate into fibrous or branched network structures. For example, actin, tubulin, haemoglobin-S, insulin, and fibrin form fibrous assemblies, denatured proteins form branched networks, and casein forms micellar aggregates. Results on these materials are interesting but beyond the scope of the present coverage, particularly

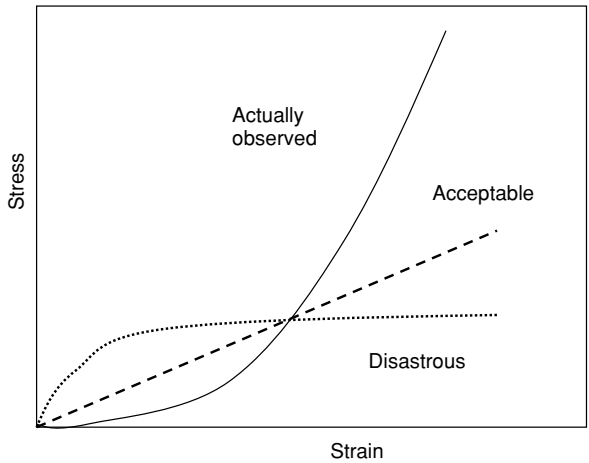

Figure 17.8 The J-shaped stress–strain curve observed for arteries, in radial deformations leading to expansion during pumping of the blood. Also shown are two hypothetical alternatives: (1) a linear dependence, which would correspond to a constant modulus (ratio of stress to strain), which would be barely acceptable, and (2) a leveling off in stress with elongation, which would be disastrous since the modulus would be *decreasing* with increasing deformation.

since most of the work reported on these materials involves their (time-dependent) viscoelastic properties.

Energy storage and hysteresis

Energy storage can be illustrated by the case of a rubber ball bouncing off a surface, as is shown schematically in Figure 17.9 (Mark, 2002a). Point a corresponds to maximum potential (stored) energy, and at point b potential energy is converted into kinetic energy. The kinetic energy is converted into elastic deformation energy upon impact with the surface, at point c. At point d, elastic energy is released and converted into kinetic energy. Finally, at point e kinetic energy is converted back into potential energy. The fraction of the original height recovered is a measure of the efficiency of the energy storage. In this case, in addition to minor effects from air resistance, the losses in stored energy are from viscous effects as chains change their spatial configurations from random to compressed and then back to random. The "resilience" measures the efficiency with which the energy is stored, and in the illustration appears to be around 70%. This experiment parallels the more familiar case of the swinging pendulum. The starting height of the weight at the end of the swinging lever again corresponds to maximum potential (stored) energy, the potential energy is converted into kinetic energy, and the kinetic energy is converted

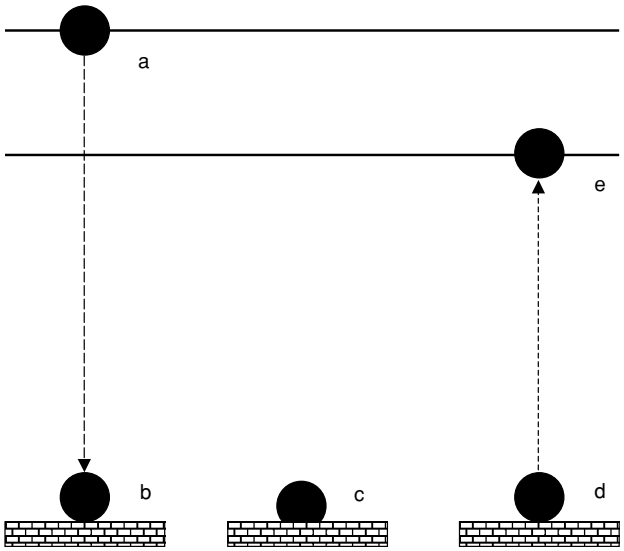

Figure 17.9 Potential energy of a rubber ball as it drops from its original position on the left (a) to the point where it is converted into kinetic energy (b), and then to elastically stored energy (c), before bouncing up (d–e) to a level corresponding to decreased potential energy.

back into potential energy. If at the end of the swing, the weight is back to 70% of its original height, then the efficiency is again 70%. In this case, the origins of the losses in stored energy arise from air resistance and friction at the pivot.

The loss in energy in the case of an elastomer can be seen more graphically by plotting stress–strain relationships at constant temperature, as is illustrated in Figure 17.10 (Mark, 2002a). The area under the curve during extension represents the energy used in the stretching, and the area under the curve during the retraction represents the energy recovered. The energy wasted in this "hysteresis" is given by the area enclosed between the two curves.

These hysteretic effects have parallels in small-molecule systems, for example in magnetization–demagnetization loops (Moore, 1983; Atkins, 1990). They are particularly important in elastomers since they correspond to wastage of energy, and overheating ("heat buildup", with accompanying increases in thermal degradation) (Mark, 2002a).

Minimizing hysteresis is very important in the case of jumping insects, such as grasshoppers and fleas. In these cases, the elastomer is a protein called resilin, and the energy is stored by their compressing a plug of this material (Erman and Mark, 1997). It is released when the insect wishes to jump, for example away from a predator, and the larger the fraction of the stored energy available the better. Release

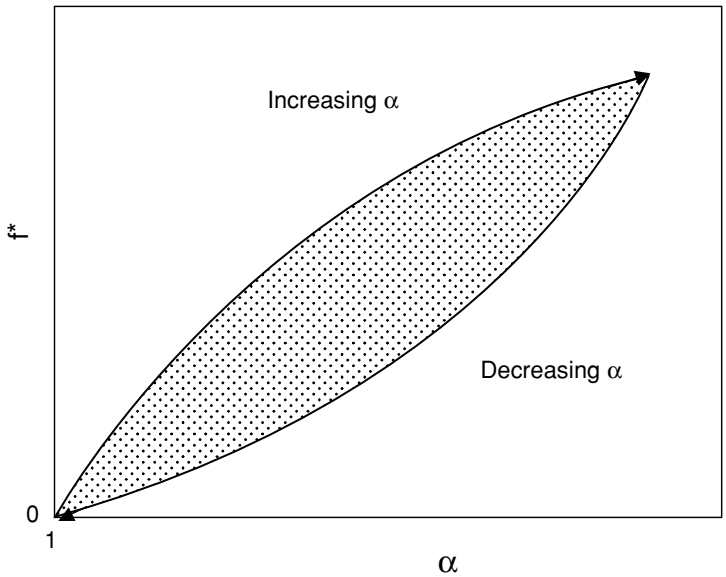

Figure 17.10 Stress–strain cycle of an elastomer at constant temperature, illustrating the occurrence of hysteresis (with the energy wasted represented by the area within the closed curve).

time is obviously also critically important, and is approximately 1 ms. Insects with more sluggish bioelastomers were presumably phased out by natural selection.

Resilin also is important in flying insects, such as dragonflies, where a plug under the wings smoothes out the flapping by alternating between being compressed and expanding. Large hysteretic effects would be bad not only because of the inefficiencies involved, but because of possible overheating of the dragonfly.

As described above, the cross linking in these bioelastomers is carefully controlled by Nature. Placing potential cross-linking sites at the ends of two stiff helical sequences may help control their spatial environment, for example their entangling with other protein repeat units (Mark, 2002a).

Trying to parallel the control nature exerts in cross linking bioelastomers, for example by end-linking reactions, is an example of "biomimicry" or "bio-inspired design". It is useful to give one illustration, however, of how such "bio-inspiration" can lead one astray (Vogel, 1994, 1998; Mark, 2002a). All of the early work trying to mimic the flight of birds by designing aircraft with flapping wings turned out to be disastrous! The successful approaches involving propellers or jets were probably not inspired at all by analogies with biological systems. Circular motions and jets of fluids for locomotion are relatively rare in biology, and are used in aqueous fluids, rather than in air.

Biosynthesis of natural rubber

A related area involves attempts to obtain a more quantitative understanding of the mechanism by which some plants can synthesize natural rubber, particularly the Hevea tree (Light and Dennis, 1989; Koyama and Steinbuchel, 2001; Tanaka, 2001). One goal is to obtain better control of the properties of the natural rubber, for example its molecular weight or molecular weight distribution. One indication of the broad range of this interest is the origins of patents in this area, which range from the Goodyear Tire & Rubber Company to Genentech, Inc.

18

Filled elastomers

Introduction

Elastomers, particularly those that cannot undergo strain-induced crystallization, are generally compounded with a reinforcing filler. The two most important examples are the addition of carbon black to natural rubber and to some synthetic elastomers (Boonstra, 1979; Rigbi, 1980; Donnet and Custodero, 2005), and silica to polysiloxane ("silicone") rubbers (Warrick *et al.*, 1979). The advantages obtained include improved abrasion resistance, tear strength, and tensile strength. Disadvantages include increases in hysteresis (and thus heat buildup) and compression set (permanent deformation).

The mechanism of the reinforcement obtained is only poorly understood in molecular terms. The network chains certainly adsorb strongly onto the particle surfaces, which would of course give an increase in the effective degree of cross linking. This is only part of the effect, however (Mullins and Tobin, 1965; Meier, 1974), but most additional molecular models seem to be highly speculative. Some elucidation might be obtained by incorporating the fillers in a more carefully controlled manner, particularly using sol–gel technology (Erman and Mark, 1997; Mark *et al.*, 2004, 2005a, b, c). We describe several such approaches, along with the incorporation of elastomeric domains in ceramic-like materials, in the remainder of this chapter.

Sol–gel generation of ceramic-like phases

Chemistry

In the most important example, hydrolysis of an alkoxysilane such as tetraethoxysilane or tetraethylorthosilicate (TEOS),

$$Si(OEt)_4 + 2H_2O \rightarrow SiO_2 + 4EtOH \qquad (18.1)$$

Table 18.1 *Some techniques for* in-situ *precipitation within an elastomer*

A.	*After cross linking*
	1. Cross link the polymer
	2. Swell with TEOS
	3. Hydrolyze some of the TEOS to silica
	4. Dry the sample
B.	*During cross linking*
	1. Dissolve TEOS into hydroxyl-terminated polymer
	2. Use some of the TEOS to end link the polymer chains
	3. Hydrolyze some of the remaining TEOS to silica
	4. Dry the sample
C.	*Before cross linking*
	1. Dissolve TEOS into an unreactive polymer
	2. Hydrolyze some of the TEOS to silica
	3. Dry the sample
	4. Cross link the filled polymer

is used to precipitate very small, well-dispersed particles of silica into a polymeric material (Erman and Mark, 1997; Mark *et al.*, 2005a, b, c). A variety of substances, generally bases, catalyze this reaction, which occurs quite readily near room temperature. Another example would be the catalyzed hydrolysis of a titanate,

$$\mathrm{Ti(OPr)_4} + 2\mathrm{H_2O} \rightarrow \mathrm{TiO_2} + 4\mathrm{PrOH} \tag{18.2}$$

in the *in-situ* precipitation of titania. Both the silica and titania thus produced give good reinforcement of a variety of elastomers. These are the same chemical reactions used in the sol–gel technology for preparing ceramics themselves (Brinker and Scherer, 1990; Sanchez *et al.*, 2002). In this case, the process first gives a swollen gel, which is then dried, fired, and densified into the final monolithic piece of ceramic, typically silica. Details of the techniques used for the *in-situ* precipitation of the particles into elastomers are given in Table 18.1.

Methods for carrying out sol–gel reactions within elastomers

The most common approach is to generate the filler after curing. In this technique the polymer is first cured or vulcanized into a network structure using any of the well-known cross-linking techniques described in Chapter 4. The network is then swelled with the silane or related molecule to be hydrolyzed, after which it is exposed to water at room temperature, in the presence of a catalyst, for a few hours. The swollen sample can be either placed directly into an excess of water containing the catalyst, or merely exposed to the vapors from the catalyst–water solution. It is

also possible to generate the catalyst and other reactants themselves *in situ*, to give composites of unusually high transparency (Rajan *et al.*, 2003). Drying the sample then gives an elastomer that is filled, and thus reinforced, with the ceramic particles resulting from the hydrolysis reaction.

Although a phase-transfer catalyst can be used in such a reaction, it was found to be unnecessary at least for relatively small specimens. Large samples could, of course, have a non-uniform distribution of particles, a possibility that has been investigated by solid-state ^{29}Si NMR spectroscopy (Garrido *et al.*, 1990, 1991).

Different alkoxysilanes can swell an elastomeric network to different extents and can hydrolyze at different rates. TEOS seems to be the best for the technique of filler precipitation after curing, as judged by the amount of silica precipitated and the extent of reinforcement obtained. Using the same criteria, basic catalysts seem more effective than acidic ones (Jiang and Mark, 1984). Some studies on the effects of catalyst concentration in particular and the hydrolysis kinetics in general have been carried out. It is found that the rate of particle precipitation can vary in a complex manner, possibly due to the loss of colloidal silica and partial deswelling of the networks when placed into contact with the catalyst solution (Mark and Ning, 1984).

Many of the studies to date have been carried out on PDMS because of the great extent to which its networks swell in TEOS. The same technique has, however, been shown to give good reinforcement of other elastomers (Mark, 1996a), for example hydrocarbon polymers such as polyisobutylene (Sun and Mark, 1987a, b). Titanates have been used in the place of silanes, with the resulting titania particles also giving significant improvements in elastomeric properties (Breiner and Mark, 1998; McCarthy *et al.*, 1998; Murugesan *et al.*, 2004).

The polymer used typically has end groups, such as hydroxyls, that can participate in the hydrolysis–condensation reactions (Erman and Mark, 1997; Mark, 2003c). Such end groups provide better bonding between the two rather disparate phases, but bonding agents may also be introduced for this purpose (Ahmad *et al.*, 1994). It is thus possible to mix hydroxyl-terminated chains (such as those of PDMS) with excess TEOS, which then serves simultaneously to tetrafunctionally end link the PDMS into a network structure and to act as the source of silica upon hydrolysis (Erman and Mark, 1997). This simultaneous curing and filling technique has been successfully used for PDMS elastomers having a unimodal distribution of chain lengths and for PDMS elastomers and thermosets having bimodal distributions. The roles of polymer and alkoxysilane may also be reversed by putting triethoxylsilyl groups at the ends of PDMS chains. Reactive groups at the surface of the *in-situ*-generated silica or titania particles then react with the chain ends to simultaneously cure and reinforce the elastomeric material (Sur and Mark, 1985).

In the previous two techniques, removal of the unreacted TEOS and the ROH by-product causes a significant decrease in volume (Novak, 1993), which could be disadvantageous in some applications. One way of overcoming this problem is by precipitating the particles into a polymer that is inert under the hydrolysis conditions, for example, vinyl-terminated PDMS. The resulting polymer–filler suspension, after removal of the other materials, is quite stable. It can be subsequently cross linked, for example, by silane reaction with the vinyl groups, with only the usual, very small change in volume occurring in any curing process.

Approximately spherical particles and their reinforcing properties

Because of the nature of the *in-situ* precipitation, the particles are well dispersed and are essentially unagglomerated (as demonstrated by electron microscopy). The mechanism for their growth seems to involve simple homogeneous nucleation, and since the particles are separated by polymer, they do not have the opportunity to coalesce. A typical transmission electron micrograph of such a filled material is shown in Figure 18.1 (Ning *et al.*, 1984). The particles are relatively monodisperse, with most of them having diameters in the range 100–200 Å. The growth of the particles in from the surface of a PDMS sample can be followed by NMR (Garrido *et al.*, 1991), utilizing ^{1}H and ^{29}Si magic-angle spinning, with two-dimensional Fourier transform spin-echo techniques. Such an approach is based on the study of ^{1}H spin-spin (T_2) relaxation times of the protons in the PDMS polymer as they are being constrained by silica-like material being generated in their vicinities. This technique is obviously non-destructive but if the sample can be sacrificed, then slices taken from it can be further studied in a gradient column with regard to density, by electron microscopy (Wang and Mark, 1994), or by X-ray or neutron scattering (Roe, 2000; Wignall, 2004).

A variety of catalysts work well in the typical hydrolysis reactions used, including acids, bases, and salts (Jiang and Mark, 1984). Basic catalysts give precipitated phases that are generally well-defined particles, whereas the acidic catalysts give more poorly defined, diffuse particles (Schaefer and Keefer, 1984; Keefer, 1990). This is illustrated in the X-ray scattering profile shown in Figure 18.2. The scattering results, specifically the intensity as a function of scattering vector, give values of the radii of gyration R_g. The terminal slopes give information on the particle surfaces, with a value of -4 corresponding to smooth particles (from basic catalysts) and -3 to "fuzzy" particles (from acidic catalysts). In some cases, particles are not formed at all, and bicontinuous (interpenetrating) phases result (Schaefer *et al.*, 1990, 1992).

Interesting "aging" effects are frequently observed in these systems. If the precipitated particles are left in contact with the hydrolysis catalyst and water they appear to reorganize, so that their surfaces become better defined and their sizes

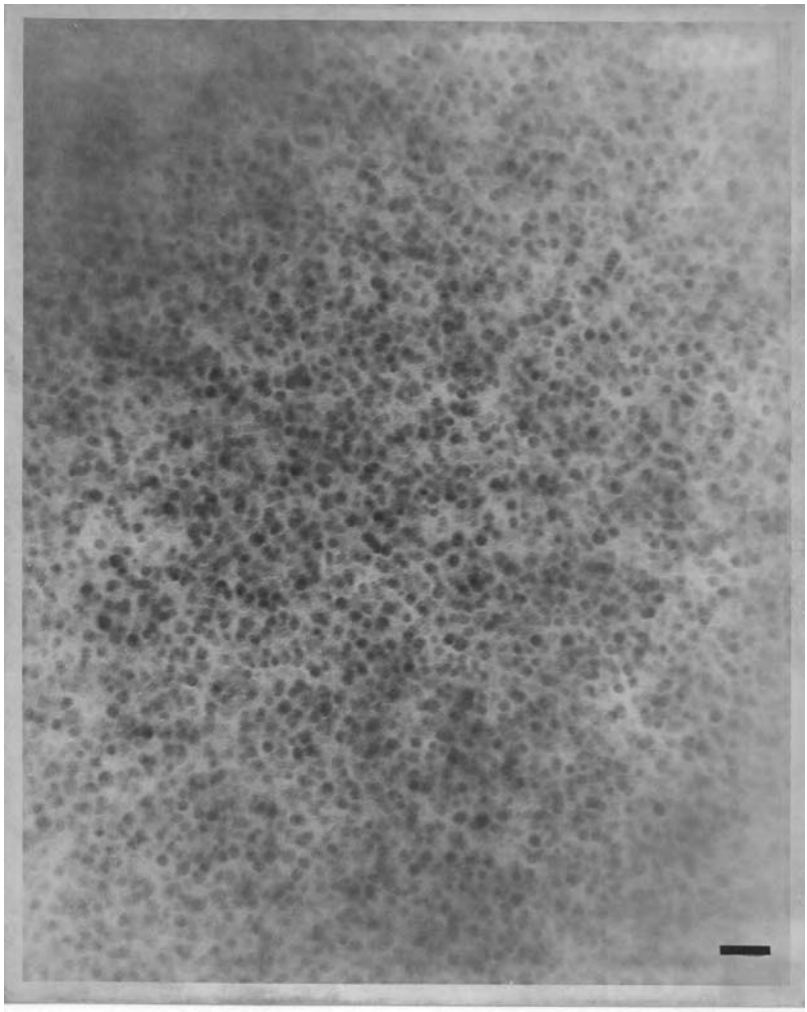

Figure 18.1 Transmission electron micrograph of a PDMS network containing 34.4 wt% *in-situ* precipitated silica particles (Ning *et al.*, 1984). The length of the bar corresponds to 1000 Å. (Reproduced by permission of John Wiley and Sons.)

become more uniform (Xu *et al.*, 1990). The process seems quite analogous to the "Ostwald ripening" (Ostwald, 1900) much studied by colloid chemists.

The reinforcing ability of such *in-situ* generated particles has been amply demonstrated for a variety of deformations, including uniaxial extension (simple elongation), biaxial extension (compression), shear, and torsion (Mark and Schaefer, 1990, Mark, 1996d, Erman and Mark, 1997). In the case of uniaxial extension, the modulus [f^*] frequently increases by more than an order of magnitude, with the isotherms generally showing the upturns at high elongations that are the signature of good

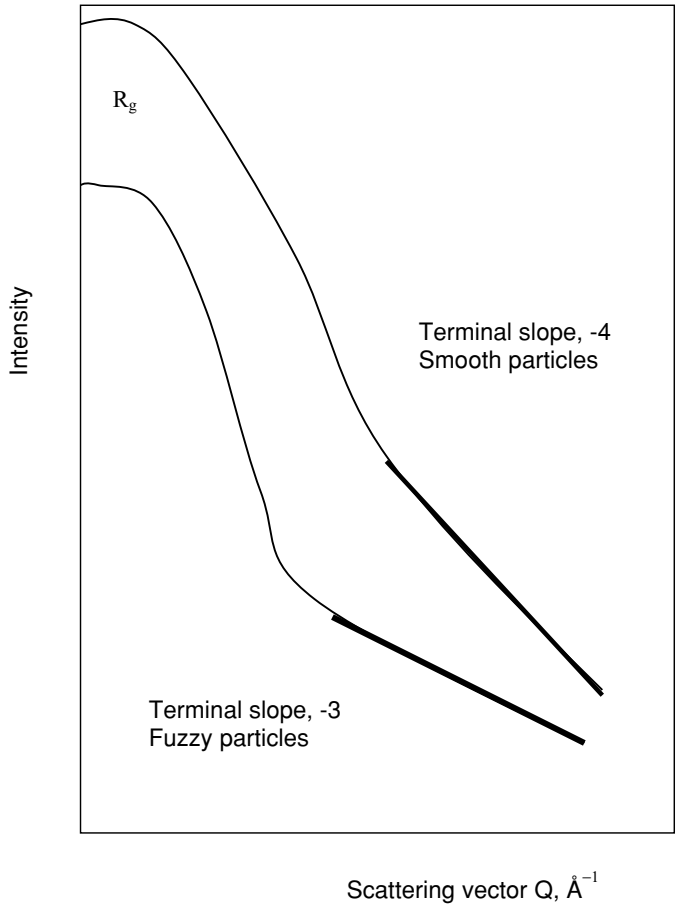

Figure 18.2 Intensity of small-angle X-ray scattering (SAXS) as a function of the scattering vector. The heavy lines emphasize the terminal slopes, which give information on the particle interfaces.

reinforcement (Mark and Ning, 1984, Mark *et al.*, 1992b). Typical results are shown in the left portion of Figure 18.3, where α is the extension (Wang *et al.*, 1991b). As is generally the case in filled elastomers, there is considerable irreversibility in the isotherms, which is thought to be due to irrecoverable sliding of the chains over the surfaces of the filler particles upon being strained. The right portion of the figure documents the reinforcement observed in equi-biaxial extension (or compression). The maxima and minima exhibited by such results will be a challenge to those seeking a better molecular understanding of filler reinforcement in general.

Some fillers other than silica, for example titania, do give stress–strain isotherms that are reversible, indicating interesting differences in surface chemistry, including increased ability of the chains to slide along the particle surfaces (Wang and

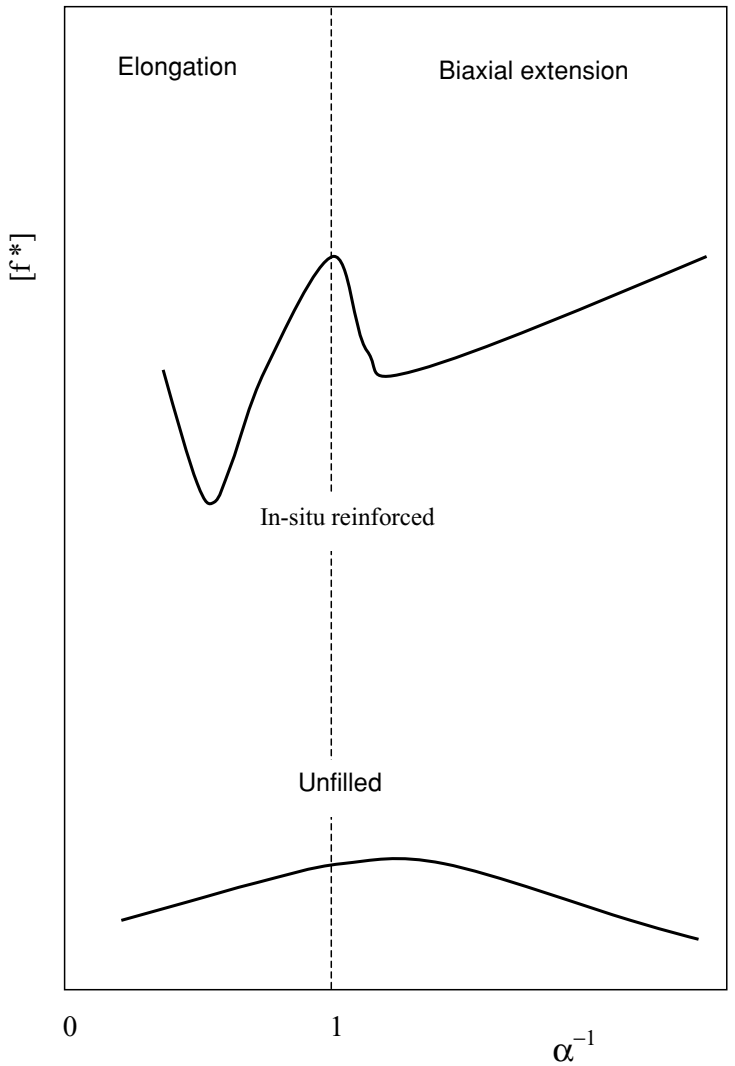

Figure 18.3 Stress–strain isotherms for *in-situ* reinforced elastomers in elongation (region to the left of the vertical dashed line, with $\alpha^{-1} < 1$), and in biaxial extension (compression) (to the right, with $\alpha^{-1} > 1$).

Mark, 1987). Such results are illustrated in Figure 18.4 (Wang and Mark, 1987). The bonding of PDMS to silica, titania, or silica–titania mixed oxide particles is however strong enough to suppress *swelling* of the polymer, as is illustrated in Figure 18.5 (Wen and Mark, 1994b). These results involve equilibrium swelling measurements obtained on unfilled and filled PDMS elastomers to estimate the degree of adhesion between elastomer and filler particles (Kraus, 1965; Wen and Mark, 1994b; Burnside and Giannelis, 1995). The results differ greatly from those

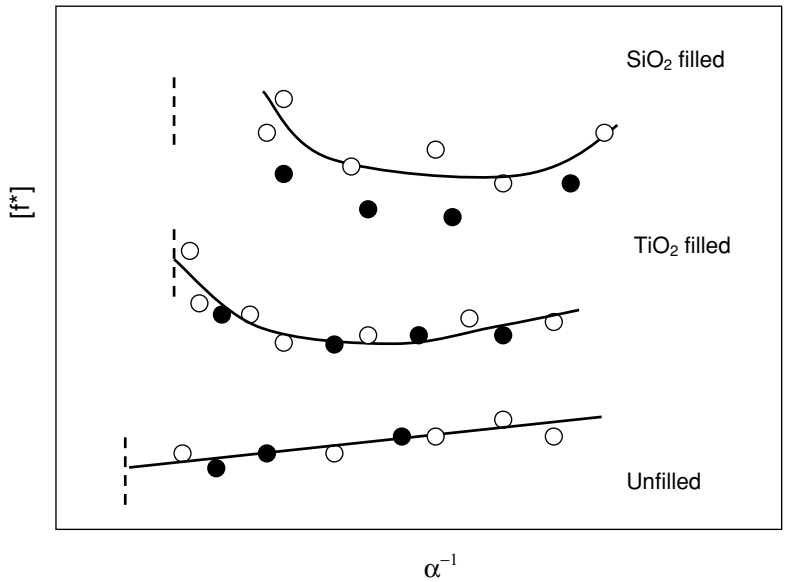

Figure 18.4 Stress–strain isotherms for elastomeric networks reinforced *in situ* with either silica or titania particles (Wang and Mark, 1987). Filled circles locate results used to test for reversibility.

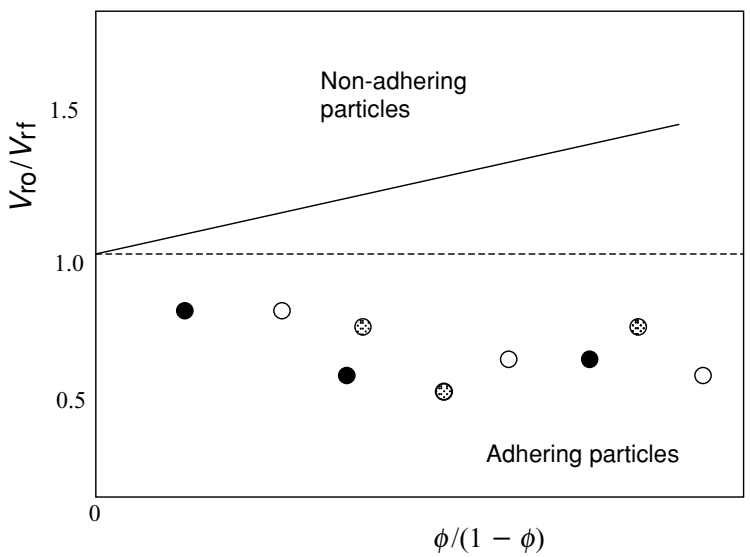

Figure 18.5 Plot of volume fraction ratio V_{ro}/V_{rf} characterizing the swelling of an unfilled PDMS network relative to that of a filled PDMS network, against filler loading expressed as volume ratio of filler to PDMS $\phi/(1-\phi)$ (where ϕ is the volume fraction of filler) (Wen and Mark, 1994b). Open, dotted, and filled circles represent results for silica, silica–titania mixed oxides, and titania.

to be expected for non-adhering fillers, indicating good bonding between the two phases. Obviously, resistance to separation from the surface in such swelling tests does not contradict the chains having considerable mobility *along* the surfaces of some types of particles, as was just described.

These *in-situ* generated silica fillers also give increased resistance to creep or compression set in cyclic deformations (Wen *et al.*, 1994). The *in-situ* filled PDMS samples showed very little compression set. The samples also exhibited increased thermal stability (Sohoni and Mark, 1992). Specifically, the samples in which the SiO_2 was introduced *in situ* had higher decomposition temperatures. A possible mechanism for this improvement would be increased capability of the *in-situ* produced silica to tie up hydroxyl chain ends that participate in the degradation reaction.

A variety of techniques have been used to further characterize these *in-situ* filled elastomers (Mark and Schaefer, 1990; Erman and Mark, 1997). Density measurements, for example, yield information on the nature of the particles. Specifically, the densities of the ceramic-type particles are significantly less than that of silica itself, and this suggests that the particles presumably contain some unhydrolyzed alkoxy groups or some voids, or both. The low-temperature properties of some of these peculiarly filled materials have also been studied by calorimetric techniques. Of particular interest is the way in which reinforcing particles can affect the crystallization of a polysiloxane, both in the undeformed state and at high elongations (Aranguren, 1998).

As already mentioned, electron microscopy (both transmission and scanning) has been used to characterize the precipitated particles. The information obtained in this way includes (1) the nature of the precipitated phase (particulate or non-particulate), (2) the average particle size, if particulate, (3) the distribution of particle sizes, (4) the degree to which the particles are well defined, and (5) the degree of agglomeration of the particles (Erman and Mark, 1997).

A number of studies using X-ray and neutron scattering (Pethrick and Dawkins, 1999; Roe, 2000; Sperling, 2001; Wignall, 2004) have also been carried out on filled elastomers (Mark and Schaefer, 1990; Schaefer *et al.*, 1990). Although the results are generally consistent with those obtained by electron microscopy, there are some intriguing differences. Of particular interest is the observation that some fillers that appear to be particulate in electron microscopy, appear to consist of continuously interpenetrating phases by scattering measurements. Additional experiments of this type will certainly be forthcoming.

Modified filler particles

If an *in-situ*-filled elastomer is extracted with a good solvent, its modulus and ultimate strength are frequently significantly increased. The effect is probably due

to hydrolytic formation of additional reactive groups on the particle surface or to removal of absorbed small molecules, thus increasing the number of sites for particle–polymer bonding.

In some applications, it may be advantageous for the filler particles to have some deformability. It may be possible to induce such deformability by using a molecule that is only partially hydrolyzable, for example, a triethoxysilane [$R'Si(OR)_3$], where R' could be methyl, ethyl, vinyl, or phenyl (Mark, 1996b).

Fillers with controlled interfaces

By choosing the appropriate chemical structures, chains that span filler particles in PDMS-based composites can be designed so that they are either durable, are breakable irreversibly, or are breakable reversibly (Vu *et al.*, 2000, 2003; Vu, 2001; Schaefer *et al.*, 2002).

Silicification and biosilicification

There has been some interest in generating silica-like particles using templates, as is done by Nature in biosilicification processes (Patwardhan and Clarson, 2003; Patwardhan *et al.*, 2003). Various particle shapes have been obtained; platelet forms would be of particular interest with regard to their abilities to provide reinforcement and decrease permeability, as occurs with the layered fillers described below.

Other inorganic particles

Polyhedral oligomeric silsesquioxanes (POSS)

These fillers are cage-like silicon–oxygen structures, and have been called the smallest possible silica particles (Haddad *et al.*, 2001; Laine *et al.*, 2001a; Lichtenhan *et al.*, 2001; Loy *et al.*, 2001; Pan *et al.*, 2003). The most common structure has eight silicon atoms, each carrying an organic group. The particles on which none of the groups are functionally reactive can be simply blended into elastomers such as PDMS using the usual mixing or compounding techniques. In this case, the inert groups are chosen to improve miscibility with the elastomeric host matrix. POSS molecules having one reactive functional group can be attached to a polymer as side chains. Those with two reactive groups can be incorporated into polymer backbones by copolymerization, and those with more than two can be used for forming cross links, within network structures.

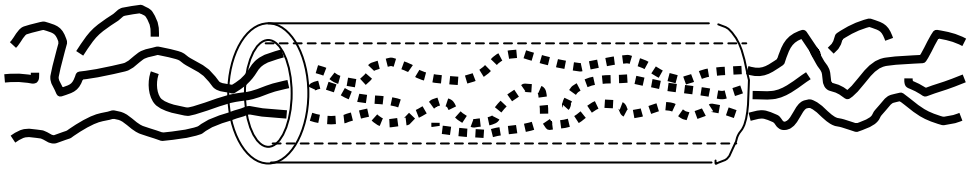

Figure 18.6 Polymer chains being threaded through a porous inorganic material such as a zeolite by polymerizing monomer that had been absorbed into one of the channels or cavities.

Porous particles

Some fillers such as zeolites are sufficiently porous to accommodate monomers, which can then be polymerized. This threads the chains through the cavities, with unusually intimate interactions between the reinforcing phase and the host elastomeric matrix (Frisch and Mark, 1996; Mark, 1999c; Kickelbick, 2003). Such an arrangement is illustrated in Figure 18.6. Unusually good reinforcement is generally obtained. Also, because of the constraints imposed by the cavity walls, these confined polymers frequently show no glass transition temperatures or melting points (Mark, 2003b; Sur *et al.*, 2003). PDMS chains have also been threaded through cyclodextrins, to form *pseudo*-rotaxanes (Okumura *et al.*, 2000).

Layered fillers

Exfoliating layered particles such as the clays, mica, or graphite is being used to provide very effective reinforcement of polymers at loading levels much smaller than in the case of solid particles such as carbon black and silica (Giannelis *et al.*, 1999; Pinnavaia and Beall, 2001; Vaia and Giannelis, 2001b; Vu *et al.*, 2001; Zhou *et al.*, 2001). Other properties can also be substantially improved, including increased resistance to solvents, and reduced permeability and flammability. A number of such studies specifically address the effects of introducing layered fillers into polysiloxanes (Burnside and Giannelis, 1995, 2000; Wang *et al.*, 1998; Bokobza and Nugay, 2001; Osman *et al.*, 2001, 2002; Bruzard and Levesque, 2002; Ma *et al.*, 2002).

Miscellaneous fillers

There are a variety of miscellaneous fillers that are of interest for reinforcing elastomers. Examples are ground-up silica xerogels (Deng *et al.*, 2000), carbon-coated silica (Kohls *et al.*, 2001), and functionalized silica particles (Bourgeat-Lami *et al.*, 1995; Espiard *et al.*, 1995, Luna-Xavier *et al.*, 2001).

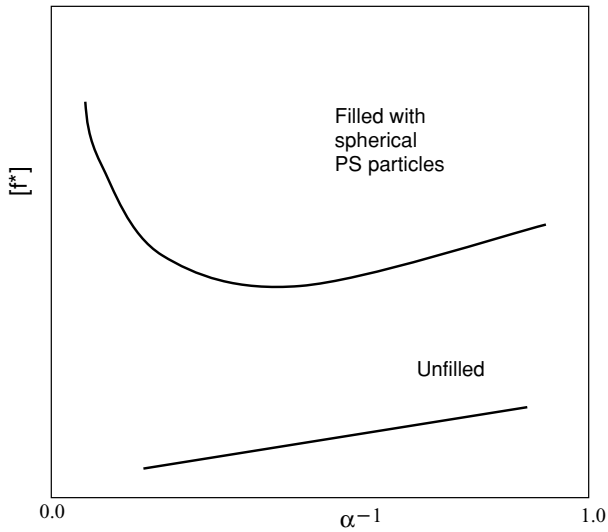

Figure 18.7 Stress–strain isotherms for PDMS–polystyrene (PS) composites (Fu and Mark, 1988). The increase in modulus without loss in extensibility is unusual.

Organic particles

Glassy particles deformable into ellipsoidal shapes

It is also possible to obtain reinforcement of an elastomer by polymerizing a monomer such as styrene to yield hard glassy domains within the elastomer (Fu and Mark, 1988, 1989). Low concentrations of styrene give low molecular weight polymer that acts more like a plasticizer than a reinforcing filler. At higher styrene concentrations, however, roughly spherical polystyrene (PS) particles are formed, and good reinforcement is obtained. The particles thus generated are relatively easy to extract from the elastomeric matrix. This means that little effective bonding exists between the two phases. It is possible, however, to get excellent bonding onto the filler particles. One way is to include some trifunctional $R'Si(OC_2H_5)_3$ in the hydrolysis, where R′ is an unsaturated group. The R′ groups on the particle surfaces then participate in the polymerization, thereby bonding the elastomer chains to the reinforcing particles. Alternatively, the $R'Si(OC_2H_5)_3$ can be used as one of the end-linking agents, to place unsaturated groups at the cross links. Their participation in the polymerization would then tie the PS domains to the elastomer's network structure. In any case, the very good reinforcement provided by the PS domains while in the roughly spherical state is shown in Figure 18.7 (Fu and Mark, 1988). The extensibility was found to remain high in spite of large increases in modulus. The PS domains have the disadvantage of having a relatively

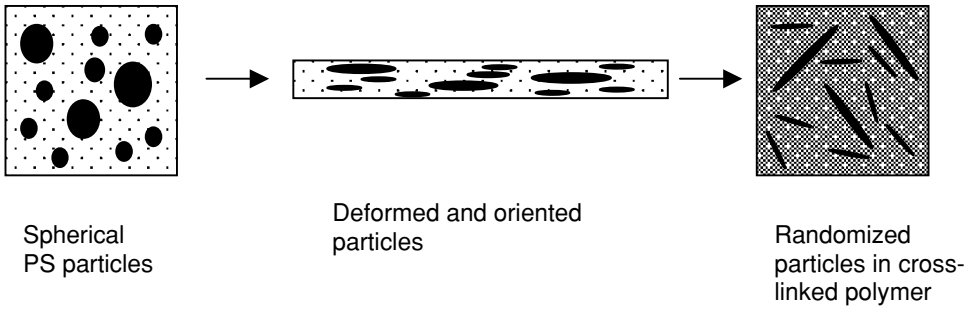

Figure 18.8 Elongation of softened spherical particles into ellipsoids by stretching the polymer matrix in which they are embedded. The orientation also introduced can be removed by dissolving away the matrix and redispersing the particles into another matrix.

low glass transition temperature ($T_g \approx 100\ ^\circ C$) (Mark, 1996a, 1999b; Brandrup *et al.*, 1999) and in being totally amorphous. Above their values of T_g they would soften and presumably lose their reinforcing ability. For this reason, similar studies have been carried out using poly(diphenylsiloxane) as the reinforcing phase (Wang and Mark, 1990b). This polymer is crystalline, and measurements on copolymers containing diphenylsiloxane blocks indicate it has a melting point (and thus a softening temperature) as high as 550 °C (Ibemesi *et al.*, 1985, 1990)! It is possible to convert the essentially spherical PS particles just described into ellipsoids (Nagy and Keller, 1989; Wang and Mark, 1990a; Ho *et al.*, 1993; Erman and Mark, 1997). First, the PS–elastomer composite is raised to a temperature well above the T_g of PS. It is then deformed, and cooled while in the stretched state. This is illustrated in Figure 18.8. The particles are thereby deformed into ellipsoids, and retain this shape when cooled. Uniaxial deformations of the composite give prolate (needle-shaped) ellipsoids, and biaxial deformations give oblate (disc-shaped) ellipsoids (Wang and Mark, 1990a; Wang *et al.*, 1991a). Prolate particles can be thought of as a conceptual bridge between the roughly spherical particles used to reinforce elastomers and the long fibers frequently used for reinforcement in thermoplastics and thermosets. Similarly, oblate particles can be considered as analogs of the much studied clay platelets used to reinforce a variety of polymers (Okada *et al.*, 1990; Giannelis, 1996; Pinnavaia *et al.*, 1996; Vaia and Giannelis, 2001a) but with dimensions and compositions that are controllable. Such ellipsoidal particles have been characterized using both scanning and transmission electron microscopy. This gives values for their axial ratios and provides a measure of the extent to which their axes were aligned in the direction of stretching. In these anisotropic materials, elongation moduli in the direction of the stretching were found to be significantly larger than those of the untreated PS–elastomer composite, whereas in the perpendicular

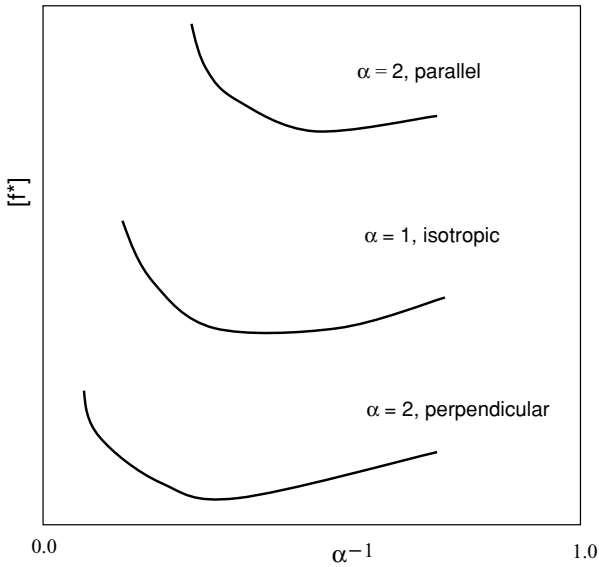

Figure 18.9 Stress–strain isotherms of a composite in which particles are oriented prolate ellipsoids (Wang and Mark, 1990a). Values of the draw ratio and testing directions are indicated on each curve.

direction they were significantly lower. This is shown in Figure 18.9 (Wang and Mark, 1990a). Such differences were to be expected from the anisotropic nature of the systems. In the case of non-spherical particles in general, degrees of orientation are also of considerable importance. One interest here is the anisotropic reinforcements such particles provide, and there have been simulations to better understand the mechanical properties of such composites (Sharaf and Mark, 2002, 2004; Mark, 2003b).

As is also illustrated in the figure, the ellipsoidal particles can be removed by dissolving away the polymer matrix and then redispersed randomly into another polymer prior to its cross linking.

Nanotubes

Carbon nanotubes are also of considerable interest with regard to both reinforcement and possible increases in electrical conductivity (Haddad *et al.*, 2001; Choi *et al.*, 2001; Lichtenhan *et al.*, 2001; Pyun *et al.*, 2001; Tamaki *et al.*, 2003). In some cases, the nanotubes have been functionalized with organic groups. There is considerable interest in characterizing the flexibility of these nanotube structures, in minimizing their tendencies to aggregate, and in maximizing their miscibilities with inorganic as well as organic polymers.

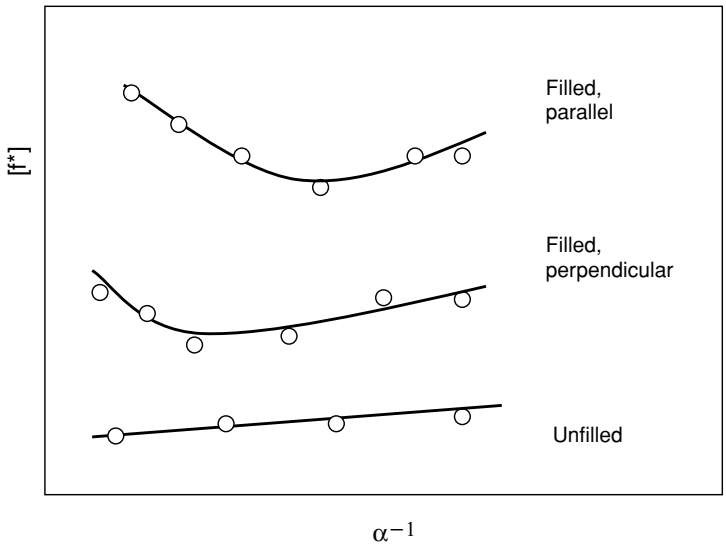

Figure 18.10 Stress–strain isotherms for elastomeric composites containing magnetically responsive particles (Sohoni and Mark, 1987). Each curve is identified by the orientation (parallel or perpendicular) of the sample strip relative to the lines of force of the magnetic field.

Metal particles

Magnetic particles

Incorporating reinforcing particles that respond to a magnetic field is important with regard to aligning even spherical particles to improve mechanical properties anisotropically (Rigbi and Mark, 1985; Sobon *et al.*, 1987; Sohoni and Mark, 1987; Calvert and Broad, 1991). Considerable anisotropy in structure and mechanical properties can be obtained, as is demonstrated for PDMS in Figure 18.10 (Sohoni and Mark, 1987). Specifically, the reinforcement is found to be significantly higher in the direction parallel to the magnetic lines of force. This technique could be combined with the *in-situ* approach by generating metal or metal oxide magnetic particles in a magnetic field (Liu and Mark, 1987; Sur and Mark, 1987), for example by the thermolysis or photolysis of a metal carbonyl. Some related work involved the use of *in-situ* techniques to generate electrically conducting fillers such as polyaniline within PDMS (Murugesan *et al.*, 2005).

Catalytic particles

In some cases, the particles generated within polymeric matrices were metals such as platinum, palladium, and silver. The matrix now served the purpose of protecting the particles in their functioning as nanocatalysts, and thus increasing their

shelf-lives (Mayer and Mark, 2000). Also, once the particles are delivered into a reaction medium, the polymer chains adsorbed onto their surfaces can improve the selectivity in some catalytic reactions (Vu and Mark, 2004). Elastomers suitable for the protective matrix would have to have low permeabilities to substances that could deactivate the nanocatalyst particles, for example oxygen and water. Polyisobutylene might be unusually good in this regard.

Simulations on fillers

Monte Carlo computer simulations have been carried out on a variety of filled elastomers, including PDMS (Mark, 1996c, 2001b, 2002b; Yuan *et al.*, 1996), in an attempt to obtain a better molecular interpretation of how such dispersed phases reinforce elastomers. The approach taken enabled estimation of the effect of the excluded volume of the filler particles on the network chains and on the elastic properties of the networks. In the first step, distribution functions for the end-to-end vectors of the chains were obtained by applying Monte Carlo methods to rotational isomeric state representations of the chains (Mark and Curro, 1983). Conformations of chains which overlapped with any filler particle during the simulation were rejected. The resulting perturbed distributions were then used in the three-chain elasticity model (Treloar, 1975) to obtain the desired stress–strain isotherms in elongation.

In one application, a filled PDMS network was modeled as a composite of cross-linked polymer chains and spherical filler particles arranged in a regular array on a cubic lattice (Sharaf *et al.*, 1994). The filler particles were found to increase the non-Gaussian behavior of the chains and to increase the moduli, as expected. It is interesting to note that composites with such structural regularity have actually been produced (Sunkara *et al.*, 1995) and some of their mechanical properties have been reported (Pu *et al.*, 1997; Rajan *et al.*, 2002). In a subsequent study, the reinforcing particles were randomly distributed within the PDMS matrix (Mark, 2002b). One effect of the filler was to increase the end-to-end separations of the chains. These results on the chain-length distributions are in agreement with some subsequent neutron scattering experiments on silicate-filled PDMS (Nakatani *et al.*, 2001). The corresponding stress–strain isotherms in elongation showed substantial increases in stress and modulus with increase in filler content and elongation that are in at least qualitative agreement with experiment.

In the case of non-spherical filler particles, it has been possible to simulate the anisotropic reinforcement obtained, for various types of particle orientations (Sharaf *et al.*, 2001; Mark, 2002b; Sharaf and Mark, 2002, 2004). Different types and degrees of particle agglomeration can also be investigated.

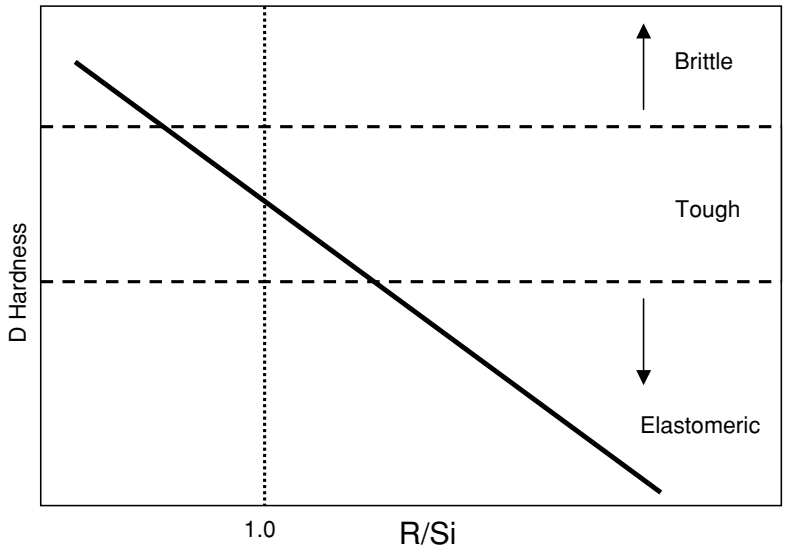

Figure 18.11 The hardness of a silica–PDMS composite as a function of the relative numbers of R alkyl groups and silicon atoms (Mark and Sun, 1987).

Polymer-modified ceramics

If the hydrolyses in silane precursor–polymer systems are carried out using relatively large amounts of the silane, then the silica generated can become the continuous phase, with the elastomeric polymer dispersed in it (Wilkes *et al.*, 1990; Hjelm *et al.*, 2001; Laine *et al.*, 2001b; Sanchez *et al.*, 2002). Again, a variety of ceramic components and polymeric components have been studied. The resultant composite is a polymer-modified glass or ceramic, frequently of very good transparency. Although its thermal stability will be inferior to that of the ceramic component itself, there are many applications for ceramic-type materials where this is not a serious problem.

As might be expected, the properties of these materials depend greatly on the relative amounts of the two phases. Properties of particular interest are modulus, impact resistance, ultimate strength, maximum extensibility, viscoelastic responses, and transparency. The hardness of such a composite, for example, can be varied by control of the molar ratio of alkyl R groups to Si atoms, as is illustrated for PDMS in Figure 18.11 (Mark and Sun, 1987). Low values of R/Si yield a brittle ceramic, and high values give a relatively hard elastomer. The most interesting range, R/Si $\cong$ 1, can yield a relatively tough ceramic of increased impact resistance.

Some improvements in impact strength in such composites are illustrated in Figure 18.12 (Wen and Mark, 1995b). It shows impact strengths of some

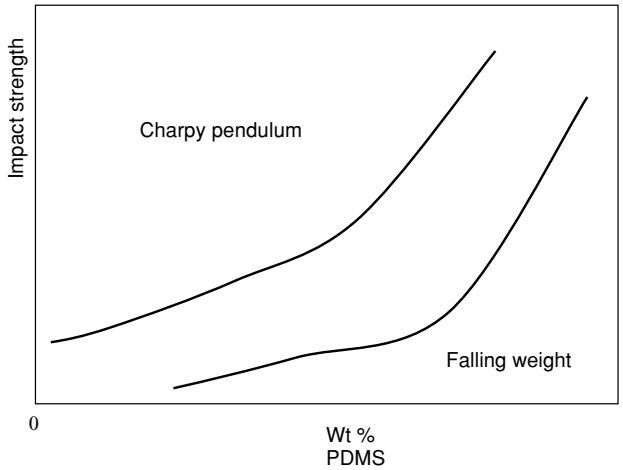

Figure 18.12 Dependence of two estimates of the impact strength on the amount of PDMS in PDMS-modified SiO_2 glasses (Wen and Mark, 1995b). The impact strengths were obtained from the Charpy pendulum impact test, or the falling-weight impact test.

PDMS–SiO_2 samples that had been determined by the Charpy pendulum test and by the falling-weight test. The samples investigated were PDMS-modified SiO_2 and SiO_2/TiO_2 glasses with PDMS contents ranging from 0 to 65 wt%. As expected, only samples with relatively high ceramic contents were sufficiently brittle to be studied in this manner. As can be seen from the figure, the larger the amount of PDMS used, the higher the impact strength.

For PDMS-modified SiO_2 glasses, structural analysis shows that this hybrid material has some degree of localized phase separation of the PDMS component, even though OH-terminated PDMS can be successfully incorporated into the SiO_2 network by chemical bonding. The PDMS component can behave as an elastomeric phase because the glass transition temperature of PDMS is far below room temperature (Mark, 1996a, 1999b; Brandrup *et al.*, 1999). When the material is subjected to an impact test, the PDMS component can absorb a great deal of energy by motions of the PDMS chains, and can ameliorate the growth of cracks and fracture. Therefore, considerable toughening of the glass can be achieved by increasing the amount of PDMS introduced. The impact resistance was also observed to increase in with increase in PDMS molecular weight, possibly due to increase in the phase separation which leads to the energy-absorbing domains (Wen and Mark, 1995b).

Also relevant here are some microscopy results. Microscopy of fracture surfaces of brittle samples typically shows smooth fracture surfaces (Reed, 1979) with little

evidence of effective resistance to either initiation or propagation of cracks. This was observed in the case of the composite silica samples having relatively low PDMS contents. In contrast, samples with high PDMS contents had fracture surfaces showing some degree of "whitening" or shearing (Wen and Mark, 1995b). This suggests that the dispersed elastomer provides a ductile, energy-absorbing response to the impacts, with increased resistance to crack propagation.

19

Current problems and new directions

Listed below are some aspects of rubberlike elasticity which are clearly in need of additional research (Mark, 2004a, b). Most have already been mentioned or will be obvious from the discussions in the preceding chapters.

- Improved understanding of dependence of the transition temperatures T_g and T_m on polymer structure
- Preparation and characterization of "high-performance" elastomers
- New cross-linking techniques
- Improved understanding of network topology
- Generalization of phenomenological theory
- More experimental results for deformations other than elongation and swelling
- Better characterization of segmental orientation, and its effects on strain-induced crystallization
- More detailed understanding of critical phenomena and gel collapse
- Additional molecular characterizations using NMR spectroscopy and various scattering techniques
- Study of possibly unique properties of bioelastomers
- Improved understanding of reinforcing effects of filler particles in a network
- Quantitative interpretation of the toughening effects of elastomers in blends and in composites, particularly the polymer-modified ceramics
- Environmental concerns ranging from elastomer synthesis to recycling

There is a real need for more high-performance elastomers, which are materials that remain elastomeric to very low temperatures and are relatively stable at very high temperatures. Some phosphazene polymers (Mark *et al.*, 1992a, 2005b) are in this category. These polymers have rather low glass transition temperatures in spite of the fact that the skeletal bonds of the chains are thought to have some double-bond character. There are thus a number of interesting problems related to the elastomeric behavior of these unusual semi-inorganic polymers. There is

also increasing interest in the study of elastomers that also exhibit the type of mesomorphic behavior described in Chapter 16.

An example of a cross-linking technique currently under development is the preparation of new triblock copolymers, similar to those of styrene–butadiene–styrene. Elastomers of this type are thermoplastic, and it is possible to reprocess them by simply heating to above the glass transition temperature of the hard phase, which makes them *reprocessable*. As mentioned in Chapter 17, more novel approaches could probably be learned by studies of the cross-linking techniques used by Nature in preparing bioelastomers.

A particularly challenging problem is the development of a more quantitative molecular understanding of the effects of filler particles, in particular carbon black in natural rubber and silica in siloxane polymers (Mark *et al.*, 2005a). As described in Chapter 18, such fillers provide tremendous reinforcement in elastomers in general, and how they do this is still only poorly comprehended. A related but even more complex problem involves much the same components, namely one that is organic and one that is inorganic. When one or both components are generated *in situ*, however, there is an almost unlimited variety of structures and morphologies that can be generated. How physical properties such as elastomeric behavior depend on these variables is obviously a challenging but important problem.

With regard to environmental concerns, it is increasingly important to be able to prepare synthetic elastomers in polymerizations that avoid organic solvents. Carrying out polymerizations in general in supercritical fluids has shown a great deal of promise in this regard (DeSimone and Tumas, 2003; Folk and DeSimone, 2003; Wood *et al.*, 2004).

There have been a variety of studies on the effects of polymers on the environment (Andrady, 2003), but the major focus here will be on elastomers in general and on tires in particular, since tires make up by far the largest bulk of any elastomer application.

Once a tire is no longer usable on a vehicle, there are only a very small number of alternative uses, such a bumpers on boats and wharves. Simply discarding the tires is not a reasonable alternative since there are so many of them and they have little biodegradability. One useful alternative is simply to burn them and at least get some of their energy content through their use as a fuel source. In the case of synthetic rubbers this can be thought of as simply borrowing the organic materials used in their manufacture, and then only later extracting their energy content when burning them as a fuel. Another approach is to grind the rubber into fine particles, cryogenically if necessary. Dissolution methods are of course inapplicable since the elastomers are essentially always cross linked into network structures. In any case, such ground-up particles can be blended into asphalt for road surfaces, or into virgin

rubbers if the properties of the blend are not unacceptably compromised. Degrading the chains all the way to the monomers generally does not seem feasible.

The most environmentally useful approach would be to devulcanize (uncross link) the rubber product, which could then be re-cross linked. In this case, even relatively low-volume elastomers such as the polysiloxanes or fluoroelastomers are also of interest because of the value (cost) of these products. Although a number of methods have been used for such devulcanization (Masaki *et al.*, 2004), the recent focus has been on the use of ultrasonic energy (De *et al.*, 2005; Isayev, 2005). This process can be carried out continuously, without the need for any chemicals. Applications to date have included natural rubber (Isayev, 2005), butadiene rubber (Oh *et al.*, 2004), styrene–butadiene rubber (SBR) (Isayev *et al.*, 1997), butyl rubber (Feng and Isayev, 2005), ethylene–propylene–diene monomer rubber (Yun and Isayev, 2003), polyurethane rubber (Ghose and Isayev, 2004), unfilled poly(dimethylsiloxane) (PDMS) (Shim *et al.*, 2002), silica-filled PDMS (Shim and Isayev, 2001, 2003; Shim *et al.*, 2003), and a complicated blend-mixture "ground-tire rubber" (Yun and Isayev, 2003). Although no chemicals are required, water has been found to facilitate the devulcanization of silica-filled PDMS (Shim and Isayev, 2003). The devulcanized material is then revulcanized, either as is or in a blend with virgin elastomer. Of course, in either case, any filler present in the unvulcanized elastomer is carried over into the new product. It will be important to optimize conditions for maximizing the properties of the final materials.

Properties typically measured include sol and gel fractions, the mechanical properties before and after devulcanization and revulcanization, and the mechanical properties as a function of composition in the case of blends. Nuclear magnetic resonance has also been used to measure molecular mobility and diffusion characteristics of the products before and after revulcanization (Shim *et al.*, 2002, 2003). Of particular interest here will be the presence of dangling network fragments.

The cleavage of the main chains means their molecular weight distribution can be significantly altered. In the case of SBR (Isayev *et al.*, 1997) and EPDM (Yun and Isayev, 2003), this has actually led to a bonus, specifically properties better than those of the virgin material! This is possibly due to the process generating bimodal network-chain distributions, the advantages of which have already described in Chapter 13.

Appendix A

Relationships between ν, ξ, and M_c

In this section we derive Eqs. (4.2) and (4.3) for a perfect network and then discuss their forms for an imperfect network.

An acyclic giant molecule or a tree (Flory, 1976) forms a convenient starting point. An example of such a tree is shown in Figure A.1. Lines denote chains, and dots represent labeled points that join with each other to form junctions or cross links.

Formation of ξ connections of labeled points reduces their number to $\nu - \xi + 1 \cong \nu - \xi$ and also introduces ξ independent cyclic paths. The number of such cyclic paths, ξ, is the *cycle rank* of the network, and ν is the number of network chains. In a perfect network there are no dangling chains and loops, and the functionality of each junction is greater than 2. If the labeled points of a tree are connected to form a perfect network, then the number μ of junctions is given by

$$\mu = \nu - \xi + 1 \cong \nu - \xi \tag{A.1}$$

The reader may verify Eq. (A.1) easily by forming a sample perfect network from a tree. Eliminating μ from Eqs. (A.1) and (4.1) leads to Eq. (4.2). An alternate form of this equation,

$$\xi = (\phi/2 - 1)\mu \tag{A.2}$$

is obtained by eliminating ν between Eqs. (A.1) and (4.1).

The density ρ of the network is defined as

$$\rho = \nu M_c / N_A V_0 \tag{A.3}$$

where M_c is the average molecular weight between junctions, N_A is Avogadro's number, and V_0 is the volume of the perfect network during its formation. If the network is formed in solution, V_0 is the total volume of polymer and solvent, and ρ is the density in this state. Substituting ν from Eq. (A.3) into Eq. (4.2) leads to Eq. (4.3).

The cycle rank ξ is the essential and universal parameter that characterizes the structure and elasticity of a network. The Helmholtz elastic free energy and the force of a network are both proportional to ξ (Duiser and Staverman, 1965; Graessley, 1975a, b). This is true for an imperfect network as well as a perfect one.

The characterization of the number of chains and junctions that contribute to the elastic activity of an imperfect network is outlined briefly by Flory (1982) and the references cited therein.

Equations (4.1) and (4.2) continue to hold exactly for an imperfect network if ν, μ, and ϕ are redefined. Thus

$$\begin{gathered} \mu' = 2\nu'/\bar{\phi} \\ \xi - 1 \simeq \xi = (1 - 2/\bar{\phi})\nu' \end{gathered} \tag{A.4}$$

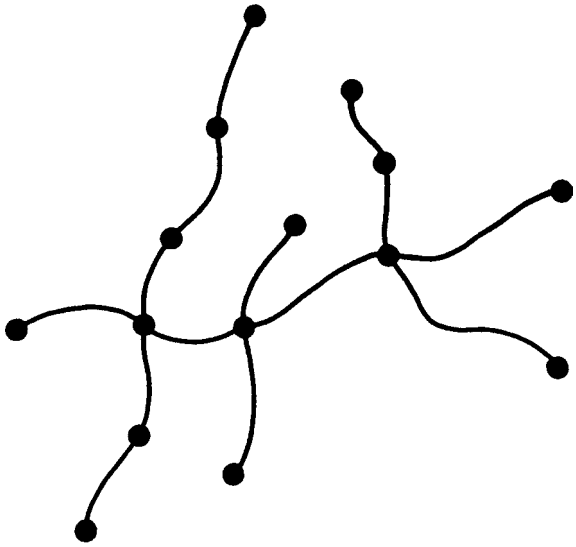

Figure A.1 A giant acyclic molecule or a tree. Lines denote chains, and dots are labeled points capable of reacting with other labeled points to form junctions.

where μ' is the number of junctions of functionality 3 or more, and ν' is the total number of chains excluding loops and dangling chains. Two chains separated by one bifunctional junction or by a series of them are considered to be a single chain and therefore contribute only unity to ν'. $\bar{\phi}$ is the average junction functionality. The reader may verify Eqs. (A.4) by constructing an imperfect network.

A theoretical estimate of M_c for all types of imperfections is not definitely established. A simple relation may be written, however, for a tetrafunctionally cross-linked imperfect network with no defects other than chain ends. The cycle rank for such a network is given (Queslel and Mark, 1985a) as

$$\xi = \frac{\rho}{2M_c}\left(1 - 3\frac{M_c}{M_n}\right) \tag{A.5}$$

where M_n is the molecular weight of the primary chains before cross linking. Derivation of Eq. (A.5) requires some discussion, which may be found in the paper by Queslel and Mark (1985a).

Appendix B

Relationships between $\langle \bar{r}^2 \rangle$, $\langle (\Delta r)^2 \rangle$, $\langle r^2 \rangle_0$, ϕ

The end-to-end vector $\boldsymbol{r}$ of a network chain is expressed in terms of its average value $\boldsymbol{r}$ and instantaneous fluctuations $\boldsymbol{\Delta r}$ from this mean by Eq. (5.11). According to the phantom network theory (Flory, 1976), the instantaneous distributions of $\boldsymbol{r}$, $\bar{\boldsymbol{r}}$ and $\boldsymbol{\Delta r}$, which are assumed to be Gaussian, are

$$\begin{aligned} W(\boldsymbol{r}) &= (\gamma/\pi)^{3/2} \exp\left(-\gamma r^2\right) \\ X(\bar{\boldsymbol{r}}) &= (\chi/\pi)^{3/2} \exp\left(-\chi \bar{r}^2\right) \\ \Psi(\Delta \boldsymbol{r}) &= (\psi/\pi)^{3/2} \exp(-\psi (\Delta r)^2) \end{aligned} \tag{B.1}$$

where

$$\gamma = \frac{3}{2\langle r^2 \rangle_0} \qquad \chi = \frac{3}{2\langle \bar{r}^2 \rangle_0} \qquad \psi = \frac{3}{2\langle (\Delta r)^2 \rangle_0} \tag{B.2}$$

The distribution of $\boldsymbol{r}$ may be written in terms of the distribution of $\bar{\boldsymbol{r}}$ and $\Delta \boldsymbol{r}$ as

$$W(\boldsymbol{r}) = \int X(\bar{r}) \Psi(\boldsymbol{r} - \bar{\boldsymbol{r}}) \mathrm{d}\bar{r} \tag{B.3}$$

where the argument of ψ follows from Eq. (5.11). Replacing $\langle (\Delta r)^2 \rangle$ in Eq. (B.1) by the square of the magnitude of the vector $(\boldsymbol{r} - \bar{\boldsymbol{r}})$, substituting Eqs. (B.1) into Eq. (B.3), and performing the integration over $\bar{r}$ results in

$$1/\psi + 1/\chi = 1/\gamma \tag{B.5}$$

The parameters ψ and γ are related for a phantom network (Eichinger, 1972; Graessley, 1975b; Pearson, 1977) by the following expression:

$$\psi = (\phi/2)\gamma = 3\phi/4\langle r^2 \rangle_0 \tag{B.6}$$

Derivation of Eq. (B.6) requires a knowledge of network topology. Replacing ψ in Eq. (B.6) by $3/2\langle (\Delta r)^2 \rangle$ leads to Eq. (5.16). Use of Eq. (B.4) or (B.5) together with (B.6) leads to Eq. (5.16).

Appendix C

Equations of state for miscellaneous deformations from the constrained junction theory

The stress in a deformed network is given by Eq. (7.7) in which ΔA_{el} is the elastic free energy of the network. From Chapters 6 and 7 the elastic free energy for the constrained junction model is

$$\begin{aligned}\Delta A_{\text{el}} &= \Delta A_{\text{ph}} + \Delta A_{\text{c}} \\ &= \frac{\xi kT}{2}\left\{\sum_t \lambda_t^2 - 3 + \frac{\mu}{\xi}\sum_t [B_t + D_t - \ln(B_t+1)(D_t+1)]\right\}\end{aligned} \tag{C.1}$$

where

$$B_t = \kappa^2(\lambda_t^2 - 1)(\lambda_t^2 + \kappa)^{-2} \qquad D_t = \lambda_t^2 \kappa^{-1} B_t \tag{C.2}$$

Substitution into Eq. (7.7) leads to

$$\tau_t = \left(\frac{\xi kT}{2V}\right)\lambda_t \sum_t \left(1 + \frac{\mu}{\xi}K_t\right)\frac{\partial \lambda_t^2}{\partial \lambda_t} \tag{C.3}$$

where

$$\begin{aligned}K_t &= K\left(\lambda_t^2\right) = B_t\left[\dot{B}_t(B_t+1)^{-1} + \kappa^{-1}\left(\lambda_t^2\dot{B}_t + B_t\right)\left(B_t + \kappa\lambda_t^{-2}\right)^{-1}\right] \\ \dot{B}_t &= \partial B_t/\partial\lambda_t^2 = B_t\left[\left(\lambda_t^2 - 1\right)^{-1} - 2\left(\lambda_t^2 + \kappa\right)^{-1}\right]\end{aligned} \tag{C.4}$$

For uniaxial extension, substituting Eqs. (7.9a,b) into Eq. (C.3) leads to

$$\tau_1 = \left(\frac{\xi kT}{V}\right)\left(\frac{V}{V_0}\right)^{2/3}\left[\alpha^2 - \alpha^{-1} + \left(\frac{\mu}{\xi}\right)(\alpha^2 K_1 - \alpha^{-1}K_2)\right] \tag{C.5}$$

The final term in the square brackets in Eq. (C.5) is the term due to constraints on the junctions. Without this term, Eq. (C.5) reduces to the phantom network expression given by Eq. (7.11) (with $F = \xi/2$). The force f acting on the network is obtained by multiplying both sides of Eq. (C.5) by the deformed area. The reduced force then follows from the definition given by Eq. (7.13), as

$$[f^*] = \left(\frac{\xi kT}{V_{\text{d}}}\right)v_{2\text{c}}{}^{2/3}\left[1 + \left(\frac{\mu}{\xi}\right)\frac{\alpha K_1 - \alpha^{-2}K_2}{\alpha - \alpha^{-2}}\right] \tag{C.6}$$

For biaxial extension, using Eqs. (7.17) in Eq. (C.3) leads to

$$\begin{aligned}\tau_1 &= \left(\frac{\xi kT}{V}\right)\left(\frac{V}{V_0}\right)^{2/3}\left[\alpha_1^2 - \frac{1}{\alpha_1^2\alpha_2^2} + \left(\frac{\mu}{\xi}\right)\alpha_1^2 K_1 - \frac{K_3}{\alpha_1^2\alpha_2^2}\right] \\ \tau_2 &= \left(\frac{\xi kT}{V}\right)\left(\frac{V}{V_0}\right)^{2/3}\left[\alpha_2^2 - \frac{1}{\alpha_1^2\alpha_2^2} + \left(\frac{\mu}{\xi}\right)\alpha_2^2 K_2 - \frac{K_3}{\alpha_1^2\alpha_2^2}\right]\end{aligned} \tag{C.7}$$

The stresses in pure shear are obtained by letting $\alpha_2 = 1$ and $\alpha_1 = \alpha$ in Eq. (C.7):

$$\begin{aligned}\tau_1 &= \left(\frac{\xi kT}{V}\right)\left(\frac{V}{V_0}\right)^{2/3}\left[\alpha^2 - \frac{1}{\alpha^2} + \left(\frac{\mu}{\xi}\right)\alpha^2 K_1 - \frac{K_3}{\alpha^2}\right] \\ \tau_2 &= \left(\frac{\xi kT}{V}\right)\left(\frac{V}{V_0}\right)^{2/3}\left[1 - \frac{1}{\alpha^2} + \left(\frac{\mu}{\xi}\right)\left(K_2 - \frac{K_3}{\alpha^2}\right)\right]\end{aligned} \tag{C.8}$$

Appendix D

Thermodynamics of the relationship of stress to temperature

The thermodynamics of highly elastic materials is most clearly developed by consideration of a particular type of strain. Most useful for this purpose is uniaxial deformation (elongation or compression), since such deformation is particularly simple to visualize and characterize, and is by far the most widely studied experimentally. In this appendix, general thermodynamic relations for stress–temperature relations are given for uniaxial deformation and the thermoelastic relations used in Chapter 9 are derived.

The thermodynamic quantities of primary interest are the changes in energy E and entropy S with deformation, more particularly the dependence of these quantities on the configurations of the polymer chains making up the elastomeric network. Since both E and S also depend on the volume V of the system, the thermodynamic analysis will proceed through the Helmholtz free energy $A \equiv E - TS$, the free energy function most convenient in the case of systems maintained at constant volume. From the above definition of A, and the first law of thermodynamics in the form $\mathrm{d}E = \mathrm{d}Q + \mathrm{d}W$, the change in A is given with complete generality by

$$\mathrm{d}A = \mathrm{d}E - T\,\mathrm{d}S - S\,\mathrm{d}T = \mathrm{d}Q + \mathrm{d}W - T\,\mathrm{d}S - S\,\mathrm{d}T \tag{D.1}$$

where $\mathrm{d}Q$ is the heat absorbed by the system, $\mathrm{d}W$ is the work done on the system, and T is the absolute temperature. The work term includes contributions from changes in volume and of length; thus,

$$\mathrm{d}A = \mathrm{d}Q + f\,\mathrm{d}L - p\,\mathrm{d}V - T\,\mathrm{d}S - S\,\mathrm{d}T \tag{D.2}$$

where f is the external force of deformation and L is the length of the sample. Restriction of this equation to reversible processes permits use of the relationship $\mathrm{d}Q = T\,\mathrm{d}S$ and, under these conditions,

$$d\mathrm{A} = f\,\mathrm{d}L - p\,\mathrm{d}V - S\,\mathrm{d}T \tag{D.3}$$

It then follows directly that

$$f = \left(\frac{\partial A}{\partial L}\right)_{T,V} \tag{D.4}$$

and

$$f = \left(\frac{\partial E}{\partial L}\right)_{T,V} - T\left(\frac{\partial S}{\partial L}\right)_{T,V} \tag{D.5}$$

The entropy, similarly obtained from Eq. (D.3), is given by

$$S = -\left(\frac{\partial A}{\partial T}\right)_{L,V} \tag{D.6}$$

Elongation ($dL > 0$) is characterized by positive values of f, and compression ($dL < 0$) by negative values. Both types of deformation of course cause increases in W and A, with the minimum value of the free energy occurring at the length L_i of the undeformed sample.

For a process at constant volume, one of the Maxwell relations obtained from the coefficients of Eq. (D.3) is $[\partial(\partial A/\partial L)_{T,V}/dT]_{L,V} = [\partial(\partial A/\partial T)_{L,V}/dL]_{T,V}$, which yields

$$\left(\frac{\partial f}{\partial T}\right)_{L,V} = -\left(\frac{\partial S}{\partial L}\right)_{T,V} \tag{D.7}$$

Substitution of this result into Eq. (D.5) gives one form of the thermodynamic equation of state for elastic materials:

$$f = \left(\frac{\partial E}{\partial L}\right)_{T,V} + T\left(\frac{\partial f}{\partial T}\right)_{L,V} \tag{D.8}$$

This equation closely parallels the general thermodynamic equation of state:

$$p = -\left(\frac{\partial E}{\partial V}\right)_{T} + T\left(\frac{\partial p}{\partial T}\right)_{V} \tag{D.9}$$

obtained from $dA = -p\,dV - S\,dT$ and $(\partial S/\partial V)_T = (\partial p/\partial T)_V$, and widely used for example to characterize materials in the gaseous phase. In further analogy with the properties of gases, an ideal elastomer is defined as one in which $(\partial E/\partial L)_{T,V}$ is zero for all values of L. It should be emphasized, however, that deviations from this type of ideality are, to an excellent approximation, entirely due to change in intramolecular interactions along the network chains. For this reason, there are no limiting experimental conditions under which all elastomers exhibit ideal thermoelastic behavior. In this regard, ideality of elastomers is fundamentally different from that of gases, all of which behave ideally of course in the limit of infinitesimally small pressure. For such a material, the force will be directly proportional to the absolute temperature, as can readily be seen from Eq. (D.8). (The more restrictive conditions specified by the subscripts in Eq. (D.8) reflect the fact that three independent variables (e.g., T, L, V or T, L, p) must be specified to describe the thermodynamic state of an elastomeric material).

Equation (D.8) serves to resolve the total force into its energetic and entropic components defined by

$$f_e = \left(\frac{\partial E}{\partial L}\right)_{T,V} \tag{D.10}$$

$$f_S = T\left(\frac{\partial f}{\partial T}\right)_{L,V} = f - f_e \tag{D.11}$$

The ratio of the energetic contribution f_e to the total force f is then simply

$$\frac{f_e}{f} = -\left(\frac{T}{f}\right)\left(\frac{\partial f}{\partial T}\right)_{L,V} = -T\left[\frac{\partial \ln (f/T)}{\partial T}\right]_{L,V} \tag{D.12}$$

This thermodynamic equation is fundamental to the interpretation of the force–temperature or thermoelastic data; it applies to both elongation and compression, provided of course that negative values of the force obtained in compression are converted to positive numbers to permit taking the logarithm of the quantity f/T.

Elongation–temperature measurements have in fact been carried out at constant volume as specified by Eq. (D.12). Unfortunately, however, small but thermodynamically significant changes in volume generally accompany the alteration of the temperature of an elastomeric material and the nullification of such changes by means of an imposed hydrostatic pressure presents serious experimental difficulties. It therefore becomes almost imperative, for practical reasons, to turn to the thermodynamic analysis of deformations carried out under the much simpler condition of constant pressure. For this purpose, however, one needs to use a force–deformation relation, and the temperature coefficient then becomes dependent on the type of the relation adopted. In the following, we use the simple equation of state given by Eq. (9.3). Dividing Eq. (9.3) by T and taking the logarithm leads to

$$\ln\left(\frac{f}{T}\right) = \ln(2Fk) - \ln(L_\mathrm{i}) + \frac{2}{3}\ln(V) - \frac{2}{3}\ln(V_0) + \ln(\alpha - \alpha^{-2}) \tag{D.13}$$

We first differentiate both sides of Eq. (D.13) with respect to T at constant V and L. The volume of the network is assumed unchanged during the deformation from L_i to L. Therefore $L_\mathrm{i} \propto V^{1/3}$, and is taken as constant during differentiation. The only non-zero term is $\dfrac{\mathrm{d}\ln V_0}{\mathrm{d}T} = \dfrac{3}{2}\dfrac{\mathrm{d}\ln\langle r^2\rangle_0}{\mathrm{d}T}$. The derivative at constant V and L then reads as

$$\left(\frac{\mathrm{d}\ln(f/T)}{\mathrm{d}T}\right)_{V,L} = -\frac{\mathrm{d}\ln\langle r^2\rangle_0}{\mathrm{d}T} \tag{D.14}$$

At constant p and L, $\dfrac{\mathrm{d}\ln L_\mathrm{i}}{\mathrm{d}T} = \dfrac{1}{3}\dfrac{\mathrm{d}\ln V}{\mathrm{d}T} = \dfrac{1}{3}\beta$, and $\dfrac{\mathrm{d}\ln(\alpha - \alpha^{-2})}{\mathrm{d}T} = -\dfrac{1}{3}\dfrac{\alpha^3 + 2}{\alpha^3 - 1}\beta$, where β is the volume thermal expansion coefficient. Substituting these expressions into the derivative of Eq. (D.13) at constant p and L yields

$$\left(\frac{\mathrm{d}\ln(f/T)}{\mathrm{d}T}\right)_{P,L} = -\frac{\mathrm{d}\ln\langle r^2\rangle_0}{\mathrm{d}T} - \frac{\beta}{\alpha^3 - 1} \tag{D.15}$$

Eliminating the term $\dfrac{\mathrm{d}\ln\langle r^2\rangle_0}{\mathrm{d}T}$ between Eqs. (D.14) and (D.15) leads to the relation

$$\left(\frac{\mathrm{d}\ln(f/T)}{\mathrm{d}T}\right)_{V,L} = \left(\frac{\mathrm{d}\ln(f/T)}{\mathrm{d}T}\right)_{p,L} + \frac{\beta}{\alpha^3 - 1} \tag{D.16}$$

At constant p and α, $\dfrac{\mathrm{d}\ln(\alpha - \alpha^{-2})}{\mathrm{d}T} = 0$ and the derivative of Eq. (D.13) with respect to T gives

$$\left(\frac{\mathrm{d}\ln(f/T)}{\mathrm{d}T}\right)_{V,L} = \left(\frac{\mathrm{d}\ln(f/T)}{\mathrm{d}T}\right)_{p,\alpha} - \frac{\beta}{3} \tag{D.17}$$

Equations (D.16) and (D.17) are those given by Eqs. (9.4) and (9.5).

Problems

1.1 Discuss adiabatic demagnetization as a parallel to stretching and releasing a rubber band, and to compressing and expanding a gas.
1.2 Explain how an elastomer can be used as the working substance in an air conditioning device.

3.1 Consider (i) a freely jointed chain model and (ii) a polyethylene (PE) chain, each having 100 bonds, and skeletal bond lengths of 1.54 Å. The temperature is chosen to be 300 K (27 °C), and the Boltzmann constant is 1.38×10^{-20} N mm K^{-1}. Calculate the mean-squared end-to-end distance and compare the volumes occupied by the two types of chains.
3.2 Using the information in Problem 3.1, calculate the values of the spring constant K for the two types of chains.
3.3 Schematically draw a network that has exactly two trifunctional cross links, two tetrafunctional cross links, no dangling chains, and one loop.
3.4 Describe how a network might be prepared so as to have no dangling chains, but a very large number of loops.
3.5 Determine the values of the cycle rank ξ for the following network segments

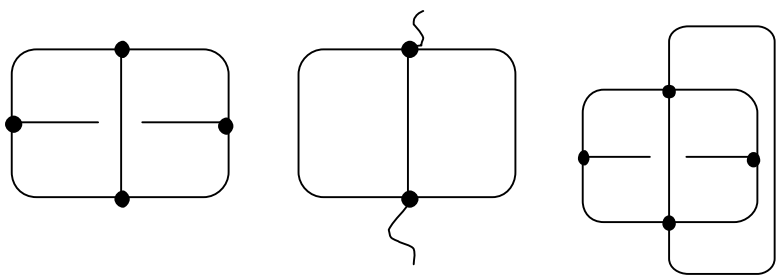

4.1 Consider a unimodal tetrafunctional network consisting of the two types of chains described in Problem 3.1. Calculate the number of chains and number of junctions per unit volume. Assume a network density of 0.9 g cm^{-3}.

5.1 What conditions (if any) are required for the following equations to be true?
A. Network chain coordinates $\langle x^2 \rangle = \langle y^2 \rangle = \langle z^2 \rangle$?
B. $\langle x^2 \rangle + \langle y^2 \rangle + \langle z^2 \rangle = \langle r^2 \rangle$?
C. ΔS (ν chains) $= \nu \Delta S$ (1 chain)?
D. $\alpha_x \alpha_y \alpha_z = 1$?

5.2 A. What would you predict for the modulus of this series arrangement of two chains of the same molecular weight, being stretched from the ends (marked with dots)? The one drawn with the heavier line has a higher modulus than the one drawn with the thinner line.

B. What would you predict for the modulus of this parallel arrangement of two chains of the same molecular weight, being stretched from the ends (marked with dots)? The one drawn with the heavier line has a higher modulus than the one drawn with the thinner line.

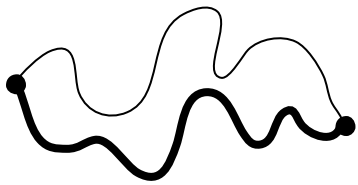

6.1 Assuming a tetrafunctional phantom network of the two types of chains described in Problem 3.1, calculate the number of junctions that share the volume of fluctuation of a given junction.

6.2 For the networks in the preceding problem, calculate the κ parameter.

6.3 Suppose an elastomer is simultaneously stretched by a factor of two in the x direction and compressed by a factor of three in the y direction. By what factor would you expect its dimensions to change in the z direction?

6.4 What would be the equation of state for a hypothetical elastomer that could be stretched in one direction without changing its dimensions in the other two directions?

6.5 What would be the elastic equation of state for a hypothetical elastomer which could be stretched equi-biaxially in two directions, without changing its dimensions in the remaining direction?

6.6 Experimental data in simple tension or compression are usually presented in terms of the familiar Mooney–Rivlin plot, where the reduced force is plotted against reciprocal extension ratio as described in Chapter 7. If the upturn in the modulus (due to crystallization or finite chain extensibility) is ignored, the curve may be extrapolated to $\alpha^{-1} = 0$ to obtain an approximation of the reduced stress for the phantom network, with $F = \xi/2$:

$$[f^*]_{\text{ph}} = (\xi / V_{\text{d}}) kT v_2^{2/3} \tag{P.1}$$

Thus $[f^*]_{\text{ph}}$ represents the shear modulus of the phantom network. As shown in Chapter 4, it may alternatively be expressed in terms of chain density by

$$[f^*]_{\text{ph}} = (1 - 2/\phi)(\nu / V_{\text{d}}) kT v_2^{2/3} \tag{P.2}$$

The corresponding equation in terms of the junction density is

$$[f^*]_{\text{ph}} = (\phi/2 - 1)(\mu / V_{\text{d}}) kT v_2^{2/3} \tag{P.3}$$

and in terms of the molecular weight M_c of the network chains is

$$[f^*]_{ph} = (1 - 2/\phi)(\nu/V_d)\rho RT/M_c \tag{P.4}$$

where ρ is the density of the bulk polymer. Experimental determination of $[f^*]_{ph}$ from the Mooney–Rivlin plot thus allows one to derive values for ν, μ, and M_c according to the above equations.

Suppose a network having tetrafunctional cross links ($\phi = 4$) that were introduced in the undiluted state ($v_{2S} = 1.00$) has a reduced force of $[f^*]_{ph} = 0.10$ N mm^{-2} at 298 K. (10^5 N m^{-2} (Pa) $= 10^{-1}$ MN m^{-2} (MPa) $= 1.02$ kg cm^{-2}). Calculate the number density of chains and cross links and the molecular weight between cross links for this network.

6.7 A typical network studied by swelling might also have been tetrafunctionally cross linked in the undiluted state, have the same value of ρ, and exhibit an equilibrium degree of swelling characterized by $v_{2m} = 0.100$ in a solvent having a molar volume

$$V_1 = 80\,\text{cm}^3\,\text{mol}^{-1}\ (\text{or}\,8.00 \times 10^4\,\text{mm}^3\,\text{mol}^{-1})$$

and an interaction parameter with the polymer corresponding to $\chi = 0.30$.
Calculate the number density of chains and cross links and the molecular weight between cross links for this network.

7.1 Derive the expressions for the small deformation modulus of elasticity for the (i) phantom network, (ii) affine network, and (iii) constrained junction models.

8.1 Suppose a network is at swelling equilibrium with a good solvent, with excess solvent present. If a non-solvent is added to the excess good solvent surrounding the network, what will happen to the degree of swelling of the network? Explain your answer.

8.2 Suppose a network consisting of natural rubber is at swelling equilibrium with a good solvent, with excess solvent present. If some uncross-linked ethylene–propylene polymer is dissolved in the excess solvent surrounding the network, what will happen to the degree of swelling of the network (increase, decrease, or stay the same)? Explain your answer.

9.1 Which of the following differentials are exact, in the Euler (Maxwell) sense?

A. $\mathrm{d}F = x^2y\,\mathrm{d}x + xy^2\,\mathrm{d}y$

B. $\mathrm{d}F = xy^2\,\mathrm{d}x + x^2y\,\mathrm{d}y$

C. $\mathrm{d}A_T = f\,\mathrm{d}l - p\,\mathrm{d}V$

9.2 Write the Euler (Maxwell) relationship obtainable from the equation

$$\mathrm{d}G = V\,\mathrm{d}p - S\,\mathrm{d}T$$

9.3 What is f_e/f for a network made up of:

A. Freely jointed chains?

B. Freely rotating chains?

9.4 If a network has $f_e/f = 0.5$, what is the relationship between the actual force f required to extend the network and the value f_S it would have if energy effects were entirely absent?

9.5 Calculate a numerical value for the non-ideality ratio f_e/f for a network having $f_e = 0.5f_S$.

9.6 Suppose a hypothetical elastomer has a force at constant volume that is proportional to the cube of the absolute temperature. Use the equation $f_S = T(\partial f/\partial T)_{V,L}$ to calculate f_e/f at 300 K for this elastomer. (A numerical answer is required.)

10.1 What is the maximum increase expected in the modulus in going from a cross-link functionality of 3 to infinity?

10.2 What type of network would be an approximation of a network having a cross-link functionality of infinity?
10.3 Why is the usual practice of drawing a cyclic to look like a circle misleading?

11.1 Two identical pieces of an elastomer are cross linked to exactly the same extent (ν/V), one in the stretched state and the other in the unstretched state. Which would you expect to have the higher modulus?
11.2 Suppose a network that was formed by cross linking in solution and subsequently dried has a certain cross-link density (per unit volume of the dried network). Suppose a second network is prepared in the dry state so as to have exactly the same cross-link density. Which should have the higher value of the modulus, and why?

13.1 Which bimodal network should show the greater improvement in mechanical properties: one with with $M_S = 200$ g/mol and $M_L = 20\,000$ g/mol, or one with $M_S = 2000$ g/mol and $M_L = 200\,000$ g/mol?
13.2 Would you expect bimodal networks to show any unusual differences in swelling equilibrium results?

16.1 In strain-induced crystallization, the crystallites generated can act as additional cross links. Would similarly generated liquid-crystalline domains be expected to behave as cross links?
16.2 Why would biaxial deformation probably be less effective than uniaxial elongation in inducing formation of a mesophase?

17.1 Describe three techniques that Nature uses to ensure that the bioelastomer elastin has good elastomeric properties.
17.2 How can you determine whether Nature uses the bimodal network approach to improve the mechanical properties of a bioelastomer such as elastin?

18.1 How can a mixture of an organosilicate and organotitanate be co-hydrolyzed to give a ceramic alloy, since the latter reacts much faster than the former?
18.2 Why might ellipsoidal particles give more reinforcement of an elastomer than spherical particles at the same weight?

Answers to problems

1.1 Lining up molecules in a magnetic field is similar to stretching an elastomer or compressing a gas in that entropy is decreased and heat is liberated. After heat is absorbed away, the field is turned off and the molecules randomize themselves, with an entropy increase paralleling that accompanying the retraction of the elastomer or expansion of a gas. The cooling effect in adiabatic demagnetization is used to reach temperatures close to absolute zero.

1.2 Absorption of heat by the usual vaporization of a volatile liquid is replaced by retraction of a stretched elastomer, and liberation of heat by condensation of the liquid is replaced by stretching of the elastomer. Retraction is carried out in the lower temperature environment and the stretching in the higher temperature environment, resulting in the transfer of heat from the lower to the higher temperature. See DeGregoria (1994), DeGregoria and Kaminski (1997).

3.1 When a chain is sufficiently long, the end-to-end distribution approaches the Gaussian limit. In fact, for all practical purposes, chains having 50 or more bonds may be characterized by a Gaussian distribution (Yoon and Flory, 1974). The mean-squared end-to-end distance for a Gaussian chain is given by $\langle r^2\rangle_0 = C_n n l^2$. For the freely jointed chain, $C_n = 1.0$, and $\langle r^2\rangle_0 = (100)(1.54)^2 = 237\,\text{Å}^2$. The chain may be assumed to occupy a spherical volume with radius $\langle r^2\rangle_0{}^{1/2} = 15.4\,\text{Å}$ and a volume V_0 of $\frac{4\pi}{3}\langle r^2\rangle_0^{3/2} = 15.3 \times 10^3\,\text{Å}^3$. For the polyethylene chain, $C_n = 6.2$ (Flory, 1969) for $n = 100$. Then, $\langle r^2\rangle_0 = (6.2)(100)(1.54)^2 = 1470\,\text{Å}^2$ or, $\langle r^2\rangle_0{}^{1/2} = 38\,\text{Å}$ and $V_0 = 230 \times 10^3\,\text{Å}^3$. Thus, the volume occupied by the PE chain is 15.4 times larger than that of the freely jointed chain.

3.2 The expression for the spring constant of a Gaussian chain is obtained from Eq. (3.5)

$$f = \left(\frac{3kT}{\langle r^2\rangle_0}\right) r, \text{ according to which the spring constant is } K = \left(\frac{3kT}{\langle r^2\rangle_0}\right).$$

Substituting the values of T and k given above, we obtain for the freely jointed chain,

$$K = \frac{(3)(1.38 \times 10^{-20}\ \text{N mm K}^{-1})(300\,\text{K})}{(237\,\text{Å}^2)\left(10^{-14}\,\text{mm}^2/\text{Å}^2\right)} = 5.2 \times 10^{-6}\,\text{N mm}^{-1}$$
$$= 0.52\,\text{pN Å}^{-1}$$

For the PE chain,

$$K = \frac{(3)(1.38 \times 10^{-20}\,\mathrm{N\,mmK^{-1}})(300\,\mathrm{K})}{\left(1470\,\mathrm{\AA}^2\right)\left(10^{-14}\,\mathrm{mm^2/\AA^2}\right)} = 0.85 \times 10^{-6}\,\mathrm{Nmm^{-1}}$$
$$= 0.085\,\mathrm{pN\,\AA^{-1}}$$

Thus, although both chains have the same number of repeat units, the freely jointed chain appears 6.1 times stiffer than the PE chain.

3.4

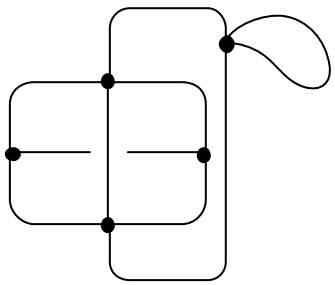

3.5 Cross link cyclic molecules.

3.6 Cutting the cycles indicates $\xi = 3$, 2, and 3.
Alternatively, use $\xi = \nu - \mu + 1$: $6 - 4 + 1 = 3$; $3 - 2 + 1 = 2$; $7 - 4 + 1 = 4$.

4.1 From Eq. (A.3), the number of chains per unit volume (assuming a molecular weight of 14 for both the freely jointed and the PE chains) is

$$\frac{\nu}{V_0} = \frac{\rho N_\mathrm{A}}{M_\mathrm{c}} = \frac{(0.9\,\mathrm{g\,cm^{-3}})(6.2 \times 10^{23}\,\mathrm{chains\,mol^{-1}})}{(100 \times 14\,\mathrm{g\,mol^{-1}})} = 4 \times 10^{20}\,\mathrm{chains\,cm^{-3}}$$

From Eq. (4.1), we have

$$\frac{\mu}{V_0} = \frac{2}{\phi}\frac{\nu}{V_0} = \left(\frac{1}{2}\right)\left(4 \times 10^{20}\,\mathrm{chains\,cm^{-3}}\right) = (2 \times 10^{20}\,\mathrm{junctions\,cm^{-3}})$$

5.1 A. Isotropic system
B. Always true
C. Elasticity entirely intramolecular
D. Constant volume

5.2 A. Close to the lower modulus
B. Close to the higher modulus

6.1 The fluctuations of junctions in the phantom network model are significant, given by Eq. (5.16), $\langle(\Delta r)^2\rangle_0 = \frac{2}{\phi}\langle r^2\rangle_0$. The number of other junctions sharing the volume in which the given junction fluctuates is given by Eq. (6.1), $\Gamma = \frac{4\pi}{3}\langle r^2\rangle_0^{3/2}\frac{\mu}{V_0}$. Substituting the values of the mean-squared chain dimensions and the junction density calculated above, gives for the freely jointed chain,

$$\Gamma = \frac{4\pi}{3}(237 \times 10^{-16}\,\mathrm{cm^2})^{3/2}\,(2 \times 10^{20}\,\mathrm{junctions\,cm^{-3}}) = 3\,\mathrm{junctions}$$

For the PE network,

$$\Gamma = \frac{4\pi}{3}(1469 \times 10^{-16}\,\text{cm}^2)^{3/2}\,(2 \times 10^{20}\,\text{junctions cm}^{-3}) = 47\,\text{junctions}$$

6.2 The κ parameter of the constrained junction model is given by Eq. (6.6)

$$\kappa = I\left(\frac{2}{\phi}\right)(N_A\rho)\left(\frac{\langle r^2\rangle}{M}\right)^{3/2} M_c^{1/2}$$

The factor I in this equation is an empirical parameter which is approximately equal to $\frac{1}{2}$ according to experimental data (Erman and Flory, 1982).

Substituting the values for the freely jointed chain,

$$\kappa = \left(\frac{1}{2}\right)\left(\frac{2}{4}\right)(6.2 \times 10^{23}\,\text{mol}^{-1})(0.9\,\text{g cm}^{-3}) \times \left(\frac{237 \times 10^{-16}\,\text{cm}^2}{1400\,\text{g mol}^{-1}}\right)^{3/2}(1400\,\text{g mol}^{-1})^{1/2} = 0.4$$

Substituting the values for the PE chain gives

$$\kappa = \left(\frac{1}{2}\right)\left(\frac{2}{4}\right)(6.2 \times 10^{23}\,\text{mol}^{-1})(0.9\,\text{g cm}^{-3}) \times \left(\frac{1469 \times 10^{-16}\,\text{cm}^2}{1400\,\text{g mol}^{-1}}\right)^{3/2}(1400\,\text{g mol}^{-1})^{1/2} = 5.6$$

The freely jointed chain network with chains of 100 bonds behaves approximately as a phantom network.

6.3 $\alpha_x\alpha_y\alpha_z = 1$, so $2(1/3)\,\alpha_z = 1$, and $\alpha_z = 3/2$.

6.4 $f^* = (\nu kT/V)\alpha$

6.5 $f^* = (2\nu kT/V)\alpha$

6.6 Taking k in units (1.381×10^{-20} N mm K^{-1} chain^{-1}) compatible with $[f^*]$ ($\alpha = \infty$) in N mm^{-2} and using the above data in Eq. (P.2) leads to $\nu/V = 4.86 \times 10^{16}$ chains mm^{-3}. Use of Avogadro's number $N_A = 6.02 \times 10^{23}$ mol^{-1}, then gives $\nu/V = 8.06 \times 10^{-8}$ mols of chains mm^{-3}.

As specified by the relationship $\mu = (2/\phi)\nu$, the density of the tetrafunctional cross links would be one-half $(2/\phi)$ of this value, $\mu/V = 4.03 \times 10^{-8}$ mols of cross links mm^{-3}. If the polymer has a density $\rho = 0.900$ g cm^{-3} (or 9.00×10^{-4} g mm^{-3}), then Eq. (P.4) gives $M_c = 1.12 \times 10^4$ g mol^{-1}.

6.7 Substituting these data into the swelling equation for a phantom network given in Chapter 8 leads to a value for the molecular weight of the network chains of $M_c = 0.708 \times 10^4$ g mol^{-1}. Using the relationships between M_c, μ, and ν and the above data gives $(\mu/V) = (2/\phi)(\rho/M_c) = 6.36 \times 10^{-8}$ mols of cross links mm^{-3} and $(\nu/V) = \rho/M_c = 12.7 \times 10^{-8}$ mols of chains mm^{-3}.

Results calculated using the more complicated constrained junction equation with a reasonable value of κ are not very different from those calculated from the equation for phantom chains.

7.1 The equation of state for the simple model is $f = \frac{2FkT}{L_i}(\alpha - \alpha^{-2})$, which may be written as $\frac{f}{A_i} = \frac{2FkT}{V_i}(\alpha^2 + \alpha + 1)(\alpha - 1)$. The stress σ is f/A_i and the strain ε is

$\alpha - 1$. Letting $\alpha \to 1$ and using the definitions of stress and strain gives the low-deformation stress–strain relationship as

$$\sigma = \left(6kT\frac{F}{V_\mathrm{i}}\right)\varepsilon$$

(i) For the phantom network model, $\dfrac{F}{V_\mathrm{i}} = \left(\dfrac{1}{2}\right)\left(\dfrac{\nu}{V_0}\right)\left(1 - \dfrac{2}{\phi}\right)$. For the network formed in the dry state, $V_\mathrm{i} = V_0$. Substituting these values gives $\dfrac{F}{V_\mathrm{i}} = \left(\dfrac{1}{2}\right)\left(4 \times 10^{20}\,\mathrm{cm}^{-3}\right)\left(1 - \dfrac{2}{4}\right) = 10^{20}\,\mathrm{cm}^{-3}$. Substituting this into the stress–strain relation gives

$$\sigma = 6\left(1.38 \times 10^{-21}\,\mathrm{N\,cm\,K}^{-1}\right)(300\,\mathrm{K})\,(10^{20}\,\mathrm{cm}^{-3})\varepsilon = 248\varepsilon\,\mathrm{N\,cm}^{-2}.$$

From this expression, we obtain the modulus of elasticity $E = 248$ N cm^{-2}, or 2.48 MPa.

We see that the modulus of the phantom network depends only on the network chain density and not on the type of the chain, i.e., whether it is freely jointed or PE.

(ii) For the affine network model, $\dfrac{F}{V_\mathrm{i}} = \dfrac{1}{2}\dfrac{\nu}{V_0}$. Using the values obtained above, we get $\dfrac{F}{V_\mathrm{i}} = \left(\dfrac{1}{2}\right)\left(4 \times 10^{20}\,\mathrm{cm}^{-3}\right) = 2 \times 10^{20}\,\mathrm{cm}^{-3}$. Following the above calculations, we obtain $\sigma = 6(1.38 \times 10^{-21}\,\mathrm{N\,cm\,K}^{-1})(300\,\mathrm{K})(2 \times 10^{20}\,\mathrm{cm}^{-3})\varepsilon = 496\varepsilon\,\mathrm{N\,cm}^{-2}$, and $E = 4.96$ MPa.

(iii) The shear modulus of the constrained junction model is given by the expression $G = \left[1 + \dfrac{\mu}{\xi}\left(\dfrac{\kappa^2 + 1}{(1+\kappa)^4}\kappa^2\right)\right]G_\mathrm{ph}$ (Erman and Mark, 2005). For incompressible materials, this is also equal to $E = \left[1 + \dfrac{\mu}{\xi}\left(\dfrac{\kappa^2 + 1}{(1+\kappa)^4}\kappa^2\right)\right]E_\mathrm{ph}$. The ratio μ/ξ is $\dfrac{\mu}{\xi} = \dfrac{2}{\phi - 2}$.

For the freely jointed chain network, we have $k = 0.4$, and

$$E = \left[1 + 1\left(\frac{0.4^2 + 1}{(1+0.4)^4}0.4^2\right)\right]2.48\,\mathrm{MPa} = 2.65\,\mathrm{MPa}$$

For the PE chain, $E = \left[1 + 1\left(\dfrac{5.6^2 + 1}{(1+5.6)^4}5.6^2\right)\right]2.48\,\mathrm{MPa} = 3.81\,\mathrm{MPa}$

8.1 Degree of swelling decreases, since thermodynamics of mixing term is less favorable.
8.2 Degree of swelling will decrease. Chemical potential of the liquid phase is lowered, or entropic advantage of solvent going into the network to mix with the chains is reduced.

9.1 A. Inexact, because $x^2 \neq y^2$
B. Exact, because $2xy = 2xy$
C. Exact, because generated by differentiation
9.2 $(\partial V/\partial T)_p = -(\partial S/\partial p)_T$
9.3 A. Zero.
B. Zero.
9.4 $f = f_\mathrm{e} + f_S$ so $f = 0.5\,f + f_S$, and $f = 2.0\,f_S$.
9.5 $f = f_\mathrm{e} + f_S$ so $f_S = f_\mathrm{e}/0.5 = 2f_\mathrm{e}$. $f = 3f_\mathrm{e}$ so $f_\mathrm{e}/\mathrm{f} = 0.33$.

9.6 $f = CT^3$ so $f_S = T(\partial f/\partial T)_{V,L} = 3CT^3$
$f_e = f - f_S$ so $f_e/f = 1 - f_S/f = 1 - 3CT^3/CT^3 = -2$

10.1 The front factor is $(1 - 2/\phi)$, so $\phi = 3$ would give 1/3 and $\phi = \infty$ would give 1. The maximum increase expected in the modulus would therefore be by a factor of 3.
10.2 A polymer with small crystallites acting as physical junctions (of very high effective functionality).
10.3 A circle would have an extremely low entropy and therefore very low probability of occurrence. This is a parallel to the low probability of the completely stretched out spatial configuration of a linear chain.

11.1 The one cross linked in the unstretched state. The other would have a lower modulus because $\langle r^2 \rangle_0$ would be larger, and there might be fewer entanglements.
11.2 The second network since the chains in the first network will have become "super-contracted" in the drying process.

13.1 The network with $M_S = 200$ g/mol and $M_L = 20\,000$ g/mol, since it is necessary for the short chains to be unusually short to take advantage of their limited extensibilities.
13.2 There should not be any unusual differences in swelling equilibrium results, since the deformations in this case are too small to take advantage of the limited extensibilities of the short chains in the bimodal elastomer.

16.1 Probably not, since the liquid-crystalline domains would presumably have too much deformability to keep chain segments constrained.
16.2 The randomization of the chain end-to-end vectors would offset some of the orientation from the stretching out of the chains.

17.1 See text in Chapter 17.
17.2 Check the amino acid sequencing in elastin to see the spacings between lysine groups, which are the potential cross-linking sites.

18.1 Start the organosilicate reaction earlier, or slow down the organotitanate by attaching ligands to it.
18.2 At the same weight, ellipsoidal particles would have a higher interfacial area, which might give greater reinforcement.

Some publications describing laboratory/classroom experiments or demonstrations

1. C. B. Arends (1960) Demonstration: Stress–strain behavior of rubber. *J. Chem. Educ.*, **37**, 41.
2. C. L. Stong (1971) Some delightful engines driven by the heating of rubber bands. *Sci. Am.*, **224** (4), 118.
3. E. A. Collins, J. Bares, and F. W. Billmeyer, Jr. (1973) Stress–strain properties. In *Experiments in Polymer Science*, New York: Wiley-Interscience, 478.
4. E. A. Collins, J. Bares, and F. W. Billmeyer, Jr. (1973) Swelling of network polymers. In *Experiments in Polymer Science*, New York: Wiley-Interscience, 481.
5. F. Rodriguez (1973) Demonstrating rubber elasticity. *J. Chem. Educ.*, **50**, 764.
6. M. Bader (1981) Rubber elasticity – A physical chemistry experiment. *J. Chem. Educ.*, **58**, 285.
7. L. H. Sperling (1982) Molecular motion in polymers. *J. Chem. Educ.*, **59**, 942.
8. G. V. S. Henderson, Jr., D. O. Campbell, V. Kuzmicz, and L. H. Sperling (1985) Gelatin as a physically crosslinked elastomer. *J. Chem. Educ.*, **62**, 269.
9. S. B. Clough (1987) Stretched elastomers. *J. Chem. Educ.*, **64**, 42.
10. C. E. Carraher, Jr. (1987) Thermodynamics and the bounce. *J. Chem. Educ.*, **64**, 43.
11. F. Rodriguez (1990) Classroom demonstrations of polymer principles. IV. Mechanical properties. *J. Chem. Educ.*, **67**, 784.
12. G. B. Kauffman, S. W. Mason, and R. B. Seymour (1990) Happy and unhappy balls: neoprene and polynorbornene. *J. Chem. Educ.*, **67**, 198.
13. F. Rodriguez, S. K. Patel, and C. Cohen (1990). Measuring the modulus of a sphere by squeezing between parallel plates. *J. Appl. Polym. Sci.*, **40**, 285.
14. J. P. Byrne (1994) Rubber elasticity. *J. Chem. Educ.*, **71**, 531.
15. T. C. Gilmer and M. Williams (1996) Polymer mechanical properties via a new laboratory tensile tester. *J. Chem. Educ.*, **73**, 1062.
16. F. Rodriguez and M. A. Acevedo (1997). A bouncemeter for measuring resilience. *J. Appl. Polym. Sci.*, **66**, 1787.

References

Aaron, B. B. and Gosline, J. M. (1981) *Biopolymers*, **20**, 1247.
Abraham, T. and McMahan, C. (2004) In *Rubber Compounding: Chemistry and Applications*, ed., B. Rodgers, New York: Marcel Dekker, Inc., p. 163.
Ahmad, Z., Wang, S. and Mark, J. E. (1994) In *Better Ceramics Through Chemistry VI*, Vol. 346. eds., A. K. Cheetham, C. J. Brinker, M. L. Mecartney, and C. Sanchez, Pittsburgh: Materials Research Society, p. 127.
Akiba, M. and Hashim, A. S. (1997) *Prog. Polym. Sci.*, **22**, 475.
Aklonis, J. J. and McKnight, W. J. (1983) *Introduction to Polymer Viscoelasticity*, New York: Wiley.
Alexander, R. M. (1966) *J. Exp. Biol.*, **44**, 119.
Allcock, H. R., Lampe, F. W. and Mark, J. E. (2003) *Contemporary Polymer Chemistry*, Third Edition, Englewood Cliffs, NJ: Prentice Hall.
Allegra, G. (1980) *Makromol. Chem.*, **181**, 1127.
Allen, G., Kirkham, M. J., Padget, J. and Price, C. (1971) *Trans. Faraday Soc.*, **67**, 1278.
Ameduri, B., Boutevin, B. and Kostov, G. (2001) *Prog. Polym. Sci.*, **26**, 105.
Amram, B., Bokobza, L., Queslel, J. P. and Monnerie, L. (1986) *Polymer*, **27**, 877.
Andrady, A. L. (Ed.) (2003) *Plastics and the Environment*, New York: Wiley-Interscience.
Andrady, A. L., Llorente, M. A. and Mark, J. E. (1980) *J. Chem. Phys.*, **72**, 2282.
Andrady, A. L., Llorente, M. A. and Mark, J. E. (1991) *Polym. Bull.*, **26**, 357.
Andrady, A. L., Llorente, M. A., Sharaf, M. A., *et al.* (1981) *J. Appl. Polym. Sci.*, **26**, 1829.
Andrady, A. L. and Mark, J. E. (1980) *Biopolymers*, **19**, 849.
Anglaret, E., Brunet, M., Desbat, B., Keller, P. and Buffeteau, T. (2005) *Macromolecules*, **38**, 4799.
Annaka, M. and Tanaka, T. (1992) *Nature*, **355**, 430.
Aprem, A. S., Joseph, K. and Thomas, S. (2004) *J. Appl. Polym. Sci.*, **91**, 1068.
Aranguren, M. I. (1998) *Polymer*, **39**, 4897.
Atkins, P. W. (1990) *Physical Chemistry*, Oxford: Oxford University Press.
Baba, M., Nedelec, J.-M., Billamboz, N. and Lacoste, J. (2003) *J. Phys. Chem. B*, **107**, 12884.
Bagrodia, S., Tant, M. R., Wilkes, G. L. and Kennedy, J. P. (1987) *Polymer*, **28**, 2207.
Bahar, I., Erbil, Y., Baysal, B. and Erman, B. (1987) *Macromolecules*, **20**, 1353.
Bahar, I., Erman, B., Bokobza, L. and Monnerie, L. (1995) *Macromolecules*, **28**, 225.
Ball, R. C., Doi, M. and Edwards, S. F. (1981) *Polymer*, **22**, 1010.
Barbara, P. F., Gesquiere, A. J., Park, S.-J. and Lee, Y. (2005) *Acc. Chem. Res.*, **38**, 602.
Barclay, G. G. and Ober, C. K. (1993) *Prog. Polym. Sci.*, **18**, 899.

Barrie, J. A. and Standen, J. (1967) *Polymer*, **8**, 97.
Bastide, J. and Boue, F. (1986) *Physica A*, **140**, 251.
Bastide, J., Duplessix, R. and Picot, C. (1984) *Macromolecules*, **17**, 83.
Batra, A., Hedden, R. C., Schofield, P. *et al.* (2003) *Macromolecules*, **36**, 9458.
Beatty, C. L. and Karasz, F. E. (1975) *J. Polym. Sci., Polym. Phys. Ed.*, **13**, 971.
Becker, N., Oroudjev, E., Mutz, S., *et al.* (2003) *Nature Materials*, **2**, 278.
Belousov, S. I., Buzin, A. I. and Godovsky, Y. K. (1999) *Polym. Sci. USSR*, **41**, 303.
Beltzung, M., Picot, C. and Herz, J. (1984) *Macromolecules*, **17**, 663.
Beltzung, M., Picot, C., Rempp, P. and Herz, J. (1982) *Macromolecules*, **15**, 1594.
Bengs, H., Finkelmann, H., Kupfer, J., Ringsdorf, H. and Schuhmacher, P. (1993) *Makromol. Rapid Commun.*, **14**, 445.
Benne, I., Semmler, K. and Finkelmann, H. (1994) *Makromol. Rapid Commun.*, **15**, 295.
Benne, I., Semmler, K. and Finkelmann, H. (1995) *Macromolecules*, **28**, 1854.
Bergmann, G. H. F., Finkelmann, H., Percec, V. and Zhao, M. (1997) *Makromol. Rapid Commun.*, **18**, 353.
Besbes, S., Cermelli, I., Bokobza, L., *et al.* (1992) *Macromolecules*, **25**, 1949.
Beyer, P. and Zentel, R. (2005) *Macromol. Rapid Commun.*, **26**, 874.
Billamboz, N., Nedelec, J. M., Grivet, M. and Baba, M. (2005) *Chem. Phys.*, **4**, 1126.
Bokinsky, G. and Zhuang, X. (2005) *Acc. Chem. Res.*, **38**, 566.
Bokobza, L., Clément, F., Monnerie, L. and Lapersonne, P. (1998) In *The Wiley Polymer Networks Group Review Series*, Vol. 1, Chapter 24, New York: John Wiley & Sons Ltd., p. 321.
Bokobza, L. and Erman, B. (2000) *Macromolecules*, **33**, 8858.
Bokobza, L. and Nugay, N. (2001) *J. Appl. Polym. Sci.*, **81**, 215.
Boonstra, B. B. (1979) *Polymer*, **20**, 691.
Borg, E. L. (1973) In *Rubber Technology*, ed., M. Morton, New York: Van Nostrand Reinhold, p. 220.
Bourgeat-Lami, E., Espiard, P., Guyot, A., *et al.* (1995) In *Hybrid Organic-Inorganic Composites*, Vol. 585, eds., J. E. Mark, C. Y.-C. Lee and P. A. Bianconi, Washington, DC: American Chemical Society, p. 112.
Brand, H. R. (1989) *Makromol. Chem., Rapid Commun.*, **10**, 57.
Brandrup, J., Immergut, E. H. and Grulke, E. A. (Eds.) (1999) *Polymer Handbook*, New York: Wiley.
Braun, J. L., Mark, J. E. and Eichinger, B. E. (2002) *Macromolecules*, **35**, 5273.
Breiner, J. M. and Mark, J. E. (1998) *Polymer*, **39**, 5483.
Brinker, C. J. and Scherer, G. W. (1990) *Sol-Gel Science. The Physics and Chemistry of Sol-Gel Processing*, New York: Academic Press.
Brintzinger, H.-H., Fischer, D., Mulhaupt, R., Reiger, B. and Waymouth, R. M. (1995) *Angew. Chem. Ed. Engl.*, **34**, 1143.
Brook, M. A. (2000) *Silicon in Organic, Organometallic, and Polymer Chemistry*, New York: John Wiley & Sons.
Brotzman, R. W. and Eichinger, B. E. (1983) *Macromolecules*, **16**, 1131.
Bruzard, S. and Levesque, G. (2002) *Chem. Mater.*, **14**, 2421.
Brydson, J. A. (1978) *Rubber Chemistry*, London: Applied Science Publishers.
Bucknall, C. B. (1977) *Toughened Plastics*, London: Applied Science Publishers.
Bueche, F. (1962) *Physical Properties of Polymers*, New York: Wiley-Interscience.
Burnside, S. D. and Giannelis, E. P. (1995) *Chem. Mater.*, **7**, 1597.
Burnside, S. D. and Giannelis, E. P. (2000) *J. Polym. Sci., Polym. Phys. Ed.*, **38**, 1595.
Bustamante, C., Marko, J. F., Siggia, E. D. and Smith, S. (1994) *Science*, **265**, 1599.

Calvert, P. and Broad, A. (1991) In *Polymers in Information Storage Technology*, ed., K. L. Mittal, New York: Plenum Press, p. 257.
Chen, R. Y. S., Yu, C. U. and Mark, J. E. (1973) *Macromolecules*, **6**, 746.
Chen, T. K. and Jan, Y. H. (1992) *J. Mater. Sci.*, **27**, 111.
Chiu, D. S. and Mark, J. E. (1977) *Coll. Polym. Sci.*, **225**, 644.
Choi, J., Harcup, J., Yee, A. F., Zhu, Q. and Laine, R. M. (2001) *J. Am. Chem. Soc.*, **123**, 11420.
Chu, S. (1991) *Science*, **253**, 861.
Ciferri, A. (Ed.) (1991) *Liquid Crystallinity in Polymers: Principles and Fundamental Properties*, New York: VCH Publishers.
Clark, A. H. and Ross-Murphy, S. B. (1987) *Adv. Polym. Sci.*, **83**, 57.
Clarson, S. J., Mark, J. E. and Semlyen, J. A. (1986) *Polym. Commun.*, **27**, 243.
Clarson, S. J., Mark, J. E. and Semlyen, J. A. (1987) *Polym. Commun.*, **28**, 151.
Clarson, S. J., Mark, J. E., Sun, C.-C. and Dodgson, K. (1992) *Eur. Polym. J.*, **28**, 823.
Clarson, S. J. and Mark, J. E. (1993) In *Siloxane Polymers*, eds., S. J. Clarson and J. A. Semlyen, Englewood Cliffs: Prentice Hall, p. 616.
Clough, S. B., Machonnachie, A. and Allen, G. (1980) *Macromolecules*, **13**, 774.
Coates, G. W. and Waymouth, R. M. (1995) *Science*, **267**, 217.
Collings, P. J. (1990) *Liquid Crystals: Nature's Delicate Phase of Matter*, Princeton: Princeton University Press.
Coran, A. Y. (1987) In *Encyclopedia of Polymer Science and Engineering*, Second Edition, New York: Wiley-Interscience.
Coran, A. Y. (2005) In *Science and Technology of Rubber*, eds., J. E. Mark and B. Erman, Amsterdam: Elsevier.
Curro, J. G. and Mark, J. E. (1984) *J. Chem. Phys.*, **80**, 4521.
Cypryk, M., Matyjaszewski, K., Kojima, M. and Magill, J. H. (1992) *Makromol. Chem., Rapid Commun.*, **13**, 39.
Davenport, R. J., Wuite, G. J. L., Landick, R. and Bustamante, C. (2000) *Science*, **287**, 2497.
Davis, W. D. (1973) In *Rubber Technology*, ed., M. Morton, New York: Van Nostrand Reinhold, p. 534.
Davis, F. J., Gilbert, A., Mann, J. and Mitchell, G. R. (1990) *J. Polym. Sci., Polym. Chem.*, **28**, 1455.
De, S. K., Isayev, A. I. and Khait, K. (2005) *Rubber Recycling*, Boca Raton, FL: CRC Press.
DeBolt, L. C. and Mark, J. E. (1987a) *Polymer*, **28**, 416.
DeBolt, L. C. and Mark, J. E. (1987b) *Macromolecules*, **20**, 2369.
DeBolt, L. C. and Mark, J. E. (1988) *J. Polym. Sci., Polym. Phys. Ed.*, **26**, 865.
de Gennes, P. G. (1979) *Scaling Concepts in Polymer Physics*, Ithaca, NY: Cornell University Press.
DeGregoria, A. J. (1994) US Patent 5,339,653.
DeGregoria, A. J. and Kaminski, T. J. (1997) US Patent 5,617,913.
Deloche, B. (1993) *Makromol. Chem., Macromol. Symp.*, **72**, 29.
Deloche, B., Dubault, A., Herz, J. and Lapp, A. (1986) *Europhys. Lett.*, **1**, 629.
Deloche, B. and Samulski, E. T. (1981) *Macromolecules*, **14**, 575.
Demirors, M. (1998) *Preprints, Div. Polym. Mat. Sci. Eng., Am. Chem. Soc.*, **79**, 162.
Deng, Q. Q., Hahn, J. R., Stasser, J., Preston, J. D. and Burns, G. T. (2000) *Rubber Chem. Technol.*, **73**, 647.
Depner, M., Deloche, B. and Sotta, P. (1994) *Macromolecules*, **27**, 5192.

DeSimone, J. M. and Tumas, W. (Eds.) (2003) *Green Chemistry Using Liquid and Supercritical Carbon Dioxide*, New York: Oxford University Press.
Disch, S., Finkelmann, H., Ringsdorf, H. and Schuhmacher, P. (1995) *Macromolecules*, **28**, 2424.
Disch, S., Schmidt, C. and Finkelmann, H. (1994) *Makromol. Rapid Commun.*, **15**, 303.
Dole, M. (Ed.) (1973) *The Radiation Chemistry of Macromolecules*, New York: Academic Press.
Donald, A. M. and Kramer, E. J. (1982) *J. Appl. Polym. Sci.*, **27**, 3729.
Donald, A. M. and Windle, A. H. (1992) *Liquid-Crystalline Polymers*, Cambridge: Cambridge University Press.
Dondos, A. and Benoit, H. (1971) *Macromolecules*, **4**, 279.
Donnet, J. and Custodero, E. (2005) In *Science and Technology of Rubber*, eds., J. E. Mark and B. Erman, Amsterdam: Elsevier.
Dubault, A., Deloche, B. and Herz, J. (1987) *Macromolecules*, **20**, 2096.
Duiser, J. A. and Staverman, A. J. (1965) In *Physics of Noncrystalline Solids*, ed., J. A. Prins, Amsterdam: North Holland Publishing.
Dusek, K. (1986) *Adv. Polym. Sci.*, **78**, 1.
Dusek, K. (Ed.) (1993a) *Responsive Gels, I*, Berlin: Springer-Verlag.
Dusek, K. (Ed.) (1993b) *Responsive Gels, II*, Berlin: Springer-Verlag.
Edwards, S. F. (1967) *Proc. Phys. Soc. (London)*, **92**, 9.
Edwards, S. F. and Vilgis, T. A. (1988) *Rep. Prog. Phys.*, **51**, 243.
Eichinger, B. E. (1972) *Macromolecules*, **5**, 496.
Eichinger, B. E. (1983) *Ann. Rev. Phys. Chem.*, **34**, 359.
Eichinger, B. E. and Akgiray, O. (1994) In *Computer Simulation of Polymers*, ed., E. A. Colbourne, White Plains, NY: Longman, p. 263.
Eichinger, B. E. and Flory, P. J. (1968) *Trans. Faraday Soc.*, **64**, 2053.
Eisenberg, A. and King, M. (1977) *Ion-Containing Polymers*, New York: Academic Press.
Erman, B. (1981) *J. Polym. Sci., Polym. Phys. Ed.*, **19**, 829.
Erman, B. (1987) *Macromolecules*, **20**, 1917.
Erman, B., Bahar, I., Kloczkowski, A. and Mark, J. E. (1990) *Macromolecules*, **23**, 5335.
Erman, B. and Flory, P. J. (1978) *J. Chem. Phys.*, **68**, 5363.
Erman, B. and Flory, P. J. (1982) *Macromolecules*, **15**, 806.
Erman, B. and Flory, P. J. (1983a) *Macromolecules*, **16**, 1601.
Erman, B. and Flory, P. J. (1983b) *Macromolecules*, **16**, 1607.
Erman, B. and Flory, P. J. (1985) *Macromolecules*, **19**, 2342.
Erman, B. and Mark, J. E. (1988) *J. Chem. Phys.*, **89**, 3314.
Erman, B. and Mark, J. E. (1997) *Structures and Properties of Rubberlike Networks*, New York: Oxford University Press.
Erman, B. and Mark, J. E. (1998) *Macromolecules*, **31**, 3099.
Erman, B. and Mark, J. E. (2005) In *Science and Technology of Rubber*, eds., J. E. Mark, B. Erman and F. R. Eirich, Amsterdam: Elsevier.
Erman, B. and Monnerie, L. (1985) *Macromolecules*, **18**, 1985.
Erman, B. and Monnerie, L. (1989) *Macromolecules*, **22**, 3342.
Erman, B. and Monnerie, L. (1992) *Macromolecules*, **25**, 4456.
Espiard, P., Guyot, A. and Mark, J. E. (1995) *J. Inorg. Organomet. Polym.*, **5**, 391.
Everaers, R. (1998) *Eur. Phys. J.*, **B 4**, 341.
Everaers, R. (1999) *New J. Phys.*, **1**, 1.
Falender, J. R., Yeh, G. S. Y. and Mark, J. E. (1979) *Macromolecules*, **12**, 1207.
Feng, W. and Isayev, A. I. (2005) *J. Mater. Sci.*, **40**, 2883.
Ferry, J. D. (1980) *Viscoelastic Properties of Polymers*, New York: Wiley.

Finkelmann, H., Kock, H.-J., Gleim, W. and Rehage, G. (1984) *Makromol. Rapid Commun.*, **5**, 287.
Fixman, M. and Alben, R. (1973) *J. Chem. Phys.*, **58**, 1553.
Flory, P. J. (1947) *J. Chem. Phys.*, **15**, 397.
Flory, P. J. (1953) *Principles of Polymer Chemistry*, Ithaca, NY: Cornell University Press.
Flory, P. J. (1961) *Trans. Faraday Soc.*, **57**, 829.
Flory, P. J. (1969) *Statistical Mechanics of Chain Molecules*, New York: Interscience.
Flory, P. J. (1973) *Pure Appl. Chem., Macromol. Chem.- 8*, **33**, 1.
Flory, P. J. (1976) *Proc. R. Soc. London, A*, **351**, 351.
Flory, P. J. (1977) *J. Phys. Chem.*, **66**, 5720.
Flory, P. J. (1982) *Macromolecules*, **15**, 99.
Flory, P. J. (1984) *Pure Appl. Chem.*, **56**, 305.
Flory, P. J. (1985a) *Polym. J.*, **17**, 1.
Flory, P. J. (1985b) *Brit. Polym. J.*, **17**, 96.
Flory, P. J., Ciferri, A. and Hoeve, C. A. J. (1960) *J. Polym. Sci.*, **45**, 235.
Flory, P. J. and Erman, B. (1982) *Macromolecules*, **15**, 800.
Folk, S. L. and DeSimone, J. M. (2003) In *Synthesis and Properties of Silicones and Silicone-Modified Materials*, Vol. 838, eds., S. J. Clarson, J. J. Fitzgerald, M. J. Owen, S. D. Smith and M. E. van Dyke, Washington, DC: American Chemical Society, p. 79.
Frechet, J. M. J. (1994) *Science*, **263**, 1710.
Fried, J. R. (2003) *Polymer Science and Technology*, Second Edition, Englewood Cliffs, NJ: Prentice Hall.
Frisch, H. L. and Mark, J. E. (1996) *Chem. Mater.*, **8**, 1735.
Frisch, H. L. and Wasserman, E. (1961) *J. Am. Chem. Soc.*, **83**, 3789.
Fu, F.-S. and Mark, J. E. (1988) *J. Polym. Sci., Polym. Phys. Ed.*, **26**, 2229.
Fu, F.-S. and Mark, J. E. (1989) *J. Appl. Polym. Sci.*, **37**, 2757.
Fyvie, T. J., Frisch, H. L., Semlyen, J. A., Clarson, S. J. and Mark, J. E. (1987) *J. Polym. Sci., Polym. Chem. Ed.*, **25**, 2503.
Galiatsatos, V. and Eichinger, B. E. (1987) *Polym. Commun.*, **28**, 182.
Galiatsatos, V. and Mark, J. E. (1987) *Macromolecules*, **20**, 2631.
Galiatsatos, V., Neaffer, R. O., Sen, S. and Sherman, B. J. (1996) In *Physical Properties of Polymers Handbook*, ed., J. E. Mark, New York: Springer-Verlag, p. 535.
Galiatsatos, V. and Subramanian, P. R. (1994) US Patent 5,376,738.
Ganicz, T. and Stanczyk, W. A. (2003) *Prog. Polym. Sci.*, **28**, 303.
Garrido, L., Ackerman, J. L. and Mark, J. E. (1990) In *Polymer-Based Molecular Composites*, Vol. 171, eds., D. W. Schaefer and J. E. Mark, Pittsburgh: Materials Research Society, p. 65.
Garrido, L. and Mark, J. E. (1985) *J. Polym. Sci., Polym. Phys. Ed.*, **23**, 1933.
Garrido, L., Mark, J. E., Clarson, S. J. and Semlyen, J. A. (1985a) *Polym. Commun.*, **26**, 53.
Garrido, L., Mark, J. E., Clarson, S. J. and Semlyen, J. A. (1985b) *Polym. Commun.*, **26**, 55.
Garrido, L., Mark, J. E., Sun, C. C., Ackerman, J. L. and Chang, C. (1991) *Macromolecules*, **24**, 4067.
Gaylord, R. J. (1976) *J. Polym. Sci. Polym. Phys. Ed.*, **14**, 1827.
Gaylord, R. J. (1982) *Polym. Bull.*, **8**, 325.
Gaylord, R. J. (1983) *Polym. Bull.*, **9**, 181.
Gee, G. (1980) *Macromolecules*, **13**, 705.
Gee, G., Stern, J. and Treloar, L. R. G. (1950) *Trans. Faraday Soc.*, **46**, 1101.

Gent, A. N. (1969) *Macromolecules*, **2**, 262.
Gent, A. N. (Ed.) (1992) *Engineering with Rubber: How to Design Rubber Components*, New York: Hanser Publishers.
Gent, A. N., Liu, G. L. and Mazurek, M. (1994) *J. Polym. Sci., Polym. Phys. Ed.*, **32**, 271.
Ghose, S. and Isayev, A. I. (2004) *Polym. Eng. Sci.*, **44**, 794.
Giannelis, E. P. (1996) In *Biomimetic Materials Chemistry*, ed., S. Mann, New York: VCH Publishers, p. 337.
Giannelis, E. P., Krishnamoorti, R. and Manias, E. (1999) *Adv. Polym. Sci.*, **138**, 107.
Gibson, H. W., Bheda, M. C. and Engen, P. T. (1994) *Prog. Polym. Sci.*, **19**, 843.
Gilles, P.-P., Milano, J.-C. and Vernet, J.-L. (2003) *Macromol. Chem. Phys.*, **204**, 2222.
Gleim, W. and Finkelmann, H. (1987) *Makromol. Chem.*, **188**, 1489.
Godovsky, Y. K. (1986) *Adv. Polym. Sci.*, **76**, 31.
Godovsky, Y. K. (1992) *Angew. Macromol. Chemie*, **202/203**, 187.
Godovsky, Y. K., Makarova, N. N., Papkov, V. S. and Kuzmin, N. N. (1985) *Makromol. Chem.*, **6**, 443.
Godovsky, Y. K. and Papkov, V. S. (1999) In *Polymer Data Handbook*, ed., J. E. Mark, New York: Oxford University Press, p. 394.
Godovsky, Y. K., Papkov, V. S. and Magonov, S. N. (2001) *Macromolecules*, **34**, 976.
Godovsky, Y. K. and Valetskaya, L. A. (1991) *Polym. Bull.*, **27**, 221.
Godovsky, Y. K., Valetskaya, L. A. and Papkov, V. S. (1991) *Makromol. Chem., Makromol. Symp.*, **48/49**, 433.
Goldstein, A. N., Esher, C. M. and Alivisatos, A. P. (1992) *Science*, **256**, 1425 and pertinent references cited therein.
Gong, C. and Gibson, H. W. (1997) *J. Am. Chem. Soc.*, **119**, 8585.
Gong, J. P., Katsuyama, Y., Kurokawa, T. and Osada, Y. (2003) *Adv. Mater.*, **15**, 1155.
Gonzalez-Leon, J. A., Acar, M. H., Ryu, S.-W., Ruzette, A.-V. G. and Mayes, A. M. (2003) *Nature*, **426**, 424.
Gosline, J. M. (1980) In *The Mechanical Properties of Biological Materials*, eds., J. F. V. Vincent and J. D. Currey, Cambridge: Cambridge University Press, p. 331.
Gosline, J. M. (1987) *Rubber Chem. Technol.*, **60**, 417.
Gosline, J. M. (1992) In *Concepts of Efficiency in Comparative Physiology*, ed., R. W. Blake, Cambridge: Cambridge University Press.
Gottlieb, M., Macosko, C. W., Benjamin, G. S., Meyers, K. O. and Merrill, E. W. (1981) *Macromolecules*, **14**, 1039.
Grady, B. P. and Cooper, S. (2005) In *Science and Technology of Rubber*, eds., J. E. Mark and B. Erman, Amsterdam: Elsevier.
Graessley, W. W. (1975a) *Macromolecules*, **8**, 186.
Graessley, W. W. (1975b) *Macromolecules*, **8**, 865.
Graessley, W. W. (1993) In *Physical Properties of Polymers*, eds., J. E. Mark, A. Eisenberg, W. W. Graessley *et al.*, Washington, DC: American Chemical Society, p. 97.
Graessley, W. W. (2003) *Polymeric Liquids and Networks: Structure and Properties*, New York: Garland Science.
Graessley, W. W. (2004) *Polymeric Liquids and Networks: Dynamics and Rheology*, New York: Garland Science.
Granzier, H. L. and Pollack, G. H. (Eds.) (2000) *Elastic Filaments of the Cell*, New York: Kluwer Academic.
Grayson, S. M. and Frechet, J. M. J. (2001) *Chem. Rev.*, **101**, 3819.
Greene, A., Smith, K. J., Jr. and Ciferri, A. (1965) *Trans. Faraday Soc.*, **61**, 2772.
Grinberg, V. Y., Dubovik, A. S., Kuznetsov, D. V. *et al.* (2000) *Macromolecules*, **33**, 8685.

Grobler, J. H. A. and McGill, W. J. (1993) *J. Polym. Sci., Polym. Phys. Ed.*, **31**, 575.
Guth, E. and Mark, H. (1934) *Monatsh. Chem.*, **65**, 93.
Haddad, T. S., Lee, A. and Phillips, S. H. (2001) *Polym. Preprints*, **42(1)**, 88.
Hagn, C., Wittkop, M., Kreitmeier, S. *et al.* (1997) *Polym. Gels Networks*, **5**, 327.
Hammerschmidt, K. and Finkelmann, H. (1989) *Makromol. Chem.*, **190**, 1089.
Hanna, S. and Windle, A. H. (1988) *Polymer*, **29**, 207.
Hanus, K.-H., Pechhold, W., Soergel, F., Stoll, B. and Zentel, R. (1990) *Coll. Polym. Sci.*, **268**, 222.
Hanyu, A. and Stein, R. S. (1991) *Makromol. Chem., Macromol. Symp.*, **45**, 189.
He, X.-Z., Zhang, B.-Y., Xiao, L.-J., Wang, Y. and Wu, H.-Q. (2005) *J. Appl. Polym. Sci.*, **97**, 498.
Hedden, R. C., McCaskey, E., Cohen, C. and Duncan, T. M. (2001) *Macromolecules*, **34**, 3285.
Hedden, R. C., Saxena, H. and Cohen, C. (2000) *Macromolecules*, **33**, 8676.
Heinrich, G. S. and Straub, E. (1983) *Acta Polym.*, **34**, 589.
Heinrich, G. S. and Straub, E. (1984) *Acta Polym.*, **35**, 115.
Heinrich, G. S. and Straub, E. (1987a) *Polym. Bull. (Berlin)*, **17**, 247.
Heinrich, G. S. and Straub, E. (1987b) *Polym. Bull. (Berlin)*, **17**, 255.
Hergenrother, W. L., Hilton, A. S. and Lin, C. J. (2004) *Rubber Chem. Technol.*, **77**, 646.
Herz, J. E., Rempp, P. and Burchard, W. (1978) *Adv. Polym. Sci.*, **26**, 105.
Higgins, J. S. and Benoit, H. (1994) *Neutron Scattering from Polymers*, Oxford: Clarendon Press.
Hild, G. (1998) *Prog. Polym. Sci.*, **23**, 1019.
Hinckley, J. A., Han, C. C., Moser, B. and Yu, H. (1978) *Macromolecules*, **11**, 836.
Hirschmann, H., Meier, W. and Finkelmann, H. (1992) *Makromol. Chem., Rapid Commun.*, **13**, 385.
Hjelm, R. J., Nakatani, A. I., Gerspacher, M. and Krishnamoorti, R. (Eds.) (2001) *Filled and Nanocomposite Polymer Materials*, Warrendale, PA: Materials Research Society.
Ho, C. C., Hill, M. J. and Odell, J. A. (1993) *Polymer*, **34**, 2019.
Hoei, Y., Ikeda, Y. and Sasaki, M. (2003) *J. Phys. Chem. B*, **107**, 1483.
Hoeve, C. A. J. and Flory, P. J. (1974) *Biopolymers*, **13**, 677.
Hoeve, C. A. J. and O'Brien, M. K. (1963) *J. Polym. Sci. Part A*, **1**, 1947.
Holden, G., Legge, N. R., Quirk, R. and Schroeder, H. E. (Eds.) (1996) *Thermoplastic Elastomers*, Munich: Hanser Publishers.
Holmes, G. A. and Letton, A. (1994) *Polym. Eng. Sci.*, **34**, 1635.
Huang, W., Frisch, H. L., Hua, Y. and Semlyen, J. A. (1990) *J. Polym. Sci., Polym. Chem. Ed.*, **26**, 1807.
Hugel, T. and Seitz, M. (2001) *Makromol. Rapid Commun.*, **22**, 989.
Hummer, G. and Szabo, A. (2005) *Acc. Chem. Res.*, **38**, 504.
Ibemesi, J., Gvozdic, N., Keumin, M., Lynch, M. J. and Meier, D. J. (1985) *Preprints, Div. Polym. Chem., Inc.*, **26(2)**, 18.
Ibemesi, J., Gvozdic, N., Keumin, M., Tarshiani, Y. and Meier, D. J. (1990) In *Polymer-Based Molecular Composites*, Vol. 171, eds., D. W. Schaefer and J. E. Mark, Pittsburgh: Materials Research Society, p. 105.
Ignatz-Hoover, F. and To, B. H. (2004) In *Rubber Compounding: Chemistry and Applications*, ed., B. Rodgers, New York: Marcel Dekker, Inc., p. 505.
Inomata, K., Yamamoto, K. and Nose, T. (2000) *Polym. J.*, **32**, 1044.
Isayev, A. I. (2005) In *Science and Technology of Rubber*, eds., J. E. Mark, B. Erman and F. R. Eirich, San Diego: Academic, p. 663.
Isayev, A. I., Kim, S. H. and Levin, V. Y. (1997) *Rubber Chem. Technol.*, **70**, 194.

Iwata, K. and Ohtsuki, T. (1993) *J. Polym. Sci., Polym. Phys. Ed.*, **31**, 441.
Jackson, C. L. and McKenna, G. B. (1991) *J. Non-Cryst. Solids*, **131–133**, 221.
James, H. M. and Guth, E. (1947) *J. Chem. Phys.*, **15**, 669.
James, H. M. and Guth, E. (1953) *J. Chem. Phys.*, **21**, 1039.
Janshoff, A., Neitzert, M., Oberdorfer, Y. and Fuchs, H. (2000) *Angew. Chem. Int. Ed.*, **39**, 3213.
Jeram, E. M. and Striker, R. A. (1976) US Patent 3,957,713.
Jia, Y.-G., Zhang, B.-Y., Sun, Q.-J. and Chang, H.-X. (2004) *Coll. Polym. Sci.*, **282**, 1077.
Jiang, C.-Y. and Mark, J. E. (1984) *Makromol. Chemie*, **185**, 2609.
Johnson, R. M. and Mark, J. E. (1972) *Macromolecules*, **5**, 41.
Kaminsky, W. (1996) *Macromol. Chem. Phys.*, **197**, 3907.
Kaneko, Y., Watanabe, Y., Okamoto, T., Iseda, Y. and Matsunaga, T. (1980) *J. Appl. Polym. Sci.*, **25**, 2467.
Kanesaka, S., Kimura, H., Kuroki, S., Ando, I. and Fujishige, S. (2004) *Macromolecules*, **37**, 453.
Kaufhold, W., Finkelmann, H. and Brand, H. R. (1991) *Makromol. Chem.*, **192**, 2555.
Kavanagh, G. M. and Ross-Murphy, S. B. (1998) *Prog. Polym. Sci.*, **23**, 533.
Keefer, K. D. (1990) In *Silicon-Based Polymer Science. A Comprehensive Resource*, Vol. 224, eds., J. M. Zeigler and F. W. G. Fearon, Washington, DC: American Chemical Society.
Kellermayer, M. S. Z., Smith, S. B., Granzier, H. L. and Bustamante, C. (1997) *Science*, **276**, 1112.
Khokhlov, A. R. (1992) In *Responsive Gels: Volume Transitions I.*, ed., K. Dusek, Berlin: Springer Verlag, p. 125.
Khokhlov, A. R. and Philippova, O. E. (1996) In *Solvents and Self-Organization of Polymers*, ed., S. E. Webber, Dordrecht: Kluwer Academic Publishers, p. 197.
Khokhlov, A. R. and Philippova, O. E. (2002) In *Polymer Gels and Networks*, eds., Y. Osada and A. R. Khokhlov, New York: Marcel Dekker, p. 163.
Kickelbick, G. (2003) *Prog. Polym. Sci.*, **28**, 83.
Kilian, H.-G. (1990) *Proceedings, Network Group Meeting*, Jerusalem.
Kilian, H. G., Enderle, H. F. and Unseld, K. (1986) *Colloid Polym. Sci.*, **264**, 866.
Kim, C. S. Y., Ahmad, J., Bottaro, J. and Farzan, M. (1986) *J. Appl. Polym. Sci.*, **32**, 3027.
Kiriy, A., Gorodyska, G., Minko, S. *et al.* (2003) *J. Am. Chem. Soc.*, **125**, 11202.
Kloczkowski, A., Mark, J. E. and Erman, B. (1991) *Macromolecules*, **24**, 3266.
Kloczkowski, A., Mark, J. E. and Erman, B. (1995a) *Macromolecules*, **28**, 5089.
Kloczkowski, A., Mark, J. E. and Erman, B. (1995b) *Comput. Polym. Sci.*, **5**, 37.
Koenig, J. L. (2004) In *Physical Properties of Polymers.* Third Edition, eds., J. E. Mark, K. L. Ngai, W. W. Graessley *et al.*, Cambridge: Cambridge University Press, p. 377.
Kohjiya, S., Urayama, K. and Ikeda, Y. (1997) *Kautschuk Gummi Kunstoffe*, **50**, 868.
Kohls, D., Beaucage, G., Pratsinis, S. E., Kammler, H. and Skillas, G. (2001) In *Filled and Nanocomposite Polymer Materials*, Vol. 661, eds., R. J. Hjelm, A. I. Nakatani, M. Gerspacher and R. Krishnamoorti, Warrendale, PA: Materials Research Society.
Kojima, M., Magill, J. H., Franz, U., White, M. L. and Matyjaszewski, K. (1995) *Makromol. Chem. Phys.*, **196**, 1739.
Kokufuta, E., Matsukawa, S. and Tanaka, T. (1995) *Macromolecules*, **28**, 3474.
Koo, C. M., Wu, L., Lim, L. S. *et al.* (2005) *Macromolecules*, **38**, 6090.
Koyama, T. and Steinbuchel, A. (Eds.) (2001) *Biopolymers, Vol. 2: Polyisoprenoids*, New York: Wiley-VCH.
Kraus, G. (Ed.) (1965) *Reinforcement of Elastomers*, New York: Interscience.

Kremer, F., Skupin, H., Lehmann, W., Gebhardt, E. and Zentel, R. (2001) *Makromol. Symp.*, **175**, 247.
Kuhn, W. (1934) *Kolloid-Z*, **68**, 2.
Kuhn, W. (1936) *Kolloid-Z.*, **76**, 258.
Kuhn, W. and Grün, F. (1942) *Kolloid-Z.*, **101**, 248.
Kumaki, J. and Hashimoto, T. (2003) *J. Am. Chem. Soc.*, **125**, 4907.
Kundler, I. and Finkelmann, H. (1995) *Makromol. Rapid Commun.*, **16**, 679.
Kuo, A. C. M. (1999) In *Polymer Data Handbook*, ed., J. E. Mark, New York: Oxford University Press, p. 411.
Kupfer, J. and Finkelmann, H. (1991) *Makromol. Rapid Commun.*, **12**, 717.
Kupfer, J. and Finkelmann, H. (1994) *Makromol. Chem. Phys.*, **195**, 1353.
Lacey, D., Beattie, H. N., Mitchell, G. R. and Pople, J. A. (1998) *J. Mater. Chem.*, **8**, 53.
Laine, R. M., Choi, J. and Lee, I. (2001a) *Adv. Mater.*, **13**, 800.
Laine, R. M., Sanchez, C., Giannelis, E. and Brinker, C. J. (Eds.) (2001b) *Organic/Inorganic Hybrid Materials – 2000*, Warrendale, PA: Materials Research Society.
Lee, C. L., Maxson, M. T. and Stebleton, L. F. (1979) US Patent 4,162,243.
Leung, Y.-K. and Eichinger, B. E. (1984a) *J. Chem. Phys.*, **80**, 3877.
Leung, Y.-K. and Eichinger, B. E. (1984b) *J. Chem. Phys.*, **80**, 3885.
Li, H., Rief, M., Oesterhelt, F. and Gaub, H. E. (1998) *Adv. Mater.*, **3**, 316.
Li, Y. and Tanaka, T. (1992) *Annu. Rev. Mater. Sci.*, **22**, 243.
Liberman, M. H., Abe, Y. and Flory, P. J. (1972) *Macromolecules*, **5**, 550.
Liberman, M. H., DeBolt, L. C. and Flory, P. J. (1974) *J. Polym. Sci., Polym. Phys. Ed.*, **12**, 187.
Lichtenhan, J. D., Schwab, J. and Reinerth, W. A., Sr. (2001) *Chem. Innov.*, **31**, 3.
Light, D. R. and Dennis, M. S. (1989) *J. Biol. Chem.*, **264**, 18569.
Lillie, M. A. and Gosline, J. M. (1990) In *Physical Networks: Polymers and Gels*, eds., W. Burchard and S. B. Ross-Murphy, London: Elsevier Applied Science, p. 391.
Lin, W., Bian, M., Yang, G. and Chen, Q. (2004) *Polymer*, **45**, 4939.
Liphardt, J., Onoa, B., Smith, S. B., Tinoco, I., Jr. and Bustamante, C. (2001) *Science*, **292**, 733.
Liu, S. and Mark, J. E. (1987) *Polym. Bull.*, **18**, 33.
Llorente, M. A. and Mark, J. E. (1980) *Macromolecules*, **13**, 681.
Llorente, M. A. and Mark, J. E. (1981) *J. Polym. Sci., Polym. Phys. Ed.*, **19**, 1107.
Llorente, M. A., Mark, J. E. and Saiz, E. (1983) *J. Polym. Sci., Polym. Phys. Ed.*, **21**, 1173.
Llorente, M. A., Rubio, A. M. and Freire, J. J. (1984) *Macromolecules*, **17**, 2307.
Loffler, R. and Finkelmann, H. (1990) *Makromol. Rapid Commun.*, **11**, 321.
Loy, D. A., Baugher, C. R., Schnieder, D. A., Sanchez, A. and Gonzalez, F. (2001) *Polym. Preprints*, **4**2(1), 180.
Luna-Xavier, J.-L., Bourgeat-Lami, E. and Guyot, A. (2001) *Coll. Polym. Sci.*, **279**, 947.
Ma, J., Shi, L., Yang, M. *et al.* (2002) *J. Appl. Polym. Sci.*, **86**, 3708.
Madkour, T. M. and Hamdi, M. S. (1996) *J. Appl. Polym. Sci.*, **61**, 1239.
Madkour, T. M., Kloczkowski, A. and Mark, J. E. (1994) *Comput. Polym. Sci.*, **4**, 95.
Madkour, T. and Mark, J. E. (1993) *Polym. Bulletin*, **31**, 615.
Madkour, T. M. and Mark, J. E. (1994a) *Comput. Polym. Sci.*, **4**, 79.
Madkour, T. M. and Mark, J. E. (1994b) *Comput. Polym. Sci.*, **4**, 87.
Madkour, T. M. and Mark, J. E. (2002) *J. Polym. Sci., Polym. Phys. Ed.*, **40**, 840.
Mandelkern, L. (1989) In *Comprehensive Polymer Science*, ed., G. Allen, Oxford: Pergamon Press, p. 363.

Mandelkern, L. (2003) *Crystallization of Polymers*, Cambridge: Cambridge University Press.
Mark, J. E. (1973) *Rubber Chem. Technol.*, **46**, 593.
Mark, J. E. (1975) *Rubber Chem. Technol*, **48**, 495.
Mark, J. E. (1976) *Macromol. Rev.*, **11**, 135.
Mark, J. E. (1979a) *Makromol. Chemie, Suppl.*, **2**, 87.
Mark, J. E. (1979b) *Polym. Eng. Sci.*, **19**, 409.
Mark, J. E. (1979c) *Polym. Eng. Sci.*, **19**, 254.
Mark, J. E. (1979d) *Acc. Chem. Res.*, **12**, 49.
Mark, J. E. (1981) *J. Chem. Educ.*, **58**, 898.
Mark, J. E. (1982a) *Rubber Chem. Technol.*, **55**, 762.
Mark, J. E. (1982b) *Adv. Polym. Sci.*, **44**, 1.
Mark, J. E. (1989) *J. Appl. Polym. Sci., Symp.*, **44**, 209.
Mark, J. E. (1990) In *Silicon-Based Polymer Science: A Comprehensive Resource*, Vol. 224, eds., J. M. Zeigler and F. W. G. Fearon, Washington, DC: American Chemical Society, p. 47.
Mark, J. E. (1993) In *Physical Properties of Polymers*, eds., J. E. Mark, A. Eisenberg, W. W. Graessley *et al.*, Washington, DC: American Chemical Society, p. 3.
Mark, J. E. (1994) *Acc. Chem. Res.*, **27**, 271.
Mark, J. E. (Ed.) (1996a) *Physical Properties of Polymers Handbook*, New York: Springer-Verlag.
Mark, J. E. (1996b) *Polym. Eng. Sci.*, **36**, 2905.
Mark, J. E. (1996c) *J. Comput.-Aided Mats. Design*, **3**, 311.
Mark, J. E. (1996d) *Hetero. Chem. Rev.*, **3**, 307.
Mark, J. E. (1999a) *Rubber Chem. Technol.*, **72**, 465.
Mark, J. E. (Ed.) (1999b) *Polymer Data Handbook*, New York: Oxford University Press.
Mark, J. E. (1999c) In *Molecular Catenanes, Rotaxanes and Knots*, eds., J.-P. Sauvage and C. Dietrich-Buchecker, Weinheim: Wiley-VCH, p. 223.
Mark, J. E. (2000) In *Applied Polymer Science – 21st Century*, eds., C. D. Craver and C. E. Carraher, Jr., Washington, DC: American Chemical Society, p. 209.
Mark, J. E. (2001a) *Makromol. Symp.*, **171**, 1.
Mark, J. E. (2001b) In *2001 International Conference on Computational Nanoscience*, Hilton Head Island, SC, eds., M. Laudon and B. Romanowicz, Boston: Nanoscience Hilton Head Island, SC, Computational Publications, p. 53.
Mark, J. E. (2002a) *J. Chem. Educ.*, **79**, 1437.
Mark, J. E. (2002b) *Mol. Cryst. Liq. Cryst.*, **374**, 29.
Mark, J. E. (2003a) *J. Phys. Chem., Part B*, **107**, 903.
Mark, J. E. (2003b) *Macromol. Symp., Kyoto Issue*, **201**, 77.
Mark, J. E. (2003c) *Prog. Polym. Sci.*, **28**, 1205.
Mark, J. E. (2003d) *Macromol. Symp., St. Petersburg Issue*, **191**, 121.
Mark, J. E. (2004a) *Acc. Chem. Res.*, **37**, 946.
Mark, J. E. (2004b) *Mol. Cryst. Liq. Cryst., Bucharest Meeting*, **417**, 75.
Mark, J. E. (2005a) In *New Book of Knowledge*, ed., K. Fitzsimons, Danbury, CT: Grolier, Scholastic Library Publishing, p. 344.
Mark, J. E. (Ed.) (2005b) *Physical Properties of Polymers Handbook*, New York: Springer-Verlag.
Mark, J. E., Abou-Hussein, R., Sen, T. Z. and Kloczkowski, A. (2005a) *Polymer*, **46**, 8894.
Mark, J. E., Allcock, H. R. and West, R. (1992a) *Inorganic Polymers*, Englewood Cliffs, NJ: Prentice Hall.

Mark, J. E., Allcock, H. R. and West, R. (2005b) *Inorganic Polymers*, Second Edition, New York: Oxford University Press.
Mark, J. E. and Andrady, A. L. (1981) *Rubber Chem. Technol.*, **54**, 366.
Mark, J. E. and Curro, J. G. (1983) *J. Chem. Phys.*, **79**, 5705.
Mark, J. E., Eisenberg, A., Graessley, W. W., Mandelkern, L. and Koenig, J. L. (1984) *Physical Properties of Polymers*, Washington, DC: American Chemical Society.
Mark, J. E., Eisenberg, A., Graessley, W. W. *et al.* (1993) *Physical Properties of Polymers*, Third Edition, Washington, DC: American Chemical Society.
Mark, J. E. and Erman, B. (Eds.) (1992) *Elastomeric Polymer Networks*, Englewood Cliffs, NJ: Prentice Hall.
Mark, J. E. and Erman, B. (1998) In *Polymer Networks*, ed., R. F. T. Stepto, Glasgow: Blackie Academic, Chapman & Hall.
Mark, J. E. and Erman, B. (2001) In *Performance of Plastics*, ed., W. Brostow, Cincinnati: Hanser, p. 401.
Mark, J. E., Erman, B. and Eirich, F. R. (Eds.) (2005c) *Science and Technology of Rubber*, Amsterdam: Elsevier.
Mark, J. E. and Llorente, M. A. (1981) *Polym. J. (Tokyo)*, **17**, 265.
Mark, J. E., Ngai, K. L., Graessley, W. W. *et al.* (2004) *Physical Properties of Polymers*. Third Edition, Cambridge: Cambridge University Press.
Mark, J. E. and Ning, Y.-P. (1984) *Polym. Bull.*, **12**, 413.
Mark, J. E. and Ning, Y.-P. (1985) *Polym. Eng. Sci.*, **25**, 824.
Mark, J. E. and Odian, G. (1984) *Polymer Chemistry Course Manual*, Washington, DC: American Chemical Society.
Mark, J. E., Rahalkar, R. R. and Sullivan, J. L. (1979) *J. Chem. Phys.*, **70**, 1794.
Mark, J. E. and Schaefer, D. W. (1990) In *Polymer-Based Molecular Composites*, Vol. 171, eds., D. W. Schaefer and J. E. Mark, Pittsburgh: Materials Research Society, p. 51.
Mark, J. E. and Sun, C.-C. (1987) *Polym. Bull.*, **18**, 259.
Mark, J. E. and Sung, P.-H. (1982) *Rubber Chem. Technol.*, **55**, 1464.
Mark, J. E., Wang, S., Xu, P. and Wen, J. (1992b) In *Submicron Multiphase Materials*, Vol. 274, eds., R. H. Baney, L. R. Gilliom, S.-I. Hirano and H. K. Schmidt, Pittsburgh, PA: Materials Research Society, p. 77.
Mark, J. E. and Zhang, Z.-M. (1983) *J. Polym. Sci., Polym. Phys. Ed.*, **21**, 1971.
Marszalek, P. E., Oberhauser, A. F., Pang, Y.-P. and Fernandez, J. M. (1998) *Nature*, **396**, 661.
Masaki, K., Ohkawara, S.-I., Hirano, T., Seno, M. and Sato, T. (2004) *J. Appl. Polym. Sci.*, **91**, 3342.
Mason, P. (1979) *Cauchu*. *The Weeping Wood*, Australian Broadcasting Commission, Sydney.
Matsuo, E. S. and Tanaka, T. (1992) *Nature*, **358**, 482.
Mattice, W. L. and Suter, U. W. (1994) *Conformational Theory of Large Molecules: The Rotational Isomeric State Model in Macromolecular Systems*, New York: Wiley.
Mayer, A. B. R. and Mark, J. E. (2000) *Mol. Cryst. Liq. Cryst.*, **354**, 221.
McCarthy, D. W., Mark, J. E., Clarson, S. J. and Schaefer, D. W. (1998) *J. Polym. Sci., Polym. Phys. Ed.*, **36**, 1191.
Meier, D. J. (1974) *Appl. Polym. Sci. Symp.*, **24**, 67.
Menduina, C., Freire, J. J., Llorente, M. A. and Vilgis, T. (1986) *Macromolecules*, **19**, 1212.
Meon, W., Blume, A., Luginsland, H.-D. and Uhrlandt, S. (2004) In *Rubber Compounding: Chemistry and Applications*, ed., B. Rodgers, New York: Marcel Dekker, Inc., p. 285.

Miller, D. R. and Macosko, C. W. (1987) *J. Polym. Sci., Polym. Phys. Ed.*, **25**, 2441.
Miller, K. J., Grebowicz, J., Wesson, J. P. and B. Wunderlich (1990) *Macromolecules*, **23**, 849.
Mitchell, G. R., Davis, F. J. and Ashman, A. (1987) *Polymer*, **28**, 639.
Miyata, T., Masuko, T., Kojima, M. and Magill, J. H. (1994) *Makromol. Chem. Phys.*, **195**, 253.
Molenberg, A., Moller, M. and Sautter, E. (1997) *Prog. Polym. Sci.*, **22**, 1133.
Monnerie, L. (1983) *Faraday Symp. Chem. Soc.*, **18**, 1.
Mooney, M. (1948) *J. Appl. Phys.*, **19**, 434.
Moore, W. J. (1983) *Basic Physical Chemistry*, Englewood Cliffs, NJ: Prentice Hall.
Morawetz, H. (1985) *Polymers: The Origins and Growth of a Science*, New York: Wiley-Interscience.
Morton, M. (Ed.) (1987) *Rubber Technology*, New York: Van Nostrand Reinhold.
Mott, P. H. and Roland, C. M. (2000) *Macromolecules*, **33**, 4132.
Mullins, L. and Tobin, N. R. (1965) *J. Appl. Polym. Sci.*, **9**, 2993.
Munch, J. P., Candau, S., Duplessix, R. *et al.* (1976) *J. Polym. Sci., Polym. Phys. Ed.*, **14**, 1097.
Murugesan, S., Sur, G. S., Beaucage, G. and Mark, J. E. (2005) *Silicon Chem.*, **2**, 217.
Murugesan, S., Sur, G. S., Mark, J. E. and Beaucage, G. (2004) *J. Inorg. Organomet. Polym.*, **14**, 239.
Myers, C. L. (1999) In *Polymer Data Handbook*, ed., J. E. Mark, New York: Oxford University Press, p. 776.
Na, Y.-H., Kurokawa, T., Katsuyama, Y. *et al.* (2004) *Macromolecules*, **37**, 5370.
Nagai, K. (1964) *J. Chem. Phys.*, **40**, 2818.
Nagy, M. and Keller, A. (1989) *Polym. Commun.*, **30**, 130.
Nakatani, A. I., Chen, W., Schmidt, R. G., Gordon, G. V. and Han, C. C. (2001) *Polymer*, **42**, 3713.
Nasir, M. and Teh, G. K. (1988) *Eur. Polym. J.*, **24**, 733.
Nele, M., Mohammed, M., Xin, S., Collins, S. and Dias, M. L. (2001) *Macromolecules*, **34**, 3830.
Netz, R. R. (2001) *Macromolecules*, **34**, 7522.
Ngai, K. L. (2004) In *Physical Properties of Polymers*. Third Edition, eds., J. E. Mark, K. L. Ngai, W. W. Graessley *et al.*, Cambridge: Cambridge University Press, p. 72.
Nieuwenhuizen, P. J., Reedijk, J., van Duin, M. and McGill, W. J. (1997) *Rubber Chem. Technol.*, **70**, 368.
Ning, Y.-P., Tang, M.-Y., Jiang, C.-Y., Mark, J. E. and Roth, W. C. (1984) *J. Appl. Polym. Sci.*, **29**, 3209.
Nisato, G. and Candau, S. J. (2002) In *Polymer Gels and Networks*, eds., Y. Osada and A. R. Khokhlov, New York: Marcel Dekker, p. 131.
Noda, I. (1991) *Nature*, **350**, 143.
Nor, H. M. and Ebdon, J. R. (1998) *Prog. Polym. Sci.*, **23**, 143.
Noshay, A. and McGrath, J. E. (1977) *Block Copolymers: Overview and Critical Survey*, New York: Academic Press.
Novak, B. M. (1993) *Adv. Mater.*, **5**, 422.
Obata, Y., Kawabata, S. and Kawai, H. (1970) *J. Polym. Sci., Part A-2*, **8**, 903.
Oberhauser, A. F., Marszalek, P. E., Erickson, H. P. and Fernandez, J. M. (1998) *Nature*, **393**, 181.
Ogden, R. W. (1986) *Rubber Chem. Technol.*, **59**, 361.
Ogden, R. W. (1987) *Polymer*, **28**, 379.

Oh, J. S., Isayev, A. I., Wagler, T., Rinaldi, P. and von Meerwall, E. (2004) *J. Polym. Sci., Polym. Phys.*, **42**, 1875.
Oikawa, H. (1992) *Polymer*, **33**, 1116.
Okada, A., Kawasumi, M., Usuki, A. *et al.* (1990) In *Polymer-Based Molecular Composites*, Vol. 171, eds., D. W. Schaefer and J. E. Mark, Pittsburgh: Materials Research Society, p. 45.
Okamoto, Y., Miyagi, H., Kakugo, M. and Takahashi, K. (1991) *Macromolecules*, **24**, 5639.
Okay, O. D., Durmaz, S. and Erman B. (2000) *Macromolecules*, **33**, 4822.
Okumura, H., Okada, M., Kawaguchi, Y. and Harada, A. (2000) *Macromolecules*, **33**, 4297.
Onoa, B., Dumont, S., Liphardt, J. *et al.* (2003) *Science*, **299**, 1892.
Oppermann, W. and Rennar, N. (1987) *Prog. Coll. Polym. Sci.*, **75**, 49.
Ortiz, C. and Hadziioannou, G. (1999) *Macromolecules*, **32**, 780.
Osman, M. A., Atallah, A., Kahr, G. and Suter, U. W. (2002) *J. Appl. Polym. Sci.*, **83**, 2175.
Osman, M. A., Atallah, A., Muller, M. and Suter, U. W. (2001) *Polymer*, **42**, 6545.
Ostwald, W. (1900) *Z. Physik. Chem.*, **34**, 495.
Out, G. J. J., Turetskii, A. A., Moller, M. and Oelfin, D. (1994) *Macromolecules*, **27**, 3310.
Out, G. J. J., Turetskii, A. A., Snijder, M., Moller, M. and Papkov, V. S. (1995) *Polymer*, **36**, 3213.
Pak, H. and Flory, P. J. (1979) *J. Polym. Sci., Polym. Phys. Ed.*, **17**, 1845.
Pan, G., Mark, J. E. and Schaefer, D. W. (2003) *J. Polym. Sci., Polym. Phys. Ed.*, **41**, 3314.
Papkov, V. S., Turetskii, A. A., Out, G. J. J. and Moller, M. (2002) *Int. J. Polym. Mater.*, **51**, 369.
Patel, S. K., Malone, S., Cohen, C., Gillmor, J. R. and Colby, R. H. (1992) *Macromolecules*, **25**, 5241.
Patwardhan, S. V. and Clarson, S. J. (2003) *Mater. Sci. Eng. C*, **23**, 495.
Patwardhan, S. V., Durstock, M. F. and Clarson, S. J. (2003) In *Synthesis and Properties of Silicones and Silicone-Modified Materials*, Vol. 838, eds., S. J. Clarson, J. J. Fitzgerald, M. J. Owen, S. D. Smith and M. E. van Dyke, Washington, DC: American Chemical Society, p. 366.
Pearson, D. S. (1977) *Macromolecules*, **10**, 696.
Peppas, N. A. and Langer, R. (1994) *Science*, **263**, 1715.
Percec, V. and Hsu, C.-S. (1990) *Polym. Bull.*, **23**, 463.
Perkins, T. T., Dalal, R. V., Mitsis, P. G. and Block, S. M. (2003) *Science*, **301**, 1914.
Perkins, T. T., Quake, S. R., Smith, D. E. and Chu, S. (1994a) *Science*, **264**, 822.
Perkins, T. T., Smith, D. E. and Chu, S. (1994b) *Science*, **264**, 819.
Perkins, T. T., Smith, D. E., Larson, R. G. and Chu, S. (1995) *Science*, **268**, 83.
Pethrick, R. A. and Dawkins, J. V. (Eds.) (1999) *Modern Techniques for Polymer Characterization*, New York: Wiley & Sons, Inc.
Philippova, O. E. (2000) *Polym. Sci. Ser. C.*, **42**, 208.
Pinnavaia, T. J. and Beall, G. (Eds.) (2001) *Polymer-Clay Nanocomposites*, New York: Wiley.
Pinnavaia, T. J., Lan, T., Wang, Z., Shi, H. and Kaviratna, P. D. (1996) In *Nanotechnology. Molecularly Designed Materials*, Vol. 622, eds., G.-M. Chow and K. E. Gonsalves, Washington, DC: American Chemical Society, p. 250.
Pochan, J. M., Beatty, C. L., Hinman, D. D. and Karasz, F. E. (1975) *J. Polym. Sci., Polym. Phys. Ed.*, **13**, 977.
Pollard, M., Russell, T. P., Ruzette, A. V., Mayes, A. M. and Gallot, Y. (1998) *Macromolecules*, **31**, 6493.

Premachandra, J., Kumudinie, C. and Mark, J. E. (2002) *J. Macromol. Sci., Pure Appl. Chem.*, **39**, 301.
Premachandra, J. and Mark, J. E. (2002) *J. Macromol. Sci., Pure Appl. Chem.*, **39**, 287.
Pu, Z., Mark, J. E., Jethmalani, J. M. and Ford, W. T. (1997) *Chem. Mater.*, **9**, 2442.
Pyun, J., Matyjaszewski, K., Kowalewski, T., Mather, P. T. and Chun, S. B. (2001) *Abstracts, Chicago Am. Chem. Soc. Meeting*.
Quan, X. (1989) *Polym. Eng. Sci.*, **29**, 1419.
Queslel, J. P. and Mark, J. E. (1985a) *Adv. Polym. Sci.*, **71**, 229.
Queslel, J. P. and Mark, J. E. (1985b) *J. Chem Phys*, **82**, 3449.
Queslel, J. P. and Mark, J. E. (1989) In *Comprehensive Polymer Science*, ed., G. Allen, Oxford: Pergamon Press, p. 271.
Rajan, G. S., Mark, J. E., Seabolt, E. E. and Ford, W. T. (2002) *J. Macromol. Sci. – Pure Appl. Chem.*, **A39**, 39.
Rajan, G. S., Sur, G. S., Mark, J. E., Schaefer, D. W. and Beaucage, G. (2003) *J. Polym. Sci. B, Polym. Phys.*, **41**, 1897.
Rajan, G. S., Vu, Y. T., Mark, J. E. and Myers, C. L. (2004) *Eur. Polym. J.*, **40**, 63.
Read, B. F. and Stein, R. S. (1968) *Macromolecules*, **1**, 116.
Reed, P. E. (1979) In *Developments in Polymer Fracture: 1*, ed., E. H. Andrews, London: Applied Science Publishers.
Rehahn, M., Mattice, W. L. and Suter, U. W. (1997) *Adv. Polym. Sci.*, **131/132**, 1.
Rennar, N. and Oppermann, W. (1992) *Coll. Polym. Sci.*, **270**, 527.
Riande, E. and Diaz-Calleja, R. (2004) *Electrical Properties of Polymers*, New York: Marcel Dekker.
Riande, E. and Saiz, E. (1992) *Dipole Moments and Birefringence of Polymers*, Englewood Cliffs, NJ: Prentice Hall.
Rief, M., Oesterhelt, F., Heymann, B. and Gaub, H. E. (1997) *Science*, **275**, 1295.
Rigbi, Z. (1980) *Adv. Polym. Sci.*, **36**, 21.
Rigbi, Z. and Mark, J. E. (1985) *J. Polym. Sci., Polym. Phys. Ed.*, **23**, 1267.
Rigbi, Z. and Mark, J. E. (1986) *J. Polym. Sci., Polym. Phys. Ed.*, **24**, 443.
Rivlin, R. S. (1948a) *Philos. Trans. R. Soc. London, A*, **241**, 379.
Rivlin, R. S. (1948b) *Philos. Trans. R. Soc. London, A*, **240**, 459.
Rivlin, R. S. (1948c) *Philos. Trans. R. Soc. London, A*, **240**, 491.
Rivlin, R. S. (1948d) *Philos. Trans. R. Soc. London, A*, **240**, 509.
Rivlin, R. S. and Saunders, D. W. (1951) *Philos. Trans. R. Soc. London, A*, **243**, 251.
Roe, R.-J. (2000) *Methods of X-Ray and Neutron Scattering in Polymer Science*, Oxford: Oxford University Press.
Roland, C. M. and Peng, K. L. (1991) *Rubber Chem. Technol.*, **64**, 790.
Roland, C. M. and Warzel, M. L. (1990) *Rubber Chem. Technol.*, **63**, 285.
Ronca, G. and Allegra, G. (1975) *J. Chem. Phys.*, **63**, 4990.
Rubinstein, M. and Panyukov, S. (2002) *Macromolecules*, **35**, 6670.
Ruzette, A.-V. G., Banerjee, P., Mayes, A. M. and Russell, T. P. (2001) *J. Chem. Phys.*, **114**, 8205.
Saalwachter, K. (2003) *J. Chem. Phys.*, **119**, 3468.
Saalwachter, K. (2004) *J. Chem. Phys.*, **120**, 454.
Saalwachter, K. and Kleinschmidt, F. (2004) *Macromolecules*, **37**, 8556.
Sakrak, G., Bahar, I. and Erman, B. (1994) *Macromol. Theory Simul.*, **3**, 151.
Sanchez, C., Laine, R. M., Yang, S. and Brinker, C. J. (Eds.) (2002) *Organic/Inorganic Hybrid Materials – 2002*, Warrendale, PA: Materials Research Society.
Santangelo, P. G. and Roland, C. M. (1994) *Rubber Chem. Technol.*, **67**, 359.
Santangelo, P. G. and Roland, C. M. (1995) *Rubber Chem. Technol.*, **68**, 124.

Santangelo, P. G. and Roland, C. M. (2003) *Rubber Chem. Technol.*, **76**, 892.
Schaefer, D. W., Jian, L., Sun, C.-C. *et al.* (1992) In *Ultrastructure Processing of Advanced Materials*, eds., D. R. Uhlmann and D. R. Ulrich, New York: Wiley, p. 361.
Schaefer, D. W. and Keefer, K. D. (1984) *Phys. Rev. Lett.*, **53**, 1383.
Schaefer, D. W., Mark, J. E., McCarthy, D. W. *et al.* (1990) In *Polymer-Based Molecular Composites*, Vol. 171, eds., D. W. Schaefer and J. E. Mark, Pittsburgh: Materials Research Society, p. 57.
Schaefer, D. W., Vu, B. T. N. and Mark, J. E. (2002) *Rubber Chem. Technol.*, **75**, 795.
Schroeder, C. M., Babcock, H. P., Shaqfeh, E. S. G. and Chu, S. (2003) *Science*, **301**, 1515.
Schuler, B. (2005) *Chem. Phys. Chem.*, **6**, 1206.
Schwaiger, I., Sattler, C., Hostetter, D. R. and Rief, M. (2002) *Nature Materials*, **1**, 233.
Seitz, M., Friedsam, C., Jostl, W., Hugel, T. and Gaub, H. E. (2003) *Chem. Phys. Chem.*, **4**, 986.
Semmler, K. and Finkelmann, H. (1995) *Makromol. Chem. Phys.*, **196**, 3197.
Seog, S., Dean, D., Plaas, A. H. K. *et al.* (2002) *Macromolecules*, **35**, 5601.
Shadwick, R. E. and Gosline, J. M. (1985) *J. Exp. Biol.*, **114**, 239.
Shah, G. B. (1996) *Macromol. Chem. Phys.*, **197**, 2201.
Shah, G. B. (2004) *J. Appl. Polym. Sci.*, **94**, 1719.
Sharaf, M. A. (1992) *Int. J. Polym. Mater.*, **18**, 237.
Sharaf, M. A., Kloczkowski, A. and Mark, J. E. (1994) *Comput. Polym. Sci.*, **4**, 29.
Sharaf, M. A., Kloczkowski, A. and Mark, J. E. (2001) *Comput. Theor. Polym. Sci.*, **11**, 251.
Sharaf, M. A. and Mark, J. E. (1991) *J. Macromol. Sci., Macromol. Rep.*, **1**, 67.
Sharaf, M. A. and Mark, J. E. (1993) *Polym. Gels Networks*, **1**, 33.
Sharaf, M. A. and Mark, J. E. (1995) *J. Polym. Sci., Polym. Phys. Ed.*, **33**, 1151.
Sharaf, M. A. and Mark, J. E. (2002) *Polymer*, **43**, 643.
Sharaf, M. A. and Mark, J. E. (2004) *Polymer*, **45**, 3943.
Shen, M. and Croucher, M. (1975) *J. Macromol. Sci. Rev. Macromol. Chem.*, **C12**, 287.
Shenoy, D. K., Thomsen, D. L., Keller, P. and Ratna, B. R. (2003) *J. Phys. Chem.*, **107**, 13755.
Shibanov, Y. D. (1989) *Polym. Sci. USSR*, **31**, 2653.
Shim, S. E. and Isayev, A. I. (2001) *Rubber Chem. Technol.*, **74**, 303.
Shim, S. E. and Isayev, A. I. (2003) *J. Appl. Polym. Sci.*, **88**, 2630.
Shim, S. E., Isayev, A. I. and von Meerwall, E. (2003) *J. Polym. Sci., Polym. Phys.*, **41**, 454.
Shim, S. E., Parr, J. C., von Meerwall, E. and Isayev, A. I. (2002) *J. Phys. Chem. B*, **106**, 12072.
Slaughter, B. D., Unruh, J. R., Price, E. S. *et al.* (2005) *J. Am. Chem. Soc.*, **127**, 12107.
Smith, K. J. (1976) *Polym. Eng. Sci.*, 16, 168.
Smith, S. B., Cui, Y. and Bustamante, C. (1996) *Science*, **271**, 795.
Smith, T. L., Haidar, B. and Hedrick, J. L. (1990) *Rubber Chem. Technol.*, **63**, 256.
Sobon, C. A., Bowen, H. K., Broad, A. and Calvert, P. D. (1987) *J. Mater. Sci. Lett.*, **6**, 901.
Sohoni, G. B. and Mark, J. E. (1987) *J. Appl. Polym. Sci.*, **34**, 2853.
Sohoni, G. B. and Mark, J. E. (1992) *J. Appl. Polym. Sci.*, **45**, 1763.
Sotta, P. (1998) *Macromolecules*, **31**, 8417.
Sotta, P. and Deloche, B. (1990) *Macromolecules*, **23**, 1999.
Sotta, P. and Deloche, B. (1993) *J. Chem. Phys.*, **100**, 4591.
Sotta, P., Deloche, B. and Herz, J. (1991) *Makromol. Chem., Macromol. Symp.*, **45**, 177.
Sotta, P., Deloche, B., Herz, J. *et al.* (1987) *Macromolecules*, **20**, 2769.
Sotta, P., Higgs, P. G., Depner, M. and Deloche, B. (1995) *Macromolecules*, **28**, 7208.

Sperling, L. H. (1981) *Interpenetrating Polymer Networks and Related Materials*, New York: Plenum Press.
Sperling, L. H. (2001) *Introduction to Physical Polymer Science*, New York: Wiley Interscience.
Stepto, R. F. T. (1986) In *Advances in Elastomers and Rubber Elasticity*, eds., J. Lal and J. E. Mark, New York: Plenum Press.
Stein, R. S. and Hong, S. D. (1976) *J. Macromol. Sci. Phys.*, **B12**, 125.
Straube, E., Urban, V., Pykhout-Hintzen, W., Richter, D. and Glinka, C. J. (1995) *Phys. Rev. Lett.*, **74**, 4464.
Strick, T., Allemand, J.-F., Croquette, V. and Benisimon, D. (2001) *Phys. Today*, **53**, 46.
Su, T.-K. and Mark, J. E. (1977) *Macromolecules*, **10**, 120.
Sun, C.-C. and Mark, J. E. (1987a) *J. Polym. Sci., Polym. Phys. Ed.*, **25**, 1561.
Sun, C.-C. and Mark, J. E. (1987b) *J. Polym. Sci., Polym. Phys. Ed.*, **25**, 2073.
Sunkara, H. B., Jethmalani, J. M. and Ford, W. T. (1995) In *Hybrid Organic-Inorganic Composites*, Vol. 585, eds., J. E. Mark, C. Y.-C. Lee and P. A. Bianconi, Washington, DC: American Chemical Society, p. 181.
Sur, G. S. and Mark, J. E. (1985) *Eur. Polym. J.*, **21**, 1051.
Sur, G. S. and Mark, J. E. (1987) *Polym. Bull.*, **18**, 369.
Sur, G. S., Sun, H., Lee, T. J., Lyu, S. G. and Mark, J. E. (2003) *Coll. Polym. Sci.*, **281**, 1040.
Suzuki, A. and Tanaka, T. (1990) *Nature*, **346**, 345.
Talroze, R. V., Gubina, T. I., Shibaev, V. P. and Plate, N. A. (1990) *Makromol. Rapid Commun.*, **11**, 67.
Tamaki, R., Choi, J. and Laine, R. M. (2003) *Chem. Mater.*, **15**, 793.
Tammer, M., Li, J., Komp, A., Finkelmann, H. and Kremer, F. (2005) *Makromol. Chem. Phys.*, **206**, 709.
Tan, N. C. B., Bauer, B. J., Plestil, J. *et al.* (1999) *Polymer*, **40**, 4603.
Tanaka, T. (1978) *Phys. Rev. Lett.*, **40**, 820.
Tanaka, T. (1981) *Sci. Am.*, **244**, 124.
Tanaka, T. (1992) In *Polyelectrolyte Gels*, Vol. 480, eds., R. S. Harland and R. K. Prud'homme, Washington, DC: American Chemical Society, p. 1.
Tanaka, T., Sun, S.-T., Hirokawa, Y. *et al.* (1987) *Nature*, **325**, 798.
Tanaka, Y. (2001) *Rubber Chem. Technol.*, **74**, 355.
Tanaka, Y., Kagami, Y., Matsuda, A. and Osada, Y. (1995) *Macromolecules*, **28**, 2574.
Tanaka, Y., Kuwabara, R., Na, Y.-H. *et al.* (2005) *J. Phys. Chem. B.*, **109**, 11559.
Tang, M.-Y., Letton, A. and Mark, J. E. (1984) *Coll. Polym. Sci.*, **262**, 990.
Termonia, Y. (1990) *Macromolecules*, **23**, 1481.
Toki, S., Sics, I., Hsiao, B. S. *et al.* (2004) *J. Polym. Sci., Polym. Phys.*, **42**, 956.
Toki, S., Sics, I., Hsiao, B. S. *et al.* (2005) *Macromolecules*, **38**, 7064.
Tomalia, D. A. (1995) *Sci. Am.*, **272(5)**, 62.
Tomalia, D. A. and Frechet, J. M. J. (2002) *J. Polym. Sci., Polym. Chem.*, **40**, 2719.
Trabelsi, S., Albouy, P.-A. and Rault, J. (2004) *Rubber Chem. Technol.*, **77**, 303.
Treloar, L. R. G. (1943a) *Trans. Faraday Soc.*, **39**, 36.
Treloar, L. R. G. (1943b) *Trans. Faraday Soc.*, **39**, 241.
Treloar, L. R. G. (1975) *The Physics of Rubber Elasticity*, Oxford: Clarendon Press.
Tsuchiya, M., Tsuji, K., Maki, K. and Tanaka, T. (1994) *J. Phys. Chem.*, **98**, 6187.
Turetskii, A. A., Out, G. J. J., Klok, H.-A. and Moller, M. (1995) *Polymer*, **36**, 1303.
Ullman, R. (1979) *J. Chem. Phys.*, **71**, 436.
Ullman, R. (1982) In *Elastomers and Rubber Elasticity*, ed., J. E. Mark and J. Lal, Washington, DC: American Chemical Society Publications.

Urayama, K. and Kohjiya, S. (1997) *Polymer*, **38**, 955.
Urayama, K. and Kohjiya, S. (1998) *Eur. Phys. J. B*, **2**, 75.
Urry, D. W., Venkatachalam, C. M., Long, M. M. and Prasad, K. U. (1982). In *Conformation in Biology: The Festschrift Celebrating the Sixtieth Birthday of G. N. Ramachandran*, eds., R. Srinivasan and R. H. Sarma, New York: Adenine Press.
Vaia, R. A. and Giannelis, E. P. (2001a) *Polymer*, **42**, 1281.
Vaia, R. A. and Giannelis, E. P. (2001b) *MRS Bull.*, **26** (5), 394.
Vasilevskaya, V. V. and Semenov, A. N. (1994) *Polym. Sci. USSR*, **36**, 1535.
Venkatraman, S. (1993) *J. Appl. Polym. Sci.*, **48**, 1383.
Viers, B. D. (1998) Ph.D. Thesis, University of Cincinnati.
Vilgis, T. A. and Boué, F. (1986) *Polymer*, **27**, 1154.
Vilgis, T. A., Boué, F. and Edwards, S. F. (1989) In *Molecular Basis of Polymer Networks*, Vol. 42, eds., A. Baumgartner and C. E. Picot, Berlin: Springer, p. 170.
Vilgis, T. A. and Erman, B. (1993) *Macromolecules*, **26**, 6657.
Vogel, S. (1994) *Life in Moving Fluids: The Physical Biology of Flow*, Princeton: Princeton University Press.
Vogel, S. (1998) *Cats' Paws and Catapults: Mechanical Worlds of Nature and People*, New York: W. W. Norton.
Voishchev, V. S., Popov, I. V., Sazhin *et al.* (1999) *Polym. Sci. USSR, A*, **41**, 311.
Volkenstein, M. (1963) *Configurational Statistics of Polymer Chains*, New York: Interscience.
Vollrath, F. (1992) *Sci. Am.*, **266(3)**, 70.
von Lockette, P. R. and Arruda, E. M. (1999) *Macromolecules*, **32**, 1990.
Vu, B. T. N. (2001) M.S. Thesis in Chemistry, University of Cincinnati.
Vu, B. T. N., Mark, J. E. and Schaefer, D. W. (2000) *Preprints, American Chemical Society Division of Polymeric Materials: Science and Engineering*, **83**, 411.
Vu, B. T. N., Mark, J. E. and Schaefer, D. W. (2003) *Composite Interfaces*, **10**, 451.
Vu, Y. T. and Mark, J. E. (2004) *Coll. Polym. Sci.*, **282**, 613.
Vu, Y. T., Mark, J. E., Pham, L. H. and Engelhardt, M. (2001) *J. Appl. Polym. Sci.*, **82**, 1391.
Waddell, W. H. and Tsou, A. H. (2004) In *Rubber Compounding: Chemistry and Applications*, ed., B. Rodgers, New York: Marcel Dekker, Inc., p. 133.
Wagner, J. and Phillips, P. J. (2001) *Polymer*, **42**, 8999.
Wall, F. T. (1942) *J. Chem. Phys.*, **10**, 132.
Wall, F. T. and Flory, P. J. (1951) *J. Chem. Phys.*, **19**, 1435.
Wampler, W. A., Carlson, T. F. and Jones, W. R. (2004) In *Rubber Compounding. Chemistry and Applications*, ed., B. Rodgers, New York: Marcel Dekker, Inc., p. 239.
Wang, J., Hamed, G. R., Umetsu, K. and Roland, C. M. (2005) *Rubber Chem. Technol.*, **78**, 76.
Wang, S., Long, C., Wang, X., Li, Q. and Qi, Z. (1998) *J. Appl. Polym. Sci.*, **69**, 1557.
Wang, S.-B. and Mark, J. E. (1987) *Polym. Bull.*, **17**, 271.
Wang, S. and Mark, J. E. (1990a) *Macromolecules*, **23**, 4288.
Wang, S. and Mark, J. E. (1990b) *J. Mater. Sci.*, **25**, 65.
Wang, S. and Mark, J. E. (1992) *J. Polym. Sci., Polym. Phys. Ed.*, **30**, 801.
Wang, S. and Mark, J. E. (1994) *J. Macromol. Sci., Macromol. Rep.*, **A31**, 253.
Wang, S., Xu, P. and Mark, J. E. (1991a) *Macromolecules*, **24**, 6037.
Wang, S., Xu, P. and Mark, J. E. (1991b) *Rubber Chem. Technol.*, **64**, 746.
Wang, X.-J. and Warner, M. (1997) *Macromol. Theory Simul.*, **6**, 37.
Ward, I. M. (1975) *Structure and Properties of Oriented Polymers*, London: Applied Science Publishers.

Warner, M. and Terentjev, E. M. (1996) *Prog. Polym. Sci.*, **21**, 853.
Warner, M. and Terentjev, E. M. (2003a) *Liquid Crystal Elastomers*, New York: Oxford University Press.
Warner, M. and Terentjev, E. M. (2003b) *Macromol. Symp.*, **200**, 81.
Warrick, E. L., Pierce, O. R., Polmanteer, K. E. and Saam, J. C. (1979) *Rubber Chem. Technol.*, **52**, 437.
Weis-Fogh, T. (1961) *J. Mol. Biol.*, **3**, 520.
Weis-Fogh, T. and Andersen, S. O. (1970) *Nature*, **227**, 718.
Wen, J. and Mark, J. E. (1994a) *Polym. J.*, **26**, 151.
Wen, J. and Mark, J. E. (1994b) *Rubber Chem. Technol.*, **67**, 806.
Wen, J. and Mark, J. E. (1995a) *J. Appl. Polym. Sci.*, **58**, 1135.
Wen, J. and Mark, J. E. (1995b) *Polym. J.*, **27**, 492.
Wen, J., Mark, J. E. and Fitzgerald, J. J. (1994) *J. Macromol. Sci., Macromol. Rep.*, **A31**, 429.
Wendorff, J. H. (1991) *Angew. Chem., Int. Ed. Eng.*, **30**, 405.
Wignall, G. D. (2004) In *Physical Properties of Polymers*, Third Edition, eds., J. E. Mark, K. L. Ngai, W. W. Graessley *et al.*, Cambridge: Cambridge University Press, p. 424.
Wilkes, G. L., Brennan, A. B., Huang, H.-H., Rodrigues, D. and Wang, B. (1990) In *Polymer-Based Molecular Composites*, Vol. 171, eds., D. W. Schaefer and J. E. Mark, Pittsburgh: Materials Research Society, p. 15.
Williams, M. C., Rouzina, I. and Bloomfield, V. A. (2002) *Acc. Chem. Res.*, **35**, 159.
Winokur, M. J. and West, R. (2003) *Macromolecules*, **36**, 7338.
Wirpsza, Z. (1993) *Polyurethanes: Chemistry, Technology, and Applications*, New York: Ellis Horwood and Prentice Hall.
Witten, T. A. (2004) *Structured Fluids: Polymers, Colloids, Surfactants*, New York: Oxford University Press.
Wood, C. D., Cooper, A. I. and DeSimone, J. M. (2004) *Curr. Opinion Solid State Mater. Sci.*, **8**, 325.
Wrana, C., Reinartz, K. and Winkelbach, H. R. (2001) *Macromol. Mater. Eng.*, **286**, 657.
Wu, W.-L., Hu, J.-T. and Hunston, D. L. (1990) *Polym. Eng. Sci.*, **30**, 835.
Xu, P. and Mark, J. E. (1992) *Polymer*, **33**, 1843.
Xu, P., Wang, S. and Mark, J. E. (1990) In *Better Ceramics Through Chemistry IV*, Vol. 180, eds., B. J. J. Zelinski, C. J. Brinker, D. E. Clark and D. R. Ulrich, Pittsburgh: Materials Research Society, p. 445.
Xu, Q., Zhang, W. and Zhang, X. (2002) *Macromolecules*, **35**, 871.
Yamamoto, S., Tsujii, Y. and Fukuda, T. (2000) *Macromolecules*, **33**, 5995.
Yang, Y., Kloczkowski, A., Mark, J. E., Erman, B. and Bahar, I. (1995) *Macromolecules*, **28**, 4920.
Yanyo, L. C. and Kelley, F. N. (1987) *Rubber Chem. Technol.*, **60**, 78.
Yeh, H. C., Eichinger, B. E. and Anderson, N. H. (1982) *J. Polym. Sci., Polym. Phys. Ed.*, **20**, 2575.
Yen, L. Y. and Eichinger, B. E. (1978) *J. Polym. Sci., Polym. Phys. Ed.*, **16**, 121.
Yoon, D. Y. and Flory, P. J. (1974) *J. Chem. Phys.*, **61**, 5366.
Yu, C. U. and Mark, J. E. (1974) *Macromolecules*, **7**, 229.
Yuan, Q. W., Kloczkowski, A., Mark, J. E. and Sharaf, M. A. (1996) *J. Polym. Sci., Polym. Phys. Ed.*, **34**, 1647.
Yun, J. and Isayev, A. I. (2003) *Rubber Chem. Technol.*, **76**, 253.
Yun, J., Oh, J. S. and Isayev, A. I. (2001) *Rubber Chem. Technol.*, **74**, 317.
Zapp, R. L. and Hous, P. (1973) In *Rubber Technology*, ed., M. Morton, New York: Van Nostrand Reinhold, p. 249.

Zentel, R. and Brehmer, M. (1995) *CHEMTECH*, **25(5)**, 41.
Zentel, R. and Benalia, M. (1987) *Makromol. Chem.*, **188**, 665.
Zentel, R. and Reckert, G. (1986) *Makromol. Chem.*, **187**, 1915.
Zentel, R., Reckert, G., Bualek, S. and Kapitza, H. (1989) *Makromol. Chem.*, **190**, 2869.
Zhang, Q., Jaroniec, J., Lee, G. and Marszalek, P. E. (2005) *Angew. Chem. Int. Ed. Engl.*, **44**, 2723.
Zhang, W. and Zhang, X. (2003) *Prog. Polym. Sci.*, **28**, 1271.
Zhang, W., Zou, S., Wang, C. and Zhang, X. (2000) *J. Phys. Chem. B.*, **104**, 10258.
Zhang, X.-B., Li, Z.-S., Lu, Z.-Y. and Sun, C.-C. (2002) *Macromolecules*, **35**, 106.
Zhang, Y.-Q., Tanaka, T. and Shibayama, M. (1992) *Nature*, **360**, 142.
Zhang, Z.-M. and Mark, J. E. (1982) *J. Polym. Sci., Polym. Phys. Ed.*, **20**, 473.
Zhou, D. and Mark, J. E. (2004) *J. Macromol. Sci. Pure Appl. Sci.*, **41**, 1221.
Zhou, W., Mark, J. E., Unroe, M. R. and Arnold, F. E. (2001) *J. Macromol. Sci. Pure Appl. Chem.*, **A38**, 1.
Zubarev, E. R., Talroze, R. V., Yuranova, T. I., Vasilets, V. N. and Plate, N. A. (1996) *Makromol. Rapid Commun.*, **17**, 43.

Index